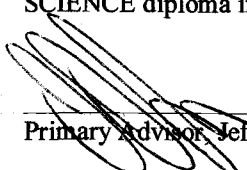
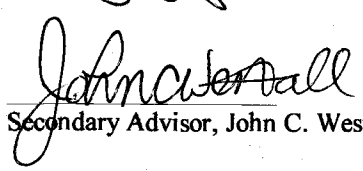


Incorporation of Aerodynamic and Boundary Layer Resistances in determining initial evaporation rates of pesticides from turf grass

presented by Michael Conway
Bioresource Research
Oregon State University
Corvallis, OR 97331
June 14, 1999

I certify this dissertation meets the minimum requirements to be accepted as a thesis for a BACHELORS OF SCIENCE diploma in Bioresource Research.


Primary Advisor, Jeffrey J. Jenkins, Environmental and Molecular Toxicology, Agricultural Chemistry Extension


Secondary Advisor, John C. Westall, Department of Chemistry

Oregon State University
Bioresource Research
4017 Ag & Life Science
Corvallis, OR 97331-7304

Codirector of the Department of Bioresource Research (Anita Azarenko, John Hays)

Incorporation of Aerodynamic and Boundary Layer Resistances in determining initial evaporation
rates of pesticides from turf grass

presented by Michael Conway
Bioresource Research
Oregon State University
Corvallis, OR 97331
June 14, 1999

I certify this dissertation meets the minimum requirements to be accepted as a thesis for a BACHELORS OF
SCIENCE diploma in Bioresource Research.



Primary Advisor, Jeffrey J. Jenkins, Environmental and Molecular Toxicology, Agricultural Chemistry Extension



Secondary Advisor, John C. Westall, Department of Chemistry

**Incorporation of Aerodynamic and Boundary Layer Resistances in
determining initial evaporation rates of pesticides from turf grass**

Michael Conway
Department of Bioresource Research
Oregon State University
Corvallis, OR 97331
June 14, 1999

Abstract:

Evaporative loss rates of pesticides, following application to turfgrass, were measured using the Backward-Time Lagrangian stochastic Dispersion model (Flesch, Wilson, *Journal of Applied Meteorology*, 34, pp. 1320-1332. All pesticides were applied to a 22.8 m x 22.8 m orchard ryegrass turf plot near Corvallis, Oregon. Solar radiation, ambient temperature, surface temperature, relative humidity, wind direction and wind speed at four heights were monitored continuously. Growth inhibitor was applied to the turf plot several days before pesticide application to maintain a constant mowed grass height and aerodynamic roughness length during the experiment. Pesticides were applied as mixtures to allow direct comparison of evaporative loss. Mixtures studied were chlorpyrifos + triadimefon, chlorpyrifos + triadimefon + ethofumesate, triclopyr (acetic acid) + propiconazole + cyfluthrin. Airborne flux estimates were correlated with temperature, solar radiation, wind speed, time, and vapor pressure of the active ingredient. Over short time periods (2 hrs) volatile loss correlated most strongly with solar radiation, surface temperature and the vapor pressure of the active ingredient. A Clausius Clapeyron relationship (log vapor pressure vs. $1/\text{Temperature (K)}$) was observed between flux and surface temperature for most pesticides. A fugacity-based model, which attempts to predict initial evaporative loss rates from turf grass, is introduced in this paper. Input parameters for the fugacity model include the vapor pressure of the active ingredient, surface temperature, wind profile information, atmospheric stability, surface roughness, molecular diffusion coefficient of the pesticide and average upwind fetch distance to the center of the plot. Assumptions of the predictive model, which are thought to exist during the period immediately following application, are 1) the vapor pressure of the pesticide on the leaf surface is equivalent to the vapor pressure of the active ingredient at a given leaf temperature, 2) molecular diffusion of the pesticide vapor is the rate limiting step in the evaporative process, 3) an equation proposed by Shephard (*Quart. J. R. Met. Soc.*, 84, pp. 205-224, 1953), which is in agreement with results from wind tunnel data for thorium-B, heat and water exchange between grass and an airstream (Chamberlain *Proc. Roy. Soc. London A*290, 236-265, 1966), is believed to be adequate in estimating the aerodynamic resistance to transfer between the region in the turf canopy where molecular diffusion occurs and a reference height in the equilibrated boundary layer of the airstream, 4) A height three times the thickness of the equilibrated boundary layer can be inserted into Shephard's equation as a fictitious height where the concentration of the evaporating substance is zero.

A comparison between measured values of flux using Backward-Time Lagrangian stochastic Dispersion (BTLSD) model and flux values predicted by the fugacity method are generally within an order of magnitude apart, with the fugacity model consistently over-estimating the flux determined by the BTLSD model. This is thought to be due to errors in surface temperature measurements and the assumption of a saturated vapor occurring over the area of the treated surface. A comparison between measured BTLSD model flux values normalized for pesticide vapor pressure, calculated aerodynamic resistance (estimated by the fugacity model) and application spray density show a progressive decrease in difference indicating the theory underlying the fugacity model could have physical significance.

Symbols and Abbreviations

The following symbols and abbreviations are frequently referred to in the dissertation. Other symbols which appear once are only described in the text.

a_w - a_w' - a_w'' -parameter representing extinction coefficient of momentum in a particular crop canopy.

B^{-1} -the reciprocal Stanton number, represents the difference in momentum and scalar transfer from a surface.

BTLS-Backward-time Lagrangian stochastic dispersion model. An improved form of the TPS model for estimating surface flux from airborne concentrations and wind speed above an evaporating surface. The improvements are the ability to calculate Φ for any height downwind from an evaporating surface in a homogeneous, turbulent air stream.

C_D -the wind drag coefficient of a surface (dimensionless).

C_s -concentration of a compound or scalar at the surface (quantity/volume).

C_z -airborne concentration of a compound at height z above a surface (quantity/volume).

d_0 - displacement height, scaling factor used in the wind profile equation for objects larger than a few centimeters.

D_a -diffusion coefficient of a compound (m^2/s).

D.S.L.-Dynamic sub-layer, the air zone above the crop canopy.

E_a or E_z eddy diffusion coefficient of a substance (m^2/s).

F -flux-the amount of a substance passing through an area per period of time (mass/area/time).

h or h_0 height of the canopy (m).

ΔH_{vap} or ΔH_{sub} -enthalpy of vaporization or sublimation (kiloJoules/mol).

I.B.L. - Interfacial boundary layer, the air zone above a surface whose flow features are affected directly as a result of the wake patterns of the roughened features of the surface.

k -Von Kármán's constant (0.4), or decay constant of pesticide flux with time following application.

K_h -Henry's law partition constant (ratio of the concentration of substance per volume to concentration per volume of water under standard conditions, C_{air}/C_{water} ; $T=298$ Kelvins, barometric pressure=1 atmosphere).

Kow-octanol/water partition constant, (ratio of the concentration of substance per volume of octanol to concentration of compound per volume of water, $C_{octanol}/C_{water}$, $T=298$ Kelvins).

L- 1. Distance of travel for an air parcel in the direction of mean wind speed, 2. Mixing length size for an eddy, 3. Monin Obukhov path length, a measure of the atmospheric stability (m).

m or $m.w.$ molecular weight of a substance (g/mol).

L_{crit} -the critical path length, the distance of travel where turbulent diffusion surpasses molecular diffusion (m).

P - partial pressure or vapor pressure (pascals).

r_a aerodynamic resistance to transport of a scalar between two heights in the **DSL** (s/m).

r_b additional boundary resistance to transport, accounts for difference in momentum and scalar transport properties in the **ISL** (s/m).

r_T total resistance to transport of a scalar, the sum of r_a and r_b (s/m)

Ri-Richardson number, measurement of atmospheric stability $Ri>0$, stable; $Ri=0$, neutral, $Ri<0$, unstable.

R- Ideal gas constant 8.3145 (Joules/Kelvin/mol).

Re-Reynolds number, determines whether turbulent or laminar flow of a fluid exists in an air stream.

Re*-Roughness Reynolds number, determines whether turbulent or laminar flow exists in the air region in contact with a roughened surface.

Sc-Schmidt number (v/D_a), the ratio of the molecular diffusion coefficients for momentum v and a compound D_a in air.

ΔS_{vap} or ΔS_{sub} - entropy of vaporization or sublimation (Joules/Kelvin/mol).

S.V.D. Saturated vapor density-the mass per volume of a gaseous substance when the partial pressure of a gas is in equilibrium with its vapor pressure (mass/volume).

**Incorporation of Aerodynamic and Boundary Layer
resistances in estimating initial pesticide evaporation rates
from turf grass.**

Michael Conway
Department of Bioresource Research
Oregon State University
Corvallis, OR 97331
Draft: 5/17/99

T-temperature (K).

TPS-Theoretical Profile Shape method, a method of determining the surface flux of a compound from airborne concentration and wind speed measurements at a single height above the center of a circular evaporating surface.

t-time.

u- wind speed at height z (m/s).

u*-frictional velocity (m/s).

v-velocity of fluid parcel (m/s).

x-upwind distance from the edge of a treated surface, or surface of new aerodynamic roughness (m).

z-height, typically the height of measurement above a surface (m).

ZINST*-ideal height sampling height for the Theoretical Profile Shape (TPS) method.

z_0 -roughness length for momentum, extrapolated height at which the wind speed becomes zero (m).

z_{0s} -the roughness length for a scalar, the extrapolated height at which the scalar concentration is equivalent to **S.V.D.** or C_s (m).

α -exponential decay constant for scalar with canopy depth.

δ_i -thickness of the internal boundary layer at distance x downstream from an edge of a new surface.

The internal boundary layer is an air layer which is affected, in any degree, by the properties of the surface which it moves over. Thus if a pesticide is evaporating from the surface, the internal boundary is the thickness of the air layer which contains some airborne pesticide residue. The thickness is often between 1/10 and 1/30 the upwind distance from the edge of the surface [48] (m).

δ_{eq} -thickness of the equilibrated boundary layer. This is the lowest section of the internal boundary layer where the air has completely equilibrated with the properties of the surface below. Flux of any quantity (momentum, vapor, or heat) is constant with height in this zone (m).

$\psi(z)$ -atmospheric stability parameter, $\psi(z)=0$, neutral; $\psi(z)>0$, unstable, $\psi(z)<0$, stable

ρ -air density (g/cm^3).

Φ -ideal or normalized flux value for the **TPS** model for a circular plot of radius R, roughness length, z_0 , sampling height z and atmospheric stability L.

T-shear, or downward flux of momentum in an air stream ($kg/m/s^2$).

ν -kinematic viscosity (molecular diffusion coefficient of momentum) $15.5 \times 10^{-6} m^2/s$ in air @ 25 °C.

List of Figures

Figure 1: Reproduced data from Jenkins et. al. [3], airborne flux data for pendimethalin from turf grass Day 1, 2 (between p. 2 and 3).

Figure 2: Reproduced data from Jenkins et. al. [3]. log Flux vs. $1/T$ (K) of pendimethalin from turf grass (between p. 2 and 3).

Figures 3-9: Correlation of surface temperature and flux estimated from airborne concentrations using the Backward-Time stochastic Lagrangian method [45, 46] on a Clausius Clapeyron scale (log Flux ($\mu\text{g}/\text{m}^2$) vs. $1/T$ (K)) for two hour air sampling intervals during the first couple of days following application.

Figure 3: Triadimefon, Application 1, 1995, (log Flux vs. $1/T$ (K)).

Figure 4: Triadimefon, Application 1, 1996 (log Flux vs. $1/T$ (K)).

Figure 5: Chlorpyrifos, Application 1, 1995, (log Flux vs. $1/T$ (K)).

Figure 6: Chlorpyrifos, Application 1, 1996 (log Flux vs. $1/T$ (K)).

Figure 7: Ethofumesate, Application 1, 1996 (log Flux vs. $1/T$ (K)).

Figure 8: Triclopyr, Application 2, 1996 (log Flux vs. $1/T$ (K)).

Figure 9: Propiconazole, Application 2, 1996 (log Flux vs. $1/T$ (K)).

Figure 10: Rate limiting step in a sequence of steps governs the rate of the sequence [1].

Figure 11: Clausius Clapeyron Relationship of vapor pressure (p) and Temperature (T) eq 3.

Figure 12: Diagram of laminar fluid flow.

Figure 13: Diagram of turbulent fluid flow.

Figure 14: Turbulent $[E(z)]$ and Molecular Transport Scales (v).

Figure 15: The displacement term d_0 in equation 25 for wind profiles over tall and short crops (corn and grass).

Figure 16: Effect of Atmospheric Stability on Wind Profiles (equation 26).

Figure 17: Linear/log plot of wind profiles above a surface during neutral atmospheric conditions (eq. 30).

Figure 18: Extrapolated Wind Profiles (eq. 30) and Observed Wind profiles in a crop canopy (see equations 33, 34, & 35).

Figure 19: Roughness Length vs. Grass Height for short grass (1.5 cm-4.5 cm). Data obtained from Deacon, 1953 [19].

Figure 20: Dynamic Sublayer and Interfacial Boundary Layer regions

Figure 21: Two dimensional view of momentum deposition and pesticide evaporation under steady state transfer conditions.

Figure 22: Extrapolated roughness lengths for momentum z_0 and an evaporating scalar z_{0s} .

Figure 23: Contrast of surfaces with Permeable (top) and Bluff (bottom) roughness features.

Figure 24: Internal and equilibrated boundary layer formation over a transition in roughness length.

Figure 25: Internal and equilibrated boundary layer formation over an evaporative surface.

Figure 26: Simulated values of ϕ vs. height (eq. 63) above the center for a circular plot of given roughness z_0 and radius R [16].

Figure 27: Experimental Setup for measuring pesticide volatilization for a turf plot using the TPS method [16].

Figure 28: Actual vs. Ideal plot conditions for the TPS method.

Figure 29: Plot of generated values of ϕ ($z=0.73$ m, $z_0=.0045$ m, plot dimension 22.8 m x 22.8 m) using the Backward-Time Lagrangian stochastic Dispersion model [45], vs. upwind distance from treated edge (m). Calculation for specific plot conditions courtesy of T. Flesch [46].

Figure 30: Two hour averaged wind profiles above the turf plot, Day 0, App.1 '95.

Figure 31: Two hour averaged wind profiles above the turf plot, Day 0, App.1 '96.

Figure 32: Two hour averaged wind profiles above the turf plot, Day 0, App.2 '96.

Figure 33: Plot of z_0 vs Re^* to determine whether change in roughness length during Application 1, Day=0 in 1995 was due a to transition in flow regimes [24, 26].

Figure 34: Plot $u^*/u(70)$ vs. Re^* to determine whether change in roughness length during Application 1,

Day=0 in 1995 was due a to transition in flow regimes [24, 26].

Figure 35: Sample plot of z_0 vs. average wind speed $u(z)$ Application 1, Day=0 in 1995.

Figure 36: Sample plots of z_0 vs. frictional velocity u^* on Application 1, Day=0 in 1995.

Figure 37: Plot of solar radiation and surface and ambient temperatures on a cloudless day (Day 2, App. 1996).

Figure 38: Flux vs. Solar Radiation on a clear Day (Day 2, App.1, 1996).

Figure 39: Flux vs. Solar Radiation on a cloudy day (Day 1, App.1, 1996).

Figure 40: Flux vs. Ambient and Surface Temperature on a clear day (Day 2, App.1, 1996).

Figure 41: Flux vs. Ambient and Surface Temperature on a cloudy day (Day 1, App.1, 1996).

Figure 42: Flux vs. Wind speed at the sampling height (Day 2, App.1, 1996).

Figure 43: Flux vs. Wind speed at the sampling height (Day 1, App.1, 1996).

Figure 44: Plot of Total Flux and Total Solar Radiation during mid-day (12:00-16:00) on days following application date (Day 0) Application 1, 1995.

Figure 45: Plot of Flux normalized for Solar Radiation (Flux/S.R.) during mid-day (12:00-16:00) Application 1, 1995 on days following application date (Day 0).

Figure 46: Plot of Total Flux and Total Solar Radiation during mid-day (12:00-14:00) on days following application date (Day 0) Application 1, 1996.

Figure 47: Plot of Flux normalized for Solar Radiation (Flux/S.R.) during mid-day (12:00-14:00) Application 1, 1996 on days following application date (Day 0).

Figure 48: Plot of Total Flux and Total Solar Radiation during mid-day (12:00-14:00) on days following application date (Day 0) Application 2, 1996.

Figure 49: Plot of Flux normalized for Solar Radiation (Flux/S.R.) during mid-day (12:00-14:00) Application 2, 1996 on days following application date (Day 0).

Figure 50-56: Plot of log Flux ($\mu\text{g}/\text{m}^2/\text{hr}$) vs. $1/\text{Temperature}$ (K) for the BTLSD model (equation 67) and fugacity model (equation 63) using surface temperature measurements.

Figure 50: Triadimefon, Application 1, 1995.

Figure 51: Triadimefon, Application 1, 1996.

Figure 52: Chlorpyrifos, Application 1, 1995.

Figure 53: Chlorpyrifos, Application 1, 1996.

Figure 54: Ethofumesate, Application 1, 1996.

Figure 55: Triclopyr, Application 2, 1996.

Figure 56: Propiconazole, Application 2, 1996.

Figure 57: %loss of active ingredient applied due to volatilization vs. vapor pressure of the active ingredient (25 °C) for all applications.

Figure 58: %loss of active ingredient applied due to volatilization vs. air/octanol partition coefficient (K_{ao}) of the active ingredient (25 °C) for all applications.

Figure 59: %loss of active ingredient applied due to volatilization vs. Henry's partition coefficient (K_h) of the active ingredient (25 °C) for all applications.

Figure 60: %loss of active ingredient applied due to volatilization vs. Henry's partition coefficient (K_{ow}) of the active ingredient (25 °C) for all applications.

Figure 61: Exponential decay constant of flux normalized for solar radiation (Flux/S.R.) vs. vapor pressure of the active ingredient @ 25 °C.

Figure 62: Exponential decay constant of flux normalized for solar radiation (Flux/S.R.) vs. air/octanol partition coefficient (K_{ao}) of the active ingredient @ 25 °C.

Figure 63: Exponential decay constant of flux normalized for solar radiation (Flux/S.R.) vs. Henry's partition coefficient the active ingredient @ 25 °C.

Figure 64: Exponential decay constant of flux normalized for solar radiation (Flux/S.R.) vs. octanol water partition coefficient (K_{ow}) of the active ingredient @ 25 °C.

Figure 66: Sensitivity Analysis of % change in flux estimated by the predictive model with % change in environmental parameters (wind speed u^* , saturated vapor density S.V.D., average plot radius R , surface temperature T , molecular diffusion coefficient D_a , atmospheric stability L , and roughness length z_0).

Figure 67: Sensitivity analysis of % change in flux estimated by the predictive model vs. % change in thermodynamic parameters of the active ingredient (Temperature T , enthalpy of vaporization ΔH , and entropy of vaporization ΔS) log scale.

Figure 68: Measured flux ($\mu\text{g}/\text{m}^2/\text{hr}$) for all pesticide applications during the day of application (log scale).

Figure 69: Measured flux ($\mu\text{g}/\text{m}^2/\text{hr}$), normalized for the saturated vapor density ($\mu\text{g}/\text{m}^3$) of the active ingredient at the measured surface temperature*, for all pesticide applications during the application date, Day 0 (log scale).

Figure 70: Measured flux ($\mu\text{g}/\text{m}^2/\text{hr}$), normalized for the saturated vapor density ($\mu\text{g}/\text{m}^3$) of the active ingredient at the measured surface temperature* and the application density ($\mu\text{g}/\text{m}^2$), for all pesticide applications during the application date, Day 0 (log scale).

Figure 71: Measured flux ($\mu\text{g}/\text{m}^2/\text{hr}$), normalized for the saturated vapor density ($\mu\text{g}/\text{m}^3$) of the active ingredient at the measured surface temperature* and the aerodynamic resistance (hr/m) for all pesticide applications during the application date, Day 0 (log scale).

Figure 72: Measured flux ($\mu\text{g}/\text{m}^2/\text{hr}$), normalized for the saturated vapor density ($\mu\text{g}/\text{m}^3$) of the active ingredient at the measured surface temperature*, the application density ($\mu\text{g}/\text{m}^2$), and the aerodynamic resistance (hr/m) for all pesticide applications during the application date, Day 0 (log scale).

Figure 73: Measured flux ($\mu\text{g}/\text{m}^2/\text{hr}$), normalized for the saturated vapor density ($\mu\text{g}/\text{m}^3$) of the active ingredient at the measured surface temperature*, the application density ($\mu\text{g}/\text{m}^2$), and the aerodynamic resistance (hr/m) for all pesticide applications during day after the application date, Day 1 (log scale).

Figure 74: Experimental setup differences between years 1995 and 1996.

List of Tables

Table 1 (p.11): Chemical Description of Pesticides used in Turf Grass Applications.

Table 2 (p.11): Application Summary for study of pesticide volatilization from turf grass.

Table 3: Roughness Lengths for Grass at Wind velocities between 2-8 m/s at height of 2 m [19].

Table 4: Measured values of B^{-1} for various substances for grass and grass-like surfaces [25,32].

Table 5: Measured vs. Predicted values of B^{-1} for grass and grass-like surfaces in Wind Tunnels [25].

Table 6: Typical Air Sampling Schedule on Days following Pesticide Application.

Table 7: Generated values of Φ ($z=0.73$ m, $z_0=0.0045$ m, plot dimension 22.8 m x 22.8 m) using the Backward-Time Lagrangian stochastic Dispersion model [45].

Table 8: Parameter inputs for the Theoretical Profile Shape (TPS) and Fugacity models in estimating pesticide loss from a turf grass surface. 'X' symbols denotes parameter requirement for the model.

Table 9: Percent change in Flux estimated by equation 61 ($z_0=0.0045$, $D_a=0.04$ cm^2/s , $x=14$ m, $u^*=20$ cm/s , S.V.D.=100 $\mu\text{g}/\text{m}^3$, $T=25$ $^\circ\text{C}$, $L=\infty$) due to input parameter deviation.

Table 10: Summary of calculated wind profile parameters u^* , z_0 , L , from two hour-averaged wind speed readings at 41, 70, 140 and 280 cm heights during Day 0 of each pesticide application.

Table 11: Pesticide flux results, Application 1, 1995 (table 1, 95:resistsummary6.xls).

Table 12: Pesticide flux results, Application 1, 1996 (table 1, 96:resistsummary6.xls).

Table 13: Pesticide flux results, Application 2, 1996 (table 2, 96:resistsummary6.xls).

Table 14: Comparison between measured vs. predicted flux results, Day 0, for all pesticide applications.

Introduction

According to a Pesticide Industry Sales and Usage report (1990, 1991) [4], pesticide usage in the United States has stabilized at 1.1 billion pounds of active ingredient per year. Increased awareness and concern of the fate of these chemicals in the environment has prompted investigative studies to determine their environmental behavior following introduction into an environmental system.

Volatilization is a significant mechanism by which pesticide residues attenuate from a target area (relative to degradation, metabolization, runoff and leaching) and can be a dominant process by which pesticides disperse and redistribute in the general environment [2]. In extreme cases, losses due to volatilization can exceed 90% of amount applied [2]. In order to estimate long-range transport, toxicological risk, and efficacy of pesticides reaching and remaining in their target area, an understanding of the mechanisms and key variables which govern pesticide evaporation is needed. Research on this topic has resulted in collaborations between agronomists, soil scientists, micro-meteorologists and chemists.

Much study to date has focused on measuring volatilization of pesticides from soil surfaces [2]. Models using parameters of soil porosity, moisture and organic carbon content, wind-speed, humidity and temperature have been developed to predict pesticide evaporation given certain environmental conditions. However, little research has been conducted to understand volatilization from the second major component in agriculture, the foliar surface [2]. Pesticide evaporation from foliar surfaces can also be a significant route by which the chemical leaves the target area. Taylor [2] reported a 46% loss of heptachlor and 12% of dieldrin within eight hours following application to short orchard grass. For pendamethalin, a less volatile compound, Cooper [5] reported 13% loss by Day 5 following grass application under relatively cool May conditions.

A probable reason for lack of research in this area is that foliar surfaces are living systems subject to high variability. Leaf surface anatomies, physical and chemical properties can vary widely between different plant and crop varieties. Foliar characteristics such as surface area, roughness, dermal thickness, epicuticular wax concentrations, rate of leaf growth, and a myriad of other properties including diurnal and seasonal metabolic changes, could affect the adsorption, penetration, metabolization, and overall volatilization of a particular chemical. An added complexity is that these processes would be pesticide specific due to differences in physical/chemical properties of each pesticide. Research and development of models to accurately predict volatilization from different foliar surfaces would seem exceedingly complicated and expensive with little ability to cross results from one plant or chemical study to another.

Turf Grass, a model leaf surface for understanding factors which govern pesticide evaporation

The advantages of using turf grass, as opposed to another crop, for studying factors which affect pesticide evaporation, are that the canopy completely covers the soil, eliminating it as source of interference in determining volatile loss from the leaf surface; the short canopy simplifies the need to account for the effect of shading, wind patterns and temperature gradients and the vertical density of pesticide deposits in the turf canopy, the homogenous low-profile surface creates an even aerodynamic roughness ideal for use of micrometeorology based models such as the Theoretical Profile Shape method [16], which estimate evaporative loss rates from a surface (flux) from airborne concentration measurements and information on wind profiles above the plot.

In the first of an ongoing series of field studies conducted by Jenkins [3] to determine factors which affected volatile loss from foliar, Jenkins measured airborne and dislodgeable foliar (surface) residue concentrations for two weeks following application of pendamethalin to Kentucky bluegrass. Volatile loss measurements normalized for wind speed were correlated with temperature, solar radiation and dislodgeable foliar surface residue concentrations (residues which penetrated the leaf surface were assumed to be unavailable for volatilization and were not measured in this study) [3]. Two observations of particular note were volatile loss rates, or flux ($\mu\text{g}/\text{m}^2/\text{hr}$), on a single day appeared to be strongly correlated with sunlight (Fig. 1), with the maximum flux occurring during the noon hours when the sun was at its highest point. A strong correlation between flux and temperature was also observed. A plot of $\log \text{Flux}$ vs. $1/\text{Temperature}$ (K^{-1}) for the first two days of flux data displayed a linear correlation indicative a Clausius Clapeyron relationship ($\log \text{Vapor Pressure}$ vs. $1/T$ (K^{-1})) (Fig. 2) indicating the vapor density of the compound over the leaf surface (determined by vapor pressure) was the primary factor determining loss intensity on a single day [3]. Loss rates, on days following the date of pesticide application, appeared to be well-correlated with dislodgeable surface residue [3].

Jenkins continued to conduct volatilization studies of pesticides from turf grass [13]. His latest series of experiments have involved simultaneous application of different compounds, with contrasting physical properties, to a turf plot and attempting to relate relative flux trends to physical properties of the pesticides and environmental factors (Table 1 and 2). Analysis of the weather data and airborne concentrations from these latest series of experiments have yielded similar trends, with the same relationship of $\log \text{flux}$ vs $1/T$ (K) for measured loss rates in close time proximity (Fig. 3-9). Surface residues from these new sets of experiments have not been analyzed so a correlations between airborne losses and surface residues cannot be conducted.

Developing a Predictive Model

Given available data of pesticide volatile loss rates from turf grass and an awareness of the known

Figure 1: Reproduced data from Jenkins et. al. [3]. Diel flux of airborne residues following application of pendimethalin 60 WDG at 340 mg/m² to turfgrass. Source strength represented by $F_z(0)$, measured by the Theoretical Aprofile Shape method for the day of application (Day 1) and the following day (Day 2).

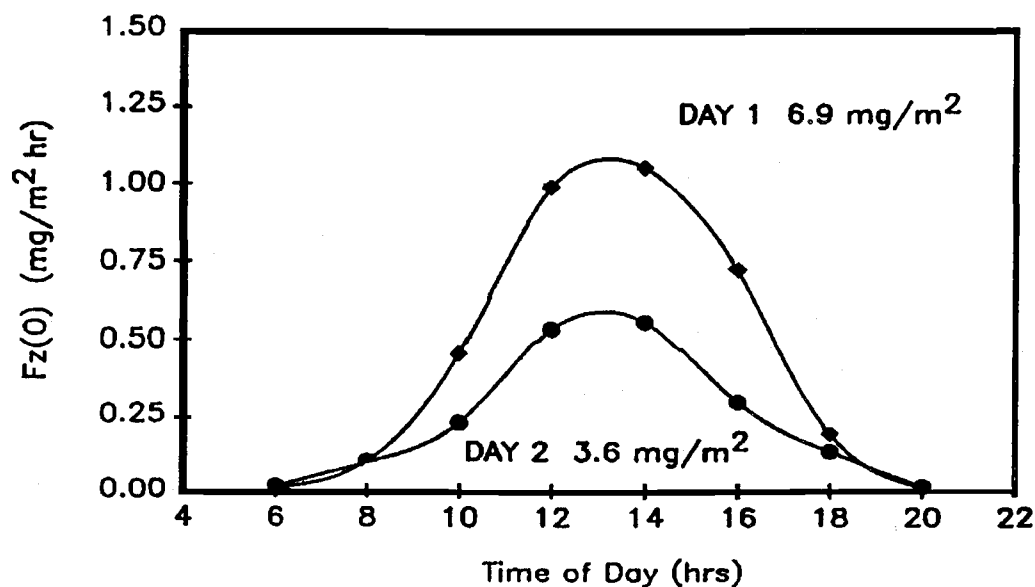
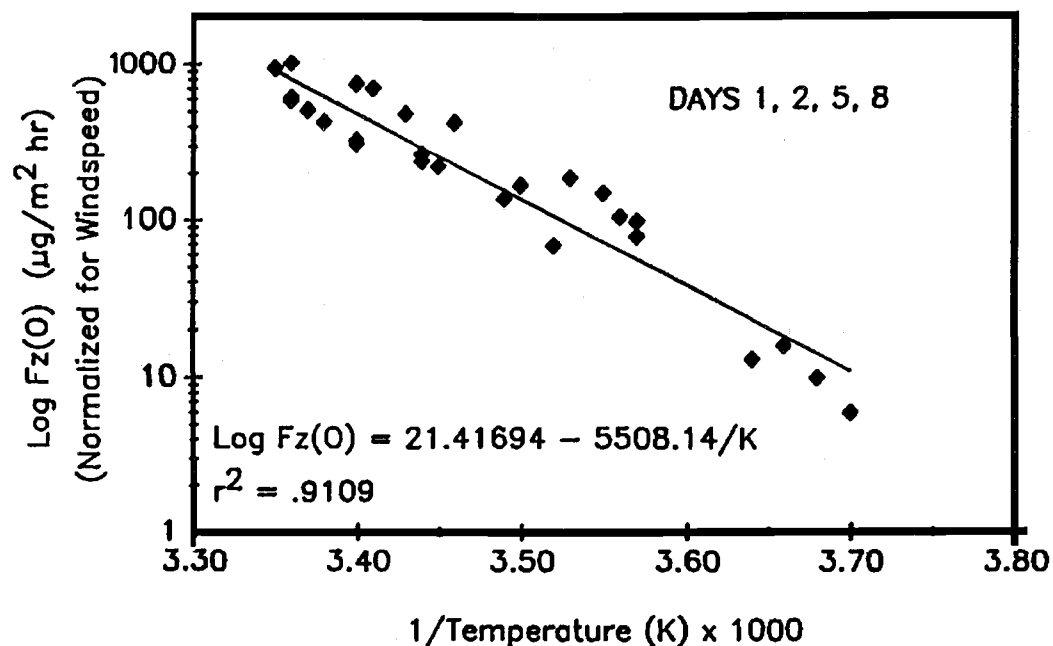
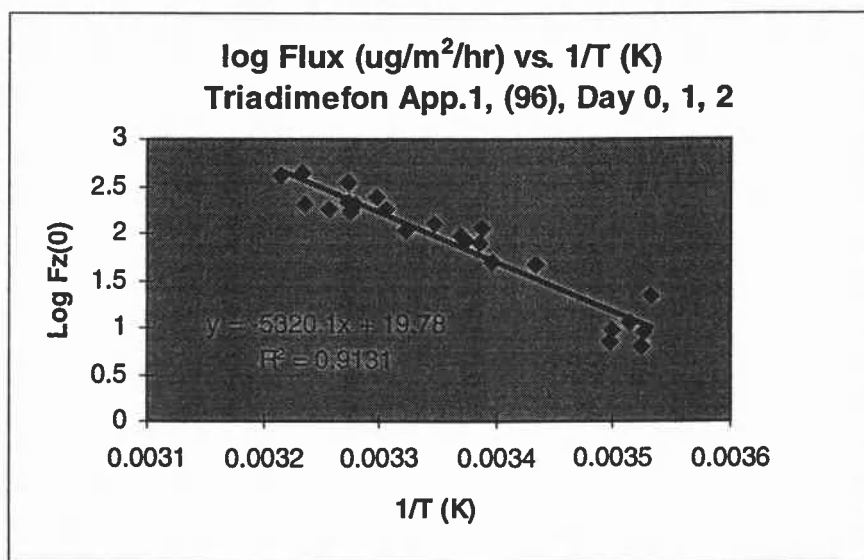
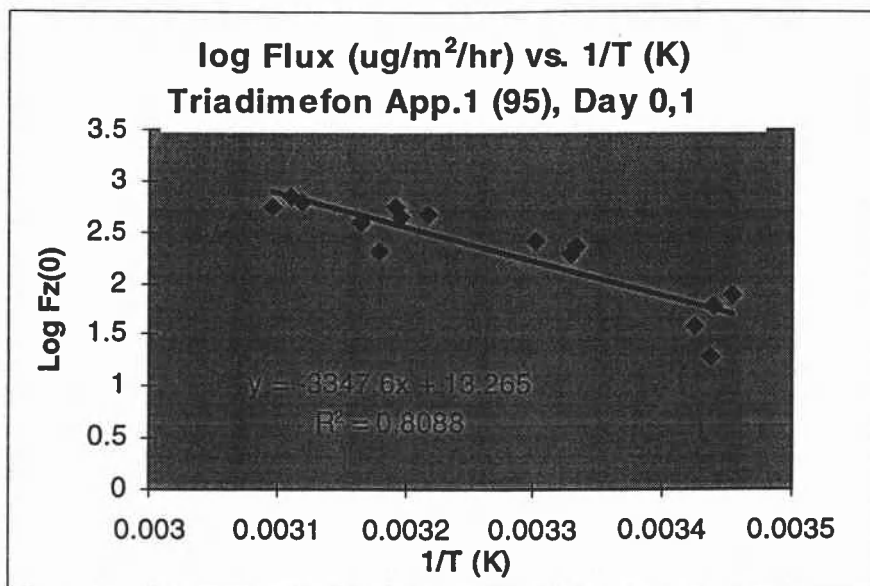


Figure 2: Reproduced data from Jenkins et. al [3]. Relationship between temperature and wind speed pendimethalin flux ($F_z(0)$) for each 2-hour sampling interval (0600-20:00) for days 1, 2, 5, and 8 of the Theoretical Profile Shape method study. Only two of the data points are from Day 5 and 8.

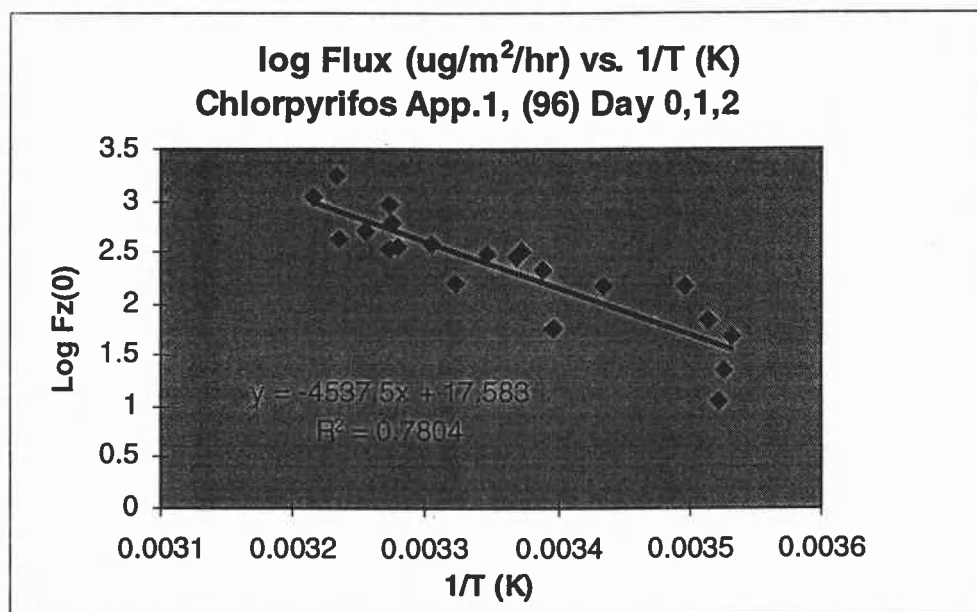
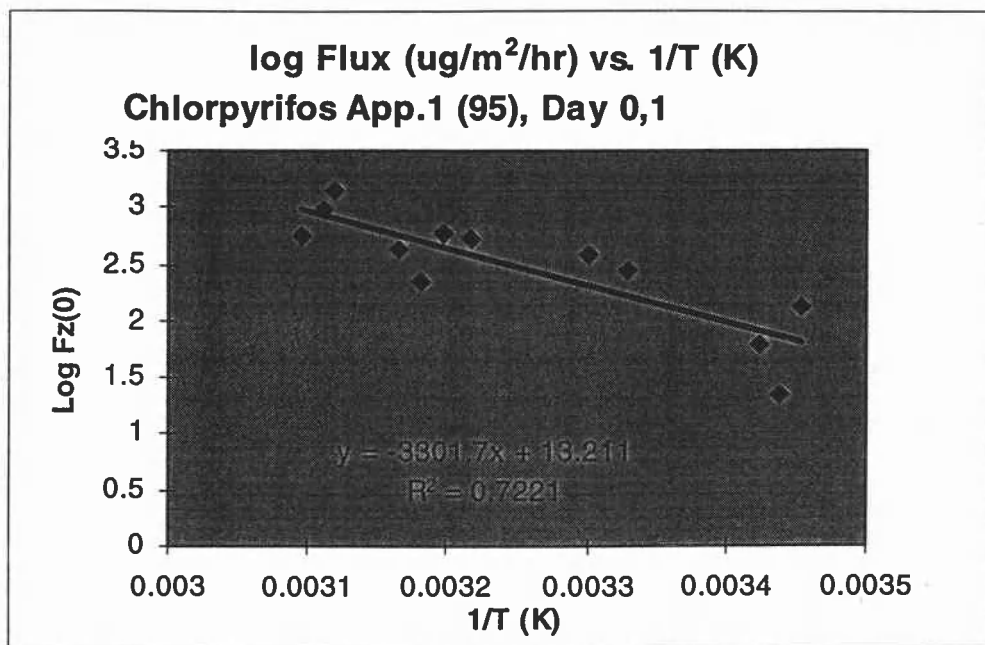


Figures reprinted from: J.J. Jenkins, A.S. Curtis, and R.J. Cooper, "Two Small-Plot Techniques for Measuring Airborne and Dislodgeable Residues of Pendimethalin Following Application to Turfgrass." A.C.S. Symposium Series: Pesticides in Urban Environments #522, ACS, Washington DC, 1993 [3].

Figures 3-4: Flux estimated by the Backward-Time stochastic Lagrangian method [45, 46] and surface temperature. Two hour air sampling intervals. Log flux ($\mu\text{g}/\text{m}^2$) vs. $1/T$ (K).



Figures 5-6: Flux estimated by the Backward-Time stochastic Lagrangian method [45, 46] and surface temperature. Two hour air sampling intervals. Log flux ($\mu\text{g}/\text{m}^2$) vs. $1/T$ (K).



Figures 7-8: Flux estimated by the Backward-Time stochastic Lagrangian method [45, 46] and surface temperature. Two hour air sampling intervals. Log flux ($\mu\text{g}/\text{m}^2$) vs. $1/T$ (K).

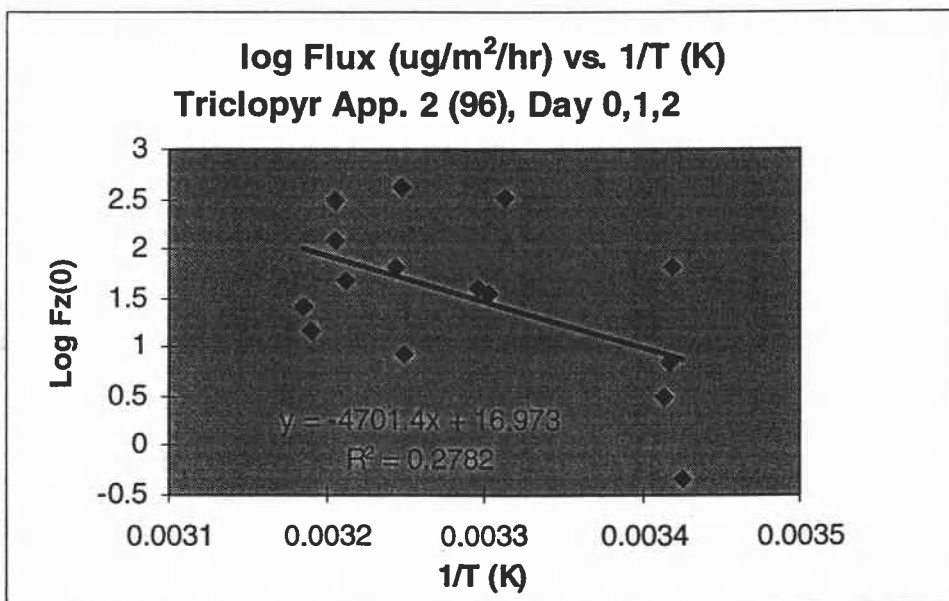
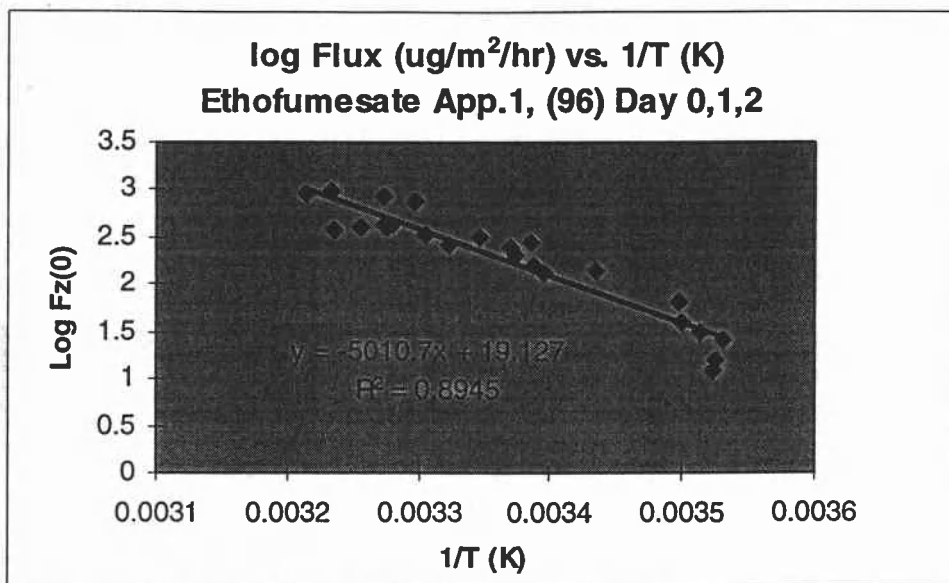


Figure 9: Flux estimated by the Backward-Time stochastic Lagrangian method [45, 46] and surface temperature. Two hour air sampling intervals. Log flux ($\mu\text{g}/\text{m}^2$) vs. $1/T$ (K).

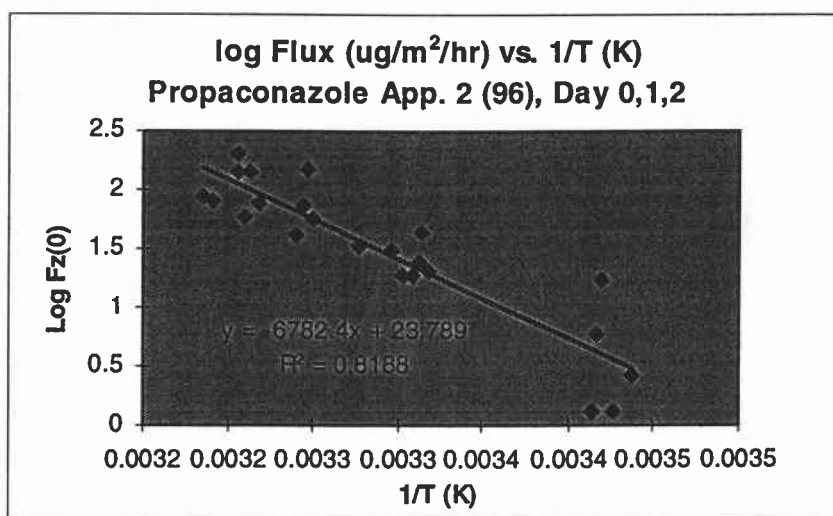


Figure 10: Rate limiting step in a sequence of steps governs the rate of the sequence [1].

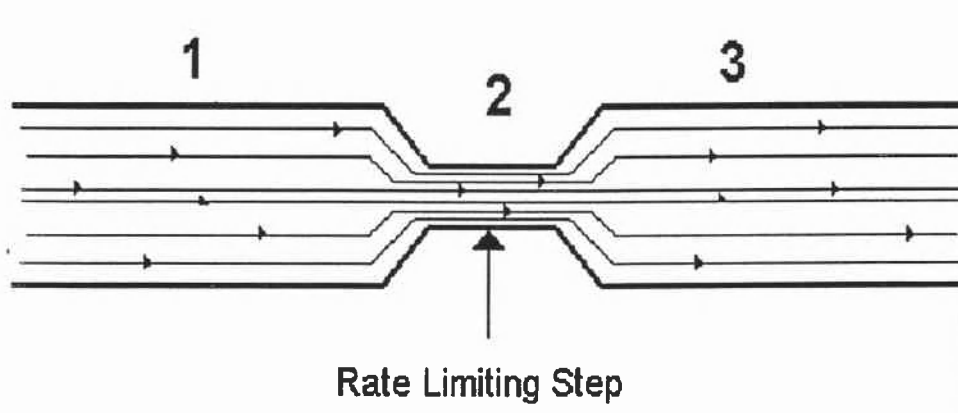
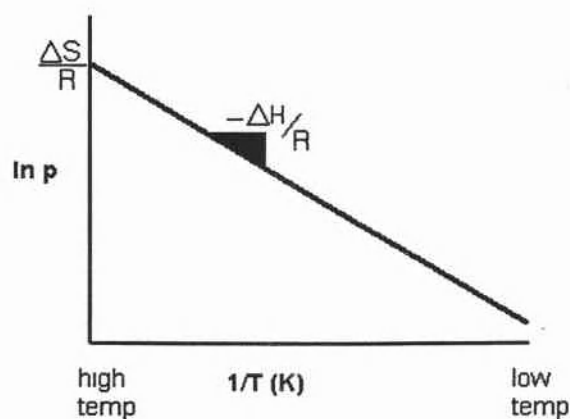


Figure 11: Clausius Clapeyron Relationship of vapor pressure (p) and Temperature (T) eq 3.



correlations of flux vs. temperature and flux attenuation with diminishing surface concentrations on days following application, it is a goal of this researcher to develop a model that will predict the volatile losses from turf grass as a function of chemical properties, temperature and other environmental factors. Since correlations cannot be currently established between dislodgeable surface residues and airborne concentrations, which is of significance during later periods of the experiment when surface residues diminish, the focus of the predictive model will be a single day. The effect of diminishing pesticide concentrations on the leaf surface, during such a short period, is assumed to be an unimportant factor in causing variations in evaporative loss rates. An emphasis will be placed on predicting evaporative loss on the day immediately following application when most of the pesticide evaporation is thought to occur from deposits rather than pesticide immediately in contact with the leaf surface. In such a case the majority of pesticide evaporation is thought to be occurring from itself rather than pesticide adsorbed to the leaf surface and the literature value of vapor pressure is more likely to represent the actual vapor pressure of the pesticide on the leaf surface.

The approach to developing a predictive model was inspired by the Fugacity Approach. The proposed model is a combination of elements of the fugacity approach and conventions developed by micrometeorologists and engineers to model heat, mass and momentum transfer between a turbulent air stream and a roughened surface.

The Fugacity Approach:

The term fugacity was initially put forward by G.N. Lewis in 1901 to describe the "fleeing" tendency of a chemical from one phase to another. Although this concept has traditionally been used to describe condensation, volatilization, precipitation or sublimation of a compound between from one phase and another in laboratory settings, Mackay [1] has broadened its approach to describe chemical partitioning of a chemical between different environmental phases (air, water, soil, biota etc.). It has now become a useful approach to describing fate and transport of a chemical in a broad variety of environmental systems [2,6]. These three steps have been gleaned from the Fugacity approach in modeling chemical transport between phases:

- 1) Divide an environmental system into compartments where the chemical has a different relative free energy each phase. The relative free energy difference (Gibbs energy of phase transition) determines the the fleeing tendency (fugacity) of a chemical from one compartment to another. A chemical will have a tendency to partition from a compartment where it has a higher fugacity to a compartment where it is lower in fugacity.
- 2) Boundaries between compartments are delineated where the transport of a chemical compound between phases is assumed to be in steady state or static equilibrium (concentration difference between two phases does not change with time).

3) If a mechanism of chemical transport between phases is composed of a series of linked, sequentially-occurring steps, the rate of the entire process can be simplified in terms of the rate-limiting step (Figure 10). Justification: If a transition process is composed of three steps and the second step is the slowest, step two will be the *rate-limiting* step or "bottle-neck". This creates the condition of steady state transport in the second step, even if the *rates* of the first and third steps change to a slight degree.

Step 1:

The two environmental phases that will presently be considered for the fugacity approach to viewing pesticide evaporation from a turf grass surface are: 1) pesticide in a deposit on the leaf surface and 2) pesticide in a vapor in the air above the deposit. *The measurement of fugacity for a chemical between a solid and vapor form is the chemical's vapor pressure.*

Step 2:

Pesticide evaporation is believed to be composed of two linked sequentially-occurring processes:

Volatilization-conversion of the pesticide in a deposit on the leaf surface from a solid to a vapor.

Diffusion-vertical transport of the pesticide vapor along a concentration gradient from the leaf surface (source of pesticide vapor) to the atmosphere (sink of pesticide vapor).

The air zones above the evaporating surface which will be considered are: 1) the region in the canopy where the vapor concentration is equivalent to the vapor pressure of the pesticide on the leaf surface, and 2) the zone above the surface where the vapor concentration becomes infinitely dilute. *The boundary which separates these two air zones will be defined in terms of an aerodynamic transport resistance, which is the sum of the vapor transport processes which occur in the boundary layer.*

Step 3:

Which of the sequentially-linked processes in volatilization and diffusion is the rate limiting step, and therefore justifies the assumption that evaporation is a steady state process? This requires an analysis of the steps in volatilization and diffusion.

Volatilization and Diffusion

Each of these two processes will now be described and then applied specifically to the case of pesticide evaporation from turf grass.

Volatilization

The conversion of a pesticide from a pure solid (C_s) or liquid to a gas (C_g) can be written as a chemical

equation:



The energy change of the molecules undergoing this transition is equivalent to the difference in Gibbs free energy (ΔG) of the molecule in each state.

$$\Delta G = \Delta H - T\Delta S \quad (2)$$

ΔG -Gibbs free energy of vaporization/sublimation (Joule·mol⁻¹)
 ΔH , the enthalpy of sublimation/vaporization (Joule·mol⁻¹)
 ΔS , the entropy of volatilization/sublimation (Joule·K⁻¹·mol⁻¹)
T-Temperature of the evaporating system (gas/solid or liquid) (K)

The enthalpy (ΔH) is defined as the amount of energy required to remove a mole of molecules from the attractive forces of its neighboring molecules which retain the substance in the solid or liquid form. The entropy (ΔS) is the measurement of disorder, or the change in the number of states available to a molecule when it volatilizes. These two thermodynamic parameters predict what proportion of a population of molecules have the energy undergo phase transition and move into the vapor phase, at a particular temperature (T). A measurement of a compound's volatility is its vapor pressure (P). The Clausius Clapeyron equation is used to predict the vapor pressure of a compound volatilizing from a solid (sublimation) or liquid (vaporization) at a particular temperature.

$$\ln P = -\frac{\Delta H}{RT} + \frac{\Delta S}{R} \quad (3)$$

ΔH , the enthalpy of sublimation (sub) or vaporization (vap) (Joule·mol⁻¹)
 ΔS , the entropy of volatilization/sublimation (Joule·K⁻¹·mol⁻¹)
R-Ideal gas constant (8.145 Joule·Kelvin⁻¹·mol⁻¹)
T-Temperature of the evaporating system; deposit and vapor (K)
P-Partial pressure of evaporating substance (pa)

Assuming a constant value of ΔH over a small temperature range 0-30°C, empirical measurements of a compound's vapor pressure at several temperatures can provide a linear equation ($\ln P$ vs. $1/T$) to predict the vapor pressure of a compound (providing there are no phase changes) at a given temperature (Fig. 11) [6]. The concentration of chemical in the vapor phase (vapor density) can be calculated from a chemical's vapor pressure using the ideal gas law:

$$\text{VaporDensity}(\text{g/m}^3) = \text{mol.wt} * \frac{P}{R * T} \quad (4)$$

R-Ideal gas constant (8.145 Joule·Kelvin⁻¹·mol⁻¹)
T-Temperature of the evaporating system (gas/solid or liquid)
P-Partial pressure of evaporating substance (pa)

mol.wt.-molecular weight of the compound (g/mol)

For pesticide registration in the U.S., the E.P.A. currently requires a vapor pressure to be published by the manufacturer for the active ingredient at a single temperature, typically at 25 °C [43]. These vapor pressure values, in addition to other physiochemical properties of the active ingredient, have been tabulated for many pesticides and have been compiled in various handbooks [7]. Unfortunately, for many semivolatile compounds including pesticides, published vapor pressure values can vary within an order of magnitude, depending on the source and method of measurement. Therefore reliability of these measurements in estimating vapor concentration is not guaranteed.¹

Efforts to develop an accurate temperature sensitive model for pesticide evaporation are further limited by the scarcity of reported vapor pressure measurements at various temperatures. Currently E.P.A. requires the manufacturer to publish a single vapor pressure at a single temperature for the active ingredient [43]. A range of vapor pressure measurements at various temperatures are needed to determine the vapor concentrations at various temperatures. For compounds where a vapor pressure is reported for a single temperature, saturated vapor concentrations can only be estimated at that temperature. For compounds where vapor pressures have been reported for multiple temperatures, the constants ΔH and ΔS can be determined from equation 3 and saturated vapor concentrations at a range temperatures can be estimated (Figure 11).

Because of the current lack of precision of vapor measurements at a single temperature and the scarcity of reported vapor pressure measurements at different temperatures, reliability of the estimated vapor pressures for the above listed compounds using the Clausius Clapeyron equation should be greatly questioned, especially in cases where measurements are obtained from different sources. It is guessed that the estimated vapor pressures are probably within an order of magnitude of their true value.

Vapor Pressure of the pesticide on the leaf surface

Although the vapor pressure measurement of a pesticide in its pure form reflects its escaping tendency from an environment of identical molecules, it probably does not accurately represent the actual vapor pressure of the active ingredient from a pesticide deposit or film on a leaf surface in an agricultural setting. Pesticides are not applied in the form of their active ingredient, but in formulations which contain oils, wetters, and surfactants (collectively called adjuvants). These added components affect the reflection and spreading behavior of the pesticide droplet upon impact, and also the drying and formation of the deposit. A pesticide in a deposit on the leaf surface might be surrounded by molecules other than

¹ For a list of vapor pressure values reported for a single compound, see [3].

Table 1: Chemical Description of Pesticides used in Turf Grass Applications.

Compound	Class	m.w. (g/mol)	Vapor Pressure (pa) @ Temperature (°C) [ref]	ΔH (kJ/mol)	ΔS (J/K/mol)
Triadimefon	triazole, conazole	294	0.0001 @ 20 °C [1] 0.002 @ 40 °C [1]	112	306
Chlorpyrifos	organophosphate, pyridine	351	0.0023 @ 20 °C [2] 0.0025 @ 25 °C [3] 0.012 @ 35 °C [3]	88	247
Ethofumesate	benzofuran	255	0.00065 @ 25 °C [4]	N/A	N/A
Triclopyr (acetic acid)	pyridine, organochlorine, pyridyloxyacetic acid	256	0.00017 @ 25 °C [5] 0.00071 @ 40 °C [5] 0.00137 @ 50 °C [5] 0.0139 @ 70 °C [5]	82	204
Propiconazole	triazole, conazole	342	0.000056 @ 25 °C [1]	N/A	N/A
Cyfluthrin	pyrethroid	434	0.0000044 @ 20 °C [4]	N/A	N/A

Reference Key for Pesticide Vapor Pressures:

- [1] Wauchope, R.D., T.M. Buttler, A.G. Hornsby, P.M. Augustijn-Beckers, and J. P. Burt. 1992. The SRS/ARS/CES pesticide properties database for environmental decision making. *Rev. Environ. Contam. Tox.* 123, 137.
[2] Suntio, L.R., Shui, W.Y. & Glotfelty, D., Mackay, D., Seiber J.N. (1988) "Critical Review of Henry's Law Constants for Pesticides," RESIDUE REV. 103:1-59
[3] AGROCHEMICALS HANDBOOK, (1983), Royal Society of Chemistry NOTTINGHAM, UK
[4] Turf and Ornamental Reference 6th ed. 1997 C&P Press, Inc NY.
[5] Ahrens' "Herbicide Handbook", 7th ed., 1994

Table 2: Application Summary for study of pesticide volatilization from turf grass

	Experiment Duration	Chemicals Applied to 520 m ² plot of Orchard Rye grass mowed to height of 1". Same plot used in all applications.	Formulation	Vapor Pressure @ 25 °C (mpa)
Application 1 1995	7/17-8/8	Triadimefon (Fungicide) 3.05 kg a.i./ha (305 mg/m ²) Chlorpyrifos (Insecticide) 1.4 kg a.i./ha (14.0 mg/m ²)	w.p. e.c.	0.231* 2.50
Application 1 1996	6/12-7/3	Triadimefon (Fungicide) 3.05 kg a.i./ha (30.5 mg/m ²) Chlorpyrifos (Insecticide) 1.86 kg a.i./ha (18.6 mg/m ²) Ethofumesate (Herbicide) 2.5 kg a.i./ha (25.0 mg/m ²)	w.p. e.c. e.c.	0.231* 2.50 0.65
Application 2 1996	7/23-8/13	Triclopyr: Amine Salt (Herbicide) 1.14 kg a.i./ha (11.4 mg/m ²) Propiconazole (Fungicide) 2.16 kg a.i./ha (21.6 mg/m ²) Cyfluthrin (Insecticide) 0.15 kg a.i./ha (1.5 mg/m ²)	e.c. e.c. e.c.	0.17 (acetic acid) 0.056 0.0044*
Application 3 1996	9/11-10/1	Diazinon (Insecticide) 4.4 kg a.i./ha (43.9 mg/m ²) Prodiamine (Herbicide) 1.1 kg a.i./ha (109 mg/m ²) Fenarimol (Fungicide) 1.4 kg a.i./ha (142 mg/m ²)	e.c. dry flowable e.c.	14.1** 0.0033 0.03

*vapor pressure @ 20 °C

**vapor pressure @ 22 °C

e.c. emulsifiable concentrate

w.p. wettable powder

its like which may cause a difference in the attractive forces which retain the pesticide in the deposit or on the leaf surface compared to its pure form and therefore the vapor pressure of the active ingredient [33].

Whether volatile loss of pesticides occurs mostly from deposits or directly from the leaf surface is a function of the chemical composition of the deposit, its physical structure (spread over leaf surface), the frequency and evenness of distribution of deposits over the leaf surface, and time following application. Deposit formation is a function of plant surface/spray droplet interactions. This is affected, to a great degree by the methods of application (drop size, and impact velocity), adjuvant properties, and the physio-chemical components of the leaf surface. The distribution of a pesticide within a deposit or film is dependent on the properties of the formulation such as concentration, solubility, pH, surface tension, ionic strength, temperature, and whether the adjuvant is a salt (surfactant) or a volatile organic [33]. There is a wealth of information and existing research in the science of formulation properties which affect deposit formation and subsequent pesticide behavior on a particular leaf surface, however, it is beyond the scope of this researcher to consider the complex interaction of each of these parameters on volatile loss behavior.

Finally, during nights and early mornings, when dew exists on the grass blades, a proportion of the pesticide deposit is imagined to be resuspended in droplet form. Due to the differences in ΔH and ΔS (eq.3) of pesticide evaporation from an aqueous emulsion environment instead of a solid pesticide deposit, it is imagined that the vapor pressure of the active ingredient would change during these time periods.

For simplification and lack of available data, it will be assumed that the vapor pressure of the active ingredient from the deposit will be similar to that of the pure active ingredient. This may be somewhat justified by the fact that volatile organic adjuvants, such as gasoline, can evaporate very quickly following application and be absent from the deposit, shortly following application. Secondly, surfactants and pesticides which have differences in polarity have, on occasion, been observed to have different redistribution pattern on the leaf surface. Bukovac [11], in his study of electron micrographs of deposits of ethephon emulsions on leaf surfaces found that the surfactant and pesticide were distributed quite differently on the foliar surface of sweet cherry leaves. In a case where the active ingredient tends to concentrate itself separately from other components in the pesticide formulation, the net attractive forces which the neighboring pesticide molecules generate may create a fleeing environment similar to when the pesticide is evaporating from its pure form, when the chemical is completely surrounded by molecules of its like. If such a case existed, the pesticide would effectively be volatilizing from itself and the assumption that the vapor pressure might be reasonable.

For lack of available data rather than completely justifiable assumptions, it will be assumed that the vapor pressure of the pesticide in the deposit will be equivalent to that of the pure active ingredient. A second assumption will be that the majority of initial evaporation takes place from the deposit instead of pesticide absorbed to the leaf surface. Pesticide evaporation, during this stage, should be relatively independent of the chemical features of the leaf surface. During the latter stages of evaporation, when less of the pesticide remains in the deposit form, the leaf surface features could have a significant effect on the vapor pressure and loss.

Relating Vapor Pressure to Rate of Evaporation:

The measurement of vapor pressure of the active ingredient occurs under conditions of static equilibrium-when the rate of condensation of the compound is equivalent to the rate of evaporation. This occurs when the average energy (temperature) of the pesticide in the vapor and solid are equivalent. In the steady-state case (as opposed to the static equilibrium), which is more likely to exist in the agricultural setting, the molecules which leave the pesticide deposit in the form of vapor and diffuse away from the leaf system causing the average energy of the remaining molecules in the deposit to decrease. This evaporative cooling, or a reduction of the temperature of the deposit through loss of latent heat, causes a reduction in vapor pressure. The pesticide deposit must therefore absorb energy from its surroundings (air or leaf surface) to return to its initial temperature and vapor pressure. Therefore it could be considered that the vapor pressure of the pesticide may not reflect the true rate of evaporation since it would be limited by the rate of heat conduction from the leaf surface to the deposit.

In support of the contrary, the latent heat demand for evaporation of water is far greater than for semi-volatile substances, such as pesticides [24]. Transpiration occurs from the stomata of the leaf surface during the daylight hours to release energy absorbed from sunlight. Since it is estimated that 95% of water loss due to transpiration occurs during the daylight hours [24] to offset heat absorbed from sunlight, and the latent heat lost through water transpiration is so much larger than that due pesticide evaporation, a reservoir of necessary energy in the leaf surface is assumed to be readily available to the pesticide deposit to maintain a saturated vapor of pesticide above it.

It will be assumed that the air immediately adjacent to the leaf surface is in equilibrium with the vapor pressure of the active ingredient in the deposit. This view relies on the assumption that volatilization is not the rate limiting step -- that the deposit can draw enough energy from the leaf surface at a rate needed to replenish the vapor lost through diffusion.

The topic of pesticide volatilization from a deposit on the leaf surface has been discussed at length. The subject of the second stage of the evaporation process, transport of pesticide vapor away from the

deposit into the atmosphere, will now be developed. Before leaving the topic of volatilization, the assumptions mentioned in the earlier discussion will be restated:

1. *During the period immediately following application, most of the pesticide evaporation takes place from discreet deposits or films instead of pesticide directly adsorbed to the leaf surface.*
2. *The vapor pressure of the pesticide in a deposit is assumed to be equivalent to the vapor pressure of the pure active ingredient.*
3. *The effect of evaporative cooling on the rate of pesticide evaporation is considered to be unimportant.*
4. *The average rate of evaporation is proportional to the compound's active ingredient vapor pressure at an estimated leaf temperature.*
5. *The vapor pressure of the pesticide estimated by the Clausius Clapeyron equation is assumed to be within an order of magnitude of the true vapor pressure.*

Diffusion

The rate of transport of any conservative property (heat, mass or momentum) in a fluid is governed by a concentration gradient (dc/dz) and a transport coefficient of the property in the medium (K). There are two generally accepted modes of transport in a fluid such as air: Molecular Diffusion and Turbulent (or Eddy) Diffusion.

Molecular diffusion generally dominates transport over short distances and in cases where the air is almost completely still. Transport, in this case, is governed by brownian motion or random molecular walk of a substance in the direction of a descending concentration gradient ($-dc/dz$). Movement of chemical, as a result of this mechanism, obeys Ficks Law:

$$F_{mol} = -D_a \frac{dc}{dz} \quad (5)$$

F_{mol} =Flux ($\mu\text{g}/\text{m}^2/\text{s}$) due to molecular diffusion mechanism of transport along z-axis.

D_a = Molecular Diffusion (m^2/s) coefficient of a compound through air (a function of fluid temperature, molar mass and molar volume).

dc/dz =concentration gradient ($\mu\text{g}/\text{m}^4$) of compound along z-axis.

The main feature of the molecular diffusion mechanism is that the fluid is stationary and the diffusion coefficient (D_a) is determined by the relative molecular size and mass of the diffusing molecule and the medium. In a stationary fluid, the size and mass of the diffusing molecule govern its mean free path and period between collisions with the molecules of the diffusing medium which resist its movement. A lighter, smaller molecule will have a greater ability to diffuse than a large, heavy molecule. A method of calculating a diffusion coefficient for an organic molecule in air @ 25°C with an estimated accuracy of 10%, using a molecule's mass (m), is reviewed in Schwarzenbach [6]:

$$D_a(@25^{\circ}C) = \frac{1.55}{m^{0.65}} \left(\frac{cm^2}{s} \right) \quad (6)$$

D_a -molecular diffusion coefficient of an organic molecule in air @ 1 atm, 25 °C (cm²/s)
 m -molecular mass of the diffusing organic molecule (g/mol)

Since temperature governs the period between molecular collisions and the collision radius of a molecule, Fuller's method can be used to normalize D_a for temperature [18]:

$$D_a(T) = \frac{1.55}{m^{0.65}} \left(\frac{cm^2}{s} \right) \times \left(\frac{T}{298K} \right)^{1.75} \quad (7)$$

T -Temperature of air system (K)

Turbulent Diffusion

Turbulent Diffusion, or transport of a property by fluid motion, is generally the dominant mechanism of transport in all areas of the atmosphere except within the first few millimeters above surfaces where molecular diffusion plays a significant role.

$$F_{turb} = -E_a \frac{dc}{dz} \quad (8)$$

F_{turb} =Flux (ug/m²/s) due to turbulent diffusion or advection of fluid along the z-axis.

E_a = Eddy (turbulent) Diffusion coefficient of a compound through in air (m²/sec).

dc/dz =concentration gradient of compound along z-axis (ug/m⁴).

Although similar in appearance to Ficks Law, the Eddy Diffusion coefficient (E_a) is a function of the structure, and intensity of fluid motion and is independent of the molecular properties of the scalar (momentum, heat or mass) being transported. Therefore E_a , for any scalar, is identical. Estimating the diffusion coefficient E_a in the direction of fluid flow (advection) can be approximated as the product of an advection length (L) and a mean fluid velocity (v) [18].

$$E_a = L \cdot v \quad (m^2/s) \quad (9)$$

The dominance of eddy diffusion over turbulent diffusion is dependent on diffusion distance (L) and fluid velocity (v) can be determined by combining the two diffusion equations and the equation for advective diffusion coefficient E_a (5, 8 & 9) to solve for the critical fluid velocity v_{crit} at which advection surpasses molecular diffusion over a given length L :

$$v_{crit} = \frac{2D_a}{L} \quad (\text{m/s}) \quad (10)$$

Also, for a given fluid velocity v , a critical length L_{crit} , can be calculated for which eddy diffusion dominates molecular diffusion:

$$L_{crit} = \frac{2D}{v} \quad (\text{m}) \quad (11)$$

The concept that an eddy transport coefficient can be viewed as the product of a velocity v and a mixing length L , in equation 9, will be used as an explanation for the derived coefficients of pesticide vapor from a grass surface.

Transport in Fluids

Before discussing pesticide transport from a surface into an air stream, it is necessary to develop some concepts of fluid flow which transport of any property such as heat, momentum or mass will depend on. These concepts apply to fluid flow in a pipe, water in a river, or air flow over a surface.

There are two types of fluid flow, laminar and turbulent. Laminar is the ideal case and can be viewed as the condition where all instantaneous fluid parcel velocities are in the direction of average flow (Fig. 12). Under laminar conditions, the viscous properties of the fluid dominate the frictional forces generated by differences in velocity of adjacent flow. Under this "hydrodynamically smooth" flow condition, the velocity profiles are idealized as adjacent linear lines pointing in the direction of flow. Transport of any property (heat, mass or momentum) in the direction of flow is by means of *advection* (transport of a property contained in a fluid parcel by fluid movement) and transport of any property perpendicular to flow is by *molecular diffusion* (brownian motion) since there are no vertical velocity components in the fluid flow.

Flow becomes turbulent when frictional forces (shear), due to differences in adjacent fluid velocity profiles, overcome the viscous properties of the fluid which maintain the laminar flow. Fluid parcel velocities in the direction perpendicular to the flow begin to occur. Turbulent flow is characterized by the presence of oscillating rotating currents (eddies) superimposed on the direction of mean fluid flow (Fig. 13). The transition between laminar and turbulent flow for any fluid is given by the dimensionless Reynolds number (Re):

$$Re = \frac{uL}{\nu} \quad (12)$$

u -mean flow velocity (m/s)
 L -flow distance (m)

Figure 12: Laminar Flow in a fluid

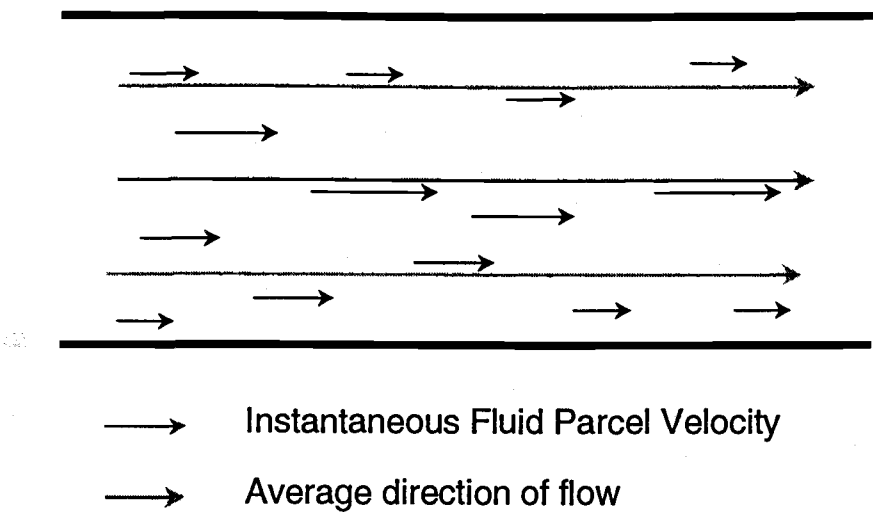
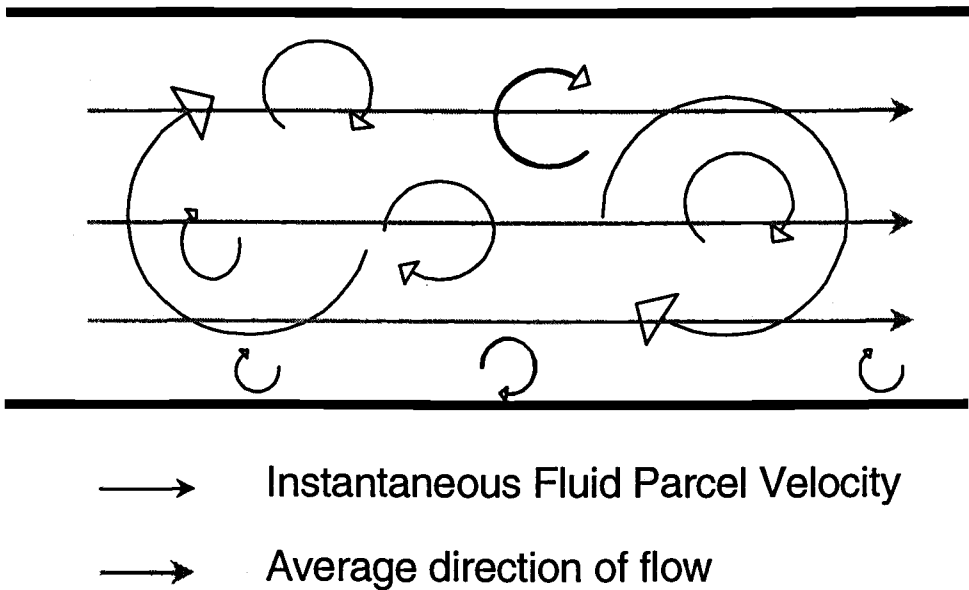


Figure 13: Turbulent Flow in a Fluid



ν -kinematic viscosity (molecular diffusion coefficient for momentum) $15.5 \times 10^{-6} \text{ m}^2/\text{s}$ for air @25 °C)
 $Re < 10^6$, laminar
 $Re > 10^6$, turbulent

These eddies are responsible for scalar transport by turbulent diffusion in the direction perpendicular to mean fluid flow. These rotating fluid parcels can be imagined as having a mixing length L and a mixing velocity, u . These concepts will now be used to describe wind speed profiles over stationary surfaces.

Wind Profiles above surfaces

The universal equation for wind speed profiles over surfaces under neutral conditions (i.e. where strong temperature gradients perpendicular to the direction of mean fluid flow do not exist) is:

$$u(z) = \frac{u_*}{k} (\ln z + C) \quad (13)$$

$u(z)$ (m/s) wind speed at height z in turbulent air stream
 z (m) vertical distance above surface
 k (dimensionless) von Kármán's constant ~ 0.4
 u_* (m/s) frictional velocity
 C -constant determined by a boundary condition (ie. where $u=0$)

The wind speed gradient (du/dz) at height z above a surface is found by taking the derivative of eq. 13:

$$\frac{du}{dz} = \frac{u_*}{kz} \quad (14)$$

The frictional velocity, u_* , is related to the shearing stress, τ , (rate of momentum loss to the surface) experienced at the surface due to friction:

$$u_* = \sqrt{\frac{\tau}{\rho}} \quad (15)$$

τ (kg/m/s²)-shear
 ρ -air density (kg/m³)
 u_* -frictional velocity (m/s)

Using equations 13 and 15, equation 8 can be written for the downward flux of momentum, τ , due to turbulent diffusion:

$$\tau = \rho u_*^2 = E_z \frac{\rho u_*}{kz} \quad (16)$$

Solving equation 16 for E_z gives:

$$E_z(z) = k u^* z \quad (17)$$

$E(z)$ (m^2/s) vertical (z) eddy diffusion coefficient of a scalar.
 z (m) vertical distance above a surface parallel to the air stream.
 k (dimensionless) von Kármán's constant ~ 0.4 .

Under neutral atmospheric conditions (ie. no strong vertical temperature gradients), the mixing length, l , (analogous to a diameter of a rotating fluid parcel) is proportional to the vertical distance, z , above a surface that is parallel with the air stream:

$$l = kz \quad (\text{m}) \quad (18)$$

l (m) mixing length.
 z (m) vertical distance above surface.
 k (dimensionless) von Kármán's constant ~ 0.4 .

In the same manner that an *advective* diffusion coefficient for laminar flow, E_a , in eq. 9 can be calculated in terms of the product of an advection length L and fluid velocity v , the *vertical* eddy diffusion coefficient $E(z)$ in equation 17 appears to be a product of a velocity u^* and a mixing length, l defined in equation 18.

The reason for the diminishing mixing length with nearness to a surface is due to the upward transmission of surface friction as shearing stress into the flowing air stream. The shearing stress, which is constant with height², causes the eddies to become unstable and progressively split into smaller rotating fluid parcels with nearness to the surface.

Wind Profiles over Smooth Surfaces

The equation of wind speed profiles over a smooth surface was shown in the classical experiments conducted by Nikarudse [35, 34], to be:

$$u(z) = \frac{u^*}{k} \left[\ln \left(\frac{k u^* z}{v} \right) \right] + 1.3 \quad (\text{m/s}) \quad (19)$$

v -kinematic viscosity (molecular diffusion coefficient for momentum).

² The momentum boundary layer above a surface is defined by Hartley [24] as the zone above the surface where shearing stress is constant with height. The equation for determining the thickness of a fully equilibrated momentum boundary layer δ_m over a roughened surface under neutral conditions is given by Munro and Oke (1975) [23]:

$$\delta_m = 0.1 x^{4/5} z_0^{1/5} \quad (22)$$

The thickness of a boundary layer δ is a function of distance (x) from the leading edge of the surface in the direction of wind flow and the roughness length, z_0 (which will be introduced). The flux of momentum (shear) is equivalent to (ρu^*). Assuming ρ (air density) is constant over a narrow vertical distance (ie. a few meters), u^* must also be constant with height.

$15.5 \times 10^{-6} \text{ m}^2/\text{s}$ in air @ 25 °C.

z (m) vertical distance above a surface parallel to the air stream.

k (dimensionless) von Kármán's constant ~ 0.4 .

$u(z)$ (m/s) average wind velocity at height z above a surface parallel to the air stream.

u^* (m/s)-frictional velocity.

Equation 19 shows that the change of momentum between the surface and height z is related to the change in diffusion coefficients for momentum (ie. $E(z)=ku^*z$ at height z and v at the surface). Transport of any property, heat, momentum or mass from a surface generally occurs first by molecular diffusion in the air layer immediately adjacent to the surface and after a short vertical distance, becomes subject to turbulent transport of vertical eddy currents. Equation 17 shows the average mixing length of the eddies in the boundary layer diminish with decreasing height above the surface until the mixing scales of the eddies $E(z)$ are on the order of the mixing scales of molecular diffusion v . When $ku^*z \gg v$, the vertical transport of a scalar (momentum, heat or mass) is solely due to eddy diffusion whereas in areas close to a surface (small z where ku^*z is on the order of v , see eq. 10 & 11) molecular diffusion plays a significant role in transport (Fig 14). The value 1.3 in eq. 19 is an empirically determined constant and corresponds to the boundary condition that $u=0$ at the plane height $z=v/(3.6ku^*)$.

Relating the change in scalar concentration between to heights to the change in diffusion coefficient between two heights in an equilibrated boundary layer.

Using equation 19 to calculate the difference in wind speeds at two heights z_2 and z_1 in an equilibrated boundary layer, it can be shown that the difference in wind velocities (momentum concentration) is due to the difference in eddy mixing scales at each height.

$$u(z_2) - u(z_1) = \frac{u^*}{k} \left[\ln \left(\frac{ku^*z_2}{ku^*z_1} \right) \right] \quad (\text{m/s}) \quad (20)$$

Since u^* and k are constant with height in the boundary layer (see footnote 1) eq. 20 simplifies to:

$$u(z_2) - u(z_1) = \frac{u^*}{k} \left[\ln \left(\frac{z_2}{z_1} \right) \right] \quad (\text{m/s}) \quad (21)$$

Since wind velocities at different heights above a surface are a means for describing eddy transport of momentum from an air stream to a surface, and the eddy correlation theory states that eddy diffusion properties of any scalar (momentum, heat or vapor) in a fully turbulent air stream are identical, *the wind velocity profiles above a surface will be used to estimate transport properties of vapor from the surface into the air stream.*

In summary, equations 13-21 show reasons why aerodynamic approaches in estimating eddy diffusion

Figure 14: Turbulent $E(z)$ and Molecular Transport Scales (ν)

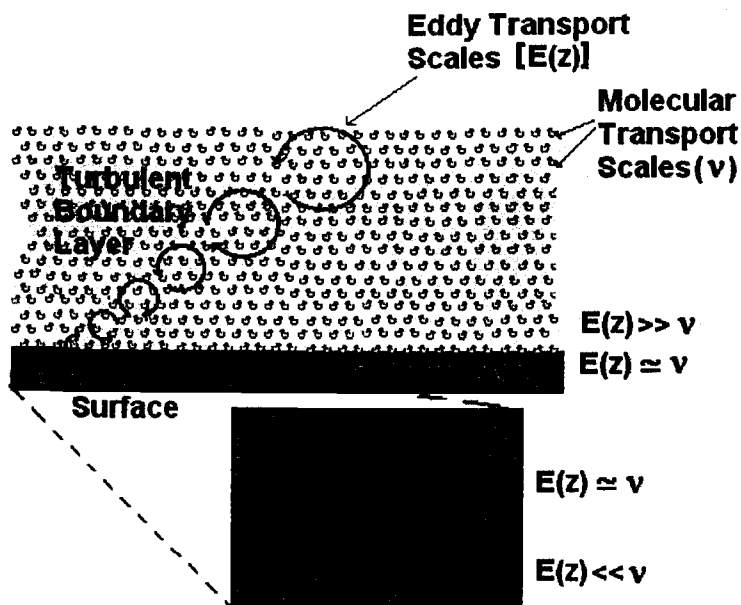


Figure 15: The displacement term d_0 in equation 25 is used for taller crops, but is omitted for turf grass.

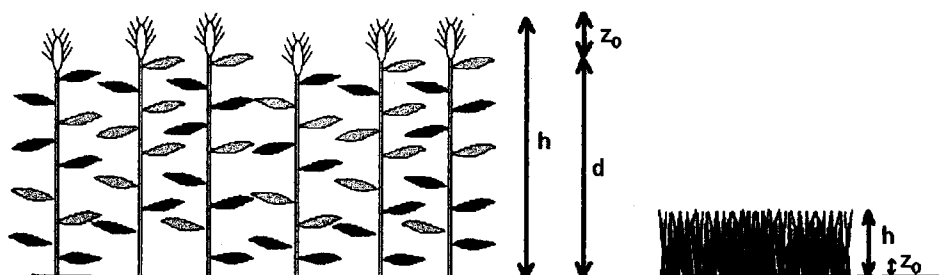
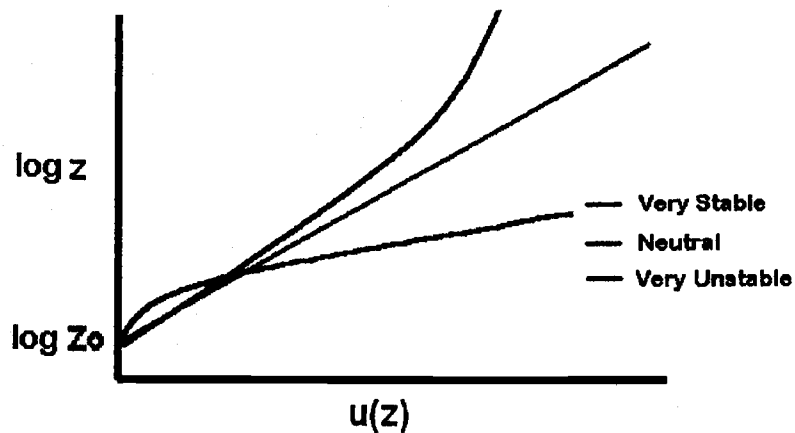


Figure 16: Effect of Atmospheric Stability on Wind Profiles (equation 26)



coefficients at various heights above surfaces use information on wind speed profiles.

Wind Profiles over Rough Surfaces:

Before relating scalar transport such as heat and vapor between surfaces and air streams to wind speed (momentum) profiles, an additional feature of momentum transport to roughened surfaces, which is absent for vapor and heat, must be discussed. There are two recognized processes by which momentum is transmitted to a surface, skin friction and form drag.

Skin Friction

Skin friction, as we have seen for smooth surfaces, is the transport of momentum across a thin, *laminar air layer* near the surface by molecular diffusion in the direction of a descending concentration gradient. Recall that laminar flow occurs when the size of the turbulent eddies in a flowing fluid are on the order of molecular diffusion (ie. $E(z) \approx D_a$). Vertical transport of a scalar in the laminar boundary layer obeys Ficks Law.

The vertical scalar concentration gradient (dc/dz) which exists across the laminar boundary near the surface is larger than at any other height above the surface where turbulent diffusion occurs since the eddy coefficient, $E(z)$, is typically several orders of magnitude greater than the molecular diffusion coefficient, D_a . To give an example of how great this difference is, the molecular diffusion coefficient for momentum, ν , is $0.155 \text{ cm}^2/\text{s}$ @ 25°C . Using a value of $u^*=20 \text{ cm/s}$, the eddy diffusion coefficient, $E(z)$ at a height of 1 m above the surface and is calculated to be $800 \text{ cm}^2/\text{s}$ (eq. 17). Combining equations 19 and 20, using the assumption of constant flux with height in a fully developed boundary layer (footnote 1), the momentum gradient ($\delta(\rho u)/\delta z$) across the laminar layer must be over 5000 times greater than the gradient which exists at 1 m above the surface!

$$F_{\text{laminar}} = F_{\text{turbulent}} \quad (23)$$

$$D_a \left[\frac{\delta(\rho u)}{\delta z} \right]_{\text{laminar}} = E_z \left[\frac{\delta(\rho u)}{\delta z} \right]_{\text{turbulent}} \quad (24)$$

Using this equality, and the knowledge that E_a is generally several orders of magnitude greater than D_a , the concentration gradient dc/dz for pesticide vapor is considered to be very high near the surface where molecular diffusion is the dominant mechanism of transport and small in areas where turbulent diffusion dominates well above the surface.

An example given in [20] of molecular thermal diffusivity is that a temperature gradient of $1 \times 10^4 \text{ K/m}$ can exist in the first few millimeters of above a surface. This corresponds to a difference of 10°C over a 1

mm thickness! The same reference states: "Those of you who have walked barefoot across a black asphalt road on a sunny summer day can testify that the surface "skin" temperature can become burning hot to the touch, even though the air temperature may be a pleasant 25 °C or 30 °C. The hot skin temperature can create a large temperature gradient in the lowest millimeters of air..." (Stull, 252).

Form Drag

Form drag is the second mechanism, by which momentum is transferred to rough surface. As opposed to skin friction, form drag is the loss of fluid momentum due to pressure exerted by the fluid on objects immersed in the flow. An example of this would be a water in a creek bed being slowed by boulders immersed in the stream or wind flow over a flat field encountering a stand of trees. Although these are extreme cases, momentum loss due to form drag can occur for any surface which has some physical roughness feature such as grass. In cases where roughened features of a surface prevent the formation of a laminar layer, turbulent flow may exist at the surface. In this case, momentum loss due to form drag occurs as eddies scour the roughened features of the surface. Transport of momentum by form drag occurs at a much greater rate than skin friction because transport is no longer limited by molecular diffusion, which is the slowest of all transport processes. The rate at which eddies can transfer their energy by form drag to the roughness elements of the surface is related by the size (l) and rotational velocity (u^*) of the eddies which exist at the surface. The following is an adaption of the universal logarithmic profile equation (equation 13) which characterizes velocity profiles over rough surfaces under neutral atmospheric conditions:

$$\bar{u}(z) = \frac{u_*}{k} \ln \left[\frac{z - d_0}{z_0} \right] \quad (\text{m/s}) \quad (25)$$

u_* - frictional velocity (m/s).

$\bar{u}(z)$ - mean wind speed at height z (m/s).

d_0 - displacement height of $z=0$ (generally omitted for short grass).

z_0 - roughness length (m).

k - von Kármán's constant (0.4).

The roughness length, z_0 , is a factor which has been determined for many surfaces, including grass, which encompasses the boundary condition (where the wind speed becomes zero) and represents the combined effect of form drag and skin friction mechanisms for momentum transfer to a roughened surface. The roughness length for a particular scalar (mass, momentum or heat) can differ for an identical surface depending on the relative differences in skin and form drag which govern transfer between a surface and an airstream.

The term d_0 is necessary in eq. 25 & 26 for many canopies with tall vegetative elements such as trees or corn, and corresponds to a height displacement of the zero plane [26, 28]. The displacement height is generally not a necessary term in eq. 25 for short grass and so will be omitted (Fig. 15) [22].

Effect of Atmospheric Stability on Wind Profiles

Vertical temperature gradients affect scalar flux by governing the vertical movement of air parcels containing the scalar, whether it is momentum, heat or vapor. During clear, sunny days, the ground becomes significantly warmer than the air. Air immediately in contact with the surface begins to expand causing the parcel to rise and cooler air to descend. Due to this cycling in unstable conditions, the vertical transport of air parcels containing momentum occurs at a much faster rate causing the steepness of the wind speed profile to be weakened. The opposite can also occur during extremely stable conditions when the ground is cooler than the air above, the wind speed profile is steeper due to a suppression in vertical transport of momentum to the surface (Fig. 16). Unstable conditions have been observed to occur in late afternoons or during clear nights [39]. A term for stability, $\psi(z)$, can be added to the wind profile equation (25) to account the effect of temperature gradients.

$$\overline{u}(z) = \frac{u^*}{k} \left[\ln\left(\frac{z}{z_0}\right) + \psi(z) \right] \quad (26)$$

$\psi(z)$ -atmospheric stability correctional term ($\psi > 0$ for stable and $\psi < 0$ for unstable conditions)

A measurement of atmospheric stability $\psi(z)$ is the Richardson number (Ri):

$$Ri = \frac{g(\Delta T \Delta z)}{T \Delta u^2} \quad (27)$$

Ri < 0 unstable conditions

Ri > 0 stable conditions

Ri = 0 neutral conditions

T-Temperature at height at which stability is being determined.

ΔT -vertical temperature gradient

Δu -vertical wind velocity gradient

Δz -vertical distance at which temperature and wind velocity gradients are being measured.

The Richardson number is essentially a vertical momentum transfer equation which is determined by vertical wind speed gradients (du/dz) and the effect of temperature with wind speed (dT/du). A more exact (although less intuitive) equation for atmospheric stability is the Monin-Obukhov path length (L). This is not to be confused with L mentioned in eq. 9-12.

$$L = \frac{-u_*^3 T_0 \rho c_p}{kgA} \quad (28)$$

$L = \infty$ m (neutral atmospheric conditions)
 $L = -5$ m (very unstable atmospheric conditions)
 $L = +5$ m (very stable atmospheric conditions)

u_* - frictional velocity
 ρ - air density
 c_p - specific heat of air
 A - sensible heat flux
 k - Von Kármán's constant (0.4)
 g - gravitational constant
 T_0 - temperature at height of measurement.

The Monin-Obukhov measurement of atmospheric stability $\Psi(z)$ in equation 28 can be written as:

$$\overline{u}(z) = \frac{u_*}{k} \left(\ln \frac{z}{z_0} + 4.7 \frac{z}{L} \right) \quad (29)$$

L - Obukhov Monin path length (not to be confused with advection length, L mentioned in eq. 9-12).
 u_* - frictional velocity.
 $u(z)$ - wind speed at height z .
 z_0 - roughness length (defined as the height at which wind speed becomes zero).
 k - Von Kármán's constant (0.4).
 z - height above the surface.

Under neutral atmospheric conditions ($L = \infty$), the second term on the right half of the equation disappears and produces a linear equation.

$$\overline{u}(z) = \frac{u_*}{k} [\ln z - \ln z_0] \quad (30)$$

The terms z_0 and u_* are scaling parameters that are specific to the momentum absorption features of the surface and the mean flow velocity of the air stream. Both parameters can be estimated by measuring wind speeds at several distances above a surface and performing a linear regression of $u(z)$ vs. $\ln z$ under neutral conditions (Fig. 17).

Physical Significance of Scaling Parameters u_* and z_0

The frictional velocity term (u_*) is related to the shearing stress τ , in eq. 15 and can be imagined to represent a tangential velocity of the eddy currents which transport of momentum to the surface. The magnitude of u_* is determined by the mean fluid flow velocity and the frictional (momentum absorption)

Figure 17: Linear/log plot of wind profiles above a surface during neutral atmospheric conditions (eq. 30)

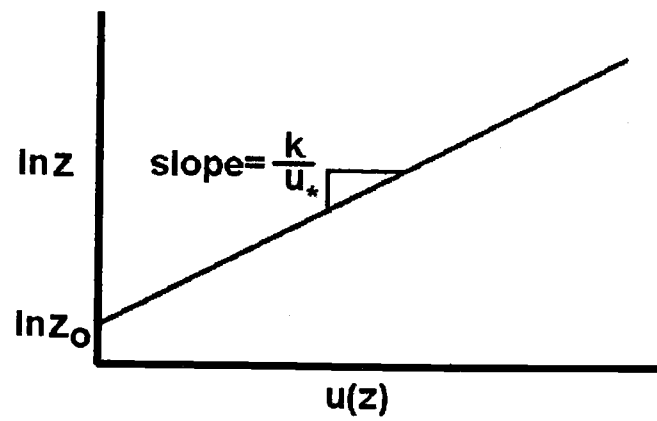
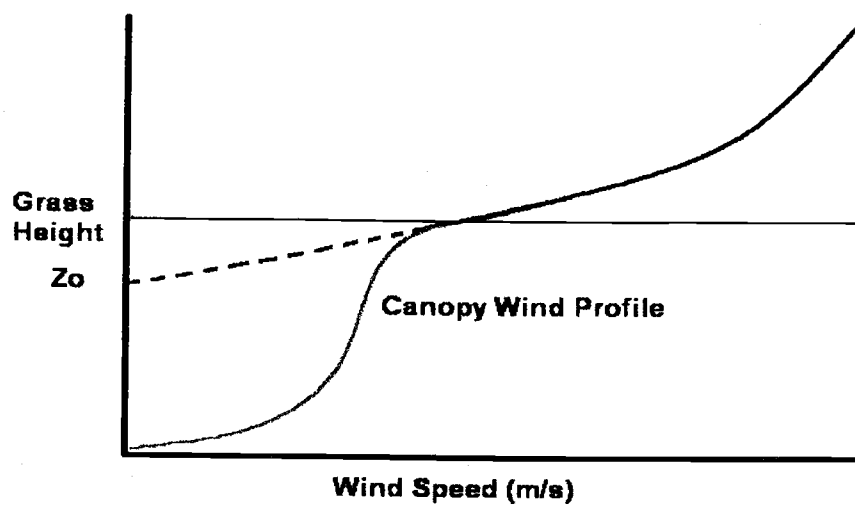


Figure 18: Extrapolated Wind Profiles (eq. 30) and Observed Wind profiles in a crop canopy (see equations 33, 34, & 35).



features of the stationary surface [35].

z_0 has the dimension of length and, according to equation (30), is the extrapolated height at which the wind speed becomes zero. For grass, it typically occurs below the height of the roughness elements (between 1/4-1/10 the height of the canopy of grass blades [19, 36]) inside the canopy. The physical significance of z_0 is debatable since it corresponds to a height where a different function of wind speed vs. height takes over (Fig. 18).

Kondo [30] described z_0 as a parameter which is related to the geometric features and spacing of the roughness elements which contribute to the drag properties of the surface. The drag coefficient C_D , which denotes the "effectiveness of momentum transfer to a surface" [30], is shown to increase with z_0 [37]:

$$C_D(z) = \frac{u_*^2}{u(z)^2} = \frac{k^2}{\left[\ln\left(\frac{z}{z_0}\right)\right]^2} \quad (31)$$

For a series of closely packed roughness elements such as turf grass, a sheltering effect of adjacent roughness elements upstream in the direction of wind causes the total bulk drag coefficient of the surface to be less than the sum of the drag contributions of the individual roughness elements. Values of z_0 are tabulated for many surfaces [9] including grass (Fig. 19, Table 2) and are generally assumed to be constant with wind velocity when turbulent flow exists at the surface, however there have been documented cases of z_0 increasing with decreasing wind speed above a surface of densely packed roughness elements such as turf grass [22, 37, 38, 39]. It is believed that a transitional flow state, which is intermediate between laminar and turbulent, exists in the canopy at lower wind speeds [38]. The change in canopy flow structure is believed to cause a decrease in the sheltering factor of adjacent roughness elements.

A criteria often used for determining whether turbulent flow occurs over a surface is the roughness Reynold's number:

$$Re^* = \left(\frac{u_* z_0}{\nu}\right) \quad (32)$$

Re^* -roughness Reynolds number
 $Re^* > b$ fully turbulent transfer of momentum
 $b > Re^* > a$ transitional (turbulent and laminar)
 $Re^* < a$ hydrodynamically smooth.

u^* -(m/s) frictional velocity
 z_0 -(m)-momentum roughness length
 ν -(m²/s)-kinematic viscosity

Similar to the Reynolds number (eq. 12), the roughness Reynolds number can be considered as a determinant of whether turbulent or molecular transport of momentum occurs at the surface. When the Re^* is greater than a critical value, b , momentum exchange to a surface is due solely to turbulent diffusion. If $Re^* < a$, momentum transfer to a surface occurs by molecular diffusion. If the conditions exists where $a < Re^* < b$, an exchange process which is intermediate between turbulent and molecular transport mechanisms is thought to exist. The values a and b appear to be different depending on the geometric properties of the surface. For a sand roughened surfaces, Nikarudse found $a=0.13$ and $b=3$, however, for grass, Deacon estimated $b=40$ [37].

Wind Speed Profiles and Mixing Lengths inside a Crop Canopy:

Equation 21 can only describe wind speed profiles above the height of the roughness elements (h_0), with z_0 being the extrapolated height at which the wind speed becomes zero. Brutsaert [26] reviews three empirical equations for mean wind speed inside a vertical crop stand:

$$\bar{u}(z) = \bar{u}(h_0) \exp\left[-a_w \left(1 - \frac{z}{h_0}\right)\right] \quad (33)$$

$$\bar{u}(z) = \bar{u}(h_0) \left[\frac{\sinh(a'_w z)}{\sinh(a'_w h_0)} \right]^{\frac{1}{2}} \quad (34)$$

$$\bar{u}(z) = \bar{u}(h_0) \left[-a''_w \left(1 - \frac{z}{h_0}\right) \right]^{-2} \quad (35)$$

$u(z)$ (m/s)- mean wind speed at height z inside the crop canopy.
 $u(h_0)$ (m/s)- mean wind speed at the height of the surface roughness elements.
 a_w - a'_w - a''_w -parameter representing extinction coefficient of momentum in a particular crop canopy.

According to Brutsaert, the three equations for wind speed are based on "markedly different assumptions concerning the eddy diffusion coefficient and the foliage drag coefficient which are not easy to verify. Nevertheless, all three functions give a mean velocity which is decaying with depth and the differences among them, when fitted to data, are usually well within the scatter observed in field experiments" [26]. Equation 33, in Brutsaert's estimation, is best understood and is most widely used for determining wind speed profiles in canopies [27].

Atmospheric Transport Zones

Since there are wind profile regions above and inside the canopy where vapor transport occurs, two zones in the lower atmosphere have been designated (Fig. 20). The *Dynamic Sublayer* (DSL) is designated as the zone above the surface where the logarithmic wind profile equation (29) is valid. Turbulent diffusion dominates as the mechanism of transport and the flow pattern is unaffected by the shape and spacing of the roughness elements [26]. This can range from a height of several hundred meters to a height near roughness elements (grass blades). The *Interfacial Boundary Layer* (IBL) is defined as the zone where the wind flow pattern is affected by the nature of the surface and transport is affected by the molecular diffusion properties of the scalar [26]. In the turf grass/air system, the IBL spans from the base of the turf canopy where the air is completely still, to the zone above the grass blades where the dynamic sublayer begins. Equations 33-35 are likely to represent wind speed profiles in the major regions of the IBL.

Although atmospheric transport is governed principally by molecular and turbulent diffusion, designating zones where each is mutually exclusive and determining the local concentration gradients is difficult. The complexity of establishing the different transport mechanisms, vertical distribution of sources and sinks and flow patterns which occur in the IBL, in addition to determining the exact height where the IBL ends and the DSL begins is difficult, if not impossible. To avoid the problem of determining the actual height and distributions of scalar sources or sinks in the canopy, and where molecular diffusion ends and turbulent diffusion begins, the scalar roughness length (z_0 momentum z_{0s} for a scalar) can be viewed under steady-state conditions, as the extrapolated height of an imaginary two-dimensional plane where the source or sink of a scalar exists for purely turbulent transfer (Fig 21). In fact, the concentration profile of a vapor being transferred to or from a surface follows a similar logarithmic profile pattern as wind speed [26, 27, 28] (Fig.22).

In this case, the existence of the IBL is ignored and the DSL is imagined to extend to the surface. The difference in transport properties in the IBL for different scalars is encompassed in the roughness length terms (z_0 and z_{0s}). z_{0s} is typically less than z_0 for the same surface because loss of momentum occurs by two mechanisms; *skin friction* (transport due to eddies above the surface and molecular diffusion near the surface) and *form drag* (momentum lost due to pressure exerted by fluid on bluff features of objects immersed in fluid flow). Although momentum transport to a surface such as turf grass occurs by both skin friction and form drag, heat and mass transport to and from a surface (including pesticide vapor) only share the mechanisms of transport inherent in skin friction [28]. Differences in z_0 and z_{0s} due to skin friction may also exist due to differences in molecular diffusion properties of the scalar (ie. size and mass). Finally, differences in the roughness lengths of different scalars may be attributed to the differences in physical locations of the sources or sinks on the surface (for example, pesticide

Table 3: Roughness Lengths for Grass at Wind velocities between 2-8 m/s at height of 2 m [19]:

Grass Length (mm)	Roughness Length z_0 (mm)
15	2
30	7
45	24 [†]
45	17 [‡]

[†]Wind speed of 2 m/s at height of 2 m

[‡]Wind speed of 6-8 m/s at height of 2 m

The decrease of roughness length for longer grass at higher wind speeds in Table 2 is believed to be due to the bending and flattening of the grass blades at higher wind speeds, causing a change in the momentum absorption features of the grass [19], and not due to a flow transition.

Figure 19: Roughness Length vs. Grass Height for short grass (1.5 cm-4.5 cm). Data obtained from Deacon, 1953 [19].

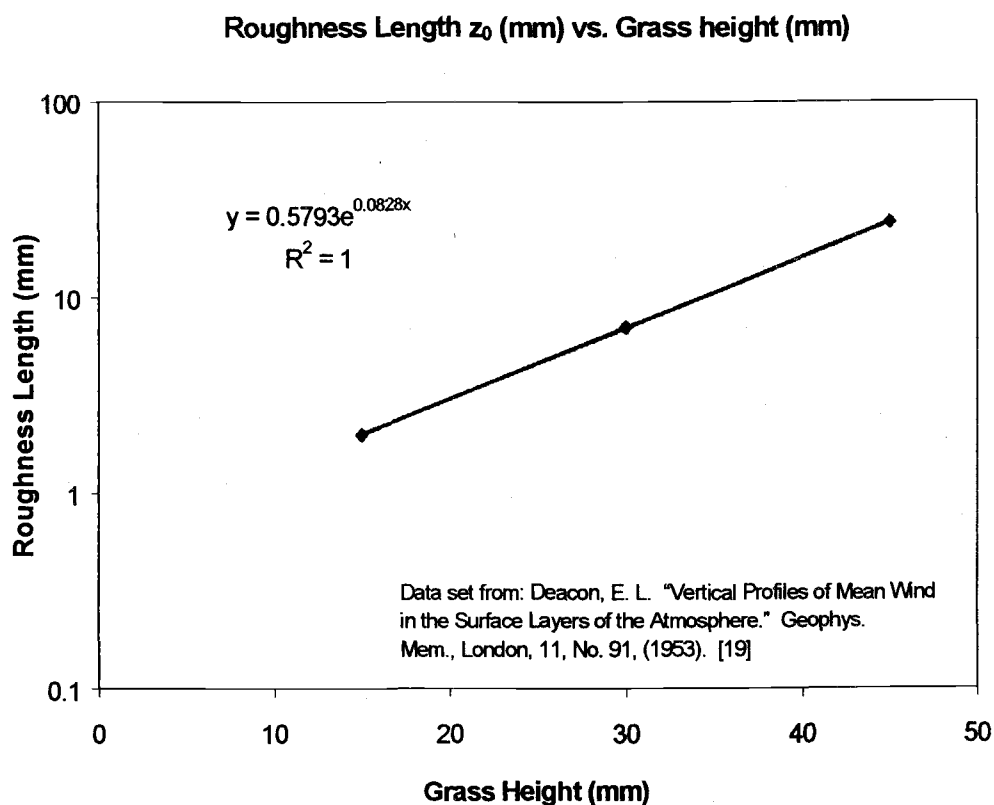


Figure 20: Dynamic Sublayer and Interfacial Boundary Layer regions

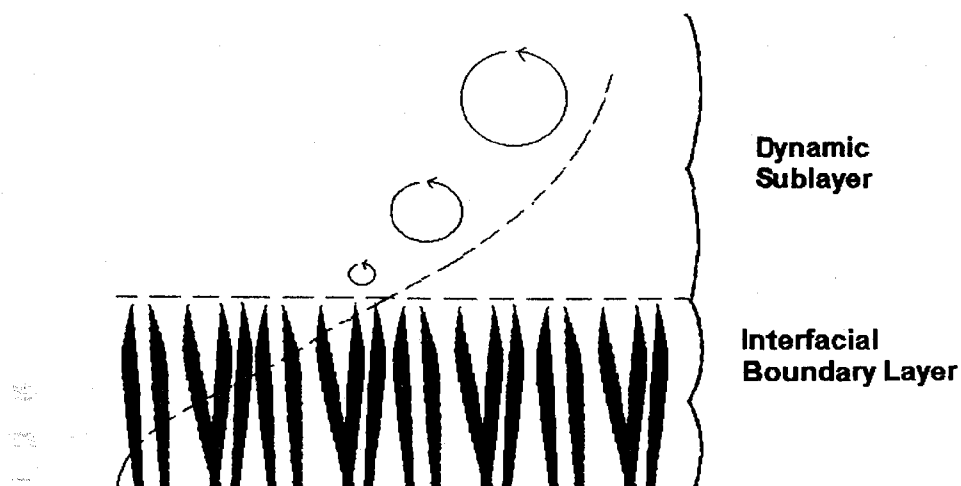


Figure 21: Two dimensional view of momentum deposition and pesticide evaporation under steady state transfer conditions. z_0 is the extrapolated height two-dimensional plane for the sink for momentum and z_{0s} the extrapolated source height for the pesticide vapor.

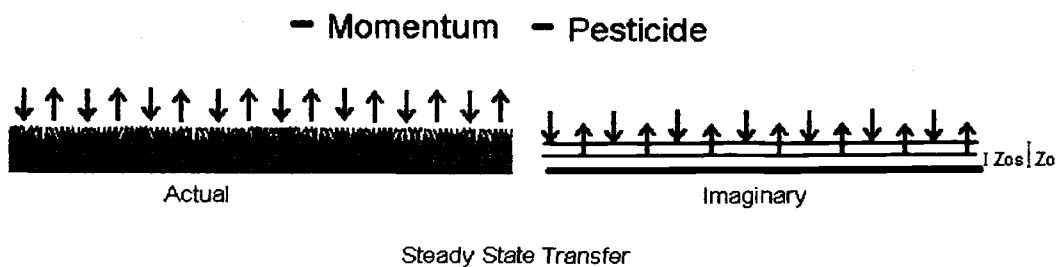
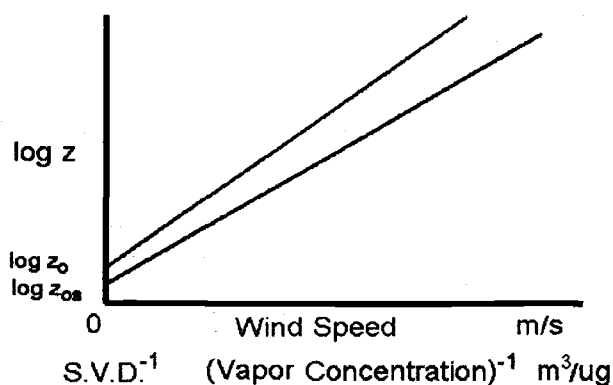


Figure 22: Extrapolated roughness lengths for momentum z_0 and an evaporating scalar z_{0s} .



z_0 momentum roughness length $u(z_0)=0$

z_{0s} scalar (vapor) roughness length $C(z_{0s})=S.V.D.$ (source vapor density).

evaporation occurs from discrete deposits or films with the densities of these deposits varying with leaf height whereas as momentum deposition may occur evenly over a leaf surface and vary with height).

In summary z_0 is extrapolated height which momentum is deposited due to turbulent diffusion and z_{0s} is the extrapolated height of the source of pesticide vapor (Fig. 21). The difference between momentum, z_0 , and scalar z_{0s} roughness lengths is due to presence of form drag in momentum deposition, differences in molecular transport properties inherent in skin friction and differences in the physical locations of sinks or sources on the surface.

Transport of Scalars between the Scalar source and the Atmosphere

The rate of transport (flux, F_z) of any conservative entity is based on a concentration gradient (dc/dz) and an exchange coefficient over the gradient (D_a or E_z). The bulk exchange coefficient for scalar transport between the surface and a reference height (z) in an air stream is thought to be a composite of the individual molecular and eddy transport processes which exist in between:

$$F_{0 \rightarrow z} = -\frac{1}{Z} \sum_0^z [D_a + E(z)] \frac{dC}{dz} dz \quad (36)$$

$F_{0 \rightarrow z}$ Rate of scalar transport between surface (0) and height (Z) in air stream
(scalar quantity/m²/s)

Assuming that flux is constant with height in the equilibrated boundary layer (the zone above the surface where the flux of a quantity is constant with height) and in regions where turbulent diffusion occurs, $E(z) > D_a$, equation 36 can be rewritten as:

$$-\int_{C_0}^{C_z} dC = F_{0 \rightarrow z} \int_0^z \frac{1}{E(z)} dz \quad (37)$$

Equation 37 is actually a form of equation 8. Integrating results in the simplified expression:

$$F_{0 \rightarrow z} = \frac{C_0 - C_z}{r_{0 \rightarrow z}} \quad (38)$$

where $r_{0 \rightarrow z}$ is the integrated resistance to transport between the surface and height z .

$$r_{0-z} = \int_0^z \frac{1}{E(z)} dz \quad (39)$$

Equation 38 resembles Ohm's law which states that the current (rate of charge flow) between two points is governed by the voltage difference and the total series resistance [26, 28, 39]:

$$\text{current} = \frac{\text{Voltage Difference}}{\text{Resistance}}$$

In the same way, the flux of a scalar between the scalar source and height z is governed by the total change in concentration between height z and the source ($C_0 - C_z$), and the total resistance to exchange between the surface and height z . The eddy and molecular diffusion coefficients represent how well a scalar is conducted in a medium. The measure of resistance is the reciprocal of the conductance.

$$\text{Resistance} = \frac{1}{\text{Conductance}}$$

The resistance to exchange (r_{0-z}) can be imagined as the sum of the inverted conductances (reciprocal molecular and eddy diffusion coefficients $E(z)$ and D_a) which exist between the scalar source (or sink) and height z in the air stream (eq. 36).

Derivation of Aerodynamic Resistance to transport (r_a) above the Canopy

According to equation 38, the vertical flux, F_z , of a scalar in the dynamic sublayer between the apparent height of a scalar source or sink $z=z_{0s}$ and the reference height, $z=h$ in the boundary layer, is governed by the concentration difference of the scalar at each height ($C_z - C_{0s}$) and the total resistance to transport (r_T) between $z=0$ and $z=h$. The scalar roughness length z_{0s} is the extrapolated height viewed by the logarithmic profile equation of the scalar source or sink (ie. the scalar roughness length) [28].

Since the downward transport of momentum to the surface and the upward transport of pesticide vapor in the boundary layer above the surface share the same mechanisms of transport, the two will be related to each other in the derivation of the transport resistance r_T . The turbulent resistance to transfer, r_{0-z} , for neutral atmospheric conditions will now be derived from equations 8, 15 and 21. This derivation is given in [28].

Using equations 8 and 17, the downward flux of momentum in the dynamic sublayer can be written as:

$$F_m(z) = E_m \frac{\partial(\rho u)}{\partial z} \quad (39)$$

The flux of an evaporating compound in the opposite direction can be written as:

$$F_c(z) = -E_c \frac{\partial(C)}{\partial z} \quad (40)$$

where:

u-wind speed (m/s)

ρ -density of air (kg/m³)

C-concentration of compound (kg/m³)

z-height (m)

E_c -turbulent diffusion coefficient of compound in air (m²/s)

E_m -turbulent diffusion coefficient of momentum in air (m²/s)

F_c -flux of compound at height z (kg/m²)

F_m -flux of momentum or shear (τ) at height z (kg/m/s²)

The eddy diffusion coefficient of the compound, (E_c) in the dynamic sublayer is equivalent to the eddy diffusion coefficient of momentum (E_m) since the turbulent diffusion coefficient of each property is dependent on the on the flow structure of air rather than the diffusing substance. Therefore $E_c = E_m$ and equations 39 and 40 can be combined:

$$-\frac{\frac{\partial(C)}{\partial z}}{F_c(z)} = \frac{\frac{\partial(\rho u)}{\partial z}}{F_m(z)} \quad (41)$$

or

$$-F_m(z) * \frac{\partial(C)}{\partial z} = F_c(z) * \frac{\partial(\rho u)}{\partial z} \quad (42)$$

The air density (ρ) is assumed to be constant from the surface to the reference height $z=h$. F_m is the shear stress (τ) in equation (16). Taking the derivative of equation 25 ($du/dz=1/ku*z$) and combining equation 16 ($F_m=\tau=\rho u^{*2}$) with eq. 42 and simplifying gives:

$$-\frac{F_c}{u * k z} = \frac{dC}{dz} \quad (43)$$

Invoking the definition of flux being constant in the boundary layer [24] (zones of the IBL and DSL where $F_c = \text{constant}$) and setting up the equation and integrating differences concentration from the height of the scalar source (z_{0s}) to the reference height $z=h$ gives:

$$-\int_{z_{0s}}^h dC = \frac{F_c}{ku_*} \int_{z_{0s}}^h \frac{1}{z} dz \quad (44)$$

and integrating:

$$C_{0s} - C_h = \frac{F_c}{ku_*} \ln\left(\frac{h}{z_{0s}}\right) \quad (45)$$

and solving for F_c :

$$F_c = \frac{(C_{0s} - C_h)}{\frac{1}{ku_*} \ln\left(\frac{h}{z_{0s}}\right)} \quad (46)$$

Comparing the denominator of 46 with the denominator of 38, we will now define the denominator of equation 46 as r_{0-z} , the aerodynamic resistance to transfer of a scalar between the surface and height z in the boundary layer:

$$r_{0-z} = \frac{1}{ku_*} \ln\left(\frac{z}{z_{0s}}\right) \quad (47)$$

The resistance terms, r_a & r_b

Using equation 47 for momentum gives the *aerodynamic resistance*, r_a , to transfer:

$$r_a(z) = \frac{1}{ku_*} \ln\left(\frac{z}{z_0}\right) \quad (48)$$

If momentum transfer to a surface and air stream is described by r_a , the resistance to transfer of another scalar from the same surface to height z can be determined from r_a by the addition of a second resistance term r_b [28]:

$$r_T(z) = r_a(z) + r_b \quad (49)$$

Where r_b is termed the *additional boundary resistance* [28] and represents the apparent differences in roughness lengths of momentum z_0 and the scalar of interest z_{0s} :

$$r_b(z) = \frac{1}{ku^*} \ln\left(\frac{z_0}{z_{0s}}\right) \quad (50)$$

Recall in the earlier discussion that the difference between z_0 and z_{0s} is due to the difference in the transport processes that exist for momentum and the scalar in the IBL. Momentum is transported to a rough surface by both form drag (bluff body effect) and skin friction, whereas transport of a scalar such as vapor occurs only as a result of the mechanisms inherent in skin friction (molecular diffusion). The addition of r_b accommodates the additional transport resistance in the IBL due to the absence of form drag and the difference in the molecular diffusion properties of momentum and the scalar. Equation 49 can now be written in the form:

$$r_T(z) = \frac{1}{ku^*} \left[\ln\left(\frac{z}{z_0}\right) + \ln\left(\frac{z_0}{z_{0s}}\right) \right] \quad (51)$$

Discussion of the physical significance of r_T , r_a , & r_b

The dimensionless resistances (or resistances normalized for wind speed), u^*r_a and u^*r_b (or $1/k \ln[z/z_0]$ and $1/k \ln[z_0/z_{0s}]$), assume a *flow structure* in both the dynamic and Interfacial Boundary Layer zones that does not change with wind velocity (ie. z_0 and z_{0s} do not change with u^*) and the *rate of vertical transport* of scalars in each of these zones is assumed to be *directly proportional* to the frictional velocity, u^* (or the mean wind speed). This is well established in the DSL where u^* is analogous to the tangential velocities of the vertical eddies. An increase in u^* corresponds to a direct increase in transfer due to advection by these eddy currents, however, because wind speeds and flow structures inside the canopy are not well understood [26] the assumption that the flow structure in the IBL (inside the turf canopy) remains constant with wind speed may not be true. This is especially the case if a transitional flow state (intermediate between turbulent and laminar flow) exists in the canopy at lower wind speeds. As stated before, a transitional flow state affects the relative contributions of skin friction and form drag in momentum deposition and change the ratio of z_0 (combination of skin friction and form drag) to z_{0s} (scalar transport by mechanisms in skin friction).

Chamberlain [25,32] measured and reviewed $1/k[\ln(z_0/z_{0s})]$ for several scalars from different surfaces. These values are published in many sources as the reciprocal Stanton number B^{-1} [28, 29, 30]

$$B^{-1} = \frac{r_b}{u^*} = \left[\frac{1}{k} \ln \left(\frac{z_0}{z_{0s}} \right) \right] \quad (52)$$

B^{-1} is a measurable parameter when the wind profile behavior is known (u^* and z_0 in eq.30), when the flux of the scalar between the surface and the air stream is measurable (F_c) and when an estimation can be made of the concentration difference of the scalar between the measurement height and the surface ($z=h$ and $z=z_{0s}$ in eq. 21). In general terms, B^{-1} represents the difference in resistance to transfer of momentum r_a and the scalar of interest r_T due to absence of form drag and difference in molecular diffusion properties of momentum and the scalar. If r_T and r_a are measurable, according to equations 49 and 51, B^{-1} is shown to be:

$$B^{-1} = \frac{r_T - r_a}{u^*} \quad (53)$$

Chamberlain [26] conducted a series of wind tunnel experiments where he measured rates of deposition of radioactive thorium (thorium-B) and evaporation of water and heat between grass and artificial grass. The following data in Table 3 from Chamberlain's experiments show that B^{-1} (or the ratio of z_0/z_{0s}) changes with u^* .

Two trends should be noted from Chamberlain's data for turf grass. Under constant temperature conditions, there is an increase of B^{-1} with u^* , giving evidence to a change in flow structure (or the relative contributions of skin and form drag to momentum deposition) with u^* . This pattern is typically observed for scalars from many surfaces including grass (see Appendix A). A second trend displayed in Table 3 is scalars with higher Schmidt numbers (ratio of kinematic viscosity, ν , to molecular diffusion coefficient, D_a) have a greater boundary resistance for particular surface than a scalar which has a lower Schmidt number. The average ratio of $B^{-1}(\text{Th})/B^{-1}(\text{H}_2\text{O})$ for $u^*=25, 50, 100$ cm/s above artificial grass is 1.6 [26]. It is believed by this author that this is due to the increase of critical molecular diffusion path length, L_{crit} with D_a in equation 11. The greater distance a molecule must travel by molecular diffusion before being susceptible to transport by eddy currents would increase the apparent resistance to transport in the IBL. *The trend of increasing B^{-1} w/ Sc is indicative of the molecular diffusion process being significant in determining the transport properties of the scalar in the ISL.*

B^{-1} for pesticides from turf grass

Since the pesticides used in this study have a similar diffusion coefficient as thorium vapor (0.035-0.042

***Table 4: Measured values of B^{-1} for various substances for grass and grass-like surfaces [25,32].**

Surface	Substance (Scalar)	Sc (v/D_a)	u^*	Re*	B^{-1}	z_0 (cm)	z_{0s} (cm) $z_{0s}=z_0 \exp(-kB^{-1})$
grass (7 cm length)	thorium-B	2.87	50	225	7.7	0.7	0.0322
short grass	thorium-B	2.87	25	32	7.9	0.2	0.0085
short grass	thorium-B	2.87	50	65	8.7	0.2	0.0062
short grass	thorium-B	2.87	100	129	10.3	0.2	0.0032
artificial grass§ (h=7.5 cm)	thorium-B	2.87	25	161	7	1	0.0608
artificial grass§ (h=7.5 cm)	thorium-B	2.87	50	323	8	1	0.0408
artificial grass§ (h=7.5 cm)	thorium-B	2.87	100	645	10.1	1	0.0176
artificial grass§ (h=7.5 cm)	water vapor	0.65	25	161	4.5	1	0.1653
artificial grass§ (h=7.5 cm)	water vapor	0.65	50	323	4.9	1	0.1409
artificial grass§ (h=7.5 cm)	water vapor	0.65	100	645	5.8	1	0.0983
short grass (open air)	heat	0.69	25	52	5.7	0.32	0.0327
short grass (open air)	heat	0.69	25	52	3.9	0.32	0.0672
*Guerra (open air) ($Z_0=7.6 \cdot Z_{0s}$ for grass)	heat/water vapor				5.07	0.32	

***Table 5: Measured vs. Predicted values of B^{-1} for grass and grass-like surfaces in Wind Tunnels.**

Surface	Sc (v/D_a)	u^*	z_0 (cm)	B^{-1} Measured [25]	B^{-1} Shephard [40]	B^{-1} Brutsaert [26] †	B^{-1} Chamberlain [32]
grass (7 cm length)	2.87	50	0.7	7.7	13.6	42.9	61.6
short grass	2.87	25	0.2	7.9	8.9	24.5	25.6
short grass	2.87	50	0.2	8.7	10.6	30.1	35.0
short grass	2.87	100	0.2	10.3	12.3	36.7	47.9
artificial grass§ (h=7.5 cm)	2.87	25	1	7	12.8	39.1	52.9
artificial grass§ (h=7.5 cm)	2.87	50	1	8	14.5	47.41	72.76
artificial grass§ (h=7.5 cm)	2.87	100	1	10.1	16.18	57.3	98.7
artificial grass§ (h=7.5 cm)	0.65	25	1	4.5	9.2	15.9	16.0
artificial grass§ (h=7.5 cm)	0.65	50	1	4.9	10.9	19.9	21.9
artificial grass§ (h=7.5 cm)	0.65	100	1	5.8	12.5	24.6	29.9
short grass (open air)	0.69	25	0.32	5.7	6.5	11.2	10.1
short grass (open air)	0.69	25	0.32	3.9	6.5	11.2	10.1

Da (cm²/s)-molecular diffusion coefficient of substance in air (25°C)

Sc-Schmidt number (v/D_a) where v is the kinematic viscosity of air (0.155 cm²/s @25°C)

u^* (cm/s)-frictional velocity

Re*-Roughness Reynolds number ($u^* \cdot z_0/v$)

B^{-1} -Reciprocal Stanton Number (defined in eq. 35)

z_0 -momentum roughness length

z_{0s} -scalar roughness length

*excerpt of Appendix 1

§-Artificial grass (height-7.5 cm, width 0.5 cm,

*Guerra (1990) estimates $Z_0/Z_{0s}=7.6$ for water and heat from turf grass [22].

†-predicted by equation 55 [40]

‡-predicted by equation 54 $a=7.3$, $m=0.25$, $n=0.45$, $c=-5.5$ [26]

§-predicted by equation 54 $a=0.5$, $m=0.25$, $n=0.8$, $c=0$ [32]

Sc=2.87, thorium-B deposition

Sc=0.65, water vapor evaporation

Sc=0.69, heat evaporation

for pesticides, 0.054 for Th), the measured values of B^{-1} for thorium-B can be used as a lower limit estimate for B^{-1} of pesticides from turf grass, however some methods of predicting B^{-1} for a scalar/surface combination at different wind speeds will be investigated.

Review of Methods for predicting B^{-1} for a Scalar/Surface Combination

There are many equations which attempt to estimate B^{-1} for certain scalar/surface/wind speed combinations. These are reviewed by Brutsaert [26] and are given a thorough treatment of their usefulness and limitations. None of these equations appears to be universally applicable to all surfaces and some work better for some surfaces than for others.

Brutsaert in his book "*Evaporation into the Atmosphere*" [26] evaluated many equations of B^{-1} for roughened surfaces. Many incorporate a product of the roughness Reynolds and Schmidt numbers:

$$B^{-1} = a \left(\frac{u_* z_0}{\nu} \right)^m \left(\frac{\nu}{D_a} \right)^n + c \quad (54)$$

$1/5 < m < 1/2$ dependent on shape, density and orientation of the leaves and on the intensity of the turbulence [26].

$1/2 < n < 2/3$ dependent on shape, density and orientation of the leaves and on the intensity of the turbulence [26].

u_* (cm/s) frictional velocity

z_0 (cm) roughness length for momentum

D_a (cm²/s) molecular diffusion coefficient of scalar

ν (cm²/s) kinematic viscosity

c -constant, probably determined for a specific boundary condition as in eq.17

a -constant specific to a surface type

Forms of equation 54 have generally worked well for predicting B^{-1} for scalar transfer between many types of flat surfaces with *bluff roughness elements*. Roughness elements characterized as having bluff features generally have geometric parameters which are similar in magnitude in their three dimensions and spacing. Examples include sand, small wave and ripple patterns, blocks, spheres, cars and buildings. However, forms of equation 54 have generally proved to be poor predictors of B^{-1} for vegetation with protruding, *permeable roughness elements* such as corn, wheat, and grass. Two surfaces, one with permeable roughness (such as grass), and the other with bluff features, each having the same drag coefficient C_D and roughness length z_0 (eq. 31) can have very different values of z_{0s} (Fig. 23) due to the relative contributions of skin friction and form drag in momentum transfer to a surface. In summary it is difficult to calculate a value of B^{-1} (a ratio of z_0 to z_{0s}) from z_0 for all surface types, since it attempts to resolve the differences in form drag and skin friction from a single lumped parameter (z_0) which incorporates both.

A method which appears to have potential for estimating B^{-1} values for vertical crop stands was originally developed by Brutsaert [27]. Brutsaert's analysis of his model for different crop canopies even incorporated the data of Chamberlain (Table 3) to determine some empirical parameters for its application to turf grass. A complete description of the assumptions and derivation of the equations used in Brutsaert's model is given in [26, 27]. Unfortunately current limitations in the knowledge of many of the input parameters of the turf grass study (such as foliage density, extinction parameter for wind speed with height in eq. 33, and the value of the eddy mixing length, l , in the canopy), compounded with many assumptions the model makes of scalar transport in the canopy³ and the few number of case studies it has been applied, prevent its application to our particular pesticide evaporation study. Despite limitations in its application to the present set of experimental data for pesticide evaporation from turf grass, Brutsaert's model appears to be a thorough approach in estimating boundary resistance terms for different scalars from turf grass and other crop canopies. It is recommended that future attempts in modeling pesticide evaporation from canopies take advantage of the opportunity to examine this model and determine its usefulness.

An equation, adapted by Chamberlain [32] from a theoretical equation proposed by Sheppard [40] for evaporation from water surfaces, appears to work fairly well for predicting B^{-1} for scalars from short grass:

$$B^{-1} = \frac{1}{ku_*} \ln\left(\frac{ku_* z_0}{D_a}\right) \quad (55)$$

u^* (m/s) frictional velocity

k von Kármán's constant ~ 0.4

z_0 (m) momentum roughness length

D_a (m²/s) molecular diffusion coefficient (for a molecule, this can be estimated from eq.6 & 7)

Predicted vs. measured values of B^{-1} for transfer of heat, water and thorium-B vapor between air streams and grass (or grass-like surfaces) using equation 55 and two other well-known forms of equation 54 are listed in Table 4 for comparison. This table is an excerpt of Appendix 1 which lists predicted vs. measured values of B^{-1} for many surfaces [25, 32].

An advantage of using eq. 55 to estimate B^{-1} as opposed to Brutsaert's model for plant canopies and forms of equation 54 is that a value of z_0 is not needed in the final equation for flux (equation 40) and,

³ For the scrutinizing reader, some of the assumptions made by Brutsaert's equation of B^{-1} for plant canopies are: 1) eq. 23 represents wind profiles in the canopy 2) The coefficients m and n in equation 37 which depend on the scalar properties and turbulence are constant with u^* 3) A constant mixing length (l) occurs in the canopy 4) C_D is constant with u^* 5) The extinction parameter for wind speed in the canopy (eq. 23) is identical to the extinction parameter of the scalar eddy viscosity with height in the canopy. 6) The value of d in eq. 21 is typically $2/3$ the height of h .

under neutral conditions, u^* is the only micrometeorological parameter required. Equation 55 appears to attempt to represent the difference in momentum and scalar roughness lengths as due to the difference in mixing viscosities which exist at the surface for momentum (ku^*z_0) and the scalar (D_a). A drawback is that equation 55 gives poor predictions of B^{-1} for surfaces with bluff features (see Appendix 1). This is likely to be due to a difference in boundary condition (constant in equation 19) which accounts for the transition characteristics between turbulent and molecular transport near the surface. Despite the uncertainty of whether equation 55 has physical significance, it appears to accurately predict measured values of B^{-1} for scalars which have a range of Schmidt values from turf grass which exceed or are lower than the Schmidt values of the pesticides in our study and so will be used to estimate the transport resistance of pesticides from turf grass. If equation 55 is used to determine B^{-1} for r_T in equation 51, for neutral atmospheric conditions it simplifies to:

$$r_T = \frac{1}{ku_*} \ln\left(\frac{ku_* z}{D_a}\right) \quad (56)$$

Equation 56 appears to represent a linear-increasing diffusion coefficient between two endpoints- D_a and $ku_* z$. The possible physical significance of equation 56 is described in Appendix 11. Using r_T in equation 56, the equation of flux for a scalar is:

$$F_z = \frac{ku_*(C_0 - C_z)}{\ln\left(\frac{ku_* z}{D_a}\right)} \quad (57)$$

According to eq. 57, the flux of a scalar from the surface will be proportional to $u^*/\ln u^*$. This agrees with the observation that an increase in u^* corresponds to higher wind speeds over a surface which maintain a low vapor concentration above the surface, causing dc/dz to increase. In addition, higher values of u^* cause E_z to increase according to eq. 17. Both an increase of E_z and dc/dz cause the flux to increase.

Effect of Atmospheric Stability on r_T and F_z

So far, r_T and F_z have been computed for neutral atmospheric conditions and the effect of atmospheric stability $\Psi(z)$ on transport resistances has been neglected (i.e: the wind profiles have been assumed to behave according to eq. 30 instead of 29). As stated before, vertical temperature gradients affect the flux by governing the vertical movement of air parcels containing the vapor which have been in contact with the surface. During unstable conditions, when the air at the surface is warmer than the overlying air above, the vertical transport of air parcels containing the evaporating substance occurs at a much faster

rate. Neglecting the stability term in equations 56 and 57 in an unstable case is likely to underestimate the actual flux. During clear nights, when the temperature of the surface is generally much cooler than the overlying air, very stable conditions exist which suppress vertical movement of air parcels, thereby decreasing the flux. The effect of stability in determining the aerodynamic resistance, r_a is proportional with height (as for wind speed in equation 29), therefore the importance of accommodating the effect of stability in the flux equation becomes more important with increasing z . The stability term, $\Psi(z)$ expressed in terms of L in equation 29 will now be incorporated into equations 56 and 57. To justify this method of incorporation, the stability correction for r_a (aerodynamic resistance to transfer of momentum) is assumed to be the same for r_T (resistance to transfer of the scalar). In other words stability does not affect the additional boundary resistance to transfer r_b or B^{-1} . Expressing the atmospheric stability term $\Psi(z)$, in terms of the Monin Obukhov path length L (i.e: $\Psi(z)=4.7*z/L$), equations 56 and 57 can be written as:

$$r_T = \frac{1}{ku_*} \left[\ln\left(\frac{ku_*z}{D_a}\right) + \frac{4.7*z}{L} \right] \quad (58)$$

$$F_z = \frac{ku_*(C_0 - C_z)}{\ln\left(\frac{ku_*z}{D_a}\right) + \frac{4.7*z}{L}} \quad (59)$$

F_z (ug/m²/hr) Flux of pesticide at height z .

Under neutral conditions, where $L=\infty$, equations 58 and 59 simplifies to equation 56 and 57. In addition to u^* , and depending on the effect of stability,, equation 59 requires an estimate of the vapor concentration in the zone of the canopy where molecular diffusion occurs (C_0) and an estimate or measurement of the scalar concentration at height z (C_z) in the equilibrated boundary layer. If molecular diffusion is the rate limiting step in the three hypothesized stages of pesticide evaporation (volatilization->molecular diffusion->turbulent diffusion), it can be assumed that a saturated vapor concentration of pesticide vapor, which is in equilibrium with the pesticide deposits, exists in areas of the turf canopy where molecular diffusion occurs. The saturated vapor density (S.V.D.) of a pesticide can be calculated from an active ingredient's vapor pressure at a specific temperature using equation 4. A height z can also be chosen in equation 53 where $C_z \ll C_s$ and the assumption can be made that $C_s - C_z \approx C_s$. This height is dependent on the thickness and concentration gradient which exists in the boundary layer.

Boundary Layer Formation and Thickness

Some discussion must now be given to boundary layer formation over surfaces. This is crucial in being able to estimate a height above the treated surface where equation 59 is valid and estimate a height where the concentration of an evaporating substance disappears ($C_s - C_z \approx C_s$). The boundary layer is a general term used to describe an air layer at a height above a surface whose properties are affected by the features of the surface below. Air moving across a water surface will possess characteristics of water vapor concentration, temperature, and turbulent structure determined by the vapor concentration, temperature and roughness features at the water surface. As this parcel of air reaches land, its properties will gradually adjust to reflect the properties of the new surface below. Two boundary layers will be discussed. An *internal boundary layer* of thickness δ_s is the depth of the air layer which is affected, in some degree by the properties of a new surface below. In this case the air has some of the properties of the new surface and some of the upwind surface. The properties near the top of the internal boundary layer will most likely be representative of the features of the previous surface whereas the lower zone will most likely reflect the properties of the new surface. The zone in the boundary layer which has fully equilibrated with the properties of the new surface is called the *equilibrated boundary layer* (Fig 24). Flux is constant with height in the equilibrated boundary layer and logarithmic wind profile is observed [23].

The depth of the internal boundary layer δ_s has been estimated to between 1/10 and 1/30 the distance of the upwind edge of the new surface [46]. If the roughness factor is included, the boundary layer thickness for short crops under neutral conditions has been observed to follow a 4/5 power increase with distance from the upwind distance from the leading edge, and be proportional to $z_0^{1/5}$ [23].

$$\delta_s = x^{4/5} z_0^{1/5} \quad (60)$$

δ_s (m) depth of the internal boundary layer above a surface.

x (m)-the average distance between the windward edge and the center of the evaporating source.

z_0 (m)-the momentum roughness length.

The equilibrated boundary layer δ_{eq} is roughly a 1/10 the depth of the internal boundary [46].

$$\delta_{eq} = 0.1 x^{4/5} z_0^{1/5} \quad (61)$$

δ_{eq} (m)-depth of the equilibrated boundary layer above a surface.

x (m)-the average distance between the windward edge and the center of the evaporating source.

z_0 (m)-the momentum roughness length.

Figure 23: Contrast of surfaces with Permeable (top) and Bluff (bottom) roughness features. Although both surfaces can have the same roughness length, the ratio of form drag to skin friction as a mechanism of momentum transfer is much greater for the surface with the bluff roughness features. The wind direction is perpendicular to the plane of the page.

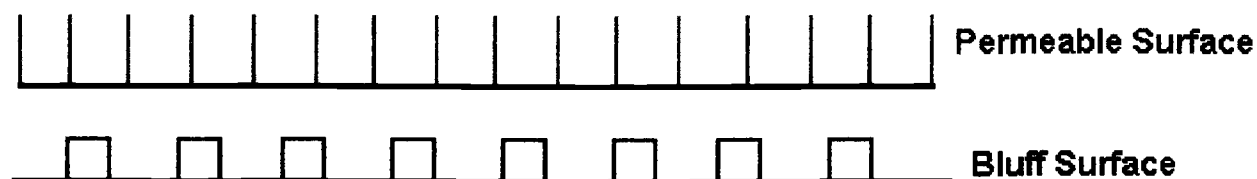


Figure 24: Boundary layer formation over a transition in roughness length. The internal boundary layer flow features are affected by the roughness features of the surface. The equilibrated boundary layer has fully adjusted to the roughness features of the surface (i.e: momentum flux is constant with height).

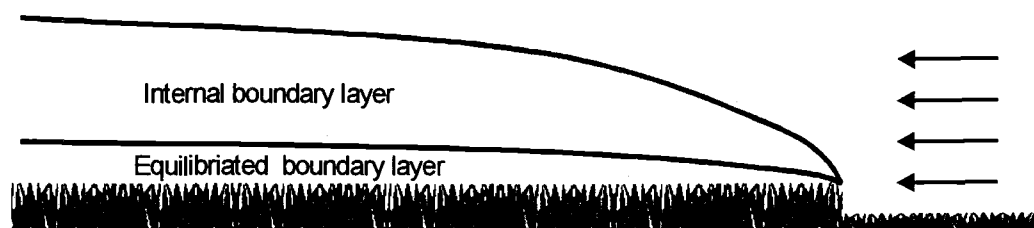
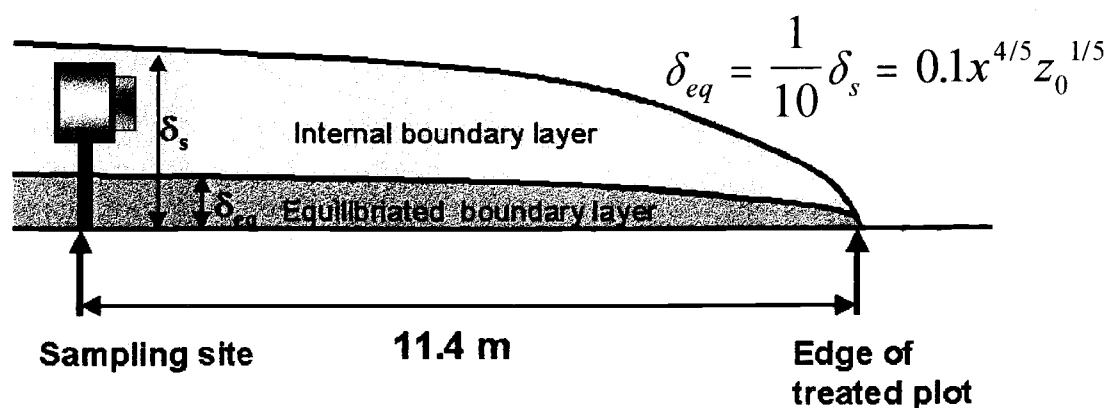


Figure 25: Boundary Layer formation over an evaporative surface. An internal boundary layer of thickness δ_s is the depth of the air layer which is affected by the evaporative properties of the surface. The equilibrated boundary layer δ_{eq} has fully adjusted to the evaporative properties of the surface (i.e: vapor flux is constant with height). According to Munro and Oke [45], the value of δ_{eq} is about 1/10 the value of δ_s and the value of each is given by the equation below.



Since the existence of the logarithmic wind profile and constant flux with height are assumptions in the derivation of equation 58, the equation for r_T only works in the equilibrated boundary layer. A problem occurs using δ_{eq} as the height z , in equation 59, where $C_s - C_z = C_s$ since the concentration of evaporating species does not disappear at this height. Although δ_s is a likely height where $C_s - C_z = C_s$ occurs, δ_s cannot be used for z since the change in concentration of the evaporating substance with height follows a different pattern than what is assumed by equation 58. Since z appears in the logarithmic form in the denominator of equation 59, a fictitious height can be chosen, with minimal error, between δ_s and δ_{eq} where the logarithmic wind profile is obeyed, the flux of the scalar is constant with height and $C_s - C_z = C_s$. A height below the half-way distance ($5 * \delta_{eq}$) between the top of the internal boundary layer and the surface is chosen since the concentration gradient is greater in the equilibrated boundary layer, where flux is constant with height, than the remainder of the internal boundary layer where flux decreases with height. This height is guessed to be roughly three times the thickness of an equilibrated boundary layer of thickness δ_{eq} given in equation 22 where x , in this case, is the distance from the windward edge of the evaporating surface to the point of measurement (i.e. in this case, x is the distance from the edge of the plot to center).

$$z = 3 * \delta_s = 0.3 x^{4/5} z_0^{1/5} \quad (62)$$

The effect of error in the assumption that $C_s - C_z = C_s$ at $3 * \delta_{eq}$ is slight since z appears in the logarithmic form of the denominator in equation 59. The sensitivity of calculated flux to change in z is discussed later. The use of equation 62 for calculating z in equation 59 accommodates the change in flux with distance from the edge of the evaporating surface due to the accumulation of vapor in the air parcel as it travels over the evaporating surface. Since concentration gradients are the driving force in flux, more evaporation will occur near the windward edge of the plot, where the vertical concentration gradients are very large, than near the leeward side. Therefore, if the same pesticides are applied to the same grass, and the same environmental conditions are experienced, the evaporation rates per area will be larger for a small plot than for a golf course.

The spatial distribution of pesticide evaporation over a plot is beyond the scope, especially when equation 62 is an assumption and its validity may change with plot size and atmospheric stability. The variable x , in equation 62, will represent the average distance between the windward edge and the center of the evaporating surface and the calculated flux at the center will represent an average for the entire plot.

Summary of Diffusion

Flux is determined by a concentration difference spanning a transport resistance, r_T in a fully formed

boundary layer, where flux of a scalar is constant with height. The fugacity method of predicting flux of pesticides from a turf surface relies on the following assumptions:

1. The concentration difference of vapor at two heights is related to the integral of the reciprocal diffusion coefficient between two heights (eq.36) . This relationship extends through both the dynamic and Interfacial Boundary Layers and assumes flux is constant with height and the eddy diffusion coefficient increases proportionally with height.
2. The eddy viscosity, E_z at height z above a surface is assumed to be equivalent to ku^*z . The viscosity at heights inside the canopy, where wind speeds and eddies have diminished and transport occurs by molecular diffusion, the viscosity is equivalent to the molecular diffusion coefficient of the pesticide.
3. Molecular diffusion dominates vapor transport at heights in the canopy where $E_z < D_a$, where D_a is the molecular diffusion coefficient of the pesticide. The molecular diffusion coefficient of a pesticide can be approximated and adjusted for temperature using equations 6 & 7.
4. A saturated vapor concentration of pesticide, which is in equilibrium with the pesticide deposits is believed to exist in the zone of the canopy where molecular diffusion occurs. This relies on the assumption that molecular diffusion is rate limiting step in the overall volatilization and transport processes.
5. A height z , is chosen for equation 59 where the concentration is guessed to be about two magnitudes lower than the vapor concentration in the canopy where molecular diffusion occurs. The height z is postulated to be about three times the thickness of the equilibrated boundary layer for the evaporating substance δ , given in equation 22.

Incorporating the assumptions from both the volatilization and transport sections, the final predictive equation for flux of a pesticide from a turf surface during the period immediately following application is:

$$F_z = \frac{ku_*[S.V.D.(T)]}{\ln\left(\frac{0.3ku_*x^{0.8}z_0^{0.2}}{D_a}\right) + \frac{1.41x^{0.8}z_0^{0.2}}{L}} \quad (63)$$

S.V.D.(T) (ug/m³) saturated density of pesticide vapor calculated from a pesticide's vapor pressure at a particular temperature and molecular weight using eq. 3 and 4

D_a (m²/s) molecular diffusion coefficient of pesticide (calculated from a the compound's molecular weight of a using eq. 6 and adjusted for temperature using eq. 7)

u^* (m/s) frictional velocity (calculated from wind speed profiles under neutral conditions using eq. 29 and 30)

k von Kármán's constant ~0.4

x (m) average distance between the edge and center of the treated plot.

$3ku_*x^{0.8}z_0^{0.2}$ (m) is the height chosen in boundary layer where $C_z < S.V.D.(T)$ this is assumed to be three times the thickness δ_{eq} given for the distance x from the windward edge of the evaporating surface by equation 62.

z_0 (m)-the momentum roughness length.

L (m)-the Monin Obukhov measurement of atmospheric stability. $L=\infty$ in neutral conditions $L= -5m$ during unstable conditions, and $L= +5m$ during stable conditions.

Equation 63 assumes zero-order kinetics, i.e. that the intensity of volatilization is independent of concentration of pesticide on the leaf surface. This ignores the effect of spray density determining the vapor concentration at the surface and the effect of decreasing canopy vapor concentration with time as the size and frequency of pesticide deposits diminish. This assumption is not supported by data collected by Jenkins [3] which shows an exponential decay pattern of flux over the duration of the experiment. Hence, equation 63 is likely to over-predict flux values. An improvement of the S.V.D.(T) term equation 41 would account for initial pesticide concentration and diminishing concentration with time. An example is given below for a simple exponential decay in flux:

$$\text{VaporConcentration } (T,t) = S.V.D.(T) * \frac{S.D.}{S.D. \text{ for } S.V.D.(T)} * e^{-kt} \quad (64)$$

Vapor Concentration (T,t)- substitute for S.V.D.(T) in eq. 41.

S.V.D.(T)-saturated vapor density of pesticide at temperature (T) (ug/m³).

S.D.-Spray Density (ug/m²).

S.D. for S.V.D.(T)-minimum spray density for grass which creates a case of saturated vapor concentration.

k-exponential decay coefficient where k=f(chemical, time, grass/surface type, average temperature, rain fall/irrigation, wind, initial spray density, photolysis, hydrolysis, leaf partition, deposit formation, spray formulation, etc.)

The form of equation 64 is debatable, since a single phase decay assumes that all of the processes which cause the pesticide vapor to diminish with time (evaporation, degradation, metabolism, etc.) is constant with time. In addition, k is probably not the same for all pesticides and is likely to be a function of many variables which cannot be determined in this study. In it's present form, equation 61 will be used to predict flux in the worst-case scenario, i.e. where pesticide exists in high enough concentrations to maintain a saturated vapor concentration of pesticide vapor over the area of the plot.

Experimental

Theoretical Profile Shape Method.

The predictive model for pesticide evaporation, which is based on aerodynamic resistances to transfer, will be compared with estimates of evaporative loss using the Theoretical Profile Shape Method.

The Theoretical Profile Shape (TPS) method of estimating gaseous mass transfer from a small plot circular plot was developed by Wilson in 1981 [16]. The plot requirements are that the plot be circular, spatially homogeneous in source strength of the evaporative substance of interest and aerodynamic surface roughness. An upwind fetch of equivalent surface roughness is required to ensure an equilibrated momentum boundary layer (eq. 61) at the height of the sampler. The size of upwind fetch is dependent on plot size and aerodynamic roughness lengths (see equation 16) and must be free from objects which have an aerodynamic element which would disrupt the wind speed profiles and turbulent homogeneity (trees, cars, etc). The TPS method is based on the Trajectory Simulation model [16] which simulates particle trajectories in a fully developed boundary layer. Theoretical concentration profiles of evaporating particles above the plot surface are generated by the averages of many simulated trajectories from the evaporating surface. The following equation is used by the TPS method to relate the product of the average measured airborne concentrations (c) and wind speed profiles (u) at a specific height (z) above the plot to the rate of loss from the evaporating surface $F_z(0)$:

$$F_{z=0} = \frac{\overline{u_z c_z}}{\Phi_{z,R,L,z_0}} \quad (65)$$

$F_{z=0}$ - flux from evaporating surface, $z=0$ ($\mu\text{g}\cdot\text{m}^{-2}\cdot\text{hr}^{-1}$)

c_z -airborne concentration of evaporating particles at height z ($\mu\text{g}/\text{m}^3$).

u_z -the average wind speed (m/s) at height z during sampling interval.

Φ_{z,R,L,z_0} -ideal flux (unit-less) defined as a factor which relates the product of the wind speed and concentration profiles at height z to the rate of loss from the surface. $\Phi=f(z, R, L, z_0)$ [16]

The normalized flux (NHF) value Φ depends on the plot radius (r), the atmospheric stability (L) and the aerodynamic roughness length (z_0). Increasing values of r , z_0 and L cause an increase in Φ . The TPS theory states that for a given plot size (r) and roughness length (z_0) *there is a height Z_{INST}^* above the center of the plot at which the dependence of Φ on L is minimal*. This height is chosen as the measurement height for wind speed (u) and airborne concentration (c) for the TPS equation since Φ remains relatively constant with varying atmospheric conditions (Fig 26).

Figure 26: Simulated values of ϕ vs. height (eq. 63) above the center for a circular plot of given roughness z_0 and radius R [16].

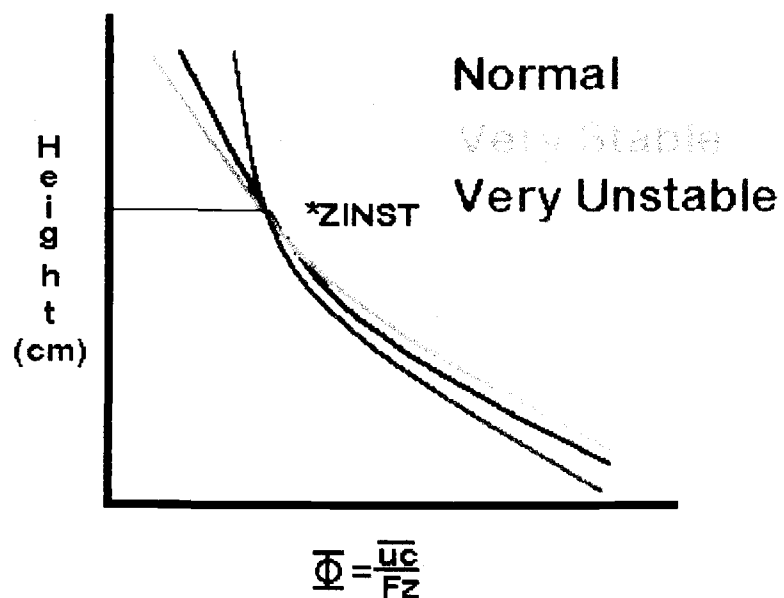
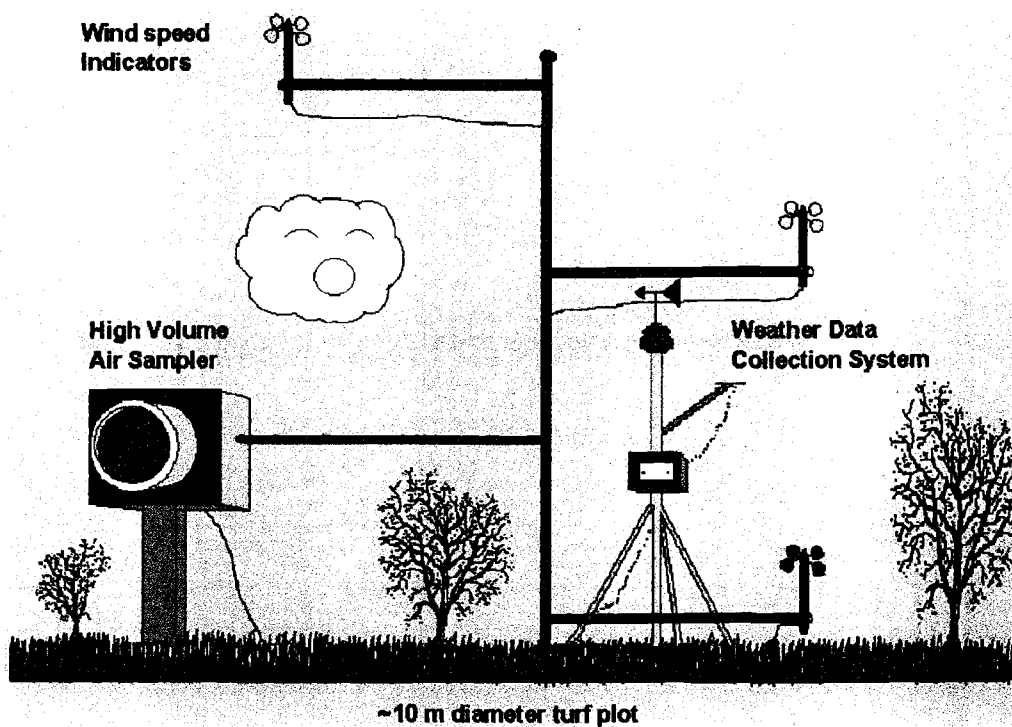


Figure 27: Experimental Setup for measuring pesticide volatilization for a turf plot using the TPS method [16].



When the requirements for the TPS method are met, it is stated to be able to estimate surface flux values within 10% of the true value[16]. Majewski compared estimates of flux of DCPA from soil using both the Thornewaite aerodynamic (TA) method (measuring wind speed and airborne concentrations at several heights in a fully developed equilibrated boundary layer) and TPS methods in an intra-plot experiment. After accounting for uncertainties in estimating flux by each method due to minor errors associated with the field site, Majewski concluded that the results of each model were within the confidence interval of the other [14]. The novel feature of the TPS method is its ability to estimate surface loss rates from airborne concentrations and wind speed measured at a *single height* above the plot. Previous models including the TA method [4] required measurements of concentrations at *several* heights above the evaporating surface and required an evaporating source several times the size required by the TPS model. The multiple sample analysis' and larger plot needed for the TA method is associated with a tremendous increase in expense.

The Experiment (Fig. 27)

All field trials were conducted at the Lewis Brown Horticulture Farm near Peoria, Oregon. Pesticides were applied to the same plot to minimize the variability associated with application, field conditions and climate. A 75' x 75' (22.8 m x 22.8 m) orchard ryegrass plot was selected based on wind patterns during the summer months. The TPS model requires the experimental plot "with a large upstream fetch of uniform conditions-uniform source strength, roughness length, wind field and turbulence" (Wilson 1982). The plot was cultivated and heavily irrigated prior to the experiment. No irrigation took place during the field trials. Growth inhibitor was applied to the turf plot several days before pesticide application to maintain a constant roughness length during the duration of the experiment.

Turf agronomists from the Horticulture Department of Oregon State University were consulted regarding pesticides combinations, application rates, and timing. For each application, an herbicide, insecticide and fungicide with contrasting vapor pressures were selected. All pesticides were applied to the same plot. Pesticides were applied at 6:00 am on Day 0 using walk-over sprayers to apply each pesticide. Rates of application were according to the manufacture label. Tank samples were obtained and analyzed to confirm the active ingredient content stated by the manufacturer.

Application timing was based on future weather predictions for clear skies and no precipitation. Clear skies were in favor to be able to view the relationship between flux intensity with solar radiation. Rainfall causes a redistribution and/or an attenuation of pesticides on the leaf surface and creates a condition which is less than ideal for comparison with fugacity-based model predictions.

A CM10 weather instrument tripod (Campbell Scientific) was situated adjacent to the plot and equipped

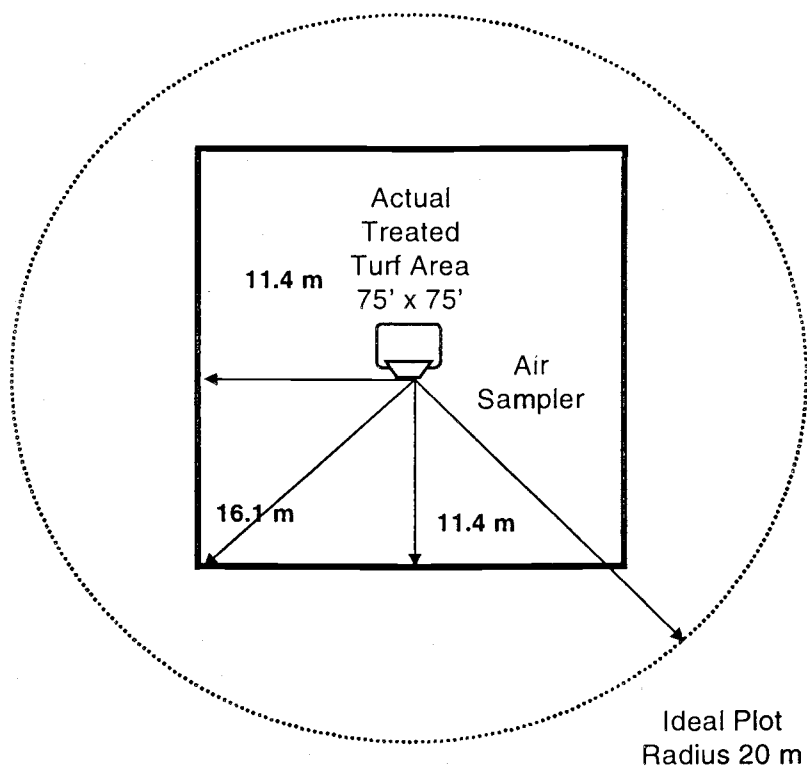
Table 6: Typical Air Sampling Schedule on Days following Pesticide Application

Day -1	Day 0*	Day 1	Day 2	Day 3	Day 5	Day 7*	Day 14*	Day 21*
	Pesticide application							
	6:00-8:00	6:00-8:00				6:00-8:00	6:00-8:00	6:00-8:00
	8:00-10:00	8:00-10:00				8:00-10:00	8:00-10:00	8:00-10:00
	10:00-12:00	10:00-12:00				10:00-12:00	10:00-12:00	10:00-12:00
12:00-14:00 (control)	12:00-14:00	12:00-14:00	12:00-4:00	12:00-14:00	12:00-14:00	12:00-14:00	12:00-14:00	12:00-14:00
	14:00-16:00	14:00-16:00				14:00-16:00	14:00-16:00	14:00-16:00
	16:00-8:00	16:00-18:00				16:00-18:00	16:00-18:00	16:00-18:00
	18:00-20:00	18:00-20:00				18:00-20:00	18:00-20:00	18:00-20:00
	20:00-6:00*	20:00-6:00*						

*Field Blank Sample Collected

#a single sample was collected during the overnight hours, 20:00-6:00.

Figure 28: Actual vs. Ideal plot conditions for the TPS method.



with instruments to measure and store local meteorological parameters. Microclimate parameters monitored continuously throughout the study included relative humidity, temperature (surface and ambient), solar radiation, wind speed profiles above the plot, and wind direction. Two soil temperature probes were positioned on a bark surface adjacent to the plot and used to record the surface temperature at the grass height. A 2.54 cm x 3 m mast with side arms was mounted in the center of the plot with four rotating cup wind speed sensors (Campbell Scientific Model 014A), wind speed above the center of the plot were recorded at 280, 140, 70 and 41 cm heights. All micro-meteorological data was collected and stored using a CR10 Datalogger (Campbell Scientific) at 1 minute intervals and averaged each half hour. Measurements of precipitation were obtained from Corvallis Hyslop farm (Appendix 4, 5, & 6).

The complete procedure for collection and processing of airborne residue samples is listed in ET&C Field SOP No. 1004-95-2. Airborne residues were collected at the determined ZINST* height (70 cm) above center the turf plot using a high volume STAPLEX TF1A air sampler with cartridges containing approximately 140 mL of Amberlite XAD-4 polymeric resin. The air samplers were calibrated to ensure accuracy of flow rate prior to the experiments. Air samples were collected during two hour intervals. Beginning and ending air-flow rates were recorded. Air flow rates were typically 1 m³ per minute. Control air samples were collected the day before application (Day -1) and analyzed to verify the absence of background concentrations of the applied pesticides. Field blanks were also prepared, labeled, shipped to the sampling site, processed, stored and analyzed in the same manner as the field residue samples.

The air sampling schedule was designed with the two-fold intent of being able to monitor diel changes in the flux intensity over the day period and to properly characterize the attenuation pattern of peak flux on receding dates from the day of pesticide application. Previous experiments, conducted by Jenkins, exhibited a diel flux pattern which correlated with daily patterns in solar radiation with a peak flux occurring during mid-day. The attenuation pattern of peak flux on days following pesticide application also showed an exponential or geometric decline (deviations were observed when measured solar radiation was significantly different or a weather event occurred between days). To characterize the decay curve of flux vs. days from the application date, the sampling dates were scheduled more frequently on days close to application. On sampling dates when flux patterns for the entire day were not measured, a sample was collected during the noon hours to estimate peak flux. Table 6 displays a typical sampling schedule for each series of pesticide applications:

Air sampling began at 0600 hours immediately following application. Samples were collected continuously for the first 2 days at 2-hour intervals from 0600 to 2000 hours. A single overnight sample was collected between 2000 to 0600 hours on the day of application and the following day.

Processing of air samples:

All samples were processed within 24 hours of collection. The sampled XAD-4 resin cartridges were stored on ice and in the dark to prevent re-volatilization of the residues. Preparation, storage and analysis of the samples occurred at the Environmental Chemistry and Toxicology (ET&C) Laboratory. Processing included quantitatively transferring the resin, with ~50 mL ethyl acetate, from the cartridge to a 150 mL glass jar with an aluminum foil-lined cap. The samples were packed, logged according to ET&C SOP No 1004-95-3 and stored in a freezer at -20°C until analysis.

Extraction and analysis Procedure

Chemical Analysis of the airborne residues was performed at the Environmental Toxicology and Chemistry Analytical Laboratory, Department of Agricultural Chemistry, Oregon State University, Corvallis, Oregon. Primary Standards were obtained for the following compounds:

1. Chlorpyrifos: CAS# 2921-88-2
Chem Service Inc., reference # 136-128B, 99.0%. 1.0 g received.
2. Triadimefon: CAS#43121-43-3
Chem Service Inc., reference #151-96A, 98%. 1.0 g received.
3. Ethofumesate: CAS#26225-79-6
Chem Service Inc., reference #137-121A, 99%. 1.0 g received.
4. Bensulide: CAS# 530-6079
Chem Service Inc., reference #136-118A, 98.0%.
5. Fenarimol: CAS# 60168-88-9
Chem Service Inc., reference #166-51A, 99.8%. 1.0 g received.
6. Propiconazole: CAS# 60207-90-1
Chem Service Inc., reference #162-44B, 96% mix of isomers .
7. Cyfluthurin: CAS# 68359-37-5
Chem Service Inc., reference #162-74B, 98% mix of isomers.
8. Diazinon: CAS# 333-41-5
Chem Service Inc., reference #174-13A, 99%.
9. Prodiamine: CAS# 29091-21-2
Sandoz Agro, Inc., reference #RS-PRO-072595, 99.91%
10. Triclopyr (butoxyester or acetic acid?):
Chem Service Inc., %

The complete procedure for the extraction and analysis of airborne samples is documented in "Determination of Airborne Residues of Turf#3 Pesticides in XAD-4 Resin by GC-MS. Project #NRI 1004-95/96". Each batch run consisted of an appropriate number of QC samples to insure batch extraction quality. No more than one field matrix blank and one fortified matrix blank were extracted for each sample set. Fortification levels were adjusted to approximate levels found in field samples.

Samples were allowed to warm to room temperature before extraction. The air samples, which included ~150 mL of wet resin/ethyl acetate, were poured from the original sample bottle to a labeled 500 mL Erlenmeyer flask. 150 mL of additional ethyl acetate was used to quantitatively transfer the resin and

residues from the sample bottle to the flask. The flasks were placed on a wrist action shaker for 1 hour. After shaking, the flasks were removed and the solvent was decanted and filtered through a glass funnel containing a Whatman #1 filter, into a 250 mL Erlenmeyer flask. An additional 75 mL of ethyl acetate was added to the original flask (still containing the resin) and replaced on the wrist action shaker for an additional fifteen minutes and decanted. This was repeated. After the third extraction, the remaining resin in the original Erlenmeyer flask was poured into the glass funnel containing the Whatman #1 filter. Three portions of 50 mL ethyl acetate were used to rinse the original Erlenmeyer flask and transfer the remaining residue to the funnel. Each rinse was allowed to soak and drain through the resin bed before adding the next.

Concentration of the solvent extracts was performed using a Turbovap II Concentrator Work Station with endpoint detection. Each solvent extraction aliquot was added to a 200 mL TV flask and placed in the TV concentrator. Enough N₂ pressure was generated to achieve a good shearing action on the solvent meniscus (~12 psi). Successive aliquots were added to the TV flasks as volume allowed. The entire sample was concentrated to the evaporation endpoint at <1 mL and exchanged twice with 5 mL of trimethylpentane (TMP). The final concentrated extract was suspended to an appropriate dilution volume for analysis and transferred to GC vials using a syringe equipped with 0.45 µm membrane filter. The GC vials were sealed and stored under refrigerated conditions for a maximum period of one week.

Analysis of the airborne residues was performed using a Hewlett Packard HP6890 GC equipped with a HP 6890 Mass Selective Detector, HP GC Autosampler Controller and Series Injector. The chromatograph included DB-17 Column (J&W 122-1732, 30 m x 250 µm, 0.25 µm film thickness). The injection port contained a 1.5 mm Quartz Liner and an HP11 mm Solsept Septa. Pulsed splitless injection was used.

GC/MS data collection and analysis was performed on a Hewlett Packard Vectra XM Series 3 Terminal Controller with HP Chemstation. A gradient oven program was used to separate the pesticides contained in each of the air samples. Select Ion Monitoring (SIM) was used to quantify the relative mass abundance of selected ion fragments for each pesticide. Relative ion abundances for each pesticide mixture were quantified using an external calibration curve $r^2 > 0.995$. High and low check standards from the interior of the calibration curve were run every six samples.

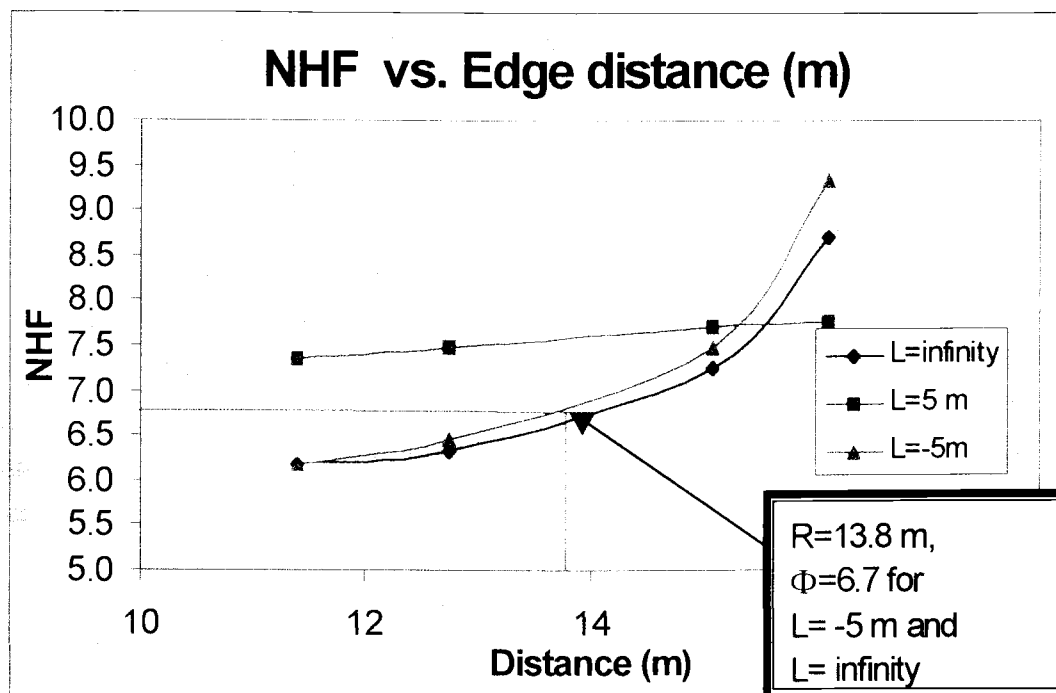
Data Analysis:

Analysis and plotting of flux results and weather data was conducted using linked Excel™ spreadsheets. The wind speed reading at 70 cm will be used as an approximate estimate of the wind speed at 73 cm, the air sampling height in equation 65. Airborne pesticide concentrations c (ug/m³) at the sampling

Table 7: Generated values of Φ ($z=0.73$ m, $z_0=.0045$ m, plot dimension 22.8 m x 22.8 m) using the Backward-Time Lagrangian stochastic Dispersion model [45], calculation for specific plot conditions courtesy of T. Flesch [46]

Wind direction normal to face of square plot ->	0°	15°	30°	45°
Upwind distance to the edge of the treated plot	11.4 m	12.75 m	15.08 m	16.12 m
L=infinity	6.17	6.33	7.25	8.70
L= -5 m	7.35	7.46	7.69	7.75
L= 5 m	6.17	6.45	7.46	9.35

Figure 29: Plot of generated values of Φ ($z=0.73$ m, $z_0=.0045$ m, plot dimension 22.8 m x 22.8 m) using the Backward-Time Lagrangian stochastic Dispersion model [45], vs. upwind distance from treated edge (m). Calculation for specific plot conditions courtesy of T. Flesch [46]



height above the plot (73 cm) were calculated by dividing the total residues collected by the air sampler (ug) by the air sampler flow rate (m³/hr), and dividing by the sampling duration (min):

$$\bar{c} \text{ (ug/m}^3\text{)} = \frac{\text{total collected residue @ 73 cm (ug)}}{\text{sampler flow rate (m}^3\text{/hr)} * \text{sampling interval (hr)}} \quad (66)$$

Average surface flux, $F(0)$ during the sampling interval was calculated from the average airborne concentrations at the sampling height (73 cm) and the wind speed u at 70 cm, using the TPS equation:

$$F_{z=0} = \frac{u_{70\text{cm}} \cdot c_{73\text{cm}}}{\Phi_{(z=73\text{cm}, R=10\text{m}, z_0=0.2\text{cm})}} \quad (67)$$

$F_{z=0}$ - flux of pesticide vapor from the turf grass (ug*m⁻²*hr⁻¹)

$c_{73\text{cm}}$ -airborne concentration pesticide vapor at the sampling height above the turf plot (ug/m³).

$u_{70\text{cm}}$ -the average wind speed (m/s) at the sampling height during the air sampling interval.

Φ -ideal flux (unit-less) defined as a factor which relates the product of the wind speed u and concentration profiles c at the sampling height to the rate of loss from the surface F . This value is generated by the BTLSD method as a function of plot radius R , roughness length z_0 , sampling height, and atmospheric stability L [45, 56].

Input parameters for the predictive (fugacity) and BTLSD models

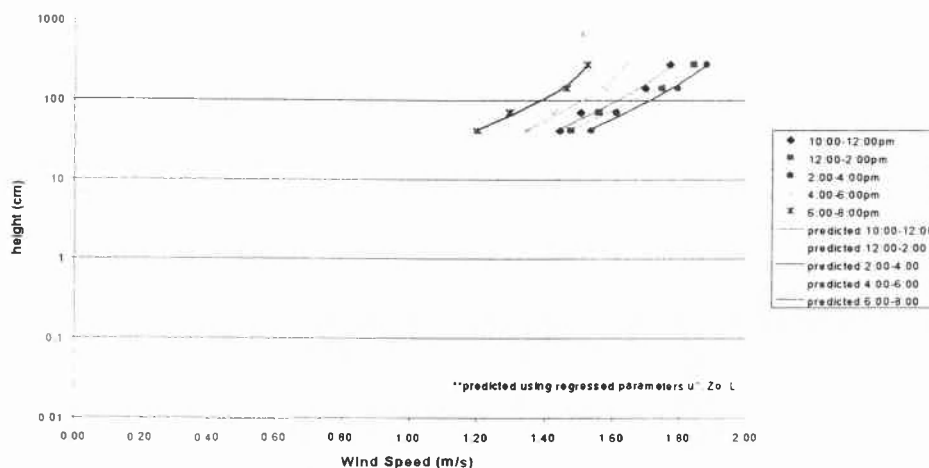
Table 8 lists the input parameters required by each model (fugacity and the Backward-Time Lagrangian stochastic models) and a brief description of the sensitivity of the flux to the input. Input parameters for the BTLSD model are: wind speed at the sampling height $u(z)$, airborne concentrations at the sampling height z , and the value normalized horizontal flux Φ at the sampling height z , which is calculated from plot radius R , roughness length z_0 , and assumptions of an equilibrated boundary layer for momentum occurring at the sampling height z . Input parameters for the fugacity model (according to equation 63) include the saturated vapor density of the active ingredient $S.V.D.(T)$ at a measured temperature $T(K)$, the frictional velocity $u^*(\text{m/s})$, roughness length $z_0(\text{m})$, the molecular diffusion coefficient in air $D_a(\text{m}^2/\text{s})$, upwind distance from the edge of the treated plot $x(\text{m})$, atmospheric stability factor $L(\text{m})$.

Determination of u^* , L , and z_0 from wind speed profiles above the plot

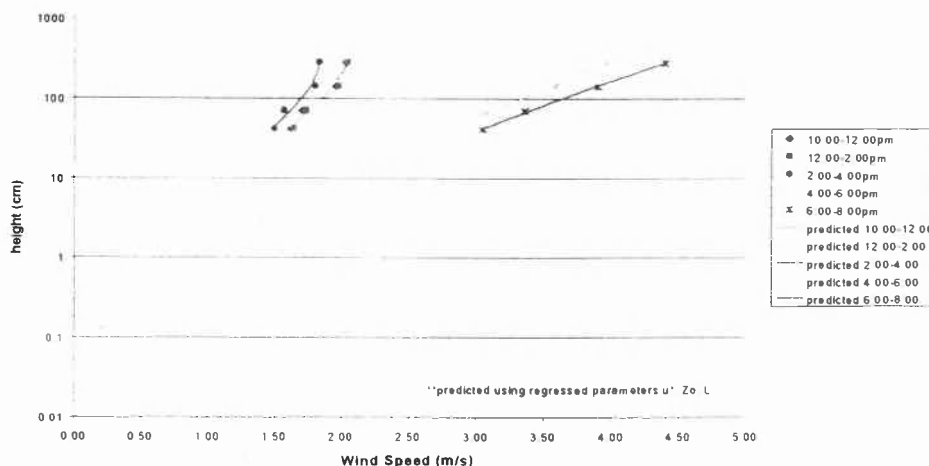
Wind speed measurements were recorded at 41, 70, 140, and 280 cm heights above the center of the plot using rotating wind cup sensors described in the previous section. The micrometeorological parameters u^* , z_0 and L are estimated from wind profiles regressions using equation 29. Empirically calculated values of roughness length z_0 , frictional velocity u^* , and atmospheric stability, in terms of the

Figures 30-32: Regressed Wind profiles above the turf plot, during Day 0, Application 1 (1995), Application 1 (1996), and Application 2 (1996).

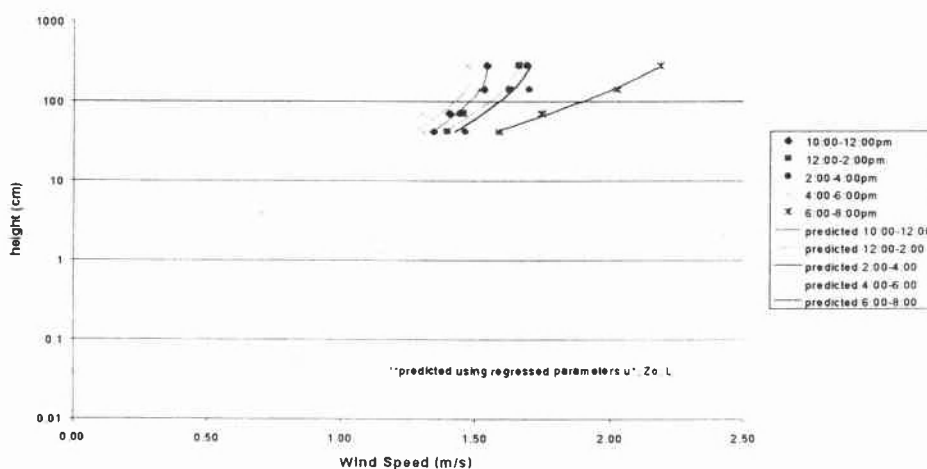
In ht (cm) vs W.S. (m/s)
Day 0, App.1 '95 July 17, Julian 198



In ht (cm) vs W.S. (m/s)
Day 0, App.1 '96 June 12, Julian 164



In ht (cm) vs W.S. (m/s)
Day 0, App.2 '96 July 23, Julian 205



Monin Obukhov path length L , were obtained using a multi-variable regression of wind speed $[u(z)]$ vs. height $[z]$, in the form of $u(z)=az +b \ln z+c$. According to equation 29, $a=u^*/k^{4.7}/L$, $b=u^*/k$ and $c=u^*/k \ln z_0$. Since von Kármán's constant k is generally agreed to have the value of 0.4, a calculation of u^* can occur from b , which facilitates a calculation z_0 from c and an estimate of L from a . The regression of $u(z)$ vs. z and calculation of u^* , L , and z_0 was conducted for wind profiles averaged over two-hour sampling intervals (Table 9). The wind speeds near the sampling height typically ranged between 0.5 and 1.5 m/s during a single day period. Plots of wind speed vs. height (Fig. 30-32) suggest that the wind cup sensors at 70 cm and 280 cm might have had a greater rotational friction (especially 280 cm). The cup-sensors were estimated by the manufacturer to have an error of 0.11 m/s and a threshold reading of 0.45 m/s. Erroneous regressions of z_0 occurred during the early mornings and overnight periods when wind speeds decreased below this threshold.

To minimize the effect of regression errors of u^* , z_0 and L , during low wind speed conditions, regressions were conducted only when the lowest wind speed indicator registered a half-hour averaged wind speed reading of at least 0.6 m/s. The average, maximum, minimum, and standard deviation of the half-hour regressed values u^* , z_0 , L and Re^* between 6:00-20:00 of Days 0 and 1 of each application, which met the criteria of $u(41 \text{ cm}) \geq 0.6 \text{ m/s}$, are listed on the following page. A complete list of the regression results for half-hour readings between 06:00 and 20:00 on Days 0 and 1 for Application 1, 95; 1, 96; and 2, 96 are listed in Appendix 4, 5, and 6.

L-Atmospheric Stability Parameter

The multivariable regression of the wind profiles to estimate z_0 , u^* and L described above was also used to estimate general ranges of the Monin Obukhov path length L . Recall that L can be used to gauge whether atmospheric conditions are very stable (where $L=-5 \text{ m}$), very stable (where $L=+5 \text{ m}$) or neutral ($L=\infty$). L can be directly measured using a sonic anemometer. The method of calculating L from the multivariable regression coefficients is not an accepted technique for determining this value by meteorologists since it uses L as a fitting parameter, making it susceptible to absorption of errors in measurement. The uncertainty is compounded by due to the fact that three regression parameters are calculated from only four data points (recall that the three parameters u^* , z_0 , and L were estimated from wind speed measurements, the effect of possible error is discussed later). The observed ranges of L , during a single day, generally fell in the expected ranges of unstable and near neutral conditions (Table 9, $L=\infty$ during neutral conditions, $L=-5$ for very unstable conditions). The importance of incorporating the effect of atmospheric stability into the TPS model becomes more important with increasing plot size and height in the predictive equation since the effect of the $\psi(z)$ becomes a greater factor in determining flux according to equation 61.

Discussion of the roughness length z_0

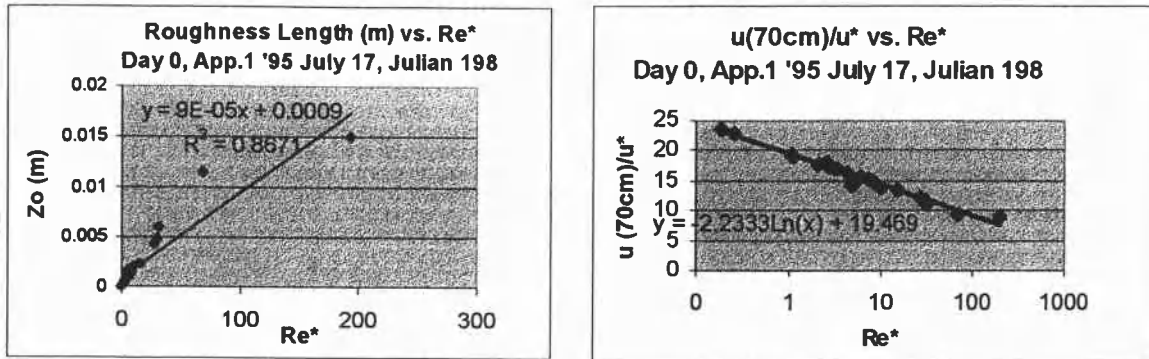
Of the parameters obtained from regression of wind speed profiles, u^* , L , and z_0 , the roughness length, z_0 is probably the most sensitive of the three to error since z_0 appears in the logarithmic form of the wind speed equation (equation 29). As stated before, the roughness length is assumed to be a constant value in cases where the air flow over the surface is fully turbulent. Empirically determined values of z_0 from regressions of measured wind speed profiles above the plot varied considerably during the period of a single day-sometimes within two orders of magnitude. To determine whether the change in observed roughness length was due to a transition in flow regimes from laminar to turbulent (the flow regime affects how momentum is transported to the surface and z_0 represents the effectiveness of the surface to absorb momentum), plots of z_0 vs. Re^* and $u(z=70\text{ cm})/u^*$ vs. Re^* were constructed (Appendix 8, Figures 33 and 34.). A correlation of z_0 vs. Re^* with a positive slope on a linear-linear (y,x) scale and a linear-log correlation between u/u^* and Re^* with a negative slope indicate the absence of a flow transition as a reason for change in z_0 [24, 26].

Figure 33 of z_0 vs. Re^* shows evidence of a transition in flow regimes at $Re^* \approx 100$, since there appears to be a slope change at this value, however it is difficult to be sure since the graph has most of its data points clustered together at low values of Re^* . The plot of u/u^* vs. Re^* (Fig. 34), for the same time interval, has a more equitable distribution of the data points in the graph range. There is no apparent change of slope which would be indicative of a flow transition, however the slope of the line (negative) is opposite to what it should be (positive) [26] indicating an anomaly in the wind speed data and/or a probable occurrence of a systematic error in the estimation of u^* and/or z_0 . This is probably due an inadequate upwind fetch of equivalent aerodynamic roughness length, necessary in creating a logarithmic wind profile which spans the height of wind sensor measurements above the center of the plot.

According to equation 61, an upwind fetch of 200 m is required to develop an equilibrated boundary layer which spans the height of wind speed measurements (280 cm). The upwind fetch of grass was approximately a tenth of this distance. A logarithmic wind profile is characteristic of an equilibrated boundary layer (constant flux of momentum with height) above a surface. Using an equation for a logarithmic wind profile where one has not completely formed would affect the accuracy of the regressed parameters u^* and L , to some degree, but would seriously affect the regressed value of z_0 since it is the parameter in equation 29 most sensitive to error.

In addition, a tree 10 m upwind from the edge of the plot during the first pesticide application in 1995 may have contributed to some turbulent interference in the wind profile over the plot (a general rule of thumb is to have interfering elements at an upwind distance at least 100 times the height of the

Figures 33 and 34: Plots of z_0 vs Re^* and $u^*/u(70)$ vs. Re^* to determine whether change in roughness length during the application date Day=0 in 1995 was due a to transition in flow regimes [24, 26]. A straight, positive slope line in each plot indicates an absence of a transition.



Figures 35 & 36: Sample plots of z_0 vs. average wind speed $u(z)$ and frictional velocity u^* to determine whether change in z_0 is attributed to wind velocity.

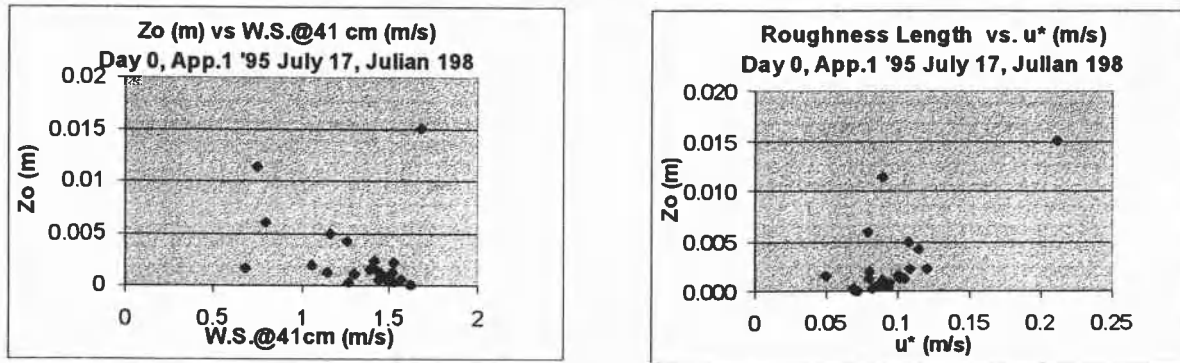
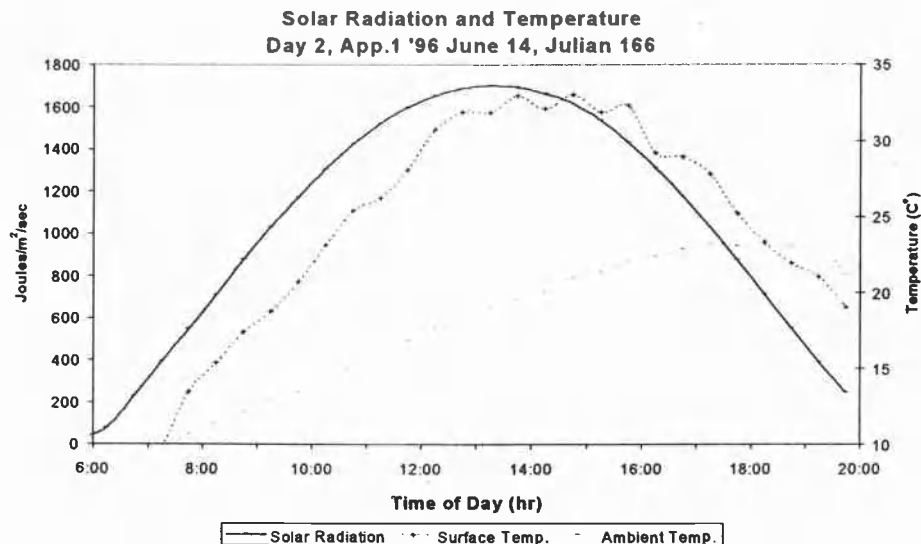


Figure 37: Plot of solar radiation and surface and ambient temperatures on a cloudless day (Day 2, App. 1996).



interfering object [44]). The tree was removed the following year while the regressed value of z_0 continued to vary. In sum, the reason for z_0 varying during a single day is not known and it is not possible to resolve the influence of a number of contributing factors.

Since the roughness length cannot be determined empirically, an estimate from the literature values displayed in Table 2 [19] will have to suffice. A literature value cannot be assumed to be completely accurate since the roughness length z_0 is dependent upon many parameters which may not be identical for all grass surfaces (foliage density, physical arrangement of grass blades relative to each other in determining the sheltering effect, individual roughness features of each grass blade etc.). A value of $z_0=0.45$ cm was estimated for grass 1" (2.5 cm) in length using literature values listed in Table 2.

Calculation of Φ using the Backward Stochastic Lagrangian Method [45]

Actual plot conditions for the experiment deviated in radius R and estimated roughness length z_0 from the plot conditions specified by the TPS model for the chosen sampling height. According to Wilson, the sampling height $z=73$ cm is based on a calculated height $ZINST^*$ for a circular plot with a 20 m radius and a roughness length $z_0=0.2$ cm. The normalized flux value for this setup is estimated to be $\Phi=9.0$ for stable and unstable atmospheric conditions ($L=+5$ m and $L=-5$ m) and 9.4 for neutral atmospheric conditions ($L=\infty$). However, in the actual case, pesticides were only applied to a square turf area of 75' by 75' (22.8 x 22.8 m) with a roughness length of 0.45 cm (estimated in Table 2 for a grass length of 1"). The distance between the air sampler and the windward edge of the treated turf area can vary between 11.4 m and 16.6 m, depending on the direction of the wind (Fig.28). A second deviation from case 3 was the roughness length. According to Table 2, a grass length of 2.5 cm generates a roughness length equivalent to $z_0=0.45$ cm instead of 0.2 cm, which is assumed by the TPS model.

Thomas Flesch performed a calculation using the backward-time Lagrangian stochastic Dispersion model (BTLSD) developed by Flesch and Wilson [45, 46] to account for the plot differences of z_0 and R . The BTLSD method is an improved form of the TPS model. It incorporates the same theory of simulated random-walk trajectories in a fully developed momentum boundary layer as the TPS model, however, instead of calculating the trajectories of all the particles leaving an evaporating surface and estimating how many particles pass the sampling location, a reverse-time simulation is conducted where an air parcel containing a number of evaporating particles is initially located at the position of the measurement device and reverse simulated (backward-calculated) to the evaporating surface (ie. how many particles, initially located at the air sampler, originate from the area of the evaporating surface). The BTLSD method is less expensive in computation time and does not require the sampling location to be at the center of a circular evaporating surface. *In fact the plot can be any shape or size and the air sampler can be positioned anywhere.* Flesch determined values of Φ for our specific plot conditions (22.8x22.8

treated surface, $z=73$ cm at the center of the square plot, $z_0=0.0045$ m) for $L=+5$ m (very stable), $L=-5$ m (very unstable) and $L=\infty$ (neutral) conditions at 0° , 15° , 30° , 45° wind angles (where the angle is 0° when the wind direction is perpendicular to the face of the square plot and 45° when the wind blows diagonally across the square plot) Table 9.

Assuming an equal probability of wind from any direction, the average distance between the air sampler and the windward edge of the treated grass is 13.86 m. Since atmospheric conditions during the day light hours are typically unstable and neutral, the average value of Φ at $L=-5$ m and $L=\infty$ at $R \sim 13.8$ m was used (Fig. 29.)

$$\Phi_{L=-5m,\infty}(R = 13.86 \text{ m}, z_0 = 0.0045 \text{ m}) = 6.7 \pm 0.5 \quad (68)$$

Although the two errors in plot radius and aerodynamic roughness length were able to be accounted for by using the BTLSD method of estimating flux from airborne residues instead of the TPS method, a third deviation in the experimental plot design which could not be corrected for was the requirement for a "large upstream fetch of uniform conditions" [16]. As stated before, during Application 1, 1995, a single tree 20 m upwind from the sampling site. This was removed the following year. The tree may have caused a turbulent wind structure slightly different from what is assumed by the BTLSD model. Although the difference is probably slight, a greater emphasis should be placed on the data collected during the data collected during 1996.

Summary and Discussion of TPS/Backward Lagrangian Stochastic Model Results

A summary of calculated BTLSD flux results for all three applications are displayed, along with environmental weather data, in Tables 11, 12 and 13.. Airborne residues were quantified for all pesticides for several days following application with the exception of Cyfluthrin in Application 2, 1996, which was non-detectable until day 21. The inability to detect Cyfluthrin during the majority of the experiment is thought to be due to the low application rate specified by the label (the application density was about ten times smaller than the other pesticides applied in this study) and the chemical's low vapor pressure.

Correlation between Observed Loss rates and Time

Average calculated flux values and instrument readings of solar radiation, surface temperature, ambient temperature and wind speed at the sampling height, were plotted on a time scale during individual days to view correlations of flux with change environmental parameters. Changes in flux on individual dates appeared to be most strongly correlated with solar radiation and surface temperature. This was especially noticeable on clear days, and less on overcast days. Peak flux during the noon hours (12:00-14:00 or 12:00-16:00) was also plotted on each sampling date (Day 0, 1, 2, 7, 14, 21) to view attenuation

Table 11: Flux results, Application 1, 1995**

	Air Sampling Period		Flux (ug/m ² /hr)		Surface	Ambient	Solar Rad.	Wind Speed	Precipitation
	Start	End	Triadimefon	Chlorpyrifos	Temp. (C)	Temp. (C)	(J/m ² /s)	@z=70 cm (m/s)	
Day 0 (July 17th)	6:50	8:00	60	548	18	19	126	0.78	
Julian 198	8:00	10:00	235	1202	27	24	874	1.27	
	10:00	12:06	544	1619	40	29	1404	1.50	
	12:06	14:00	642	1391	47	32	1639	1.56	
	14:02	16:00	697	981	48	36	1521	1.61	
	16:02	18:00	545	567	50	37	1080	1.42	
	18:02	20:00	210	229	41	36	463	1.30	
	20:00	6:03	38	61	19	22	6	1.22	
% Cumulative Loss of Amount Applied			2.0	9.7					
Day 1 (July 18th)	6:03	8:02	78	133	16	16	116	1.32	
Julian 199	10:00	12:02	259	393	30	23	911	1.18	
	12:02	14:00	443	601	40	29	1172	1.09	
	14:02	16:00	386	426	43	32	1087	1.16	
	16:02	18:00	464	544	38	31	789	2.67	
	18:02	20:03	192	275	27	27	216	3.15	
	20:03	5:59	20	22	18	19	3	0.92	
% Cumulative Loss of Amount Applied			3.3	13.3					
Day 2 (July 19th)	12:02	14:02	501	488	46	30	1557	1.24	
Julian 200	14:02	16:03	514	423	46	33	1474	1.91	
Day 3 (July 20th)	12:00	14:02	319	313	43	27	1593	1.43	
Julian 201	14:02	16:00	368	334	44	30	1468	1.75	
Day 5 (July 22th)	12:00	13:59	77	96	38	23	1330	1.34	
Julian 203	14:01	16:00	73	77	35	23	1100	1.59	
Day 7 (July 24th)	6:00	8:00	NQ	NQ	18	17	73	0.73	
Julian 205	8:11	9:59	14	21	22	18	413	0.95	
	10:00	12:02	28	37	28	21	835	1.11	
	12:02	14:00	92	121	37	23	1555	1.82	
	14:00	16:00	67	79	39	24	1520	1.57	
	16:00	18:00	89	131	38	26	1060	2.34	
	18:00	20:20	21	40	26	23	365	3.52	
Day 14 (July 31st)	6:00	8:00	NQ	NQ	13	16	64	0.98	
Julian 212	8:07	10:00	NQ	8	24	20	835	1.55	
	10:00	12:00	8	19	40	24	1374	1.80	
	12:00	14:00	15	30	46	28	1621	2.25	
	14:01	16:02	9	23	46	31	1504	2.06	
	16:02	18:02	NQ	12	44	32	1053	1.99	
	18:02	20:00	NQ	NQ	35	31	427	1.51	
Day 21 (August 7th)									0.3
Day 22 (August 8th)	6:00	8:00	NQ	NQ	11	11	81	0.76	0.5
Julian 220	8:03	10:01	NQ	NQ	22	16	777	1.03	
	10:02	12:00	NQ	8	34	20	1312	1.42	
	12:00	14:00	NQ	9	41	22	1552	1.53	
	14:00	16:00	NQ	NQ	40	23	1431	1.72	
	16:00	18:00	NQ	NQ	36	24	973	1.66	
	18:00	19:50	NQ	NQ	28	23	365	1.33	

*rainfall occurred prior to date

NQ-not quantifiable

**flux estimated from airborne concentrations using the Backward-Time Lagrangian stochastic Dispersion model (Flesch, Wilson, Journal of Applied Meteorology, 34, pp. 1320-1332)

Table 12: Flux results*, Application 1, 1996

	Air Sampling Period		Flux (ug/m ² /hr)			Surface Ambient		Solar Rad.	Wind Speed	Precipitation
	Start	End	Triadimefon	Chlorpyrifos	Ethofumesate	Temp. (C)	Temp. (C)	J/m ² /sec	(cm/s)	(mm)
								@z=70 cm		
Day 0 (June 12th)	6:41	7:59	9	166	41	13	12	382	0.78	
Julian 164	8:00	10:01	77	1046	284	22	15	941	1.46	
	10:01	12:00	242	2496	768	30	18	1457	1.71	
	12:00	14:00	450	1738	949	36	21	1683	1.73	
	14:01	16:06	405	1092	898	38	23	1490	1.56	
	16:07	17:56	341	944	851	32	24	1083	3.07	
	17:58	20:00	95	284	248	24	21	469	3.36	
	20:00	6:00	11	69	31	11	12	7	1.43	
Cummulative Loss % of Amount Applied			1.1	8.6	3.3					
Day 1 (June 13th)	6:01	8:02	7	148	64	13	10	247	0.78	
Julian 165	8:03	10:00	83	325	203	23	15	892	1.08	
	10:02	12:00	172	598	414	32	17	1235	1.36	
	12:02	14:00	178	508	409	34	19	1140	1.65	
	14:01	16:00	198	436	374	36	21	1231	1.40	
	16:01	18:00	179	377	333	29	22	797	2.03	
	18:01	20:01	110	210	157	22	19	474	3.63	
	20:03	6:00	9	23	16	10	10	8	1.13	
Cummulative Loss % of Amount Applied			1.7	11.5	4.9					
Day 2 (June 14th)	6:00	8:00	22	47	26	10	9	312	0.92	
Julian 166	8:06	10:01	47	152	138	18	12	949	1.67	
	10:03	12:00	123	308	308	26	16	1463	1.78	
	12:01	14:00	200	362	422	32	19	1684	1.85	
	14:01	16:01	220	335	418	32	21	1562	1.85	
	16:02	18:00	106	159	257	28	23	1098	1.79	
	18:01	20:00	49	57	128	21	23	475	1.66	
	20:01	6:00	6	11	12	11	11	8	0.89	
Cummulative Loss % of Amount Applied			2.2	13.1	6.3					
Day 3 (June 15th)	12:05	14:05	258	320	371	35	20	1666	1.52	
Julian 167										
Day 6 (June 18th)	12:02	14:00	126	215	176	32	17	1745	1.50	2.3
Julian 170										
Day 7 (June 19th)	6:01	8:00	3	9	9	10	11	321	1.15	0.3
Julian 171	8:01	10:00	62	107	99	18	14	967	1.72	
	10:00	12:01	40	69	60	26	17	1439	1.84	
	12:04	14:00	76	101	111	31	21	1732	1.94	
	14:01	16:00	113	108	155	30	24	1561	1.99	
	16:01	18:00	79	70	68	29	25	1136	1.88	
	18:00	20:00	13	12	21	24	25	517	1.49	
Day 14 (June 26th)	6:00	8:00	NQ	3	NQ	12	12	278	0.67	17.1*
Julian 178	8:01	10:00	13	30	28	22	16	892	0.95	
	10:00	12:00	12	36	23	35	19	1380	1.38	
	12:00	14:00	28	79	49	42	22	1611	1.40	
	14:01	16:00	8	19	12	40	24	1442	1.56	
	16:00	18:00	NQ	24	NQ	31	24	1151	3.84	
	18:00	20:00	NQ	NQ	17	26	22	549	3.93	
Day 21 (July 3rd)	6:00	8:00	6	12	10	15	14	248	1.27	2*
Julian 185	8:01	10:00	39	31	30	24	18	806	1.17	
	10:00	12:00	10	23	18	30	21	1212	1.68	
	12:00	14:01	16	39	27	31	23	1145	2.55	
	14:01	15:59	NQ	37	28	31	23	1344	3.34	
	16:00	18:00	NQ	18	NQ	26	22	463	2.73	
	18:01	20:00	NQ	NQ	NQ	20	20	121	2.77	

*rainfall occurred prior to date

NQ-not quantifiable

**flux estimated from airborne concentrations using the Backward-Time Lagrangian stochastic Dispersion model (Flesch, Wilson, Journal of Applied Meteorology, 34, pp. 1320-1332)

Table 13: Flux results*, Application 2, 1996

	Air Sampling Period		Flux (ug/m ² /hr)			Surface Temp. (C)	Ambient Temp. (C)	Solar Rad. J/m ² /sec	Wind Speed	Precipitation (mm)
	Start	End	Triclopyr	Propiconazole	Cyfluthrin				(cm/s) @z=70 cm	
Day 0 (July 23rd)	6:15	8:03	66	17	NQ	19	17	205	0.64	
Julian 205	8:03	10:00	323	42	NQ	29	24	837	1.04	
	10:00	12:00	414	147	NQ	35	27	1351	1.40	
	12:00	14:00	303	202	NQ	39	31	1614	1.45	
	14:00	16:00	121	145	NQ	39	34	1427	1.44	
	16:01	18:00	66	72	NQ	35	35	946	1.30	
	18:01	20:01	35	19	NQ	30	32	264	1.75	
	20:04	6:00	3	1	NQ	20	21	3	0.70	
Cummulative Loss % of Amount Applied			2.3	0.6						
Day 1 (July 24th)	6:01	8:00	7	6	NQ	20	17	226	0.53	
Julian 206	8:01	10:00	39	31	NQ	30	24	825	0.76	
	10:01	12:00	47	142	NQ	38	29	1413	1.10	
	12:02	14:00	26	87	NQ	41	31	1646	1.29	
	14:00	16:00	15	78	NQ	40	34	1551	1.34	
	16:00	18:00	9	56	NQ	35	34	1038	1.78	
	18:01	20:00	NQ	24	NQ	29	31	426	2.59	
	20:00	6:00	0	1	NQ	19	19	4	0.68	
Cummulative Loss % of Amount Applied			NQ	0.4						
Day 2 (July 25th)	6:01	8:00	NQ	3	NQ	18	15	200	0.57	
Julian 207	8:12	10:00	6	18	NQ	29	21	851	0.87	
	10:01	12:00	5	41	NQ	35	27	1387	1.13	
	12:00	13:55	4	59	NQ	38	30	1623	1.27	
	13:55	16:00	4	75	NQ	38	33	1505	1.50	
	16:01	18:00	NQ	33	NQ	32	34	1059	1.55	
	18:01	20:00	NQ	20	NQ	28	33	432	1.42	
	20:01	6:00	0	NQ	NQ	19	19	4	0.86	
Cummulative Loss % of Amount Applied			NQ	NQ						
Day 3 (July 26th)	12:00	14:00	NQ	43	NQ	41	31	1594	1	
Julian 208										
Day 5 (July 28th)	12:00	14:00	NQ	8	NQ	27	21	820	1	
Julian 210										
Day 7 (July 30th)	6:00	8:00	NQ	NQ	NQ	18	17	185	0.47	
Julian 212	8:01	10:00	NQ	4	NQ	25	20	796	0.67	
	10:01	12:00	NQ	19	NQ	30	23	1326	1.65	
	12:01	14:02	NQ	30	NQ	34	26	1571	1.67	
	14:03	16:00	NQ	20	NQ	34	28	1459	1.67	
	16:01	18:00	NQ	23	NQ	29	29	1014	1.75	
	18:01	20:00	NQ	NQ	NQ	24	25	405	2.77	
Day 10 (August 2nd), Julian 215										
Day 13 (August 5th)	6:00	8:00	NQ	2	NQ	13	14	156	0.45	3.6*
Julian 218	8:00	10:00	NQ	NQ	12	20	16	751	2.09	
	10:01	12:00	NQ	22	8	21	17	914	2.64	
	12:01	14:00	NQ	NQ	NQ	26	19	1396	2.15	
	14:01	16:00	NQ	NQ	NQ	25	20	590	1.44	
	16:00	18:00	NQ	NQ	NQ	30	22	1032	1.74	
	18:01	20:24	NQ	NQ	NQ	18	21	275	1.61	
Day 21 (August 13th)	6:00	8:45	NQ	NQ	NQ	14	14	120	0.48	
Julian 226	8:00	10:00	NQ	NQ	NQ	25	20	715	0.57	
	10:01	12:01	NQ	NQ	NQ	33	25	1357	1.29	
	12:10	14:00	NQ	NQ	NQ	38	29	1490	1.23	
	14:01	16:02	NQ	NQ	NQ	36	32	1367	1.00	
	16:02	18:01	NQ	NQ	NQ	33	32	928	2.47	

*rainfall occurred prior to date

NQ-not quantifiable

**flux estimated from airborne concentrations using the Backward-Time Lagrangian stochastic Dispersion model (Flesch, Wilson, Journal of Applied Meteorology, 34, pp. 1320-1332)

patterns on days following application. Given constant solar radiation, peak flux appears to decline exponentially with time following the application date (Fig. 44, 46, & 48).

Correlation of Flux with Solar Radiation on a Single Date

On clear days, pesticide flux exhibited a strong positive correlation with solar radiation (Fig. 38). In fact, on clear days, volatilization appears to correlate better with solar radiation than surface temperature (Fig. 40). This relationship is less apparent on cloudy days where solar radiation and flux measurements become erratic (Fig 39 & 41). Total flux during noon hours on days following application which were normalized for differences solar radiation (Normalized Flux=Flux/Solar Radiation) displayed an exponential decay pattern (Fig 45, 47, & 49).

The data was fitted to a single exponential decay function.

$$\frac{Flux}{S.R.} \left(\frac{ug}{MJ} \right) = \frac{F_0}{S.R.} e^{-kt} \quad (69)$$

F/S.R.(ug/MJ)-Flux (t=0) normalized for solar radiation during noon hours (12:00-16:00 in 1995, 12:00-14:00 in 1996).

F₀/S.R.(ug/MJ)-Fitted parameter of initial flux (t=0) normalized for solar radiation.

t-(days) time following application.

k-(days⁻¹) fitted decay constant for flux during the noon hour normalized for solar radiation.

A slight transition in decay slopes appeared for Application 1, 1995 and 1996 between Days 5 and 7 (Fig 45 & 47). This might signify a transition in volatilization behavior proposed by Taylor [2]. Taylor speculated that during the initial period following application, the majority of evaporation would occur from deposits instead of pesticide adsorbed to the leaf surface. Over time, as the deposits shrink, more volatilization would occur from the leaf surface. The active ingredient's vapor pressure may decrease significantly for compounds which exhibit a strong binding feature the wax and coatings of the leaf surface. Loss due to volatilization would diminish, decreasing the exponential decay constant, k. Correlations between the integrated of solar radiation and flux over a day period could be explored and account for volatilization due to energy balance methods.

Correlation of observed Flux with Ambient and Surface Temperatures

Ambient temperatures were measured at the height of the CM-10 weather monitoring system (Fig. 74) (~ 1 m) over half-hour averaged intervals. Surface temperatures were collected at the same interval using two white plastic-covered soil temperature probes laid on a wood chip or soil surface near the grass plot.

Figure 38: Flux vs. Solar Radiation on a clear Day (Day 2, App.1, 1996)

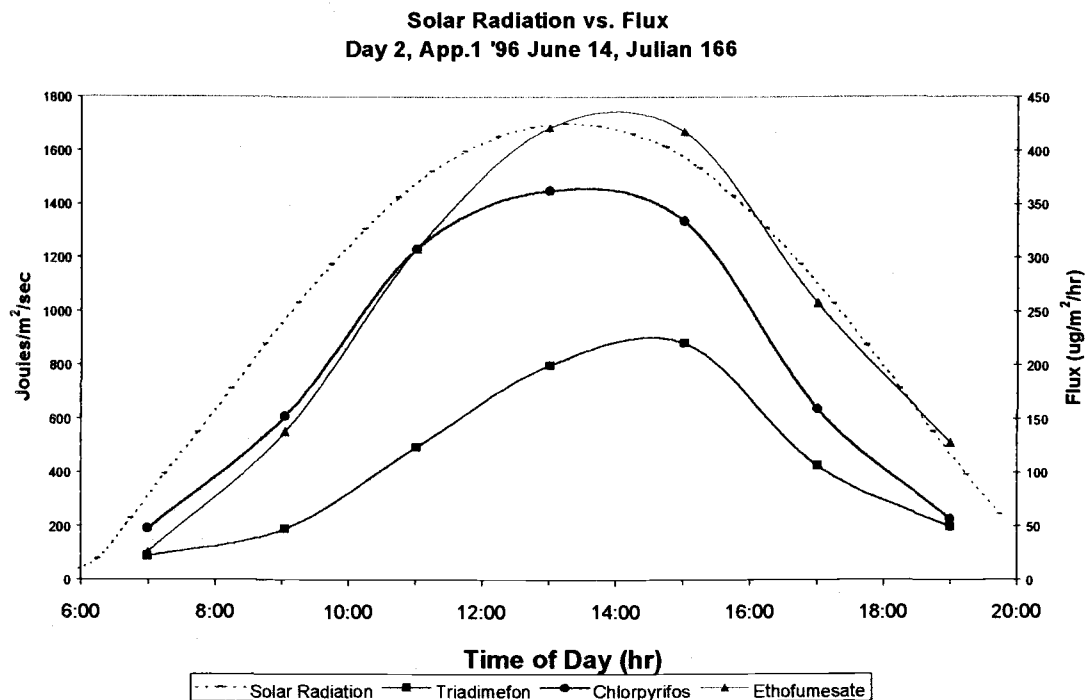


Figure 39: Flux vs. Solar Radiation on a cloudy day (Day 1, App.1, 1996)

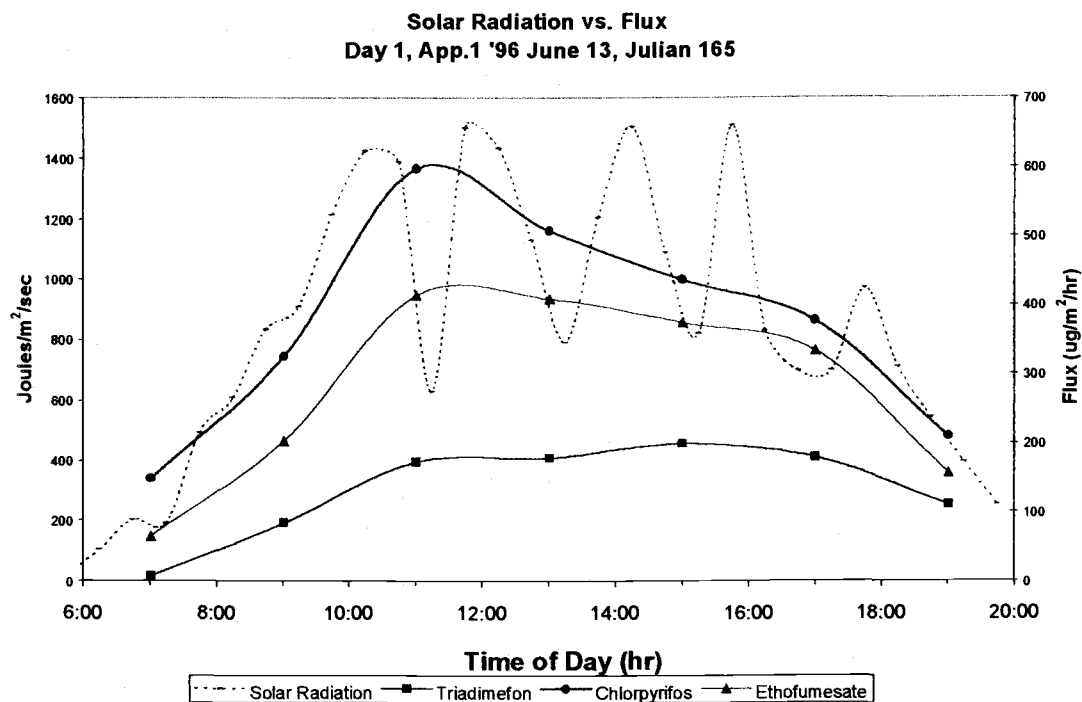
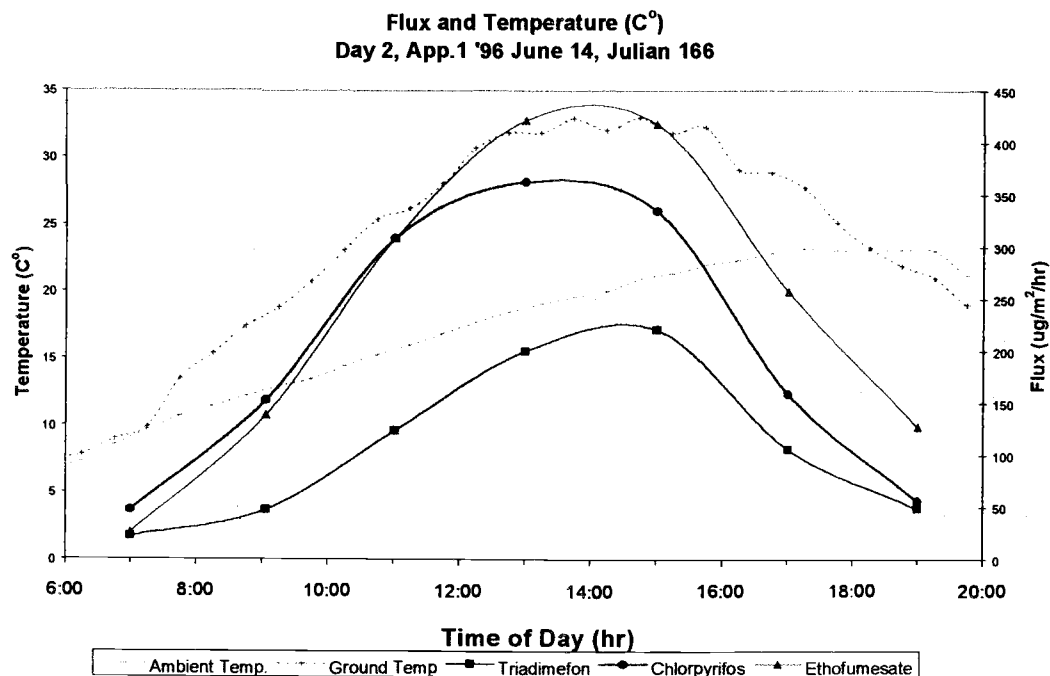


Fig -

Figure 40: Flux vs. Ambient and Surface Temperature on a clear day (Day 2, App.1, 1996).



Figure

41: Flux vs. Ambient and Surface Temperature on a cloudy day (Day 1, App.1, 1996).

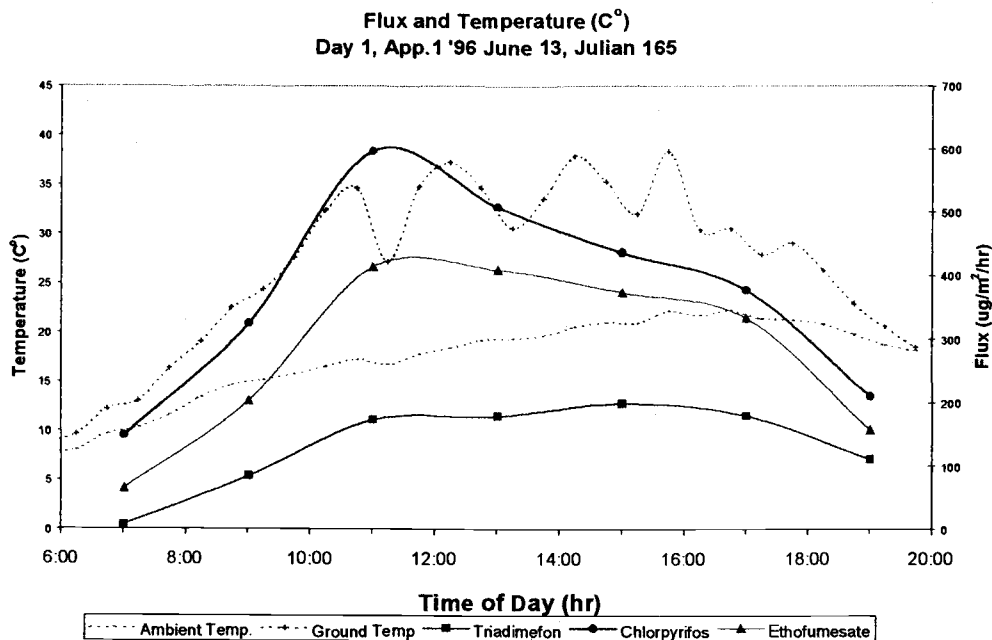


Figure 42: Flux vs. Wind speed at the sampling height (Day 2, App.1, 1996).

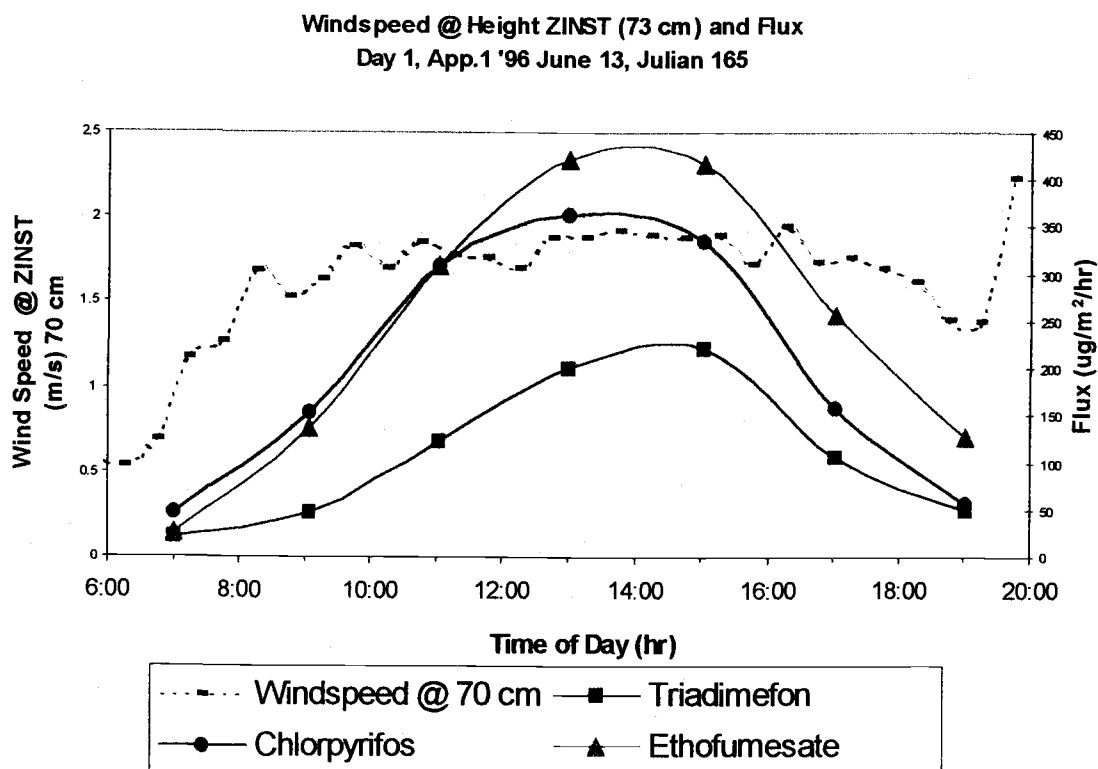


Figure 43: Flux vs. Wind speed at the sampling height (Day 1, App.1, 1996).

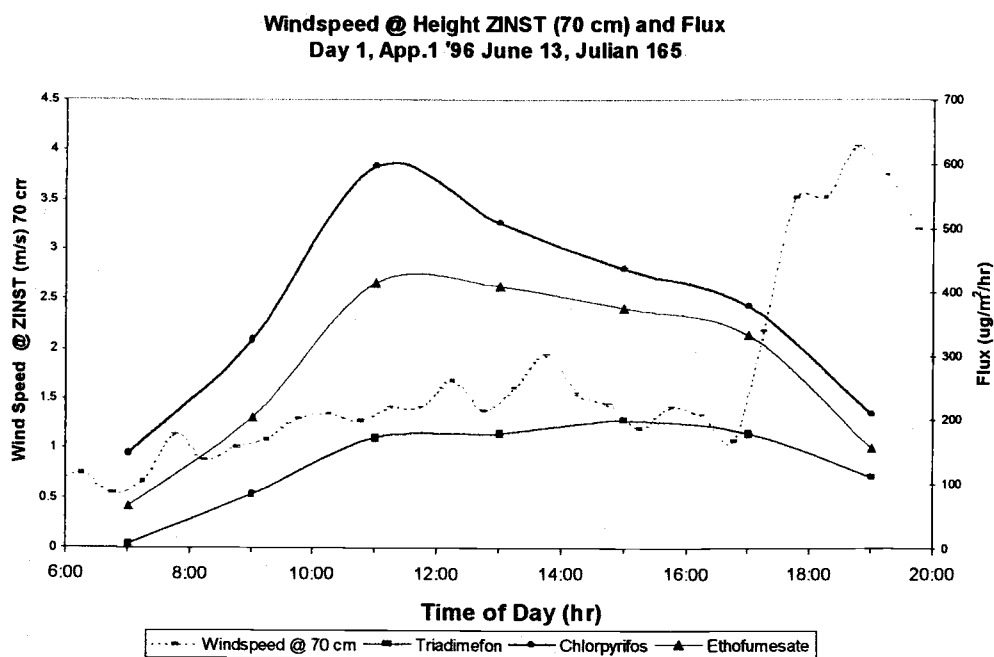


Figure 44: Plot of Total Flux and Total Solar Radiation during mid-day (12:00-16:00) on days following application date (Day 0) Application 1, 1995.

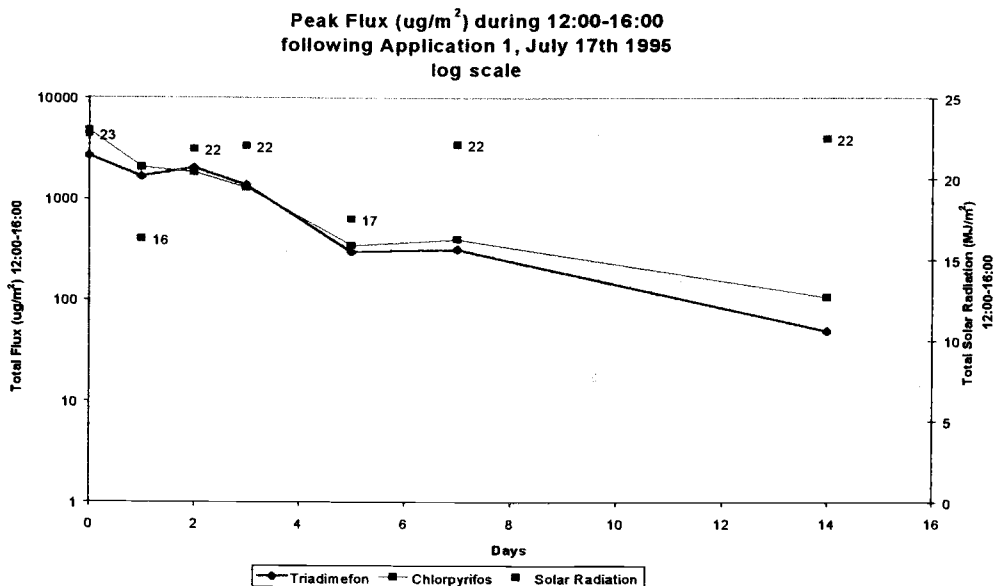


Figure 45: Plot of Flux normalized for Solar Radiation (Flux/S.R.) during mid-day (12:00-16:00) Application 1, 1995 on days following application date (Day 0).

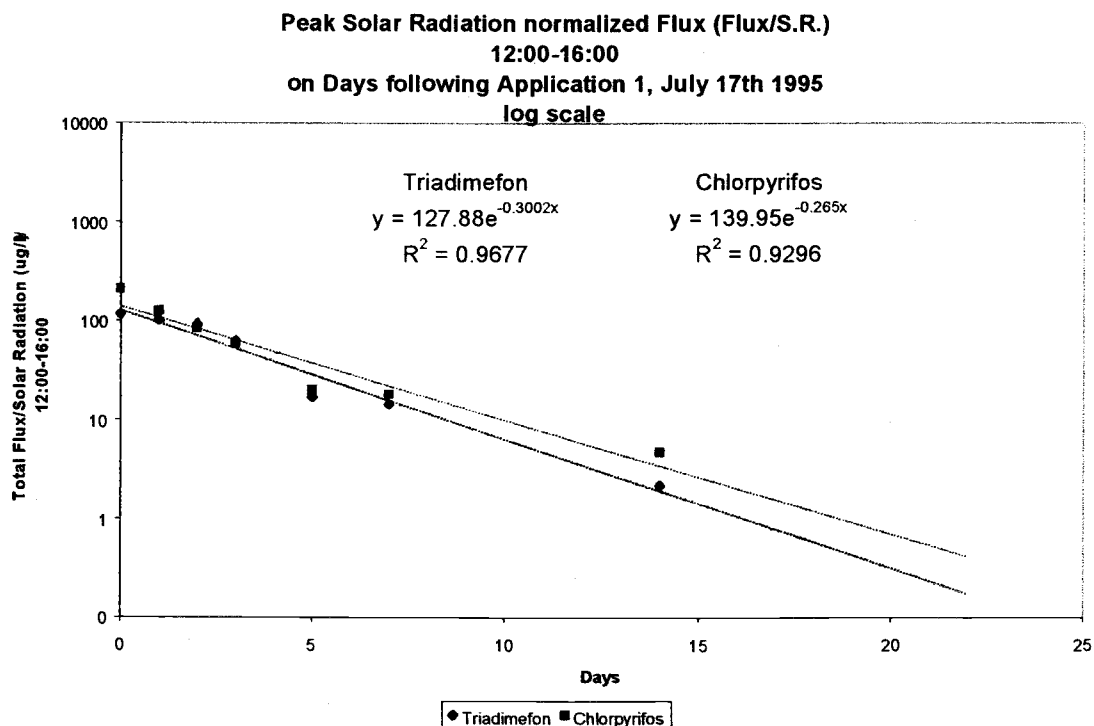


Figure 46: Plot of Total Flux and Total Solar Radiation during mid-day (12:00-14:00) on days following application date (Day 0) Application 1, 1996.

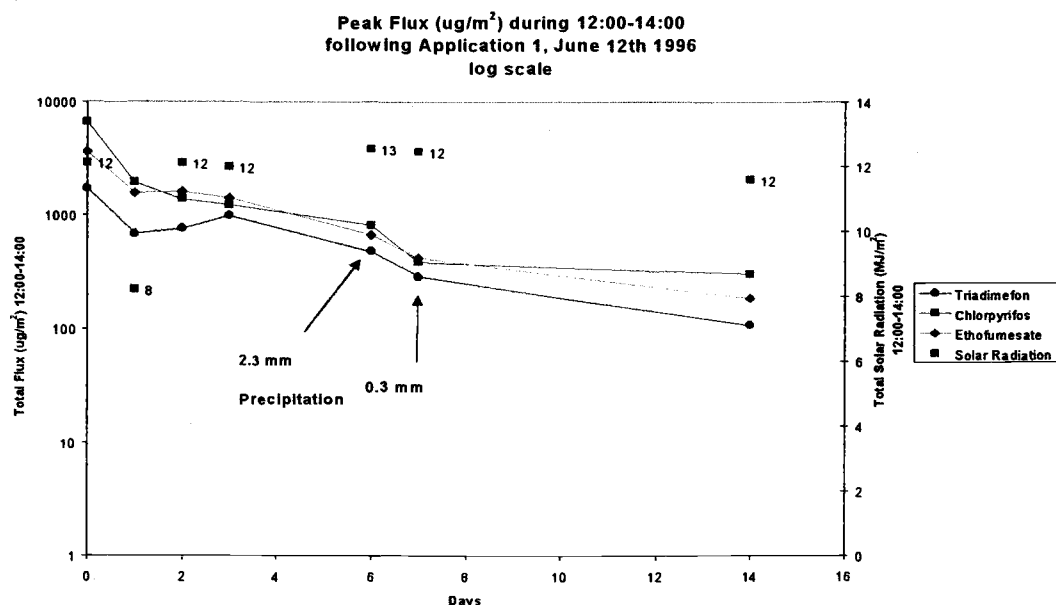


Figure 47: Plot of Flux normalized for Solar Radiation (Flux/S.R.) during mid-day (12:00-14:00) Application 1, 1996 on days following application date (Day 0).

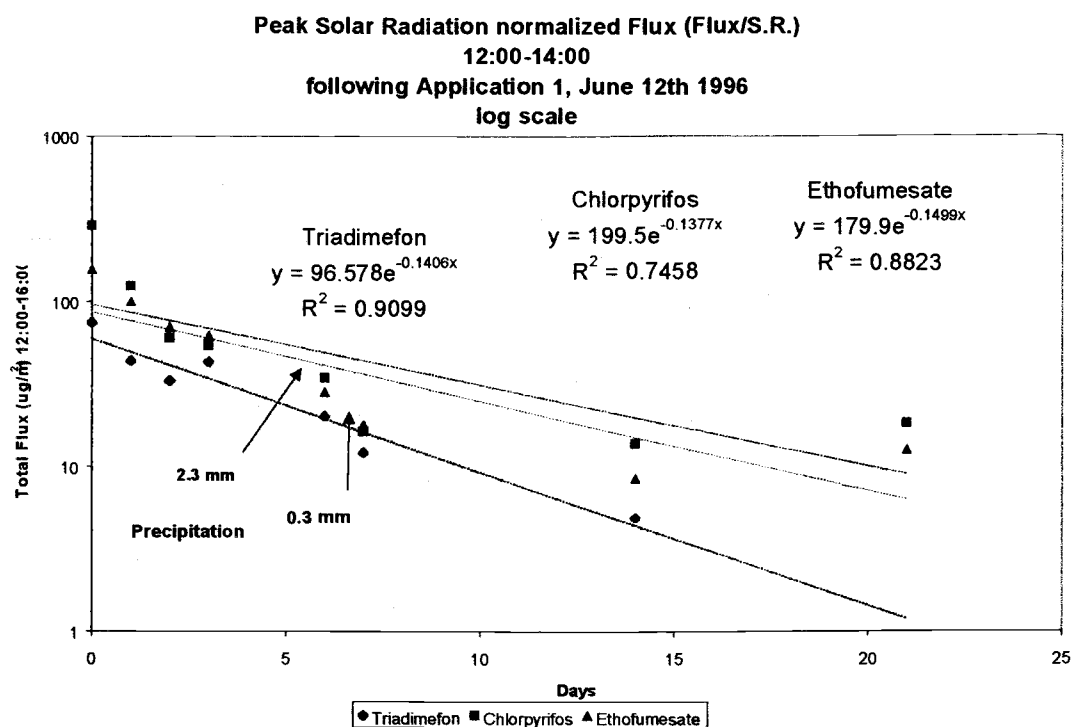


Figure 48: Plot of Total Flux and Total Solar Radiation during mid-day (12:00-14:00) on days following application date (Day 0) Application 2, 1996.

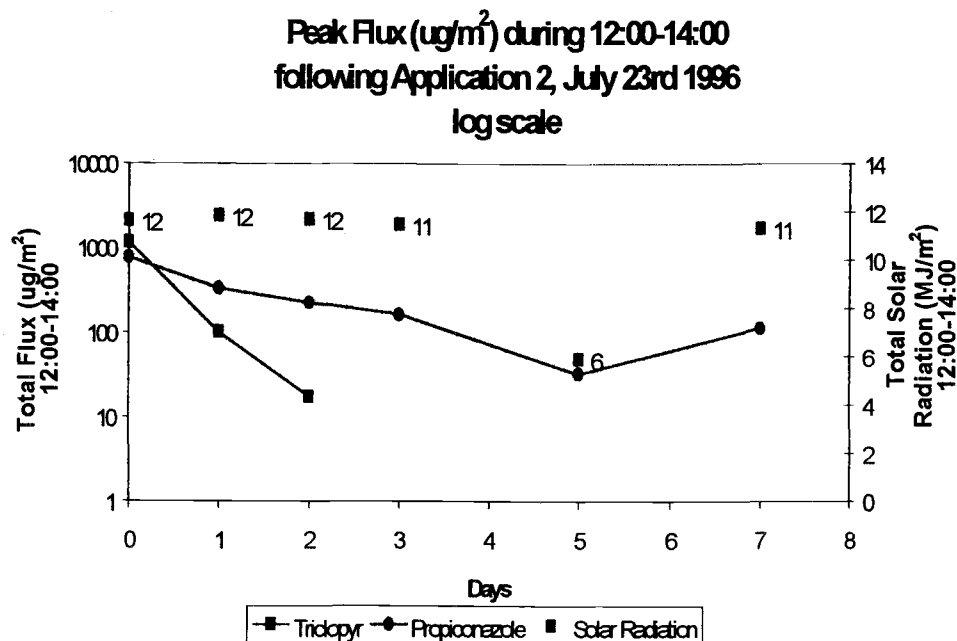
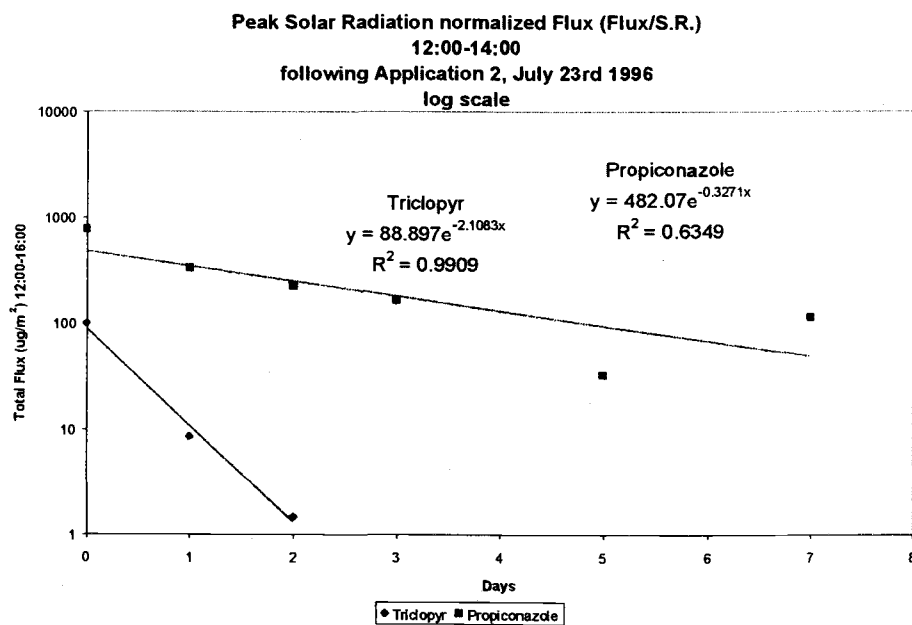


Figure 49: Plot of Flux normalized for Solar Radiation (Flux/S.R.) during mid-day (12:00-14:00) Application 2, 1996 on days following application date (Day 0).



The temperature difference between the two probes was normally a degree or two apart but could be as much as 7 °C. The average of the two readings during the two hour sampling period was used for inputs into the fugacity model. These measurements are thought to be representative of the actual surface temperature where volatilization however, it must be remembered that these surface temperature measurements *do not* actually represent the temperature at the leaf surface. The leaf surface has a different sunlight absorption and heat dissipation capacity which can vary during the day due to evapo-transpiration of the leaf surface. There is also likely to be a time delay between the temperature of the leaf surface and the air above. A surface being warmed by sunlight in the morning will gradually warm the air above it by convection until the air and surface temperatures are in equilibrium. In the same way, during the late afternoons and early evenings, when the surface is no longer being warmed by sunlight, the surface cools due to radiation and evapo-transpiration. This gradually cools the air above. The surface temperature measurements are thought to be intermediate between the ambient temperatures and the actual temperature of the leaf surface. Therefore, the following surface temperature errors are thought to exist:

Time of Day	Atmospheric Conditions	Likely Error in Surface Temperature Estimation (Fig 37)
Morning	Unstable	Actual temperature > Measured Temperature
Late Afternoon/ Early Evening	Stable	Measured Temperature > Actual Temperature

This theory may explain the skewed behavior of a plot of solar radiation and temperature profiles during the day and the plateau behavior of the log Flux vs. 1/T plots at higher temperatures (Fig. 50-56).

Clausius Clapeyron plot of flux vs. temperature (log F vs. 1/T(K))

Recall from the earlier discussion that volatile loss is believed to be proportional to the vapor pressure of the active ingredient (equation 61). According to the Clausius Clapeyron equation (eq. 3), vapor pressure is exponentially related to temperature. Plots of log Flux (ug/m²hr) vs. 1/Temp (K) during the first two days following application were created to verify the existence of the linear relationship proposed by equations 3 and 41⁴ (Fig 3-9, 50-56).

With the exception of Triclopyr a linear relationship between log Flux vs. 1/Temp. (K) was observed for all pesticides in both ambient and surface temperature plots with less scatter occurring for surface

⁴The relationship between vapor concentration and temperature is not exactly linear due to the presence of the temperature term in the denominator of equation 4, however the exponential term in eq. 3 should dominate and the linear term in equation 4 shouldn't noticeably skew the linear relationship between log Flux vs. 1/T.

Figure 50-51: Plot of log Flux ($\mu\text{g}/\text{m}^2/\text{hr}$) vs. $1/\text{Temperature}$ (K) for the BTLSD model (equation 67) and fugacity model (equation 63) for Triadimefon using surface temperature measurements. In cases where vapor pressure measurements are reported for more than one temperature a projected line is plotted for the fugacity model.

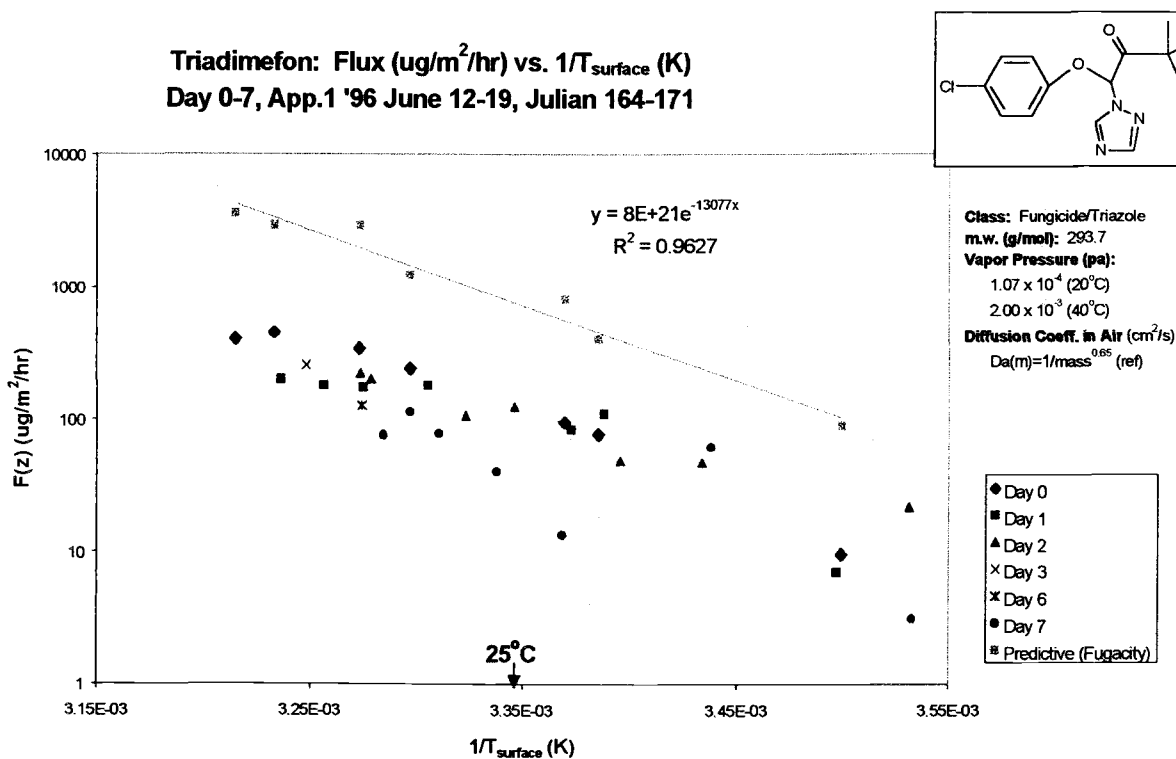
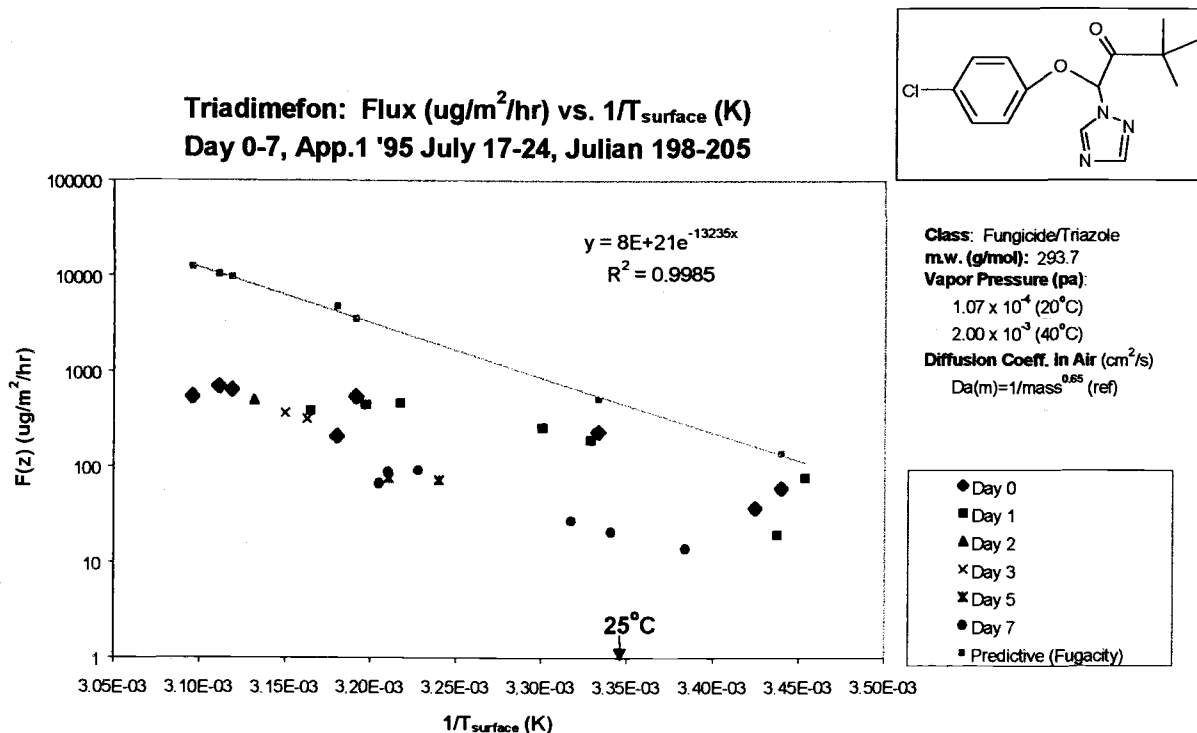


Figure 52-53: Plots of log Flux ($\mu\text{g}/\text{m}^2/\text{hr}$) vs. $1/\text{Temperature (K)}$ for the BTLSD model (equation 67) and fugacity model (equation 63) for Chlorpyrifos (1995, 1996) using surface temperature measurements. In cases where vapor pressure measurements are reported for more than one temperature a projected line is plotted for the fugacity model.

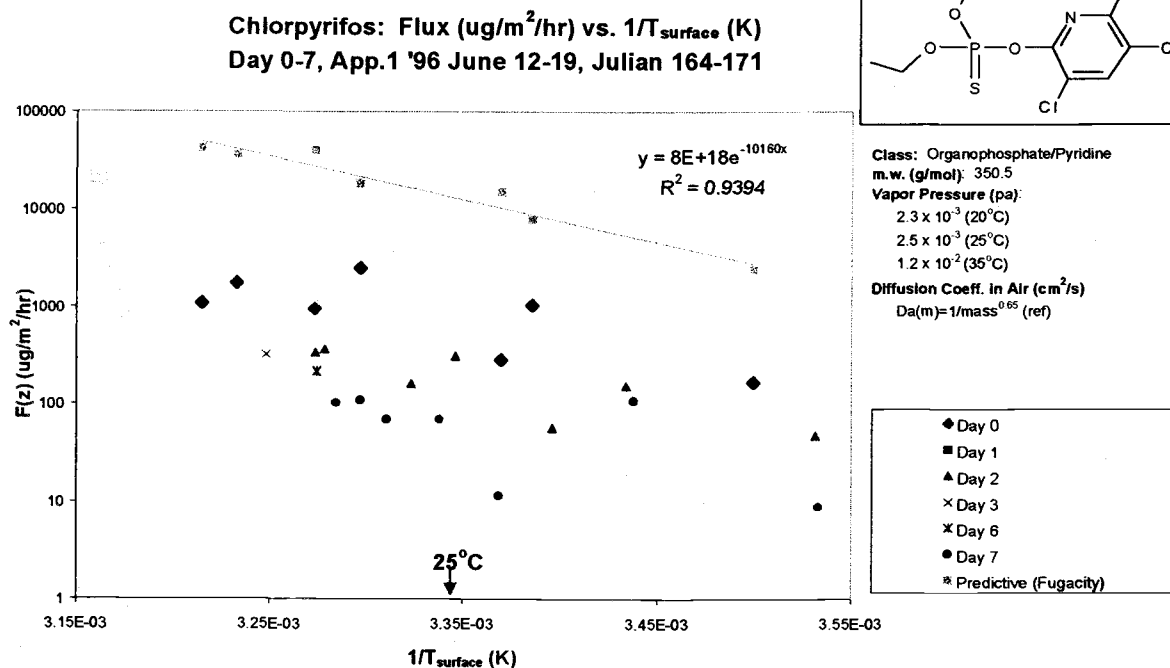
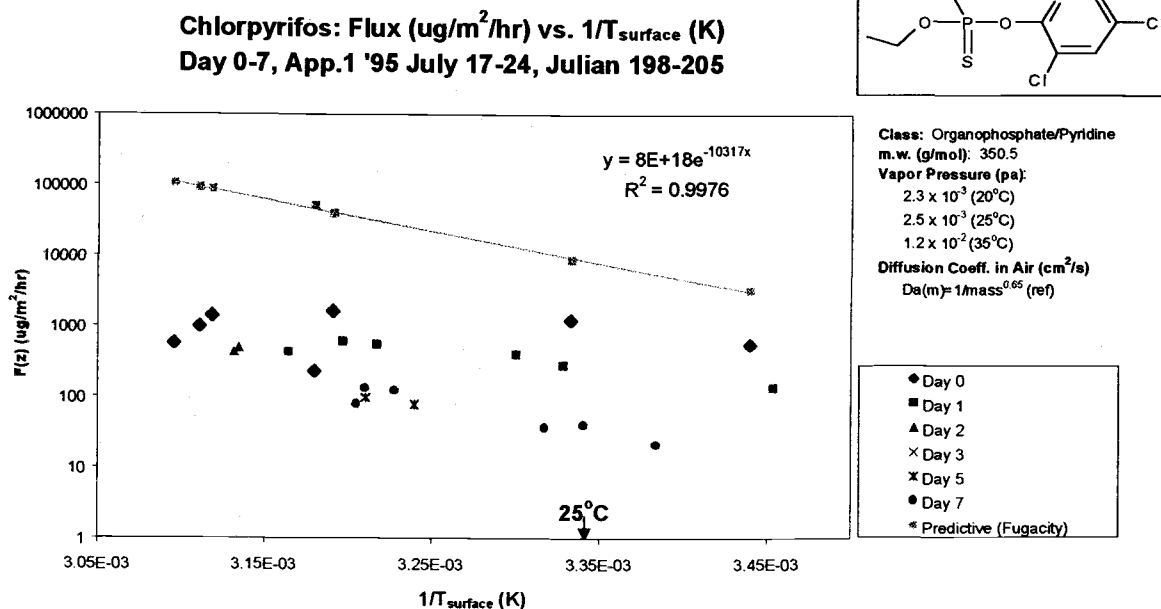


Figure 54-55: Plots of log Flux ($\mu\text{g}/\text{m}^2/\text{hr}$) vs. $1/\text{Temperature (K)}$ for the BTLSD model (equation 67) and fugacity model (equation 63) for Ethofumesate and Triclopyr using surface temperature measurements. In cases where vapor pressure measurements are reported for more than one temperature a projected line is plotted for the fugacity model.

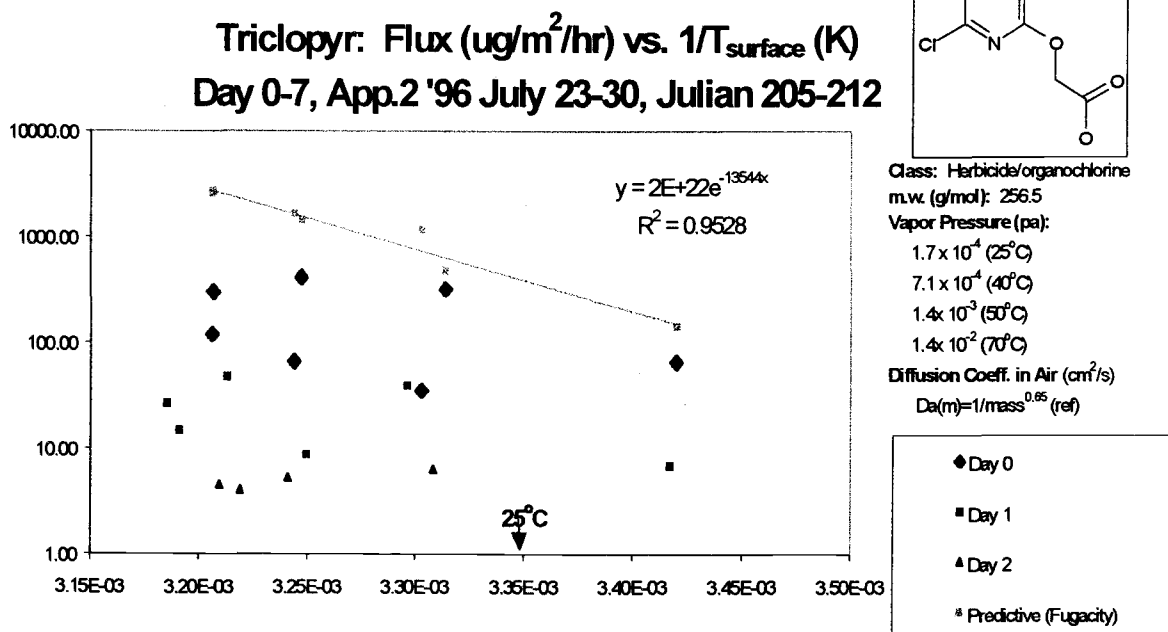
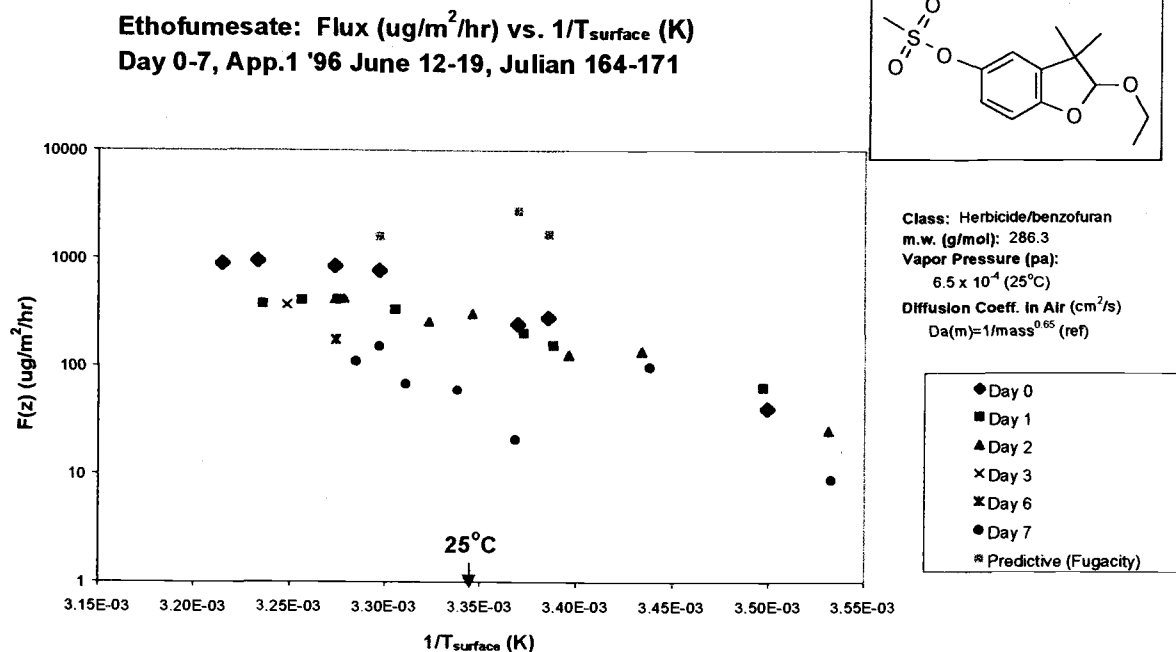


Figure 56: Plot of log Flux ($\mu\text{g}/\text{m}^2/\text{hr}$) vs. $1/T_{\text{surface}}$ (K) for the BTLSD model (equation 67) and fugacity model (equation 63) for Propiconazole using surface temperature measurements. In cases where vapor pressure measurements are reported for more than one temperature a projected line is plotted for the fugacity model.

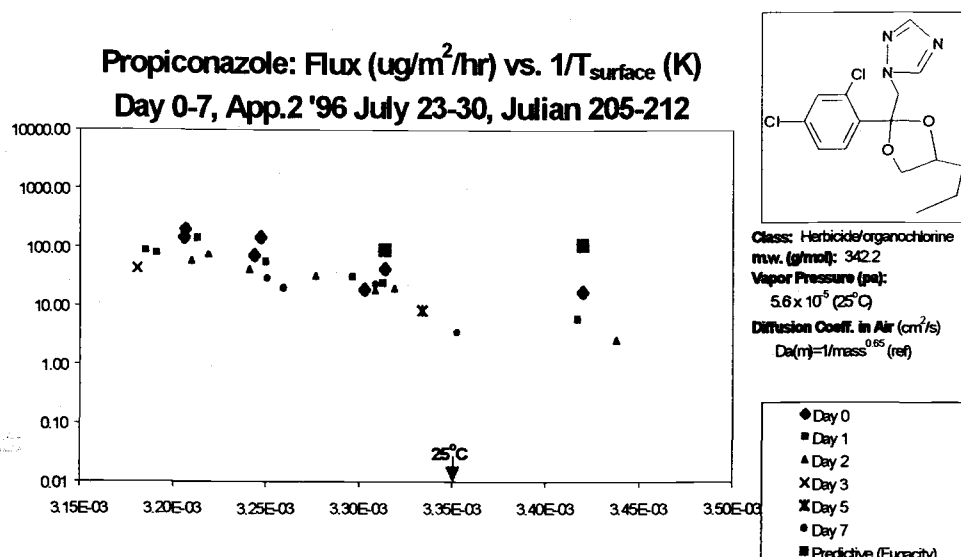


Table 8: Parameter inputs for the Theoretical Profile Shape (TPS) and Fugacity models in estimating pesticide loss from a turf grass surface. 'X' symbols denotes parameter requirement for the model.

Parameter	TPS (eq. 67)	Fugacity (eq. 63)	Relation of Flux to the parameter	If calculated, relation of parameter to measured environmental data.
$u(z)$ -wind speed at sampling height	X		$F \propto u(z)$	measured.
c airborne concentration measurements	X		$F \propto c$	accuracy of c proportional to sampling time and chemical analysis sensitivity.
Thickness of atmospheric equilibrated boundary layer for momentum δ_m and the scalar δ_{eq}	X	X	$F \propto [\ln \delta + \text{const.}]^{-1}$	$\delta \propto x^{5/4}$ for the fugacity model, where x is distance from edge of plot for the scalar and the length of the upwind fetch of equivalent z_0 for momentum (see equation 61).
S.V.D. (saturated vapor density of the active ingredient at a measured surface temperature T).		X	$F \propto \text{S.V.D.}(T)$	$\text{S.V.D.}(T) \propto \exp^{-1/T}$ (see equations 3 and 4)
z_0 measured from wind profiles or predicted for a given surface type.	X	X	$F \propto [\text{const.} - \ln z_0]$	exponentially related to wind speed log/linear regression intercept of ($\ln z_0$) of $\ln z$ vs. $u(z)$ during neutral conditions (see equation 30).
D_a pesticide diffusion coefficient (calculated).	X		logarithmic	inversely proportional to barometric pressure, molecular mass ^{0.65} , directly proportional to Temp ^{1.75} (see equation 7).
Φ (normalized flux value)	X		inversely proportional	dependent on plot radius R , stability L , roughness length z_0 and sampling height z)
L (Monin-Obukhov stability factor)	X	X	$F \propto [\text{const.} + 1/L]$	fitted to wind profile using equation 29.
u^* (estimated from wind profile)		X	directly proportional	directly proportional to wind speed.

temperature (Fig. 7, 55). A slight departure from linearity appears to occur at higher temperature when the data points are resolved for individual days (Fig 50-56). A closer look at the log Flux vs. $1/T$ for triclopyr (Fig. 55) shows a rapid attenuation during a single day. Triclopyr's unusual behavior is thought to be due to the conversion of the acetic acid group to the conjugate base ($pK_a=2.68$). The acetate form of triclopyr has a much higher solubility in water and is thought to be transported away rapidly by the plant's vascular system after penetrating the leaf surface. The process of partitioning and rapid removal would maintain a high concentration gradient across the leaf membrane explain the rapid attenuation behavior.

Differences in Triadimefon/Chlorpyrifos Flux for 1995 and 1996 applications.

A systematic difference in the slopes and intercepts of log Flux vs. $1/T$ exist for Triadimefon and Chlorpyrifos exist for the 1995 and 1996 applications. The slopes and intercept values appear consistently lower in 1995 indicating a suppression in the sensitivity of the flux to change in surface temperature measurements. A difference is also evident in the plots of normalized flux values which incorporate surface temperature measurements in normalizing flux for the saturated vapor density of a pesticide at a particular surface temperature (Figures 72 and 73). The change in relationship between flux and temperature for the same pesticides on different years is likely due to two experimental differences. During the first application in 1995, a tree on the west side of the plot cast a shade over a treated area of the grass which was typically an upwind path from the air sampler during that period of the day (Figure 74). The temperature sensors (which were attached to the weather station located on the east side of the plot during 1995) did not experience this shade and therefore, during the late afternoons, probably contributed to an overestimation of the plot temperature relative to earlier periods in the day. During 1996, the weather station relocated to the south west side of the plot and the tree was removed (Figure 74). *The absence of shading factors during the following year, in addition to a difference in positioning of the temperature sensors are possible causes for the systematic difference in the log Flux vs. $1/T$ slopes and intercepts for Triadimefon and Chlorpyrifos between years.* May 20, 1999

Correlation of Observed Flux with wind speed

No discernable correlations between wind speed at the sampling height and flux were detected. Because wind may be a weaker factor in governing flux than other factors such as temperature and solar radiation, its relationship may be obscured due to the variance of other factors (Fig 42, 43).

Correlation of initial loss percentages of the amount applied due to volatilization and active ingredient partition coefficients.

The rank of calculated initial loss rates during the first 24 hours correlated with the rank of the active ingredient's vapor pressure (Table 10). Figure 57 displays a somewhat linear correlation between vapor

pressure of the active ingredient at 25 °C and the % loss of the amount applied due to volatilization during the first 24 hours following application. This linear equation is thought to be able to estimate % loss rates vs. vapor pressure of the active ingredient from turf grass. No correlations were apparent between the air/octanol (K_{ao}), air/water (K_h), and octanol/water (K_{ow}) coefficients (Table 8, Fig. 58-60).

Attenuation vs. Active ingredient partition constants

Correlations of the decay constant k with physiochemical properties of the pesticides, including vapor pressure, octanol/water partition constant K_{ow} , air/water partition constant (Henry's Law), and air/octanol K_{ao} , showed no evidence of correlation (Fig. 61-64, Table 8).

Fugacity Model Results:

The required parameters for equation 59, which predicts the flux, are S.V.D.(T), Da , T , z , u^* , and L (Table 8). The saturated vapor density (S.V.D.) of a compound can be predicted using literature values of a compound's molecular weight and vapor pressure at temperature (T) (listed in Table 1) using equations 3 and 4. The molecular diffusion coefficients (Da) for each compound were estimated using the molecular weight of the active ingredient and adjusted for temperature using equation 7. The average surface temperature measurements during the sampling interval described above were used as inputs for T . According to equation 60, the value of z for a turf plot with an average distance between the edge of the treated plot and the center $x=13.86$ m and estimated roughness length of $z_0=4.5$ mm was calculated to have a value of approximately 83 cm, where z is approximately three times the thickness of the equilibrated boundary layer $\delta=28$ cm calculated by equation 22.

According to the assumptions made in equation 60, the height where $C_s-C_z=C_s$ (i.e: $z=3\delta$) is above the air sampling height ($z_s=73$ cm). The exactness of the chosen height z where $C_s-C_z=C_s$ in near neutral and unstable atmospheric conditions is not critical since z appears in the logarithmic form in the denominator of equation 59 for neutral atmospheric conditions and as a difference between a logarithmic term and linear term for unstable conditions. According to Table 9, a 50% error in the estimation of $z=73$ cm, where $C_s-C_z=C_s$ under neutral conditions will generate a maximum 10% error in the estimated flux. The error in height estimation becomes more critical during very stable atmospheric conditions.

The weather parameters u^* and L were calculated from wind speed profiles averaged over the sampling duration (generally two-hour periods) using equation 29. Despite the poor means of estimating L (using it as a fitting parameter in a multivariable regression instead of measuring it directly), the effect of errors contributed due to uncertainty in L to the calculated flux cannot exceed more than 10% since z is very low to the ground.

Figure 57: %loss of active ingredient applied due to volatilization vs. vapor pressure of the active ingredient (25 °C) for all applications.

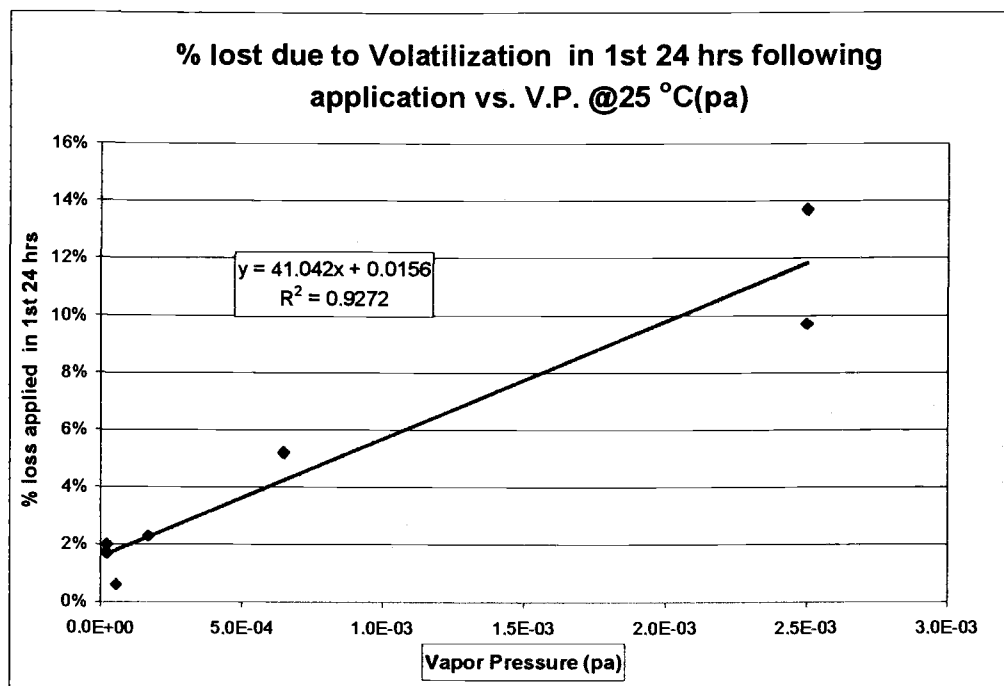
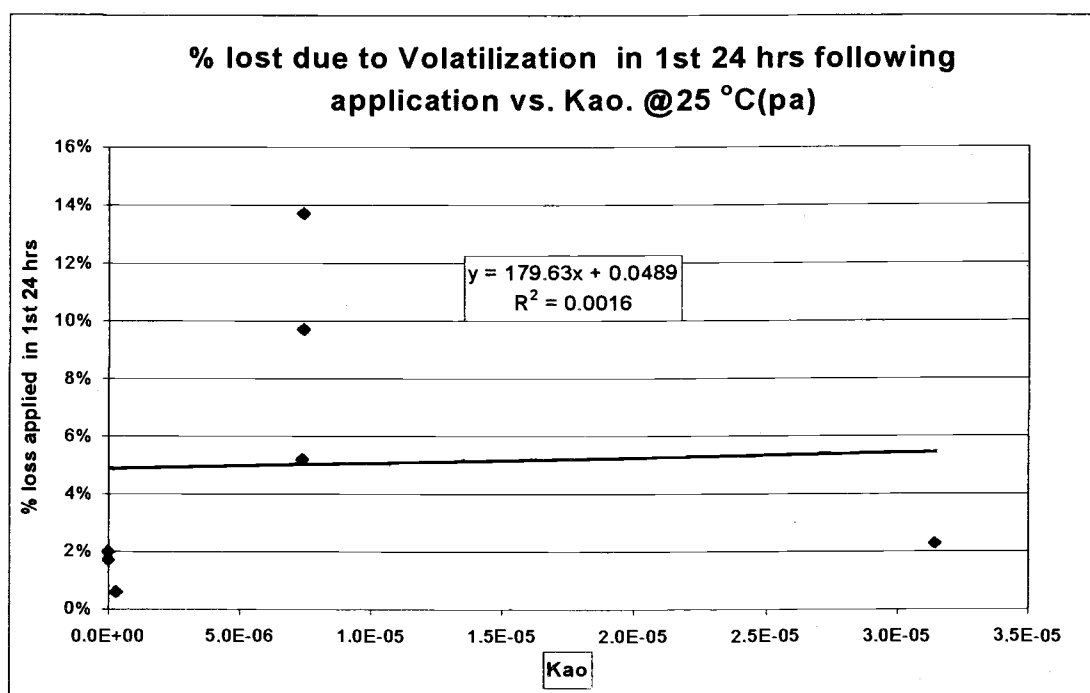


Figure 58: %loss of active ingredient applied due to volatilization vs. air/octanol partition coefficient (Kao) of the active ingredient (25 °C) for all applications.



Comparison of measured evaporative loss rates and loss parameters and partition coefficients
of the active ingredient (vapor pressure, air/octanol (Kao), air/water (Kh), octanol/water (Kow)).
(Figures 57-64)

	Volatile Loss in						
	V.P.	1st 24 hrs	F ₀ (ug/MJ)	k (day) ⁻¹	Kow	Kh	Kao
Chlorpyrifos (1:1995)	2.50E-03	9.70%	139.95	0.265	100000	7.43E-01	0.00000743
Chlorpyrifos (1:1996)	2.50E-03	13.70%	199.5	0.1377	100000	7.43E-01	0.00000743
Ethofumesate (1:1996)	6.50E-04	5.20%	179.9	0.1499	500	0.004	7.40E-06
Triclopyr (2:1996)	1.70E-04	2.30%	88.897	2.1083	2.64	8.30E-05	3.14E-05
Triadimefon (1:1995)	2.30E-05	2.00%	127.88	0.3002	1510	8.20E-06	5.4305E-09
Triadimefon (1:1996)	2.30E-05	1.70%	96.578	0.1406	1510	8.20E-06	5.4305E-09
Propiconazole (2:1996)	5.60E-05	0.60%	482.07	0.3271	630	1.92E-04	3.05E-07

Regressed exponential decay equation of flux normalized for solar radiation (Flux/S.R.)
during noon hours (12:00-16:00) App. 1, 1995, (12:00-14:00) App 1, 2, 1996.
(Figures 45, 47, 49)

$$\frac{F}{S.R.} \left(\frac{ug}{MJ} \right) = F_0 * e^{-kt}$$

Figure 59: %loss of active ingredient applied due to volatilization vs. Henry's partition coefficient (Kh) of the active ingredient (25 °C) for all applications.

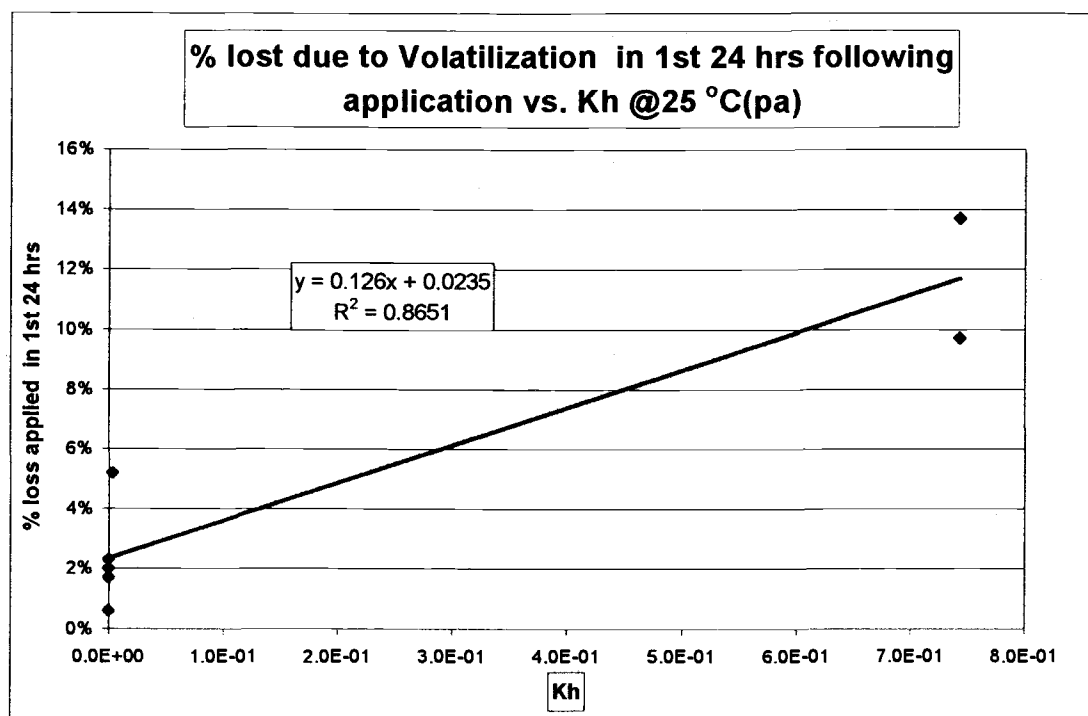


Figure 60: %loss of active ingredient applied due to volatilization vs.octanol/water partition coefficient (Kow) of the active ingredient (25 °C) for all applications.

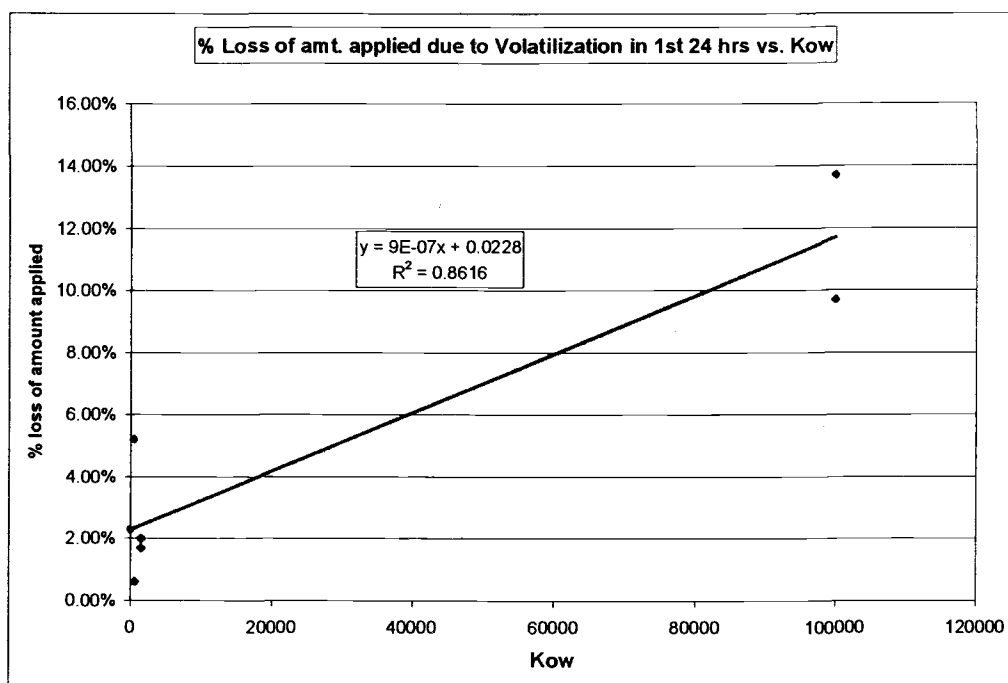


Figure 61: Exponential decay constant of flux normalized for solar radiation (Flux/S.R.) vs. vapor pressure of the active ingredient @ 25 °C.

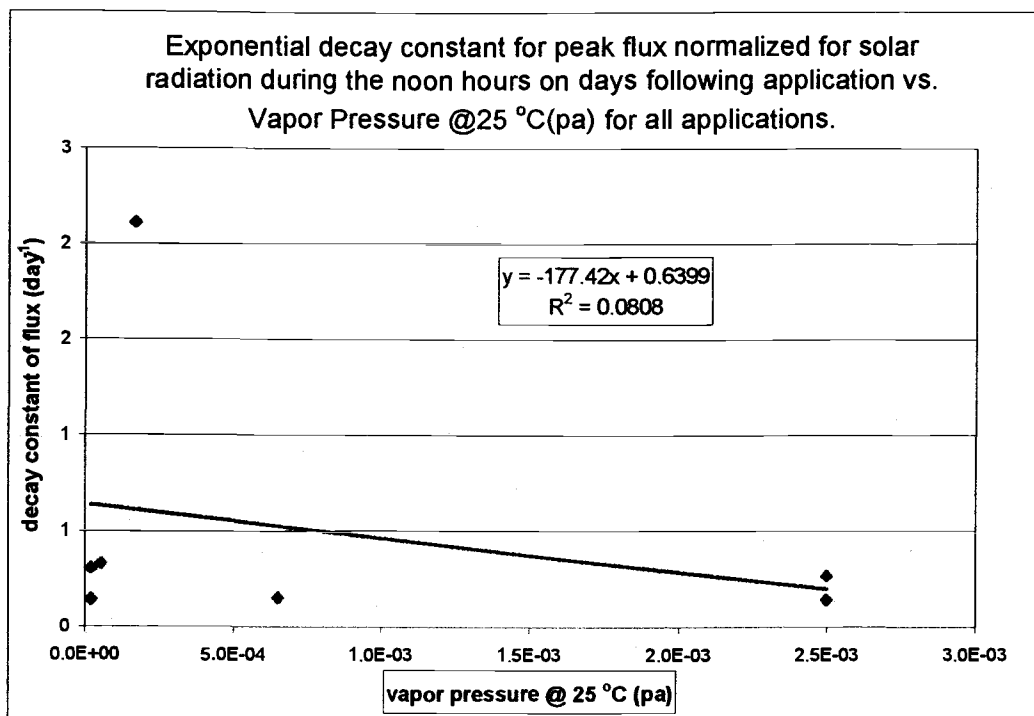


Figure 62: Exponential decay constant of flux normalized for solar radiation (Flux/S.R.) vs. air/octanol partition coefficient (K_{ao}) of the active ingredient @ 25 °C.

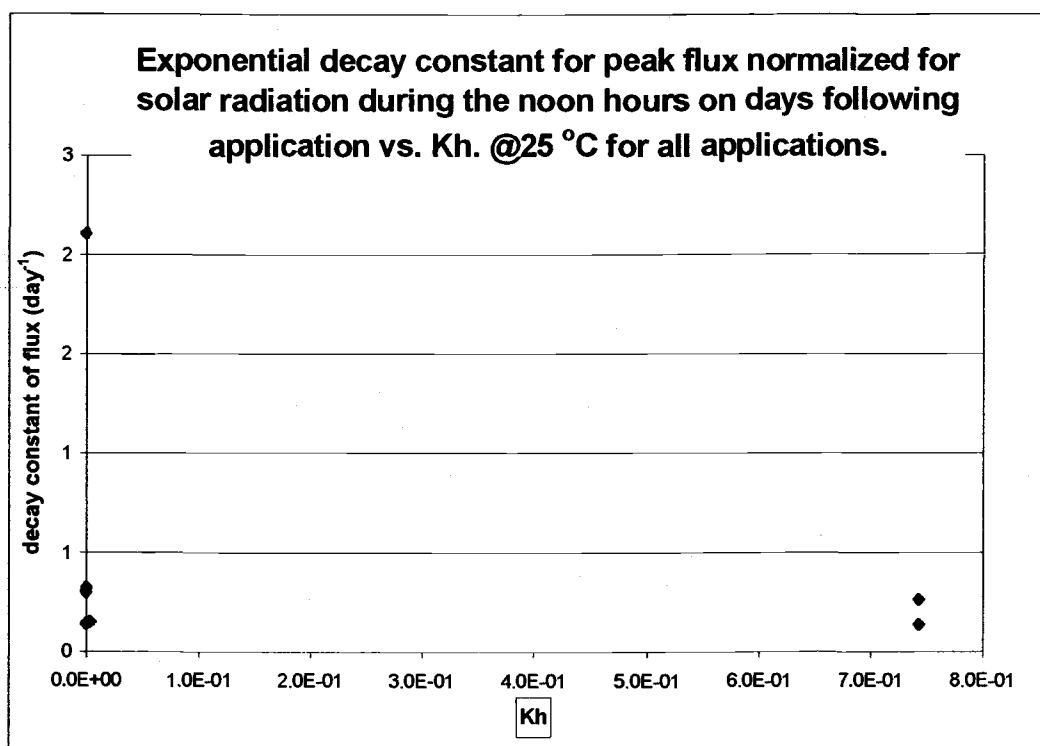


Figure 63: Exponential decay constant of flux normalized for solar radiation (Flux/S.R.) vs. Henry's partition coefficient the active ingredient @ 25 °C.

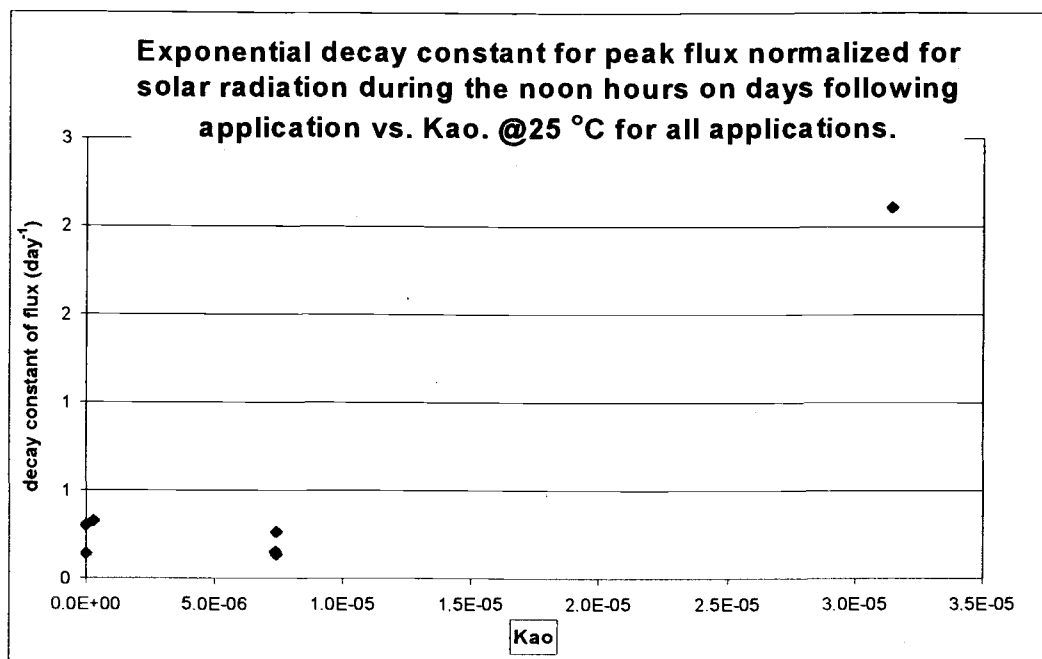
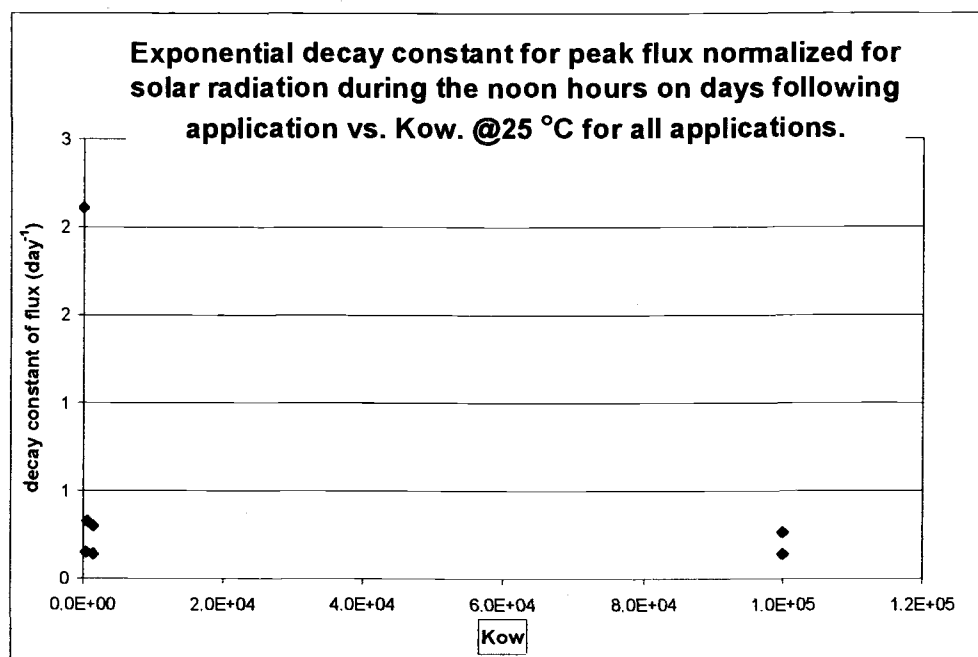


Figure 64: Exponential decay constant of flux normalized for solar radiation (Flux/S.R.) vs. octanol/water partition coefficient (Kow) of the active ingredient @ 25 °C.



Sensitivity analysis of the input parameters for the Fugacity model

Tables 8 & 9 and Figures 66 & 67 display the sensitivity of the predicted flux (eq. 3, 4, 61) due to change in the input parameters z_0 , u^* , x , T , L , D_a , S.V.D (T) ΔH and ΔS . The percent change in flux due to deviation in an input parameter is relative to a flux predicted by a standard condition observed for this turf grass study: $z_0=0.0045$, $D_a=0.04 \text{ cm}^2/\text{s}$, $x=14 \text{ m}$, $u^*=20 \text{ cm/s}$, S.V.D.=100 $\mu\text{g}/\text{m}^3$, $T=25 \text{ }^\circ\text{C}$, $L=\infty$.

According to Table 9, temperature (which determines the saturated vapor density in equation 3 and 4) is the environmental parameter whose change has the strongest influence on the predicted flux according to equation 59. Future studies on the fugacity approach of estimating evaporation loss of pesticides from turf grass should use techniques which give accurate estimates of leaf surface temperature.

Dependence of Flux on Physiochemical Parameters of the Pesticide

According to equation 3 and 4, the three parameters which determine the saturated vapor density S.V.D. of the pesticide are temperature, heat of vaporization (sublimation) ΔH_{vap} and entropy of vaporization ΔS_{vap} (sublimation). A technique of approximating ΔH_{vap} and ΔS_{vap} from a single vapor pressure at a single temperature is described in Lyman et. al [46]. Comparing the values of ΔH_{vap} and ΔS_{vap} obtained by a linear regression of measured vapor pressures at different temperatures with values of ΔH_{vap} and ΔS_{vap} predicted using the method described in Lyman appears to overestimate each of these values for this set of compounds (Table 12), giving gross overestimates of vapor pressure at temperatures higher than the reference temperature and underestimating the vapor pressure at lower temperatures. Performing a sensitivity analysis for each of the input parameters for S.V.D. in equations 3 and 4 shows that a small error in ΔH_{vap} and/or ΔS_{vap} can contribute to large errors in the estimated flux. Accurate estimates of these parameters is essential in determining flux for a given pesticide, using equation 59. Due to large differences between the estimates ΔH_{vap} and/or ΔS_{vap} the prediction method in Lyman [46] will not be used.

Comparison of Results between TPS/Backward Lagrange Stochastic and Predictive methods in predicting emission rates from Turf Grass

Plots of the predicted flux using equation 63 vs. flux estimated from airborne concentration measurements by the BTLSD model are displayed on a log Flux vs. $1/T$ (K) scale in Figures 50-56. In cases where literature values of vapor pressure exist for a particular compound for more than one temperature (Triadimefon, Chlorpyrifos, and Triclopyr), predicted fluxes are plotted for multiple temperatures and a regressed line is fitted through these points. For compounds with only a single vapor pressure value (Ethofumesate and Propiconazole), plots of predicted fluxes are only conducted at a single surface temperature (generally $25 \text{ }^\circ\text{C}$).

Table 9: Percent change in Flux estimated by equation 61 ($z_0=0.0045$, $D_a=0.04$ cm²/s, $x=14$ m, $u^*=20$ cm/s, S.V.D.=100 ug/m³, $T=25$ °C, $L=\infty$) due to input parameter deviation.

% change in environmental input parameter	25%	50%	100%	200%	400%
z_0 (m)	5.7%	2.8%	0%	-2.6%	-5.1%
D_a (m ² /s)	-21.3%	-11.9%	0%	15.6%	37.1%
x (m)	27.6%	12.1%	0%	-9.8%	-17.8%
u^* (m/s)	-65.7%	-42.2%	0%	76.2%	214.8%
S.V.D. (ug/m ³)	-75%	-50%	0%	100%	300%
	$T=5$ °C	$T=15$ °C	$T=25$ °C	$T=35$ °C	$T=45$ °C
T (°C)→S.V.D.(T)	5.88%	25.48%	0%	358.72%	1186.25%
	$L= -5$ m	$L= -100$ m	$L=inf$	$L= 100$ m	$L= 5$ m
L (m)	-13.4%	-0.8%	0%	0.8%	18.2%

S.V.D.(T) (ug/m³) saturated density of pesticide vapor calculated from a pesticide's vapor pressure at a particular temperature and molecular weight using eq. 3 and 4.

D_a (m²/s) molecular diffusion coefficient of pesticide (calculated from the compound's molecular weight of a using eq. 6 and adjusted for temperature using eq. 7)

u^* (m/s) frictional velocity (calculated from wind speed profiles under neutral conditions using eq. 29 and 30)

x (m) average distance between the edge and center of the treated plot.

$3ku^*x^{0.8}z_0^{0.2}$ (m) is the height chosen in boundary layer where $C_z \ll S.V.D.(T)$ this is assumed to be three times the thickness δ given for the distance x from the windward edge of the evaporating surface by equation 62.

z_0 (m)-the momentum roughness length.

L (m)-the Monin Obukhov measurement of atmospheric stability. $L=\infty$ in neutral conditions $L= -5$ m during unstable conditions, and $L= +5$ m during stable conditions.

T (K)- Surface Temperature or temperature of the leaf surface

Table 10: Percent change in Flux estimated by equation 3,4 and 61 ($z_0=0.0045$, $D_a=0.04$ cm²/s, $x=14$ m, $u^*=20$ cm/s, S.V.D.=100 ug/m³, $T=25$ °C, $L=\infty$, $\Delta H_{vap}=100$ KJ/mol and $\Delta S_{vap}=300$ J/K/mol) due to input parameter deviation.

% change in parameter	25%	50%	100%	200%	400%
T (K)	1.04×10^{-52}	5.93×10^{-18}	1	2.9×10^8	3.5×10^{12}
ΔH_{vap} (kJ/mol)	1.4×10^{13}	5.81×10^8	1	3.0×10^{-18}	2.6×10^{-53}
ΔS_{vap} (J/K/mol)	4.6×10^{-65}	4.34×10^{-26}	1	2.72×10^{24}	1.43×10^{60}

Table 11: Qualitative analysis in the parameters used in flux predicted by the Fugacity Model.

Parameter Input	Relation to Flux estimated by Fugacity Model.	Degree of possible error in parameter in the estimation of flux.	Suggested methods for increasing the accuracy of measurement or estimate of each parameter.
Estimation of Vapor pressure.	directly proportional	order of magnitude with current deviation in literature values	Making more accurate vapor pressure measurements at several temperatures
Estimation of Diffusion Coefficient in Air.	weakly proportional	~10%	Could adjust for change in barometric pressure. Find diffusion coefficients for P and F.
Assumption that $C_s - C_z = C_s$ is $z=3\delta$.	depends on stability L $F \propto 1/(\ln z + 4.7 \cdot z/L) + C$	will not exceed 10% for 50% error in height estimation at $z=73$ cm at $L=\infty$, -5 m	Verify assumption that $z=3\delta$ for eq. 59 is valid.
Measured Surface Temperature as an estimation of the leaf temperature.	exponentially proportional to $1/T(K)$	unknown	Use thermocouples on leaf surface.
Estimation of u^* and L from wind speed regressions.	directly proportional (u^*) weakly inversely proportional (L)	unknown	Measure L , use wind speed indicators of higher quality, make sure upwind fetch, clear of objects exists.

Table 12: Comparison between estimates of ΔH_{vap} and ΔS_{vap} based a linear regression ($\ln p$ vs. $1/T$ (K)) of measured vapor pressures at different temperatures using equation 3 and predictions of ΔH_{vap} and ΔS_{vap} using Lyman's method [46]

	ΔH_{vap} (KJ/mol) (measured)	ΔS_{vap} (J/K/mol) (measured)	ΔH_{vap} (KJ/mol) (predicted Lyman et.al)	ΔS_{vap} (J/K/mol) (predicted, Lyman et. al)
Triadimefon	111	305	427	1381
Chlorpyrifos	88	248	395	1276
Triclopyr	74	177	431	1316

Figure 66: Sensitivity Analysis of % change in flux estimated by the predictive model with % change in environmental parameters (wind speed u^* , saturated vapor density S.V.D., average plot radius R, surface temperature T, molecular diffusion coefficient D_a , atmospheric stability L, and roughness length z_0)

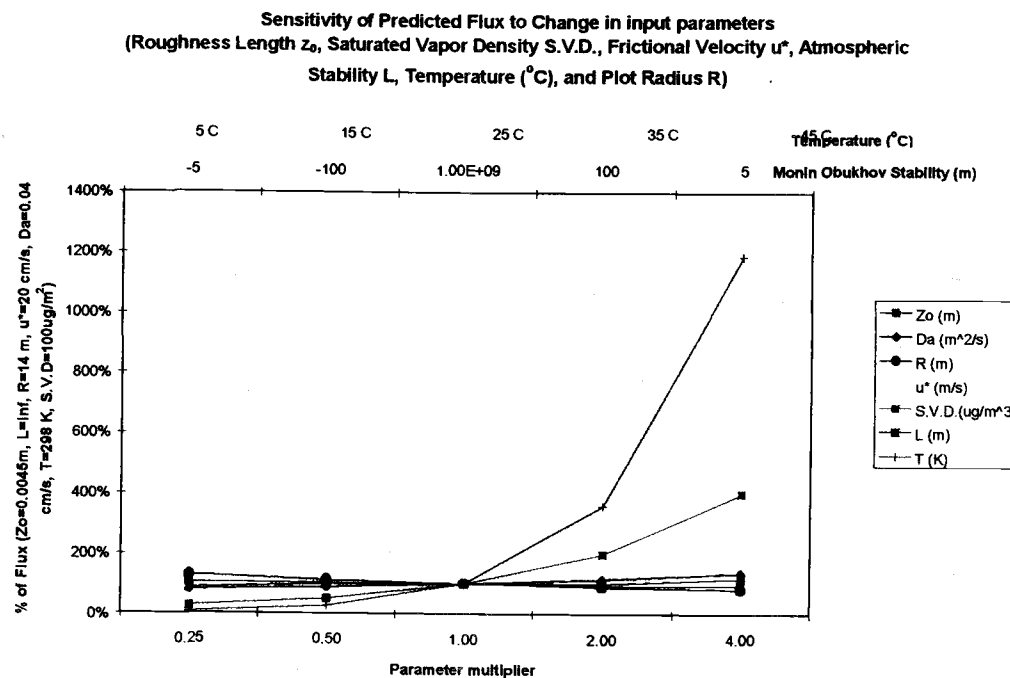


Figure 67: Sensitivity analysis of % change in flux estimated by the predictive model vs. % change in thermodynamic parameters of the active ingredient (Temperature T, enthalpy of vaporization ΔH , and entropy of vaporization ΔS) log scale.

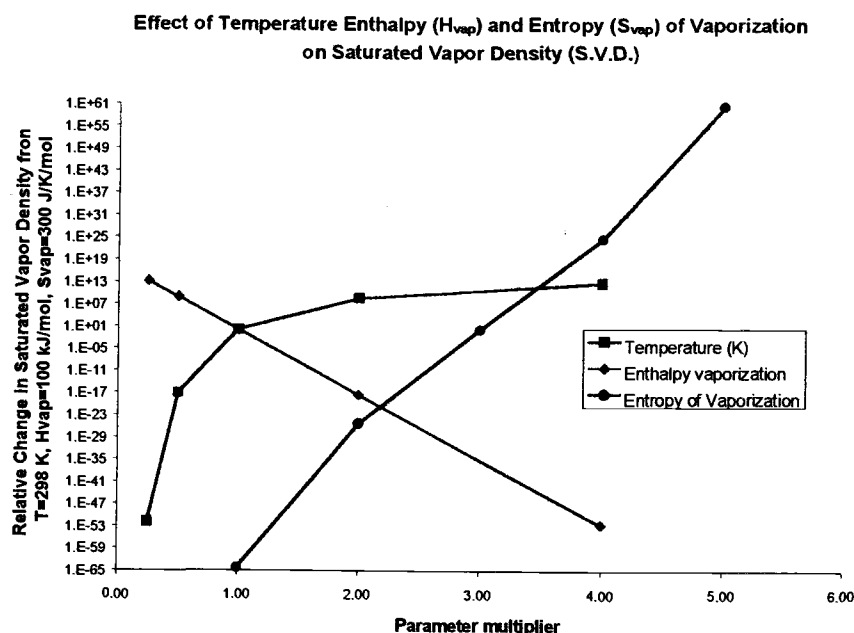


Figure 68: Measured flux ($\mu\text{g}/\text{m}^2/\text{hr}$) for all pesticide applications during the day of application (log scale).

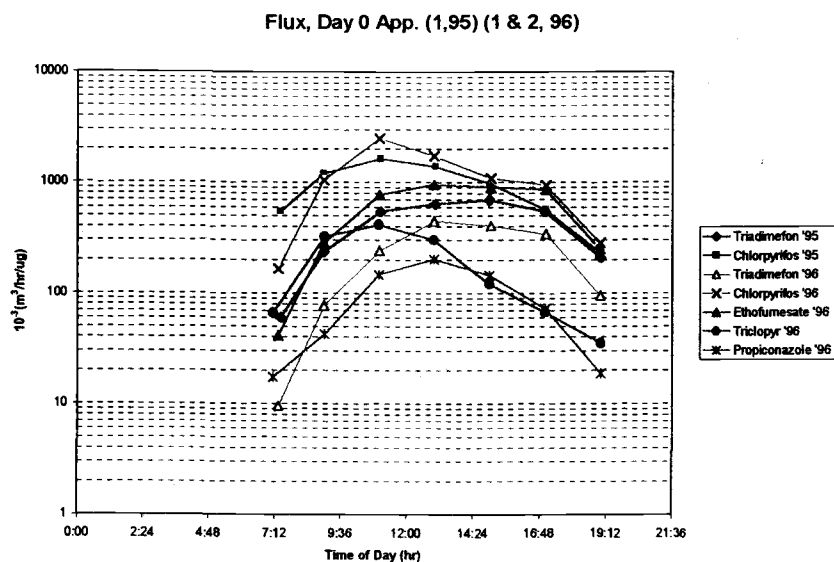
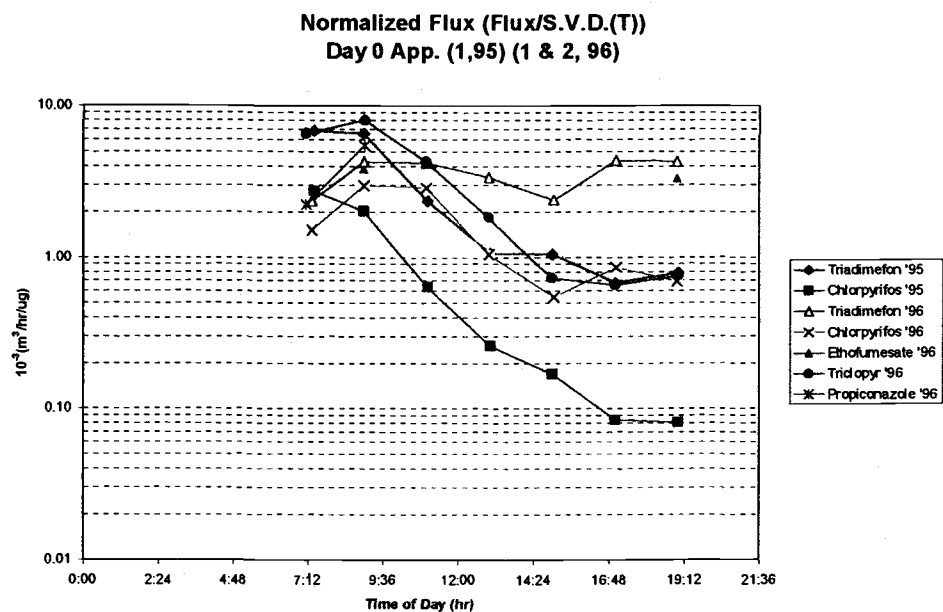


Figure 69: Measured flux ($\mu\text{g}/\text{m}^2/\text{hr}$), normalized for the saturated vapor density ($\mu\text{g}/\text{m}^3$) of the active ingredient at the measured surface temperature*, for all pesticide applications during the application date, Day 0 (log scale).



*for pesticides where vapor pressure estimates for the active ingredient are only available at a single temperature (ethofumesate and propiconazole), a normalized flux value only appears when the surface temperature coincides with the temperature of the vapor pressure measurement.

Figure 70: Measured flux ($\mu\text{g}/\text{m}^2/\text{hr}$), normalized for the saturated vapor density ($\mu\text{g}/\text{m}^3$) of the active ingredient at the measured surface temperature* and the application density ($\mu\text{g}/\text{m}^2$), for all pesticide applications during the application date, Day 0 (log scale).

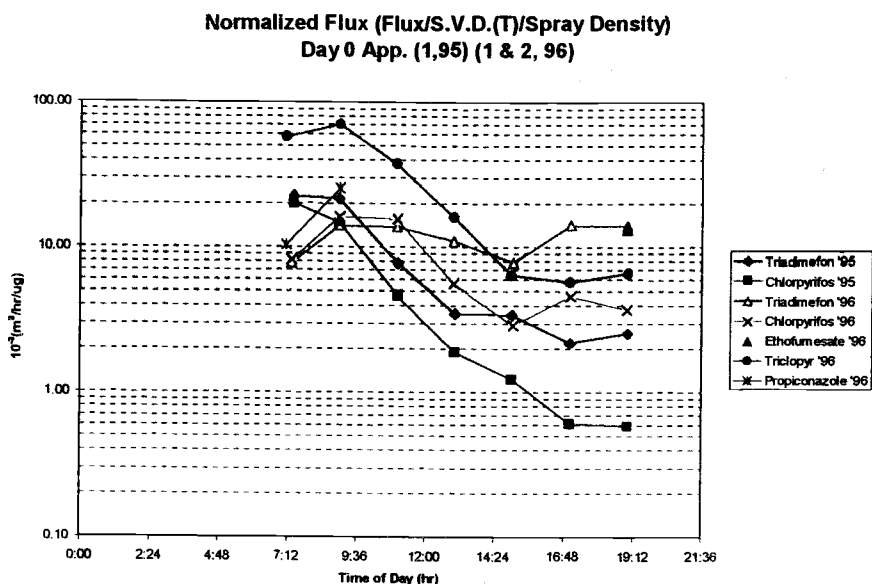
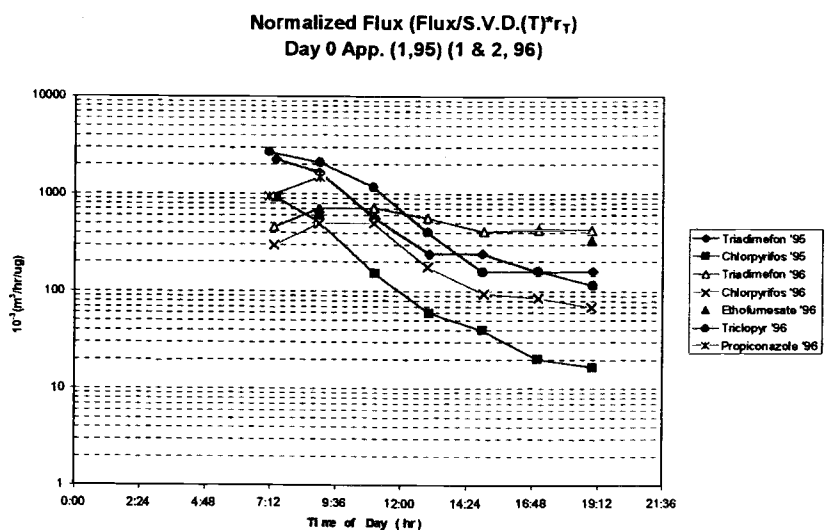


Figure 71: Measured flux ($\mu\text{g}/\text{m}^2/\text{hr}$), normalized for the saturated vapor density ($\mu\text{g}/\text{m}^3$) of the active ingredient at the measured surface temperature* and the aerodynamic resistance (hr/m) for all pesticide applications during the application date, Day 0 (log scale).



*for pesticides where vapor pressure estimates for the active ingredient are only available at a single temperature (ethofumesate and propiconazole), a normalized flux value only appears when the surface temperature coincides with the temperature of the vapor pressure measurement.

Figure 72: Measured flux ($\mu\text{g}/\text{m}^2/\text{hr}$), normalized for the saturated vapor density ($\mu\text{g}/\text{m}^3$) of the active ingredient at the measured surface temperature*, the application density ($\mu\text{g}/\text{m}^2$), and the aerodynamic resistance (hr/m) for all pesticide applications during the application date, Day 0 (log scale).

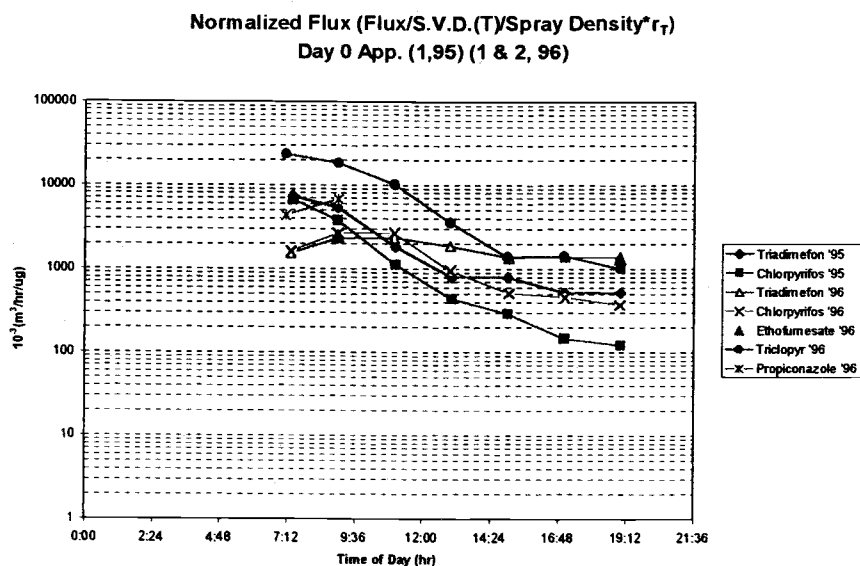
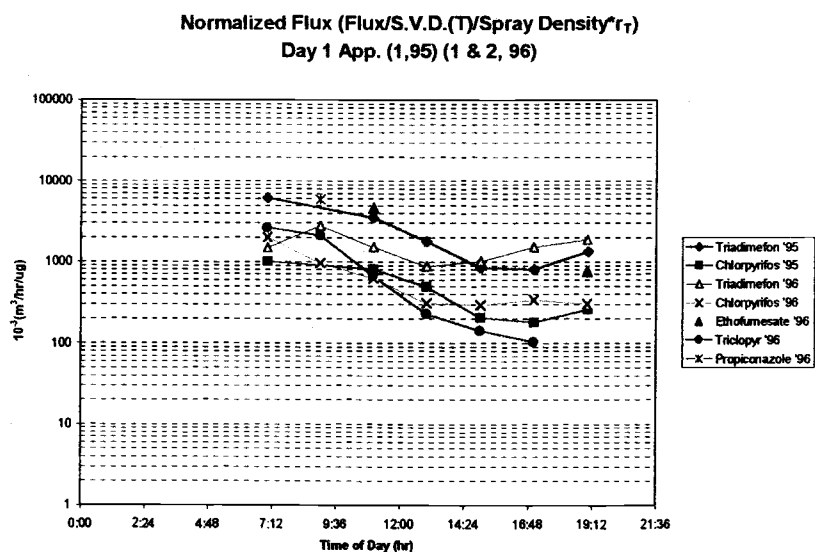
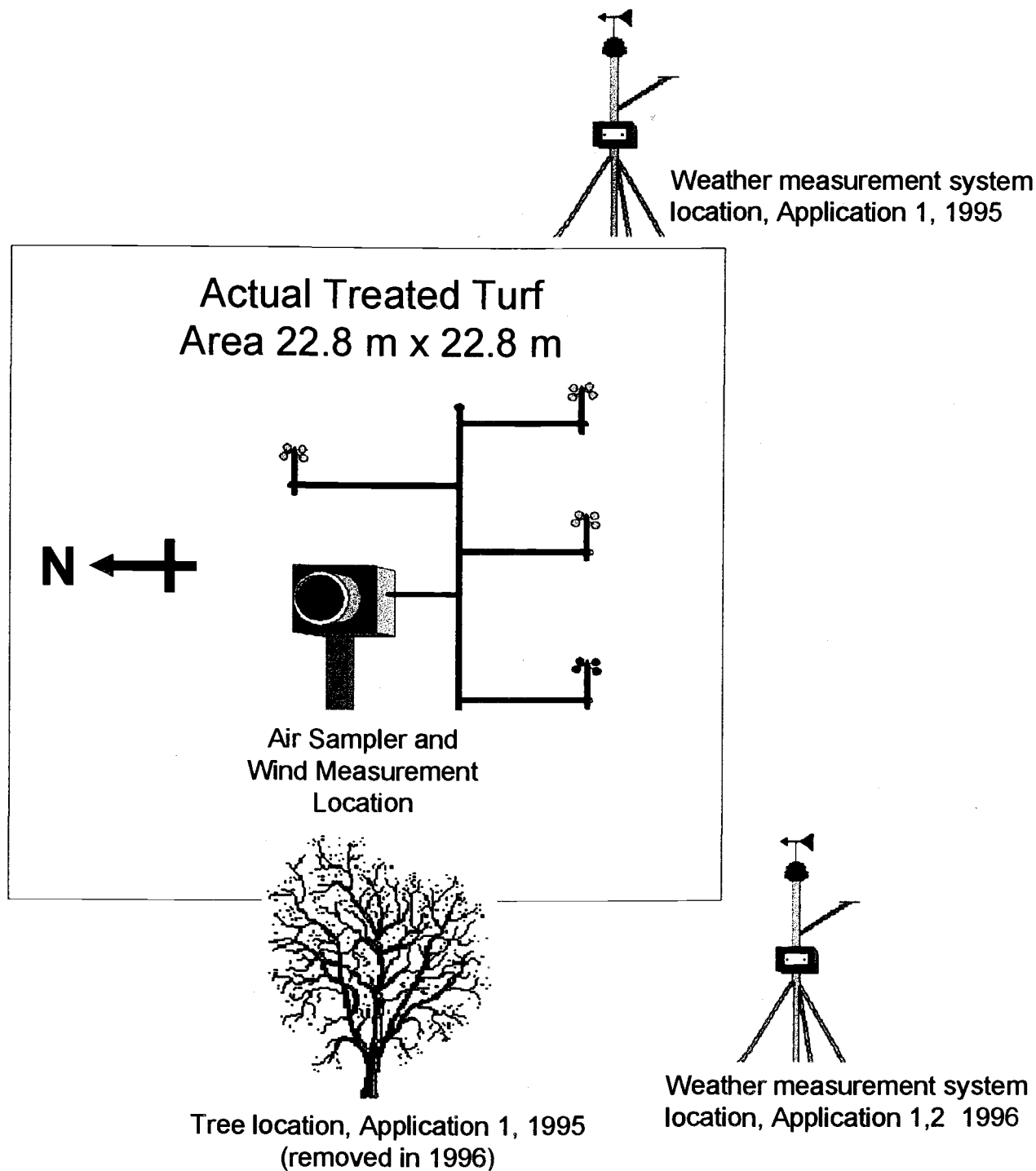


Figure 73: Measured flux ($\mu\text{g}/\text{m}^2/\text{hr}$), normalized for the saturated vapor density ($\mu\text{g}/\text{m}^3$) of the active ingredient at the measured surface temperature*, the application density ($\mu\text{g}/\text{m}^2$), and the aerodynamic resistance (hr/m) for all pesticide applications during day after the application date, Day 1 (log scale).



*for pesticides where vapor pressure estimates for the active ingredient are only available at a single temperature (ethofumesate and propiconazole), a normalized flux value only appears when the surface temperature coincides with the temperature of the vapor pressure measurement.

Figure 74: Experimental setup differences between years 1995 and 1996. 1) Difference in location of temperature/solar radiation measurement system and 2) presence of a tree upwind from the treated surface during 1995, which created shade during the later afternoons.



Discussion and Comparison of BTLSD and Fugacity flux results for Day 0.

Although the same trends of flux vs. temperature are apparent in the results of both models, the predictive model appears to consistently estimate higher values of flux with the greatest departures occurring during the noon hours. As has already been discussed, the noon-hour departure (deterioration of the linearity of the log Flux vs. $1/T$ at higher temperatures) may be due to the soil temperature probes over-estimating the temperature of the leaf surface. Aside from this, the consistent pattern of over-prediction may be indicative of systematic errors in the assumptions of the predictive model. Measured flux values for all pesticide applications on the application date (Day 0), were normalized for the major inputs of the predictive model (S.V.D.(T), r_T) in addition to the application rate (spray density) to determine which factor, if any, contributed to systematic difference between the two models (Fig 68-73). A consistent narrowing of relative differences of measured flux values for each pesticide application occurred after factoring each parameter in the fugacity model. Fig. 67-73, display the parameters of decreasing importance in the fugacity model as, S.V.D.(T), $\rightarrow r_T \rightarrow$ spray density. *The decrease in relative difference of measured BTLSD flux results with each successive step in normalization for a factor of the fugacity model gives credibility to the theory of the fugacity model. A factor which is not included in the fugacity model, but appears to determine flux intensity is the application rate (amount of active ingredient applied per area of turf grass).*

Another trend which should be noted in figures 72-73, is the serial correlation of decreasing normalized flux values with time. This may be due to suspected temperature errors described earlier (underestimation of leaf temperature in the morning and overestimation in the afternoons and evenings) or an effect of decreasing surface concentrations during a single day causing a decrease in flux. The latter is probably true for Triclopyr, since its rank of measured flux normalized for S.V.D., r_T and spray density changes dramatically from one day to the next (Day 0 to Day 1, Figures 72 and 73) however, it is not known whether this is true for the other pesticides.

In summary, the relative differences in flux values for pesticides applied for all applications appears to decrease when normalized for saturated vapor density of the active ingredient, aerodynamic resistance to transfer and to spray density. The current version of the fugacity model accounts for the first two. A refined version of the fugacity model should also account for the third. Factors which continue to cause relative differences in normalized flux values in Fig. 72 & 73 have not been able to be quantitatively discerned from this data set. Experiments conducted under more controlled conditions could test the assumptions of the fugacity model and account or rule out some of the factors suspected for causing errors. Suspected errors in the assumptions of the current version of the fugacity model are listed below:

1. *The vapor pressure of the active ingredient in the deposit is similar to the vapor pressure of the*

pure active ingredient. The constituents of the deposit and the leaf surface may be reducing the vapor pressure, at a given temperature, from its literature value.

2. *The vapor density of the active ingredient in the zone where molecular diffusion is in equilibrium with the deposit.* Currently, the predictive model assumes that the flux is independent of the amount of pesticide applied over a particular area (zero-order kinetics). This is not likely to be true due to the following observations: 1) The flux normalized for solar radiation during the noon hours, on days following application (Figures 44-49) appear to show an exponential decay pattern (indicating first order kinetics, where the flux is dependent on the amount applied or remaining) instead of a horizontal line (zero-order kinetics, where flux is independent of the amount applied or remaining). 2) Simultaneous plots of the flux measurements for all pesticides on the first day of each application normalized for S.V.D.(T), r_T , and spray density (Figures 72 and 73) show a tighter cluster than flux values which have not been normalized for spray density (Figure 71). Future studies could relate flux with the application rates and remaining foliar residue concentrations.
3. *Equation 56 may not represent the true value of r_T in the field.* Recall that equation 56 was chosen since it predicted values of r_T for lead vapor deposition, water evaporation, and heat flux from Italian rye grass in a wind tunnel [25]. In using this equation, it is assumed that the vertical source/sink distribution of lead vapor, moisture, heat and pesticide vapor are identical in the field and the tunnel. This assumption may not be valid since sunlight was not used as a source of heat to drive the evaporation process in the wind tunnel experiment. Because of a decreasing sunlight penetration with canopy depth, the height distribution of temperature and pesticide vapor may be lower in deeper areas of the canopy. The temperature measured by the probes, which are fully exposed to sunlight, may over-estimate the average temperature of the canopy. A further implication of this hypothesis would be that more volatilization would take place from pesticide residues near the surface during the initial stages of evaporation. After a period of time the remaining residues would be deeper in the canopy where the temperature is lower and the effective canopy transport resistance from the pesticide deposit to the air stream above the canopy r_{SL} would be greater. Both of these could result in a decrease in measured flux with time following pesticide application.
4. Finally, the boundary layer assumption made by this author that $C_s - C_z = C_s$ occurs at $z = 3\delta_s$ may not be true. Although the true value is likely to be between δ_{eq} and $10\delta_{eq}$, the exact value is subject to change with fetch size, atmospheric stability and the aerodynamic roughness of the surface upwind from the evaporating source. These factors cannot be fully accounted for since concentration profiles in the zone between the equilibrated boundary layer δ_{eq} and the top internal boundary layer δ_s (Figures 24 and 25) are not understood and can change depending on the distance from the leading edge, the surface type, and atmospheric stability [31].

Future Research

Future research should design experimental conditions which are ideal for both the BTLSD and fugacity models (homogeneous upwind fetch) and can best measure the parameters which each require (leaf temperature T , u^* , L , z_0). Wind tunnel experiments can also test for the occurrence of flow transitions over turf grass (change of z_0 with Re^*) at low wind speeds. Measurements of emission rates as a function of pesticide application rates or remaining surface residues could assist in the development of models which do not assume zero order kinetics and can predict flux as a function of initial application rates on dates receding application from the day of application. Vapor pressure studies, where the vapor

pressures of the active ingredient are accurately estimated for the compounds studied at a range of environmental temperatures, in addition to an understanding of how the effect of spray formulations and droplet leaf interactions affect the vapor pressure of the active ingredient, would improve the estimation of C_s or S.V.D.(T) in equation 59.

Conclusion

The predicted volatile loss rates of pesticides from turf grass are generally within an order of magnitude above those estimated by the Backward-Time Lagrangian stochastic Dispersion model (BTLSD) model during the period immediately following application. The theory is also weak in understanding the transport processes which occur in the canopy, is founded on many unverifiable assumptions and requires a large number of micrometeorological and chemical parameters which are limited in availability. In addition, the partitioning and degradation processes which begin soon after application (or after rainfall) limit its usefulness after the first day. Understanding pesticide attenuation as related pesticide partitioning rates into leaf surfaces, and degradation/metabolization could assist in developing predictive models which would forecast emission on dates further away from the date of application. Some studies have attempted to understand partitioning as a function of a chemical's Henry's constant K_h (air/water partition constant) and K_{ow} (octanol/water partition constant).

A best estimate of loss during the first 24 hrs from a plot of similar size and roughness, using the fewest parameters appears to be the regression equation of the percent loss of amount applied vs. vapor pressure (@25 °C in Figure 57).

$$\% \text{ loss of amount applied in 24 hrs} = 41.37 \cdot x + 0.0148 \quad (70)$$

-x is the vapor pressure of the active ingredient in pascals.

With equation 70 being the final and simplest addition to the previously discussed models of estimating pesticide evaporation rates from turf grass, this thesis is concluded. The parameters and assumptions of each the three models are summarized below:

1. TPS/BTLSD Method Requirements (equation 67)

Circular Plot (radius R).

Estimation of Roughness Length (z_0).

Upwind Fetch of equivalent aerodynamic roughness length, free from interfering objects

Calculation of height $z = Z_{INST}$ and Φ for plot defined by R and z_0 .

Measurements of Airborne Concentrations at height $z = Z_{INST}$.

Wind speed at height $z = Z_{INST}$ during airborne concentration measurement interval.

2. Predictive Model Inputs (equation 63)

Accurate estimates of vapor pressures of compounds.

Estimates of a molecular diffusion coefficient.

Estimates of wind profile parameters z_0 , u^* .

Measurement of L using a sonic anemometer (the necessity of this parameter depends on the size of the surface).

Upwind Fetch of equivalent aerodynamic roughness length, free from interfering objects.

Estimate of wind direction or average path length over the evaporating surface.

Evaporating surface dimensions.

Estimates of the spray density.

3. Estimate of average loss of amount applied measured during first 24 hours following application by TPS or BLSD method for turf plot $z_0=0.0045\text{cm}$, $R=14\text{ m}$ (equation 70)

Vapor pressure of active ingredient at 25 °C.

Linear equation of %loss measured by TPS in 1st 24 hrs following pesticide application vs. Vapor Pressure for Triadimefon, Chlorpyrifos, Ethofumesate, Triclopyr, Propiconazole.

Bibliography

1. Mackay D., Multimedia Environmental Models: The Fugacity Approach, (Lewis Publishers, Inc., Chelsea, Michigan, 1991), pp. 2, 20.
2. Taylor A.W., Spencer W.F., "Volatilization and Vapor Transport Processes." Chapter 7 in *Pesticides in the Soil Environment: Processes, Impacts, and Modeling*, edited H.H. Cheng, Soil Science Society of America, Madison, Wisconsin, 1990.
3. J.J. Jenkins, A.S. Curtis, and R.J. Cooper, "Two Small-Plot Techniques for Measuring Airborne and Dislodgeable Residues of Pendimethalin Following Application to Turfgrass." A.C.S. Symposium Series: Pesticides in Urban Environments #522, ACS, Washington DC, 1993.
4. Aspelin A., Grube A., Torla R., "Pesticides Industry Sales and Usage, 1990 and 1991 Market Estimates" *Biological and Economic Analysis Branch Division, Office of Pesticide Programs, E.P.A.* Washington D.C., 1992.
5. Cooper, R. J., J. J. Jenkins, and A.S. Curtis. 1990. Pendimethalin volatility following application to turfgrass. *J. Environ. Qual.* 19:508-513.
6. R. P. Schwarzenbach, P. M. Gschwend, D. M. Imboden, *Environmental Organic Chemistry*, (John Wiley and Sons, New York, NY, 1993), pp. 182-224.
7. Wauchope, R.D., T.M. Buttler, A.G. Hornsby, P.M. Augustinjn-Beckers, and J. P. Burt. 1992. The SRS/ARS/CES pesticide properties database for environmental decision making. *Rev. Environ. Contam. Tox.* 123:1-155.
8. Atkins P.W. *Physical Chemistry* 5th ed.; Freeman Publ. Co.: NY, 1994.
9. Linsley, R. K.; Kohler, M. A.; Paulhus, J. L. H. *Hydrology for engineers*, 2nd ed.; McGraw-Hill: New York, 1975; pp 42-44.
10. J. J. Jenkins, M. Conway (1997). Verbal Communication.
11. McCall, P.J., L.E. Stafford, and P.D. Gavit 1986 "Compartmental model describing the foliar behavior of tridiphane on giant foxtail." *J. Agric. Food Chem.* 34:229-234.
12. John Rhinehold, M. Conway (1997). Verbal Communication.
13. Jenkins, J. J., NRI-1004 95/96/97: Grant Proposal (1994)
14. Majewski, M. S., M. M. McChesney, and J. N. Seiber. 1991. A field comparison of two methods for measuring DCPA soil evaporation rates. *Environ. Toxicol. And Chem.* 10:301-311.
15. McCall, P.J., Stafford L.E., Zorner P.S. Gavit P.D. "Modeling the Foliar Behavior of Atrazine with and without Crop Oil concentrate on Giant Foxtail and the Effect of tridiphane on the Model Rate Constants." *J. Agric. Food chem.* 1986, 34, 235-238.
16. Wilson, J.D., G.W. Thurtell, G.E. Kidd, and E.G. Beauchamp. 1982. Estimation of the Rate of Gaseous Mass Transfer from a Surface source Plot to the Atmosphere. *Atmos. Environ.* 16(8):1861-1867.
17. Majewski, M. S., D. E. Glotfelty, K. T. Paw, and J. N. Seiber. 1990. "A Field comparison of several methods for measuring pesticide evaporation rates from soil." *Environ. Sci. Technology.* 24:1490-1497.

18. Fuller, E.N., Schettler, P.D., and Giddings, J.C., "A new method for prediction of binary gas-phase diffusion coefficient," *Ind. Eng. Chem.*, 58, 19-27 (1966).
19. Deacon, E. L. "Vertical Profiles of Mean Wind in the Surface Layers of the Atmosphere." *Geophys. Mem., London*, 11, No. 91, (1953).
20. Stull, R. B. "An Introduction to Boundary Layer Meteorology" Kluwer Academic Publishers Dordrecht, The Netherlands (1988)
21. Bukovac M.J., Leon M.J., Cooper J.A. "Spray Droplet: Plant Surface Interaction and Deposit Formation as related to Surfactants and Spray Volume."
22. Guerra, Antonio Fernando "Analysis of parameters for evaluation of canopy and aerodynamic resistances over turfgrass." Ph.D. Thesis, University of Arizona, 1990.
23. Monro D.S. and Oke A.M. (1975) Aerodynamic boundary layer adjustment over a crop in neutral stability. *Boundary-Layer Met.* 9, 53-61
24. Hartley G.S., Graham-Bryce I.J., "Physical Principles of Pesticide Behavior", Academic Press, London, (1980)
25. Chamberlain, A.C., "Transport of Gases to and from Grass and Grass-Like Surfaces", *Proc. Roy. Soc. London A290*, 236-265 (1966)
26. Brutsaert, Wilfried, *Evaporation into the Atmosphere*, D. Reidel Publishing Company, Dordrecht, Holland (1982).
27. Brutsaert, Wilfried, "Heat and Mass Transfer to and from Surfaces with Dense Vegetation or Similar Permeable Roughness.", *Boundary Layer Meteorology*, 16, (1979), 365-388
28. Monteith J. L., Unsworth M. J., *Principles of Environmental Physics*, Elsevier Publ. Co., Inc., N.Y. (1990)
30. Kondo, Junsei, "Relationship Between the Roughness Coefficient and Other Aerodynamic Parameters." *J. Meteorol. Soc. Japan*, 50, 487-488 (1971)
31. Larry Mahrt, M. Conway (1998, 1999). Verbal Communication.
32. Chamberlain, A.C., "Transport of gases to and from surfaces with bluff and wave-like roughness elements" *Q. J. Roy. Meteorol. Soc.* 94, 318-322 (1968)
33. Frear, Donald E. H., "Chemistry of Pesticides", 3rd Ed., D. Van Nostrand Company, Inc. Toronto. (Publication date not available).
34. Owen, P. R., and Thomson, W.R., "Heat Transfer Across Rough Surfaces", *J. Fluid Mech.* 15, 321-324 (1963)
35. Sutton, O. G., *Micrometeorology*, McGraw Hill, London, (1953)
36. Thom A.S., "Momentum, mass and heat exchange of vegetation." *Quart. J. Roy. Meteorol. Soc.* 98: pp. 124-134 (1972)
37. Thom A.S., "Momentum Absorption by Vegetation." *Quart. J. Roy. Meteorol. Soc.* 97: pp. 414-428 (1971)

38. Deacon, E. L. "Wind profiles and the shearing stress-an anomaly resolved." *Quart. J. R. Met. Soc.*, 83, pp. 537-540 (1957)
39. Montieth, J. L., "Gas exchange in plant communities." *Environmental Control of Plant Growth*, (L. T. Evans, Ed.), Academic Press, N.Y., pp. 95-112. (1963)
40. Sheppard, P. A., "Transfer across the Earth's surface and through the air above" *Quart. J. R. Met. Soc.*, 84, pp. 205-224. (1953)
41. Chamberlain, A.C. Garland, J.A. and Wells, "Transport of gases and particles to surfaces with widely spaced roughness elements" *Boundary-Layer Meteorology*, 29, 343-360 (1984)
42. Murphy, K.C. 1994. The determination of volatile and dislodgeable residues from pesticide-treated turf grass and an assessment of human exposure. Ph.D. Diss. University of Massachusetts, Amherst (Diss. Abstr. DAI-B 55/08 p. 3272).
43. Michael Maynard (Novartis Chemical Company) and Michael Conway - verbal communication, April 1998.
44. J.D. Wilson and K.C. Murphy (1991)-contract report.
45. Flesch, T. K., Wilson, J.D., "Backward-Time Lagrangian Stochastic Dispersion Models and their Application to Estimate Gaseous Emissions" *Journal of Applied Meteorology*, 34, pp. 1320-1332
46. Thomas K. Flesch, Michael Conway- electronic correspondence, March 31, 1999.
47. "Handbook of Chemical Property Estimation Methods." Lyman, W.J.; Reehl, W. F.; Rosenblatt, D.H., Eds.; McGraw Hill: New York, NY, 1982
48. Oke, T.R. "Boundary Layer Climates" 2nd ed., Methuen, London, 1987.

Appendix 1:

Predicted vs. measured values of B^{-1} for scalar transfer between roughened surfaces and airstreams in a wind tunnel [32, 40, 41].

Source File: boundary2.xls
 Sheet1
 Chart1

Surface	Substance	Da	Sc	u* (cm/s)	Re*	Zo (cm)	Measured	Predicted	Predicted	Predicted	Zo' (cm)	Zo'/Zo
							B ⁻¹	*Sheppard (1958) B ⁻¹	*Chamb 1984 B ⁻¹	*Chamb 1968 B ⁻¹		
grass	thorium-B	0.054	2.87	50	225.81	0.7	7.7	13.62	42.94	61.55	3.22E-02	4.60E-02
short grass	thorium-B	0.054	2.87	25	32.26	0.2	7.9	8.87	24.47	25.64	8.49E-03	4.24E-02
short grass	thorium-B	0.054	2.87	50	64.52	0.2	8.7	10.56	30.05	35.02	6.16E-03	3.08E-02
short grass	thorium-B	0.054	2.87	100	129.03	0.2	10.3	12.25	36.68	47.85	3.25E-03	1.62E-02
artificial grass	thorium-B	0.054	2.87	25	161.29	1	7	12.80	39.08	52.90	6.08E-02	6.08E-02
artificial grass	thorium-B	0.054	2.87	50	322.58	1	8	14.49	47.41	72.26	4.08E-02	4.08E-02
artificial grass	thorium-B	0.054	2.87	100	645.16	1	10.1	16.18	57.33	98.71	1.76E-02	1.76E-02
towelling	thorium-B	0.054	2.87	50	14.52	0.045	8	6.92	19.14	17.90	1.83E-03	4.08E-02
rough glass	thorium-B	0.054	2.87	25	3.23	0.02	28.5	3.25	11.57	9.10	2.24E-07	1.12E-05
rough glass	thorium-B	0.054	2.87	50	6.45	0.02	30.7	4.94	14.71	12.43	9.29E-08	4.64E-06
rough glass	thorium-B	0.054	2.87	100	12.90	0.02	35.3	6.63	18.44	16.98	1.47E-08	7.37E-07
rough glass	camphor	0.038	4.06	100	12.90	0.02	39.4	7.48	22.89	22.42	2.86E-09	1.43E-07
towelling	water vapor	0.240	0.65	25	7.26	0.045	4.7	1.59	4.63	3.97	6.87E-03	1.53E-01
towelling	water vapor	0.240	0.65	50	14.52	0.045	5.8	3.28	6.45	5.43	4.42E-03	9.83E-02
towelling	water vapor	0.240	0.65	100	29.03	0.045	8	4.97	8.62	7.41	1.83E-03	4.08E-02
artificial grass	water vapor	0.240	0.65	25	161.29	1	4.5	9.16	15.91	16.04	1.65E-01	1.65E-01
artificial grass	water vapor	0.240	0.65	50	322.58	1	4.9	10.85	19.86	21.91	1.41E-01	1.41E-01
artificial grass	water vapor	0.240	0.65	100	645.16	1	5.8	12.54	24.57	29.93	9.83E-02	9.83E-02
short grass (open air)	heat	0.225	0.69	25	51.61	0.32	5.7	6.54	11.24	10.11	3.27E-02	1.02E-01
short grass (open air)	heat	0.225	0.69	25	51.61	0.32	3.9	6.54	11.24	10.11	6.72E-02	2.10E-01
Guerra (Zo=7.6Zo' for grass) [22]							0.32	5.07				0.00E+00
cone-shaped elements (1 cm ht)	bromobenzene	0.037	4.15	65.6	126.97	0.3	16	13.11	44.90	63.75	4.98E-04	1.66E-03
2.54 cm spheres	thorium-B	0.054	2.87	15.6	50.32	0.5	21	9.95	27.94	31.32	1.12E-04	2.25E-04
2.54 cm spheres	thorium-B	0.054	2.87	31	100.00	0.5	28.4	11.63	34.11	42.66	5.83E-06	1.17E-05
2.54 cm spheres	thorium-B	0.054	2.87	70	225.81	0.5	35.6	13.62	42.94	61.55	3.27E-07	6.54E-07
2.54 cm spheres	thorium-B	0.054	2.87	104	335.48	0.5	37	14.58	47.93	73.55	1.87E-07	3.74E-07
2.54 cm spheres	thorium-B	0.054	2.87	143	461.29	0.5	43.7	15.36	52.32	84.88	1.28E-08	2.56E-08
0.79 cm spheres	thorium-B	0.054	2.87	20	18.06	0.14	12.3	7.46	20.50	19.75	1.02E-03	7.30E-03
0.79 cm spheres	thorium-B	0.054	2.87	49	44.26	0.14	19.6	9.64	26.90	29.56	5.51E-05	3.94E-04
0.79 cm spheres	thorium-B	0.054	2.87	100	90.32	0.14	25.9	11.38	33.13	40.75	4.43E-06	3.17E-05
0.79 cm spheres	thorium-B	0.054	2.87	150	135.48	0.14	28.9	12.37	37.20	48.91	1.34E-06	9.54E-06
2.54 cm cyl/5.08 cm apart	thorium-B	0.054	2.87	20	77.42	0.6	37.5	11.01	31.69	38.02	1.84E-07	3.06E-07
2.54 cm cyl/5.08 cm apart	thorium-B	0.054	2.87	47	181.94	0.6	44.6	13.09	40.42	55.85	1.07E-08	1.79E-08
2.54 cm cyl/5.08 cm apart	thorium-B	0.054	2.87	70	270.97	0.6	52.1	14.06	45.18	66.81	5.34E-10	8.90E-10
2.54 cm cyl/5.08 cm apart	thorium-B	0.054	2.87	140	541.94	0.6	67.6	15.75	54.67	91.26	1.08E-12	1.81E-12
0.79 cm cyl/1.59 cm apart	thorium-B	0.054	2.87	25	24.19	0.15	22.6	8.17	22.43	22.53	1.78E-05	1.19E-04
0.79 cm cyl/1.59 cm apart	thorium-B	0.054	2.87	50	48.39	0.15	23	9.86	27.62	30.77	1.52E-05	1.01E-04
0.79 cm cyl/1.59 cm apart	thorium-B	0.054	2.87	82	79.35	0.15	29.9	11.07	31.91	38.44	9.59E-07	6.39E-06
0.79 cm cyl/1.59 cm apart	thorium-B	0.054	2.87	107	103.55	0.15	29.8	11.71	34.45	43.34	9.98E-07	6.66E-06
0.79 cm cyl/1.59 cm apart	thorium-B	0.054	2.87	118	114.19	0.15	40	11.95	35.43	45.29	1.69E-08	1.13E-07
0.79 cm cyl/1.59 cm apart	thorium-B	0.054	2.87	170	164.52	0.15	42.3	12.84	39.29	53.37	6.73E-09	4.48E-08
0.16 cm cyl/0.32 cm apart	thorium-B	0.054	2.87	12	1.55	0.02	17.7	1.46	8.80	6.54	1.68E-05	8.42E-04
0.16 cm cyl/0.32 cm apart	thorium-B	0.054	2.87	36	4.65	0.02	13.6	4.14	13.16	10.72	8.68E-05	4.34E-03
0.16 cm cyl/0.32 cm apart	thorium-B	0.054	2.87	71	9.16	0.02	18.4	5.80	16.52	14.55	1.27E-05	6.36E-04
0.16 cm cyl/0.32 cm apart	thorium-B	0.054	2.87	121	15.61	0.02	20.3	7.10	19.58	18.50	5.95E-06	2.98E-04

¹ Data sets from Chamberlain "Transport of gases to and from surfaces with bluff and wave-like roughness elements" Q. J. Roy. Meteorol. Soc. 94, 318-322 (1968) and Chamberlain "Transport of gases to and from grass and grass-like surfaces," Proc. Roy. Soc., A, 290, p. 236 (1966)

Equation Key: $\text{*Sheppard } B^{-1} = 1/k^* \ln(ku^*z_0/Da)$ [40] $\text{*Chamberlain (1984) } B^{-1} = 7.3^*(u^*z_0/v)^{0.25}(v/Da)^{0.45} - 5.5$ [41]

$\text{*Chamberlain (1968) } B^{-1} = 0.5(u^*z_0/v)^{0.25}(v/Da)^{0.8}$ [32]

Surface	Substance	Da	Sc	u* (cm/s)	Re*	Zo (cm)	Measured B ⁻¹	*Shephard (1958) B ⁻¹	*Chamb 1984 B ⁻¹	*Chamb 1968 B ⁻¹	Zo' (cm)	Zo'/Zo
0.79 cm cyl/4.76 cm apart	thorium-B	0.054	2.87	18.5	17.90	0.15	22.9	7.43	20.44	19.67	1.58E-05	1.05E-04
0.79 cm cyl/4.76 cm apart	thorium-B	0.054	2.87	45	43.55	0.15	28.5	9.60	26.77	29.35	1.68E-06	1.12E-05
0.79 cm cyl/4.76 cm apart	thorium-B	0.054	2.87	92	89.03	0.15	40.7	11.35	32.99	40.49	1.28E-08	8.51E-08
0.79 cm cyl/4.76 cm apart	thorium-B	0.054	2.87	143	138.39	0.15	42.8	12.42	37.42	49.38	5.51E-09	3.67E-08
5.08 cm half cyl.	thorium-B	0.054	2.87	27	52.26	0.3	31.1	10.05	28.25	31.86	1.19E-06	3.96E-06
5.08 cm half cyl.	thorium-B	0.054	2.87	56.5	109.35	0.3	34.2	11.85	34.99	44.41	3.44E-07	1.15E-06
5.08 cm half cyl.	thorium-B	0.054	2.87	123	238.06	0.3	41.8	13.74	43.58	63.03	1.64E-08	5.48E-08
5.08 cm half cyl.	thorium-B	0.054	2.87	200	387.10	0.3	41	14.93	49.86	78.44	2.26E-08	7.54E-08
Wave 2.54 cm ht	thorium-B	0.054	2.87	14	18.06	0.2	24.9	7.46	20.50	19.75	9.45E-06	4.73E-05
Wave 2.54 cm ht	thorium-B	0.054	2.87	23	29.68	0.2	28.4	8.67	23.87	24.70	2.33E-06	1.17E-05
Wave 2.54 cm ht	thorium-B	0.054	2.87	50	64.52	0.2	35.8	10.56	30.05	35.02	1.21E-07	6.04E-07
Wave 2.54 cm ht	thorium-B	0.054	2.87	83	107.10	0.2	40	11.80	34.79	44.00	2.25E-08	1.13E-07
Wave 2.54 cm ht	thorium-B	0.054	2.87	104	134.19	0.2	41.7	12.35	37.09	48.70	1.14E-08	5.70E-08
Wave 2.54 cm ht	thorium-B	0.054	2.87	191	246.45	0.2	49.7	13.83	44.00	64.02	4.65E-10	2.32E-09
Wave 0.6 cm ht	thorium-B	0.054	2.87	12.7	3.28	0.04	8.6	3.29	11.64	9.16	1.28E-03	3.21E-02
Wave 0.6 cm ht	thorium-B	0.054	2.87	37	9.55	0.04	12.8	5.90	16.74	14.82	2.39E-04	5.98E-03
Wave 0.6 cm ht	thorium-B	0.054	2.87	78	20.13	0.04	17.9	7.72	21.20	20.74	3.11E-05	7.77E-04
Glass	thorium-B	0.054	2.87	9	0.00		13.5					
Glass	thorium-B	0.054	2.87	23	0.00		18.2					
Glass	thorium-B	0.054	2.87	44	0.00		16					
Glass	thorium-B	0.054	2.87	67	0.00		12.6					
Paper	thorium-B	0.054	2.87	23	0.00		16.7					
Cloth	thorium-B	0.054	2.87	23	0.00		16.4					
2.54 cm cyl/5.08 cm apart	water vapor	0.240	0.65	23	89.03	0.6	13.7	7.71	13.02	12.28	2.50E-03	4.17E-03
2.54 cm cyl/5.08 cm apart	water vapor	0.240	0.65	36	139.35	0.6	15.8	8.80	15.16	15.02	1.08E-03	1.80E-03
2.54 cm cyl/5.08 cm apart	water vapor	0.240	0.65	70	270.97	0.6	16	10.42	18.80	20.26	9.97E-04	1.66E-03
2.54 cm cyl/5.08 cm apart	water vapor	0.240	0.65	99	383.23	0.6	19.7	11.27	20.96	23.68	2.27E-04	3.78E-04
2.54 cm cyl/5.08 cm apart	water vapor	0.240	0.65	146	565.16	0.6	19.3	12.22	23.60	28.20	2.66E-04	4.44E-04
2.54 cm cyl/5.08 cm apart	water vapor	0.240	0.65	222	859.35	0.6	20.9	13.24	26.76	34.05	1.40E-04	2.34E-04
0.79 cm cyl/4.76 cm apart	water vapor	0.240	0.65	23.5	22.74	0.15	4.9	4.38	7.81	6.64	2.11E-02	1.41E-01
0.79 cm cyl/4.76 cm apart	water vapor	0.240	0.65	35	33.87	0.15	5.7	5.35	9.15	7.95	1.53E-02	1.02E-01
0.79 cm cyl/4.76 cm apart	water vapor	0.240	0.65	63.5	61.45	0.15	7.9	6.80	11.43	10.39	6.36E-03	4.24E-02
0.79 cm cyl/4.76 cm apart	water vapor	0.240	0.65	76	73.55	0.15	8.7	7.24	12.18	11.26	4.62E-03	3.08E-02
0.79 cm cyl/4.76 cm apart	water vapor	0.240	0.65	114	110.32	0.15	9.4	8.23	14.01	13.52	3.49E-03	2.33E-02
0.79 cm cyl/4.76 cm apart	water vapor	0.240	0.65	137	132.58	0.15	10.6	8.68	14.91	14.69	2.16E-03	1.44E-02
5.08 cm half cyl	water vapor	0.240	0.65	26.5	51.29	0.3	11	6.36	10.70	9.58	3.68E-03	1.23E-02
5.08 cm half cyl	water vapor	0.240	0.65	37.5	72.58	0.3	11.5	7.21	12.12	11.20	3.02E-03	1.01E-02
5.08 cm half cyl	water vapor	0.240	0.65	56	108.39	0.3	12.4	8.19	13.93	13.41	2.10E-03	7.01E-03
5.08 cm half cyl	water vapor	0.240	0.65	81	156.77	0.3	15.1	9.09	15.76	15.84	7.14E-04	2.38E-03
5.08 cm half cyl	water vapor	0.240	0.65	96	185.81	0.3	14.1	9.50	16.66	17.09	1.07E-03	3.55E-03
5.08 cm half cyl	water vapor	0.240	0.65	122	236.13	0.3	14	10.09	18.00	19.04	1.11E-03	3.70E-03
Wave-form 2.54 cm	water vapor	0.240	0.65	16.5	21.29	0.2	7.4	4.22	7.60	6.45	1.04E-02	5.18E-02
Wave-form 2.54 cm	water vapor	0.240	0.65	33	42.58	0.2	9.3	5.91	9.99	8.81	4.85E-03	2.42E-02
Wave-form 2.54 cm	water vapor	0.240	0.65	66	85.16	0.2	12.9	7.60	12.82	12.03	1.15E-03	5.74E-03
Wave-form 2.54 cm	water vapor	0.240	0.65	103	132.90	0.2	15.6	8.68	14.92	14.70	3.90E-04	1.95E-03
Wave-form 2.54 cm	water vapor	0.240	0.65	165	212.90	0.2	18	9.83	17.41	18.17	1.49E-04	7.47E-04
Wave-form 2.54 cm	water vapor	0.240	0.65	219	282.58	0.2	19	10.52	19.05	20.64	1.00E-04	5.00E-04

¹ Data sets from Chamberlain "Transport of gases to and from surfaces with bluff and wave-like roughness elements" Q. J. Roy. Meteorol. Soc. 94, 318-322 (1968) and Chamberlain "Transport of gases to and from grass and grass-like surfaces," Proc. Roy. Soc., A, 290, p. 236 (1966)

Equation Key: Boundary2.xls *Sheppard B⁻¹=1/k*ln(ku*zo/Da) [40] *Chamberlain (1984) B⁻¹=7.3*(u*zo/v)^{0.25} (v/Da)^{-0.45} [41]

*Chamberlain (1968) B⁻¹=0.5(u*zo/v)^{0.25} (v/Da)^{0.8} [32]

Appendix 2:

Master Variable List for predicted flux.

Source File: resistsummary6.xls

Var. Table

Appendix 3: Chemical properties of pesticide active ingredients used in the volatilization study.

Source File: chemdata.xls

Triadimefon
Chlorpyrifos
Ethofumesate
Triclopyr
Propiconazole
Cyfluthurin

Pesticide Partition Coefficients and Vapor Pressure Data

Application 1, 95-96

	Triadimefon*	Chlorpyrifos	Ethofumesate
Vapor Pressure (pa @ 25 C)	2.31E-04	2.50E-03	6.50E-04
V.P./V.P. Chlorpyrifos)	0.092	1	0.260
Vapor Density (ug/m³ @ 25°C)	2.7E+01	3.5E+02	7.5E+01
V.D./V.D. Chlorpyrifos)	0.077	1	0.212
95 Vapor Density/Spray Density (m⁻¹ @ 25°C)	8.95E+01	2.58E+03	N/A
V.D./S.D./V.D./S.D. Chlorpyrifos)	0.035	1	N/A
96 Vapor Density/Spray Density (m⁻¹ @ 25°C)	8.95E+01	1.9E+03	3.0E+02
V.D./S.D./V.D./S.D. Chlorpyrifos)	0.047	1	0.158
Kh (pa m³/mol) @ 25 °C	8.20E-06	7.43E-01	0.004
Kh/Kh (Chlorpyrifos)	1.10E-05	1	4.98E-03
Kow @ 25 °C	1510	100000	500
Kow/Kow (Chlorpyrifos)	1.51E-02	1	5.00E-03
Kao (Kh/Kow)	5.43E-09	7.43E-06	7.40E-06
Kao/Kao(Chlorpyrifos)	7.31E-04	1	0.996
Da@25°C (cm²/sec)	3.86E-02	3.44E-02	3.92E-02
Da/Da(Chlorpyrifos)	1.12	1	1.140
* values of Kh, Kow, Koa for 20°C			
Koc	319	9930	276
Koc/Koc (Chlorpyrifos)	0.03	1	0.028

Molecular Weights (g/mol)

Triadimefon	293
Chlorpyrifos	350
Ethofumesate	286

Application 2, 96

	Triclopyr	Propiconazole
Vapor Pressure (pa @ 25 C)	1.68E-04	5.60E-05
V.P./V.P. Propiconazole)	3.000	1
Vapor Density (ug/m³ @ 25°C)	1.7E+01	7.7E+00
V.D./V.D. Propiconazole)	2.246	1
Kh (pa m³/mol) @ 25 °C	8.30E-05	1.92E-04
Kh/Kh (Propiconazole)	0.432	1
Kow @ 25 °C	2.64	6.30E+02
Kow/Kow (Propiconazole)	0.004	1
Koa (Kow/Kh)	3.14E-05	3.05E-07
Koa/Koa(Propiconazole)	103.161	1
Da@25°C (cm²/sec)	4.21E-02	3.49E-02
Da/Da(Propiconazole)	1.206	1

* values of V.P., V.D., Kh, Kow, Koa for 20°C

Molecular Weights (g/mol)

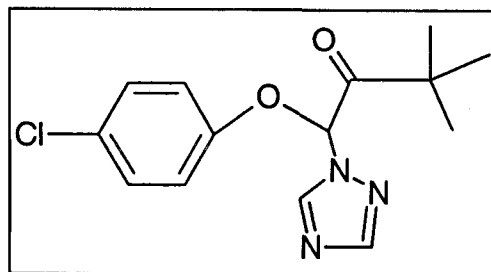
Triclopyr	256
Propiconazole	342

Triadimefon-Fungicide

Trade Name
Formulation
Physical State
CASRN
Molecular Formula
Molecular Weight (g/mol)
Chemical Family

Manufacturer(s): Bayer; Mobay

Bayleton
Wettable Powder
solid
43121-43-3
 $C_{14}H_{16}N_3O_2Cl$
293.7523
triazole, conazole



C
H
O
N
Cl

14
16
2
3
1

S
P
rings

2

Reference:

*Molar Diffusion Volume (cm^3/mol)
*Da @ 25 C (cm^2/sec) (Da=1.55/ $m^{0.65}$)
Melting Point (C)
Boiling Point (C)
Kh ($Pa\ m^3/mol$) @ 20 C
Kow @ 20 C
pKa
Koc (mL/g)
Koa=Kow/Kh ($mol/m^3/pa$)

270.2
3.86E-02
82.3
none
8.20E-06
1.51E+03
none
1.85E+08

#9PMED8, 8th ed.,p.813,1987

MILES COMPANY DATA
MILES COMPANY DATA

Claussius Clapeyron

Vapor Pressure (pa)	1.07E-04	2.00E-03
Temperature (C)	20	40
#Reference for V.P (pa) @ T (C)	Env. Cont. & Tox series Vol. 123,137	

ln (Vapor Pressure (pa))	-9.15	-6.21
1/T (K)	0.003411223	0.003193358
dH (sublimation) (J/mol)	1.12E+05	
dS (sublimation) (J/mol/K)	3.06E+02	

Case Inputs

Avg. Molecular Mass of Air (g/mol)
Molecular Volume of air (cm^3/mol)
Barometric Pressure (atm)

28.97
20.1
1

Notes

*Da @ 25 C estimated using Fuller's method (1966) in S.G.I. "Environmental Organic Chemistry" Page 195

* Molar Volume calculated using Fuller's Method to estimate diffusion Volumes of Organic Molecules (1966) found in Schwarzenbach's "Environmental Organic Chemistry" page 198

note: used a guessed value of $16.9\ cm^3/mol$ for Phosphorous in Diffusion Volume calculation

Chlorpyrifos-Insecticide

Trade Name

Formulation

Physical State

CASRN

Molecular Formula

Molecular Weight (g/mol)

Chemical Family

C

H

O

N

Cl

S

P#

rings

*Molar Diffusion Volume (cm³/mol)

*Da @25 C (cm²/sec) (Da=1.55/m^{0.65})

Melting Point (C)

Boiling Point (C)

Kh (Pa m³/mol) @ 25 C

Kow (temperature unknown)

pKa

Koc (mL/g)

Koa=Kow/Kh (mol/m³/pa)

Claussius Clapeyron

Vapor Pressure (pa)

Temperature (C)

#Reference for V.P (pa) @ T (C)

ln (Vapor Pressure (pa))

1/T (K)

dH (sublimation) (J/mol)

dS (sublimation) (J/mol/K)

Case Inputs

Avg. Molecular Mass of Air (g/mol)

Molecular Volume of air (cm³/mol)

Barometric Pressure (atm)

Notes

*Da @25 C estimated using Fuller's method (1966) in S.G.I. "Environmental Organic Chemistry" Page 195

* Molar Volume calculated using Fuller's Method to estimate diffusion Volumes of Organic Molecules (1966) found in Schwarzenbach's "Environmental Organic Chemistry" page 198

note: used a guessed value of 16.9 cm³/mol for Phosphorous in Diffusion Volume calculation

* Reference Key located at <http://www.arsusda.gov/rsml/coden.txt>

Manufacturer(s):

Dursban 4EC

Emul. Conc.

solid

2921-88-2

C₉H₁₁Cl₃NO₃PS

350.58356

organophosphate-pyridine

9

11

3

1

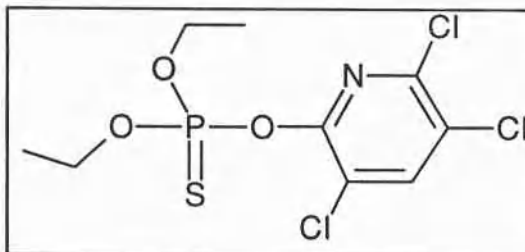
3

1

1

1

DowElanco and Makhteshim-Agan



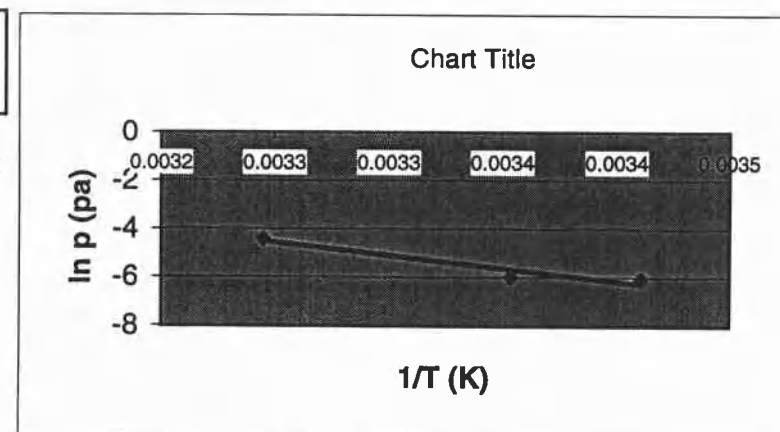
Reference:

#9ACHB2

Dow Chemical *Manufacturer*

Dow Chemical *Manufacturer*

Vapor Pressure (pa)	2.50E-03	1.20E-02	2.30E-03
Temperature (C)	25	35	20
#Reference for V.P (pa) @ T (C)	#9ACHB2,1983 ED	#9ACHB2,1983 ED	#9HRLCP
ln (Vapor Pressure (pa))	-5.99	-4.42	-6.07
1/T (K)	0.003354016	0.003245173	0.0034112
dH (sublimation) (J/mol)	8.76E+04		
dS (sublimation) (J/mol/K)	2.47E+02		



Ethofumesate-Herbicide

Trade Name

Formulation

Physical State

CASRN

Molecular Formula

Molecular Weight (g/mol)

Chemical Family

C

H

O

N

Cl

S

rings

*Molar Diffusion Volume (cm³/mol)*Da @ 25 C (cm²/sec) (Da=1.55/m^{0.65})

Melting Point (C)

Boiling Point (C)

Kh (Pa m³/mol) @ 25 C

Kow (25 C)

pKa

Koc (mL/g)

Koa=Kow/Kh (mol/m³/pa)**Claussius Clapeyron**

Vapor Pressure (pa)

Temperature (C)

*Reference for V.P (pa) @ T (C)

ln (Vapor Pressure (pa))

1/T (K)

dH (sublimation) (J/mol)

dS (sublimation) (J/mol/K)

Case Inputs

Avg. Molecular Mass of Air (g/mol)

Molecular Volume of air (cm³/mol)

Barometric Pressure (atm)

Manufacturer(s):

Prograss EC

Emul. Conc.

solid

26225-79-6

C₁₃H₁₈O₅S

286.3422

benzofuran

13

18

5

1

2

254.6

3.92E-02

70

none

3.70E-03

5.0E+02

none

1.35E+05

6.50E-04

25

#7SCHER

-7.34

0.003660983

#DIV/0!

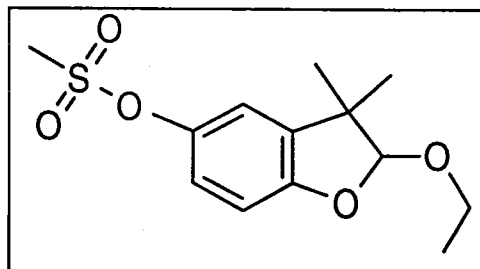
#DIV/0!

28.97

20.1

1

Kerima; NOR-AM; Schering

**Reference:**

#9ACHB2

NORAM COMPANY DATA

NORAM COMPANY DATA

Notes

*Da @ 25 C estimated using Fuller's method (1966) in S.G.I. "Environmental Organic Chemistry" Page 195

* Molar Volume calculated using Fuller's Method to estimate diffusion Volumes of Organic Molecules (1966) found in Schwarzenbach's "Environmental Organic Chemistry" page 198

note: used a guessed value of 16.9 cm³/mol for Phosphorous in Diffusion Volume calculation

chem data.xls

5/17/99

Propiconazole-Fungicide

Trade Name

Formulation

Physical State at Room Temp.

CASRN

Molecular Formula

Molecular Weight (g/mol)

Chemical Family

C

H

O

N

Cl

S

P

rings

*Molar Diffusion Volume (cm³/mol)*Da @ 25 C (cm²/sec) (Da=1.55/m^{0.65})

Melting Point (C)

Boiling Point (C)

Kh (Pa m³/mol) @ 25 C

Kow (25 C)

pKa

Koc (mL/g)

Koa=Kow/Kh (mol/m³/pa)**Claussius Clapeyron**

Vapor Pressure (pa)

Temperature (C)

#Reference for V.P (pa) @ T (C)

ln (Vapor Pressure (pa))

1/T (K)

dH (sublimation) (J/mol)

dS (sublimation) (J/mol/K)

Case Inputs

Avg. Molecular Mass of Air (g/mol)

Molecular Volume of air (cm³/mol)

Barometric Pressure (atm)

Manufacturer(s):

Banner Maxx

Emuls. Conc.

liquid

60207-90-1

C₁₅H₁₇Cl₂N₃O₂

342.2242

triazole, conazole

15

17

2

3

2

3

288

3.49E-02

124

1.92E-04

6.3E+02

1.09

3.29E+06

5.60E-05

25

Env. Cont. & Tox series Vol. 123,137 #9CIBAG

-9.79

3.35E-03

#DIV/0!

#DIV/0!

28.97

20.1

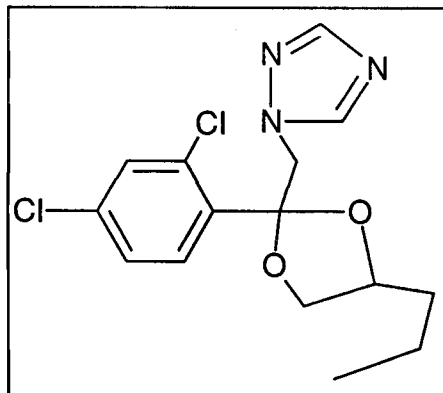
1

Reference:

#9CIBAG

#9CIBAG

#9CIBAG

**Notes**

*Da @ 25 C estimated using Fuller's method (1966) in S.G.I. "Environmental Organic Chemistry" Page 195

* Molar Volume calculated using Fuller's Method to estimate diffusion Volumes of Organic Molecules (1966) found in Schwarzenbach's "Environmental Organic Chemistry" page 198

note: used a guessed value of 16.9 cm³/mol for Phosphorous in Diffusion Volume calculation# Reference Key located at <http://www.arsusda.gov/rsml/coden.txt>

chem data.xls

5/17/99

Cyfluthurin-Insecticide

Trade Name

Formulation

Physical State at Room Temp.

CASRN

Molecular Formula

Molecular Weight (g/mol)

Chemical Family

C

H

O

N

Cl

S

F"

rings

*Molar Diffusion Volume (cm³/mol)*Da @25 C (cm³/mol) (Da=1.55/m^{0.65})

Melting Point (C)

Boiling Point (C)

Kh (Pa m³/mol) @ 20 C

Kow (20 C)

pKa

Koc (mL/g)

Koa=Kow/Kh (mol/m³/pa)**Claussius Clapeyron**

Vapor Pressure (pa)

Temperature (C)

#Reference for V.P (pa) @ T (C)

ln (Vapor Pressure (pa))

1/T (K)

dH (sublimation) (J/mol)

dS (sublimation) (J/mol/K)

Case Inputs

Avg. Molecular Mass of Air (g/mol)

Molecular Volume of air (cm³/mol)

Barometric Pressure (atm)

Manufacturer(s):

Tempo 2

Emuls. Conc.

solid

68359-37-5

C₂₂H₁₈Cl₂FNO₃

434.2951

pyrethroid

22

18

3

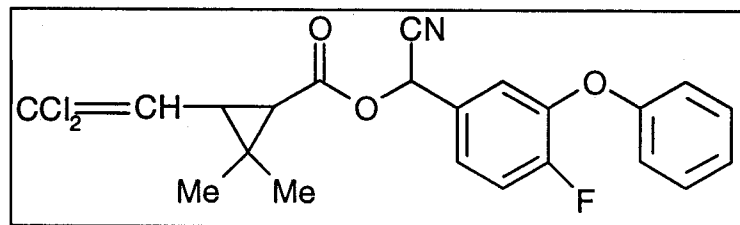
1

2

1

2

Bayer

**Reference:**

#9PMED8

#6MILES

#6MILES

#6MILES

-12.33

3.41E-03

#DIV/0!

#DIV/0!

28.97

20.1

1

Notes

*Da @25 C estimated using Fuller's method (1966) in S.G.I. "Environmental Organic Chemistry" Page 195

* Molar Volume calculated using Fuller's Method to estimate diffusion Volumes of Organic Molecules (1966) found in Schwarzenbach's "Environmental Organic Chemistry" page 198

note: used a guessed value of 5.3 cm³/mol for Fluorine in Diffusion Volume calculation

chem data.xls

5/17/99

* Reference Key located at <http://www.arsusda.gov/rsml/coden.txt>

Triclopyr (acetic acid)-Herbicide

Trade Name

Formulation

Physical State at Room Temp.

CASRN

Molecular Formula

Molecular Weight (g/mol)

Chemical Family

C
H
O
N
Cl
S
P

rings

*Molar Diffusion Volume (cm³/mol)*Da @ 25 C (cm²/sec) (Da=1.55/m^{0.65})

Melting Point (C)

Boiling Point (C)

Kh (Pa m³/mol) @ 25 C

Kow (25 C) @ pH 5

Kow (25 C) @ pH 7

Kow (25 C) @ pH 9

pKa

Koc (mL/g)

Koa=Kow (pH 5)/Kh (mol/m³/pa)**Claussius Clapeyron**

Vapor Pressure (pa)

Temperature (C)

#Reference for V.P (pa) @ T (C)

ln (Vapor Pressure (pa))

1/T (K)

dH (sublimation) (J/mol)

dS (sublimation) (J/mol/K)

Case Inputs

Avg. Molecular Mass of Air (g/mol)

Molecular Volume of air (cm³/mol)

Barometric Pressure (atm)

Notes

*Da @25 C estimated using Fuller's method (1966) in S.G.I. "Environmental Organic Chemistry" Page 195

* Molar Volume calculated using Fuller's Method to estimate diffusion Volumes of Organic Molecules (1966) found in Schwarzenbach's "Environmental Organic Chemistry" page 198

note: used a guessed value of 16.9 cm³/mol for Phosphorous in Diffusion Volume calculation# Reference Key located at <http://www.arsusda.gov/rsml/coden.txt>**Manufacturer(s):**

Turflon Ester

Emuls. Conc.

solid

55335-06-3

C₇H₄Cl₃NO₃

256.4725

pyridine; organochlorine; pyridyloxyacetic acid

7

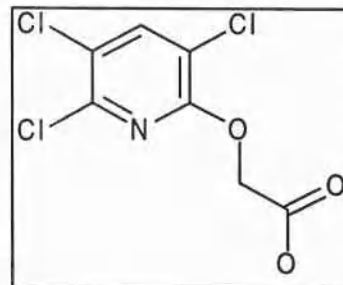
4

3

1

3

1

DowElanco<---note that Butoxyester is not active ingredient**Reference:**

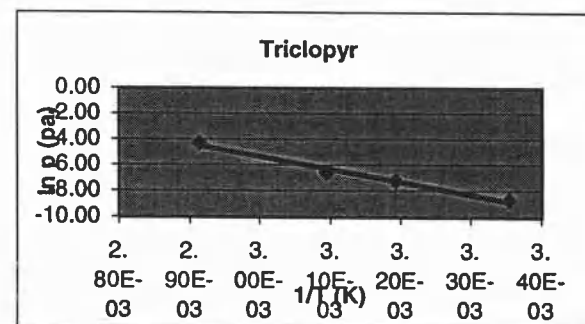
Dow Chemical *Manufacturer*

WSSA Herbicide Handbook 7th ed.

WSSA Herbicide Handbook 7th ed.

WSSA Herbicide Handbook 7th ed.

Env. Cont. & Tox series Vol. 123,138



Vapor Pressure (pa)	1.68E-04	7.07E-04	1.37E-03	1.39E-02
Temperature (C)	25	40	50	70

#Reference for V.P (pa) @ T (C)	Ahrens' "Herbicide Handbook", 7th ed., 1994			
ln (Vapor Pressure (pa))	-8.69	-7.25	-6.59	-4.28
1/T (K)	3.35E-03	3.19E-03	3.09E-03	2.91E-03
dH (sublimation) (J/mol)	8.24E+04			
dS (sublimation) (J/mol/K)	2.03E+02			

Case Inputs

Avg. Molecular Mass of Air (g/mol)	28.97
Molecular Volume of air (cm ³ /mol)	20.1
Barometric Pressure (atm)	1

Notes

*Da @25 C estimated using Fuller's method (1966) in S.G.I. "Environmental Organic Chemistry" Page 195

* Molar Volume calculated using Fuller's Method to estimate diffusion Volumes of Organic Molecules (1966) found in Schwarzenbach's "Environmental Organic Chemistry" page 198

note: used a guessed value of 16.9 cm³/mol for Phosphorous in Diffusion Volume calculation# Reference Key located at <http://www.arsusda.gov/rsml/coden.txt>

Appendix 4: Application 1, 1995

Source File: app195summary95a.xls

T1.App.1,95 (1st 2 pages)

Ch,95,1,0,SR.FI

Ch,95,1,0,T.F

Ch,95,1,0,SR.T

Ch,95,1,0,WS.FI

Ch,95,1,1,SR.FI

Ch,95,1,1,T.FI

Ch,95,1,1,SR.T

Ch,95,1,1,WS.FI

Ch,95,1,7,SR.FI

Ch,95,1,7,T.FI

Ch,95,1,7,SR.T

Ch,95,1,7,WS.FI

Ch,95,1,0.7,CCTr

Source File: fluxratio3.xls

CCTr,95,0

CCTr,95,1

CCTr,95,7

Source File: app195summary95a.xls

Ch,95,1,0.7,CCCI

Source File: fluxratio3.xls

CCCI,95,1,0

CCCI,95,1,1

CCCI,95,1,7

Source File: app195summary95a.xls

Solar Rad

Temp

Precip

Pk Flux Noon

Ch,PkFxNoon

Ch,logPkFxNoon

Ch,logPkFxNormNoon

Application 1, 1995 Airborne Residue

Application 1, 1995

										WS 1 (m/s)	WS 2 (m/s)	WS 3 (m/s)	WS 4 (m/s)
										41 cm	70 cm	140 cm	280 cm
										41	70	140	280
Day 0 (July 17th)	Air Sampling Period	Intermed.	Flux (ug/m ² /hr)	Surface	Ambient	Solar Rad.	J/m ² sec	In Ht (cm)→					
Julian 198	Start	End	Time	Triadimefon	Chlorpyrifos	Temp. (C)	Temp. (C)						
	6:50	8:00	7:25	60	548	17.55	18.58	126	3.713572067	0.66	0.78	0.83	0.85
	8:00	10:00	9:00	235	1202	26.85	24.23	874	1.22	1.27	1.45	1.49	
	10:00	12:06	11:03	544	1619	40.19	28.59	1404	1.44	1.50	1.70	1.77	
	12:06	14:00	13:03	642	1391	47.49	32.46	1639	1.48	1.56	1.75	1.84	
	14:02	16:00	15:01	697	981	48.28	35.55	1521	1.53	1.61	1.79	1.88	
	16:02	18:00	17:01	545	567	49.86	37.18	1080	1.35	1.42	1.58	1.64	
	18:02	20:00	19:01	210	229	41.28	36.35	463	1.20	1.30	1.46	1.52	
	20:00	6:03	13:01	38	61	18.86	22.02	6	1.06	1.22	1.36	1.43	
Est.Total (6:00-20:00)				5866	13073								
Day 1 (July 18th)	6:03	8:02	7:02	78	133	16.38	16.29	116	1.18	1.32	1.42	1.44	
Julian 199	10:00	12:02	11:01	259	393	29.81	22.86	911	1.09	1.18	1.25	1.24	
	12:02	14:00	13:01	443	601	39.61	28.82	1172	1.02	1.09	1.17	1.17	
	14:02	16:00	15:01	386	426	42.83	32.14	1087	1.07	1.16	1.24	1.21	
	16:02	18:00	17:01	464	544	37.65	30.91	789	2.43	2.67	2.99	3.02	
	18:02	20:03	19:02	192	275	27.24	26.82	216	2.88	3.15	3.55	3.64	
	20:03	5:59	13:01	20	22	17.77	18.96	3	0.84	0.92	1.04	1.05	
Est.Total (6:00-20:00)				3641	4741								
Day 2 (July 19th)	12:02	14:02	13:02	501	488	45.86	30.34	1557	1.17	1.24	1.35	1.35	
Julian 200	14:02	16:03	15:02	514	423	46.17	32.92	1474	1.77	1.91	2.10	2.10	
Day 3 (July 20th)	12:00	14:02	13:01	319	313	43.04	26.67	1593	1.35	1.43	1.52	1.51	
Julian 201	14:02	16:00	15:01	368	334	44.34	29.55	1468	1.65	1.75	1.91	1.91	
Day 5 (July 22th)	12:00	13:59	12:59	77	96	38.30	22.60	1330	1.27	1.34	1.41	1.44	
Julian 203	14:01	16:00	15:00	73	77	35.48	23.33	1100	1.49	1.59	1.69	1.73	
Day 7 (July 24th)	6:00	8:00	7:00	#VALUE!	#VALUE!	17.51	16.52	73	0.69	0.73	0.82	0.87	
Julian 205	8:11	9:59	9:05	14	21	22.35	18.32	413	0.91	0.95	1.01	1.06	
	10:00	12:02	11:01	28	37	28.27	20.62	835	1.06	1.11	1.16	1.19	
	12:02	14:00	13:01	92	121	36.64	22.96	1555	1.72	1.82	1.96	2.01	
	14:00	16:00	15:00	67	79	38.85	24.44	1520	1.51	1.57	1.70	1.75	
	16:00	18:00	17:00	89	131	38.34	25.67	1060	2.15	2.34	2.54	2.50	
	18:00	20:20	19:10	21	40	26.17	23.00	365	3.23	3.52	3.98	4.16	
Est.Total (6:00-20:00)													

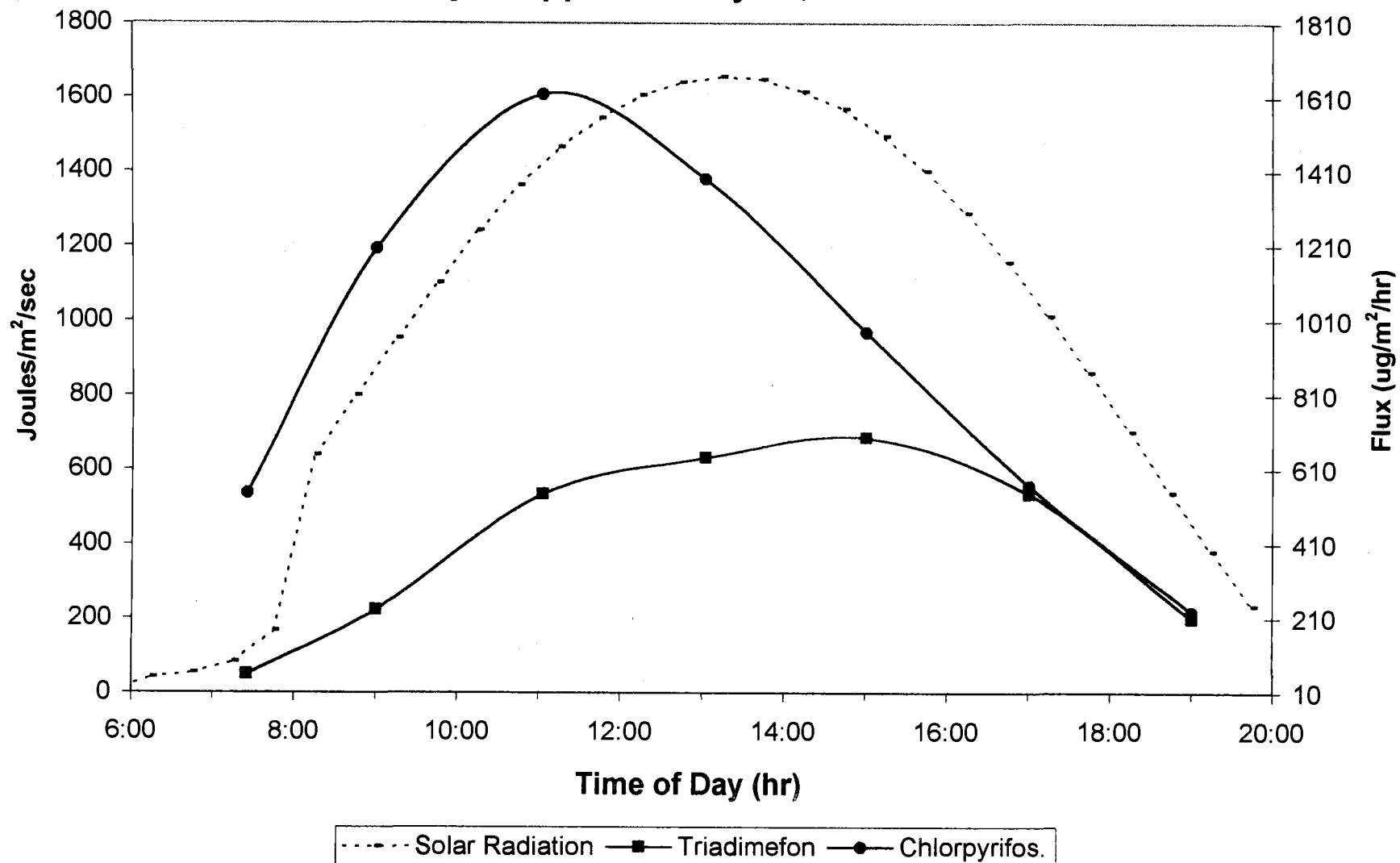
*flux estimated from airborne concentrations using the Backward-Time Lagrangian stochastic Dispersion model (Flesch, Wilson, Journal of Applied Meteorology, 34, pp. 1320-1332)

Application 1, 1995 Airborne Residue

	Air Sampling Period		Intermed. Time	Flux (ug/m ² /hr)		Surface	Ambient	Solar Rad.	WS 1 (m/s)	WS 2 (m/s)	WS 3 (m/s)	WS 4 (m/s)
	Start	End		Triadimefon	Chlorpyrifos	Temp. (C)	Temp. (C)	J/m ² sec	41 cm	70 cm	140 cm	280 cm
Day 14 (July 31st)												
Julian 212	6:00	8:00	7:00	#VALUE!	#VALUE!	12.94	15.85	64	0.98	0.98	1.18	1.24
	8:07	10:00	9:03	#VALUE!	8	23.97	19.69	835	1.48	1.55	1.78	1.86
	10:00	12:00	11:00	8	19	39.96	24.10	1374	1.71	1.80	2.02	2.10
	12:00	14:00	13:00	15	30	46.33	27.86	1621	2.16	2.25	2.53	2.66
	14:01	16:02	15:01	9	23	45.60	30.62	1504	1.97	2.06	2.32	2.42
	16:02	18:02	17:02	#VALUE!	12	44.05	31.66	1053	1.93	1.99	2.27	2.38
	18:02	20:00	19:01	#VALUE!	#VALUE!	34.72	30.66	427	1.45	1.51	1.73	1.82
Est.Total (6:00-20:00)												
Day 22 (August 8th)	6:00	8:00	7:00	#VALUE!	#VALUE!	10.92	10.86	81	0.66	0.76	0.85	0.85
Julian 220	8:03	10:01	9:02	#VALUE!	#VALUE!	22.31	15.58	777	0.53	1.03	1.13	1.13
	10:02	12:00	11:01	#VALUE!	8	33.51	19.58	1312	0.80	1.42	1.60	1.65
	12:00	14:00	13:00	#VALUE!	9	40.52	21.82	1552	1.10	1.53	1.70	1.77
	14:00	16:00	15:00	#VALUE!	#VALUE!	39.85	23.23	1431	1.43	1.72	1.92	2.01
	16:00	18:00	17:00	#VALUE!	#VALUE!	35.84	23.89	973	1.35	1.66	1.88	1.99
	18:00	19:50	18:55	#VALUE!	#VALUE!	27.59	23.17	365	0.98	1.33	1.56	1.64
Est.Total (6:00-20:00)												

*flux estimated from airborne concentrations using the Backward-Time Lagrangian stochastic Dispersion model (Flesch, Wilson, Journal of Applied Meteorology, 34, pp. 1320-1332)

Solar Radiation and Flux
Day 0, App.1 '95 July 17, Julian 198



Solar Radiation		Day 0	Day 1	Day 2	Day 3	Day 5	Day 7	Day 14	Day 22
Julian Date, 1995		0	1	2	3	5	7	14	22
Time	Time(hr)	198	199	200	201	203	205	212	220
600	5:45	7.26	6.171	4.514	5.063	1.576	2.379	2.349	0.681
630	6:15	41.86	34.86	19.83	33.69	13.53	18.75	19.59	8.25
700	6:45	54.51	77.5	47.85	61.44	52.27	49.41	40.73	52.41
730	7:15	83.8	129.7	95.2	142	120	79.8	55.15	97.9
800	7:45	167.2	220.8	181.3	205.6	201.2	143.2	142.4	164.5
830	8:15	639.1	423.5	446.1	459	279.7	238.6	596.9	533.4
900	8:45	801	653.3	621.3	737	379.2	311.1	759	701
930	9:15	954	523.7	532.8	897	422.3	485.9	916	863
1000	9:45	1100	574.1	1067	1048	457.8	616.2	1067	1011
1030	10:15	1241	559.6	1228	1180	388.7	743	1208	1154
1100	10:45	1362	500.9	1328	1304	693.5	766	1332	1292
1130	11:15	1466	1101	1398	1402	834	647	1435	1362
1200	11:45	1545	1483	1486	1496	799	1184	1521	1438
1230	12:15	1606	1543	1466	1573	920	1444	1582	1575
1300	12:45	1641	998	1570	1595	1601	1476	1625	1447
1330	13:15	1657	1108	1602	1604	1641	1957	1642	1591
1400	13:45	1650	1038	1589	1600	1159	1342	1635	1596
1430	14:15	1616	1616	1569	1569	1421	1670	1606	1533
1500	14:45	1570	1076	1523	1513	1227	1554	1553	1484
1530	15:15	1496	811	1450	1441	1349	1477	1478	1404
1600	15:45	1402	846	1355	1347	403.3	1377	1378	1303
1630	16:15	1289	1222	1249	1238	1059	1266	1263	1183
1700	16:45	1156	988	1131	1112	1132	1159	1133	1049
1730	17:15	1013	525.1	1002	981	980	984	986	905
1800	17:45	861	420.1	590.7	816	835	830	828	754
1830	18:15	702	337.1	298.2	724	681.1	671.6	665	596.9
1900	18:45	537.8	233.4	268.5	485.9	521.7	510.7	500.8	437.7
1930	19:15	379.9	192.9	159.5	346.9	365	354.3	344.5	287.6
2000	19:45	234.1	102	96.1	210.3	224	209.7	199.3	139.2
MJ/m ²		25781.25	50554980				42151140	49312620	46447740
Time (hr) 8:00-20:00		8:00-20:00					8:00-20:00	8:00-20:00	8:00-20:00

Ground Temperature C°

Julian Date, 1995		198	198	198	198	199	199	199	199	200	200	200	200
Time	Time(hr)	Ambient	Ground1	Ground2	Groundavg	Ambient	Ground1	Ground2	Groundavg	Ambient	Ground1	Ground2	Groundavg
600	6:00	15.64	13.78	13.79	13.785	16.09	14.62	14.59	14.605	16.24	16.63	16.62	16.625
630	6:30	15.68	14.17	14.35	14.26	15.95	15.13	15.1	15.115	16.28	16.79	16.78	16.785
700	7:00	16.64	16.25	17.07	16.66	16.08	15.84	15.8	15.82	16.42	17.56	17.46	17.51
730	7:30	17.64	16.95	17.13	17.04	16.27	16.66	16.64	16.65	17.07	19.01	18.81	18.91
800	8:00	19.52	17.97	18.13	18.05	16.84	17.95	17.91	17.93	17.87	20	19.94	19.97
830	8:30	21.51	19.59	20.46	20.025	17.79	19.66	19.9	19.78	19.05	21.82	21.73	21.775
900	9:00	24.02	26.58	27.74	27.16	19.03	23.62	24.06	23.84	21.09	25.64	26.09	25.865
930	9:30	25.32	29.15	28.8	28.975	19.95	23.77	23.65	23.71	22.24	26.04	26.64	26.34
1000	10:00	26.07	32.33	30.12	31.225	20.51	23.97	23.4	23.685	23.29	30.84	30.03	30.435
1030	10:30	27.14	36.63	35.57	36.1	21.63	26.48	25.39	25.935	24.89	34.45	34.38	34.415
1100	11:00	28.09	40.17	37.08	38.625	21.73	25.55	24.51	25.03	26.01	38.62	37.02	37.82
1130	11:30	28.94	43.26	38.22	40.74	22.96	31.97	29.3	30.635	26.92	40.7	37.95	39.325
1200	12:00	30.18	46.57	43.99	45.28	25.11	39.06	36.23	37.645	27.89	44.09	43.55	43.82
1230	12:30	31.07	48.3	46.32	47.31	27.19	42.8	40.83	41.815	28.85	45.6	45.35	45.475
1300	13:00	31.81	44.57	47.09	45.83	28.36	36.95	38.51	37.73	30.23	42.47	46.84	44.655
1330	13:30	33.11	49.04	50.4	49.72	29.27	39.58	38.03	38.805	30.72	46.28	48.92	47.6
1400	14:00	33.83	43.35	50.87	47.11	30.46	39.87	40.3	40.085	31.54	41.14	50.29	45.715
1430	14:30	34.41	46.82	50.58	48.7	31.62	45.22	46.04	45.63	32.26	45.05	51.07	48.06
1500	15:00	35.32	48.27	49.3	48.785	32.1	44.57	42.89	43.73	32.97	48.28	50.48	49.38
1530	15:30	36.06	50.86	44.66	47.76	32.31	42.46	39.74	41.1	33.33	47.84	42.12	44.98
1600	16:00	36.42	52.77	42.97	47.87	32.54	42.46	39.24	40.85	33.11	45.96	38.54	42.25
1630	16:30	36.8	52.67	48.95	50.81	32.83	45.96	42.8	44.38	32.89	43.22	40.98	42.1
1700	17:00	37	51.59	49.15	50.37	31.43	41.27	38.99	40.13	32.04	40.21	39.28	39.745
1730	17:30	37.4	50.78	49.47	50.125	30.18	35.05	33.64	34.345	30.72	37.54	37.02	37.28
1800	18:00	37.53	48.85	47.44	48.145	29.18	32.24	31.23	31.735	28.83	32.41	32.02	32.215
1830	18:30	37.29	46.17	45.8	45.985	28.48	30.6	29.75	30.175	26.91	27.93	27.61	27.77
1900	19:00	37.18	43.56	43.4	43.48	27.1	27.68	27.12	27.4	25.27	26.31	26.1	26.205
1930	19:30	36.92	41.11	41.25	41.18	26.19	26.75	26.27	26.51	23.49	23.93	23.77	23.85
2000	20:00	33.99	34.57	34.38	34.475	25.5	25.06	24.68	24.87	22.02	22.34	22.23	22.285

Ground Temperature C°

Julian Date, Time(hr)	201 Ambient	201 Ground1	201 Ground2	201 Groundavg	203 Ambient	203 Ground1	203 Ground2	203 Groundavg	205 Ambient	205 Ground1	205 Ground2	205 Groundavg
6:00	14.59	13.79	13.79	13.79	16.55	16.97	16.86	16.915	16.07	16.43	16.41	16.42
6:30	14.47	14.42	14.52	14.47	16.47	17.17	17.03	17.1	16.13	16.5	16.48	16.49
7:00	14.91	15.44	15.53	15.485	16.56	17.59	17.43	17.51	16.24	17.26	17.19	17.225
7:30	15.5	16.63	16.77	16.7	16.82	18.27	18.23	18.25	16.61	17.79	17.6	17.695
8:00	16.56	17.67	17.85	17.76	17.22	19.57	19.6	19.585	17.08	18.79	18.5	18.645
8:30	17.56	18.96	19.81	19.385	17.59	20.7	20.7	20.7	17.6	20.3	20.02	20.16
9:00	18.71	22.91	24.98	23.945	18.23	22.44	22.42	22.43	18.05	21.53	21.39	21.46
9:30	19.6	26.17	27.62	26.895	18.57	22.98	22.93	22.955	18.58	23.29	23.09	23.19
10:00	20.81	29.93	29.08	29.505	19	24.53	23.99	24.26	19.03	24.73	24.48	24.605
10:30	21.6	32.2	32.45	32.325	19.05	23.48	22.93	23.205	19.74	26.57	26.08	26.325
11:00	22.46	35.01	34.09	34.55	19.73	27.26	26.06	26.66	20.23	27.63	26.77	27.2
11:30	23.11	36.64	34.33	35.485	20.42	30.79	28.71	29.75	20.76	27.78	26.72	27.25
12:00	24.12	39.51	39.66	39.585	20.67	31.12	29.17	30.145	21.75	33.36	31.27	32.315
12:30	25.29	41.34	42.88	42.11	21.19	33.64	31.75	32.695	22.49	35.23	34.2	34.715
13:00	26.38	39.33	45.67	42.5	22.43	38.73	40.43	39.58	22.71	35.9	36.36	36.13
13:30	27.02	43.23	46.03	44.63	23.41	42.73	43.8	43.265	23.26	39.18	40.05	39.615
14:00	27.98	37.94	47.89	42.915	23.36	35.31	40	37.655	23.37	34.63	37.6	36.115
14:30	29.11	41.99	50.5	46.245	22.93	36.77	39.4	38.085	23.56	34.91	40.02	37.465
15:00	29.76	47.1	48.17	47.635	23.38	38.41	37.62	38.015	24.14	42.28	41.03	41.655
15:30	29.59	44.79	39.14	41.965	23.96	39.62	33.4	36.51	24.73	39.74	35.11	37.425
16:00	29.75	45.88	37.11	41.495	23.03	30.8	27.83	29.315	25.34	45.14	32.54	38.84
16:30	29.71	43.6	40.7	42.15	23.54	36	31.42	33.71	25.92	45.5	37.93	41.715
17:00	29.71	41.99	40.6	41.295	23.64	35.56	32	33.78	26.47	44.35	40.52	42.435
17:30	29.4	39.66	38.63	39.145	23.19	33.34	30.47	31.905	25.56	37.29	35.75	36.52
18:00	28.53	36.71	35.84	36.275	22.68	31.27	29.15	30.21	24.74	33.06	32.32	32.69
18:30	27.06	33.73	33.3	33.515	22.21	29.35	28.08	28.715	24.47	31.17	30.56	30.865
19:00	25.55	30.16	29.87	30.015	21.77	27.5	26.53	27.015	23.96	29.14	28.69	28.915
19:30	24.49	27.67	27.46	27.565	21.14	25.28	24.63	24.955	23.16	26.47	26.17	26.32
20:00	23.09	24.65	24.5	24.575	20.33	22.81	22.32	22.565	22.22	23.97	23.67	23.82

Ground Temperature C°

Julian Date,	212	212	212	212	220	220	220	220
Time(hr)	Ambient	Ground1	Ground2	Groundavg	Ambient	Ground1	Ground2	Groundavg
6:00	15.33	11.02	11.46	11.24	10.99	10.91	10.98	10.945
6:30	15.03	11.21	11.7	11.455	10.49	9.15	9.38	9.265
7:00	15.38	12.52	13.05	12.785	10.21	10.5	10.72	10.61
7:30	16.09	13.28	13.6	13.44	10.95	11.6	11.85	11.725
8:00	16.88	13.96	14.23	14.095	11.79	11.85	12.29	12.07
8:30	18.17	15.38	15.95	15.665	13.24	13.87	15.89	14.88
9:00	19.37	22.29	23.41	22.85	15.31	20.73	23.47	22.1
9:30	20.18	27.58	26.46	27.02	16.61	24.88	24.3	24.59
10:00	21.04	31.66	29.05	30.355	17.17	26.74	28.58	27.66
10:30	22.46	36.44	35.66	36.05	18.07	30.49	29.75	30.12
11:00	23.54	40.16	35.51	37.835	19.55	34.95	29.9	32.425
11:30	24.42	43.75	37.39	40.57	20.31	37.83	32.25	35.04
12:00	25.98	47.02	43.77	45.395	20.39	38.77	34.1	36.435
12:30	26.48	48.06	43.7	45.88	21.09	42.62	37.77	40.195
13:00	27.26	47.52	44.94	46.23	21.48	41.19	38.43	39.81
13:30	28.54	46.12	48.11	47.115	22.29	39.83	41.22	40.525
14:00	29.14	44.98	47.18	46.08	22.42	42.73	40.37	41.55
14:30	29.78	43.48	47.88	45.68	22.83	44.8	41.45	43.125
15:00	30.61	47.89	48.56	48.225	22.95	37.87	40.53	39.2
15:30	30.86	44.98	43.96	44.47	23.32	40.57	39.05	39.81
16:00	31.24	49.85	38.23	44.04	23.81	41.74	32.76	37.25
16:30	31.55	49.18	40.06	44.62	23.88	42.44	30.71	36.575
17:00	31.91	47.86	43.74	45.8	23.85	39.95	33.94	36.945
17:30	31.48	45.3	41.45	43.375	23.93	37.97	33.92	35.945
18:00	31.69	43.78	41.06	42.42	23.89	35.51	32.27	33.89
18:30	31.23	40.58	37.91	39.245	23.86	33.31	31.18	32.245
19:00	31.05	37.92	34.9	36.41	23.48	29.96	28.43	29.195
19:30	30.48	34.12	32.06	33.09	23.13	26.69	25.82	26.255
20:00	29.88	30.52	29.72	30.12	22.22	22.84	22.48	22.66

Wind speed Profile July 17th, 1995 Application 1, Day 0, Julian Date 198

Time	Height (cm) In Ht (m)-->	41	70	140	280	u* (m/s) Value	u* (m/s) Std. Err	Zo (m) Value	Zo (m) Std. Err	L (m) Value	L (m) Std. Err	R squared
600	6:00	0.463	0.485	0.502	0.535	0.01	0.01	0.000	0.0000	14.41	20.58	1.00
630	6:30	0.468	0.514	0.658	0.631	0.10	0.05	0.053	-0.0822	-9.64	-9.11	0.96
700	7:00	0.448	0.447	0.448	0.449	0.00	0.00	4.58E+128	1.55E+131	-4.03	-5.52	0.89
730	7:30	0.568	0.701	0.763	0.799	0.10	0.03	0.035	-0.0355	-10.59	-6.23	0.99
800	8:00	0.749	0.855	0.906	0.91	0.09	0.02	0.011	-0.0113	-9.05	-3.52	0.99
830	8:30	0.8	0.887	0.956	0.975	0.08	0.01	0.006	-0.0024	-10.68	-1.69	1.00
900	9:00	1.063	1.127	1.257	1.299	0.08	0.03	0.002	-0.0040	-16.20	-15.14	0.99
930	9:30	1.489	1.499	1.764	1.851	0.08	0.10	0.000	-0.0037	654.13	84879.25	0.96
1000	10:00	1.524	1.558	1.804	1.854	0.10	0.09	0.001	-0.0070	-21.92	-69.27	0.96
1030	10:30	1.306	1.403	1.532	1.611	0.09	0.01	0.001	-0.0007	-20.59	-6.48	1.00
1100	11:00	1.413	1.482	1.704	1.781	0.11	0.06	0.002	-0.0077	-23.60	-52.27	0.98
1130	11:30	1.63	1.641	1.879	1.977	0.07	0.09	0.000	-0.0006	39.71	327.41	0.96
1200	12:00	1.425	1.493	1.671	1.714	0.10	0.05	0.001	-0.0043	-15.76	-19.69	0.98
1230	12:30	1.449	1.54	1.725	1.825	0.10	0.03	0.001	-0.0027	-29.70	-47.11	1.00
1300	13:00	1.484	1.543	1.746	1.823	0.09	0.06	0.001	-0.0033	-28.89	-82.65	0.98
1330	13:30	1.396	1.472	1.667	1.752	0.10	0.04	0.002	-0.0044	-26.56	-52.90	0.99
1400	14:00	1.573	1.675	1.844	1.969	0.09	0.02	0.000	-0.0007	-57.52	-101.22	1.00
1430	14:30	1.619	1.659	1.865	1.974	0.07	0.06	0.000	-0.0005	62.36	532.80	0.98
1500	15:00	1.489	1.551	1.746	1.829	0.09	0.05	0.001	-0.0025	-32.99	-99.98	0.99
1530	15:30	1.502	1.587	1.766	1.871	0.09	0.03	0.001	-0.0016	-40.72	-92.44	1.00
1600	16:00	1.529	1.643	1.795	1.844	0.12	0.02	0.002	-0.0018	-13.18	-4.10	1.00
1630	16:30	1.444	1.527	1.677	1.759	0.09	0.02	0.001	-0.0010	-25.42	-27.81	1.00
1700	17:00	1.533	1.565	1.765	1.824	0.08	0.07	0.000	-0.0016	-31.79	-139.94	0.97
1730	17:30	1.267	1.392	1.511	1.558	0.12	0.00	0.004	-0.0006	-12.28	-0.70	1.00
1800	18:00	1.147	1.214	1.352	1.412	0.08	0.03	0.001	-0.0028	-21.00	-24.96	0.99
1830	18:30	1.163	1.27	1.412	1.473	0.11	0.01	0.005	-0.0030	-14.98	-4.56	1.00
1900	19:00	1.269	1.332	1.46	1.532	0.07	0.02	0.000	-0.0007	-32.84	-57.10	1.00
1930	19:30	0.688	0.713	0.821	0.852	0.05	0.03	0.002	-0.0070	-23.41	-63.10	0.98
2000	20:00	1.685	1.872	2.157	2.239	0.21	0.04	0.015	-0.0125	-13.39	-6.32	1.00

Wind speed Profile July 18th, 1995 Application 1, Day 1, Julian Date 199

Height (cm)	41	70	140	280	u* (m/s)	u* (m/s)	Zo (m)	Zo (m)	L (m)	L (m)	R squared
Time (hrs)	-0.89	-0.36	0.34	1.03	Value	Std. Err	Value	Std. Err	Value	Std. Err	
6:00	1.15	1.309	1.408	1.43	0.14	0.02	0.012	-0.0083	-9.87	-2.93	1.00
6:30	1.251	1.394	1.512	1.538	0.13	0.01	0.008	-0.0022	-10.46	-1.16	1.00
7:00	1.294	1.423	1.554	1.581	0.13	0.00	6.33E-03	-9.05E-04	-10.91	-0.63	1.00
7:30	1.048	1.175	1.261	1.273	0.12	0.01	0.009	-0.0048	-9.69	-2.11	1.00
8:00	1.142	1.274	1.362	1.357	0.12	0.01	0.008	-0.0039	-8.99	-1.54	1.00
8:30	1.244	1.365	1.449	1.455	0.11	0.01	0.004	-0.0022	-9.46	-1.72	1.00
9:00	1.3	1.431	1.532	1.526	0.13	0.01	0.006	-0.0014	-9.11	-0.73	1.00
9:30	1.241	1.367	1.458	1.485	0.11	0.01	0.004	-0.0025	-10.55	-2.44	1.00
10:00	1.331	1.476	1.593	1.617	0.14	0.01	0.007	-0.0021	-10.33	-1.26	1.00
10:30	1.255	1.375	1.459	1.457	0.11	0.01	0.004	-0.0019	-9.14	-1.38	1.00
11:00	1.053	1.155	1.237	1.21	0.11	0.00	0.007	0.0000	-8.32	-0.01	1.00
11:30	0.776	0.819	0.876	0.877	0.05	0.01	0.001	-0.0009	-10.17	-3.17	1.00
12:00	1.272	1.352	1.433	1.4	0.10	0.01	0.002	-0.0010	-8.16	-1.28	1.00
12:30	1.286	1.371	1.463	1.48	0.09	0.00	0.001	-0.0004	-10.93	-1.28	1.00
13:00	0.952	0.994	1.067	1.043	0.07	0.02	0.001	-0.0020	-8.55	-4.31	0.98
13:30	0.791	0.844	0.907	0.876	0.07	0.01	0.004	-0.0035	-7.94	-2.09	0.99
14:00	1.044	1.146	1.241	1.273	0.10	0.00	0.004	-0.0006	-11.65	-0.64	1.00
14:30	1.353	1.455	1.554	1.537	0.11	0.01	0.003	-0.0009	-8.89	-0.86	1.00
15:00	1.17	1.26	1.355	1.338	0.10	0.01	0.004	-0.0018	-8.92	-1.39	1.00
15:30	0.689	0.739	0.788	0.758	0.06	0.01	0.004	-0.0023	-7.66	-1.22	1.00
16:00	1.073	1.176	1.254	1.226	0.11	0.00	0.006	-0.0006	-8.23	-0.24	1.00
16:30	1.919	2.086	2.32	2.392	0.18	0.03	0.005	-0.0043	-13.24	-4.90	1.00
17:00	2.783	3.059	3.437	3.466	0.33	0.05	0.012	-0.0088	-10.66	-3.62	1.00
17:30	2.438	2.681	3.022	2.99	0.31	0.06	0.015	-0.0123	-9.56	-3.45	0.99
18:00	2.596	2.838	3.197	3.228	0.30	0.06	0.010	-0.0098	-10.92	-4.52	0.99
18:30	2.517	2.781	3.119	3.155	0.30	0.04	0.012	-0.0074	-10.75	-2.98	1.00
19:00	3.195	3.444	3.9	4.158	0.26	0.07	0.003	-0.0045	-27.78	-33.76	1.00
19:30	2.579	2.785	3.149	3.359	0.21	0.05	0.003	-0.0043	-27.37	-30.23	1.00
20:00	3.22	3.591	4.032	3.891	0.47	0.07	0.022	-0.0125	-8.46	-2.13	0.99

Precipitation Record: Application 1 1995

July 17-August 8, 1995

(Corvallis/Hyslop readings listed on website: <ftp://chaos.ats.orst.edu/pub/oregon/dly/prec1862.1f>)

Experiment Date	Calendar Date	Julian Date	Precipitation (hundredths of inches)	Precipitation (mm)
0	7/17/95	198		
1	7/18/95	199		
2	7/19/95	200		
3	7/20/95	201		
4	7/21/95	202		
5	7/22/95	203		
6	7/23/95	204		
7	7/24/95	205		
8	7/25/95	206		
9	7/26/95	207		
10	7/27/95	208		
11	7/28/95	209		
12	7/29/95	210		
13	7/30/95	211		
14	7/31/95	212		
15	8/1/95	213		
16	8/2/95	214		
17	8/3/95	215		
18	8/4/95	216		
19	8/5/95	217		
20	8/6/95	218		
21	8/7/95	219	1	0.3
22	8/8/95	220	2	0.5

Peak Flux Values during 12:00-16:00 on Days 0,1,2,3,5,7,14,22

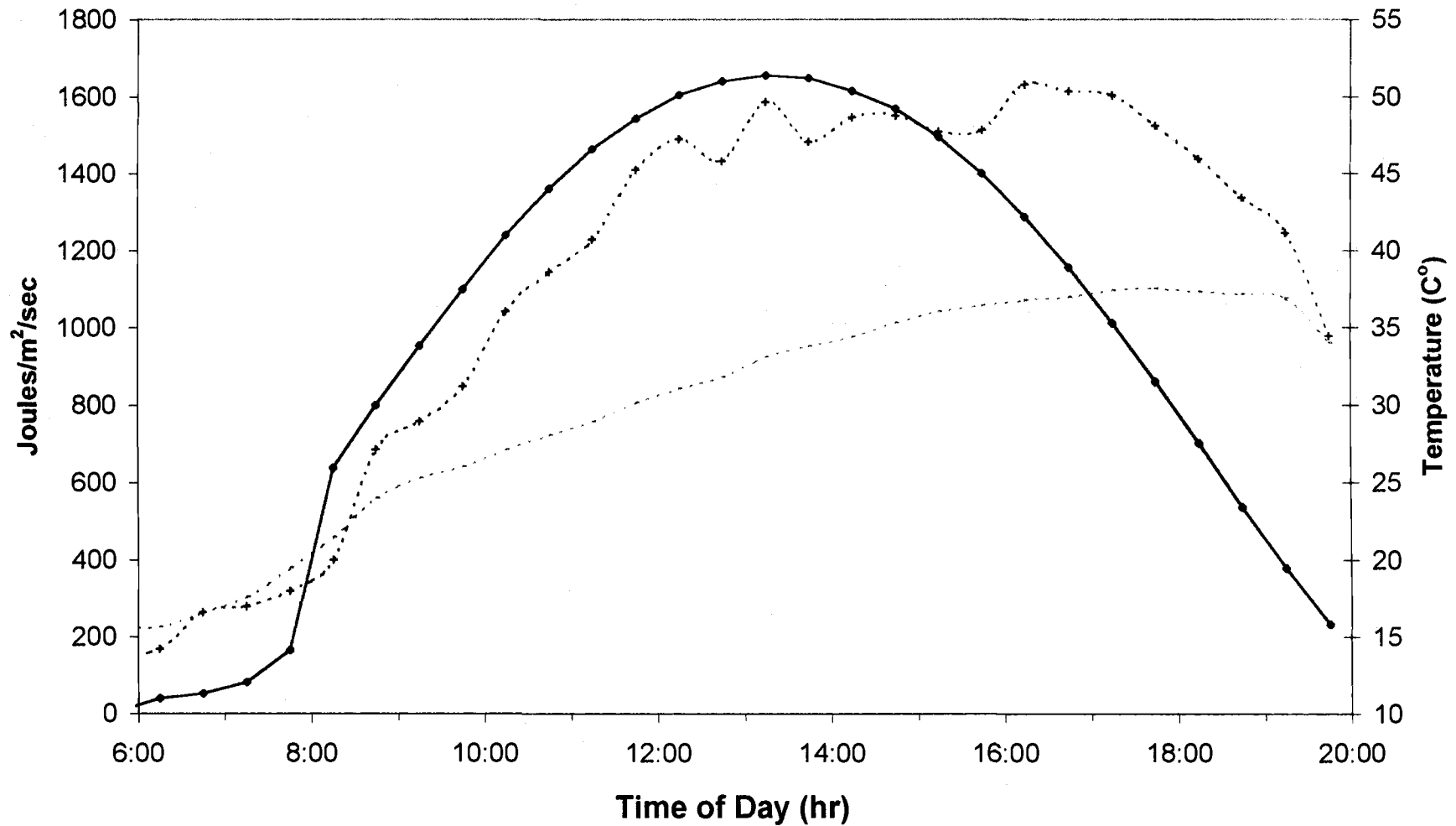
Application 1, 1995

Day	Total Flux (ug/m ²) 12:00-16:00		Total Solar Radiation 12:00-16:00 (MJ/m ²)	Flux/Solar Radiation (ug/MJ)	
	Triadimefon	Chlorpyrifos		Triadimefon	Chlorpyrifos
0	2677	4744	23	118	209
1	1657	2053	16	102	126
2	2030	1822	22	93	84
3	1375	1293	22	62	59
5	299	346	17	17	20
7	319	400	22	14	18
14	49	107	22	2	5
22	#VALUE!	#VALUE!	21		

Exponential Decay Constants of (Flux/Solar Radiation) on Days following application

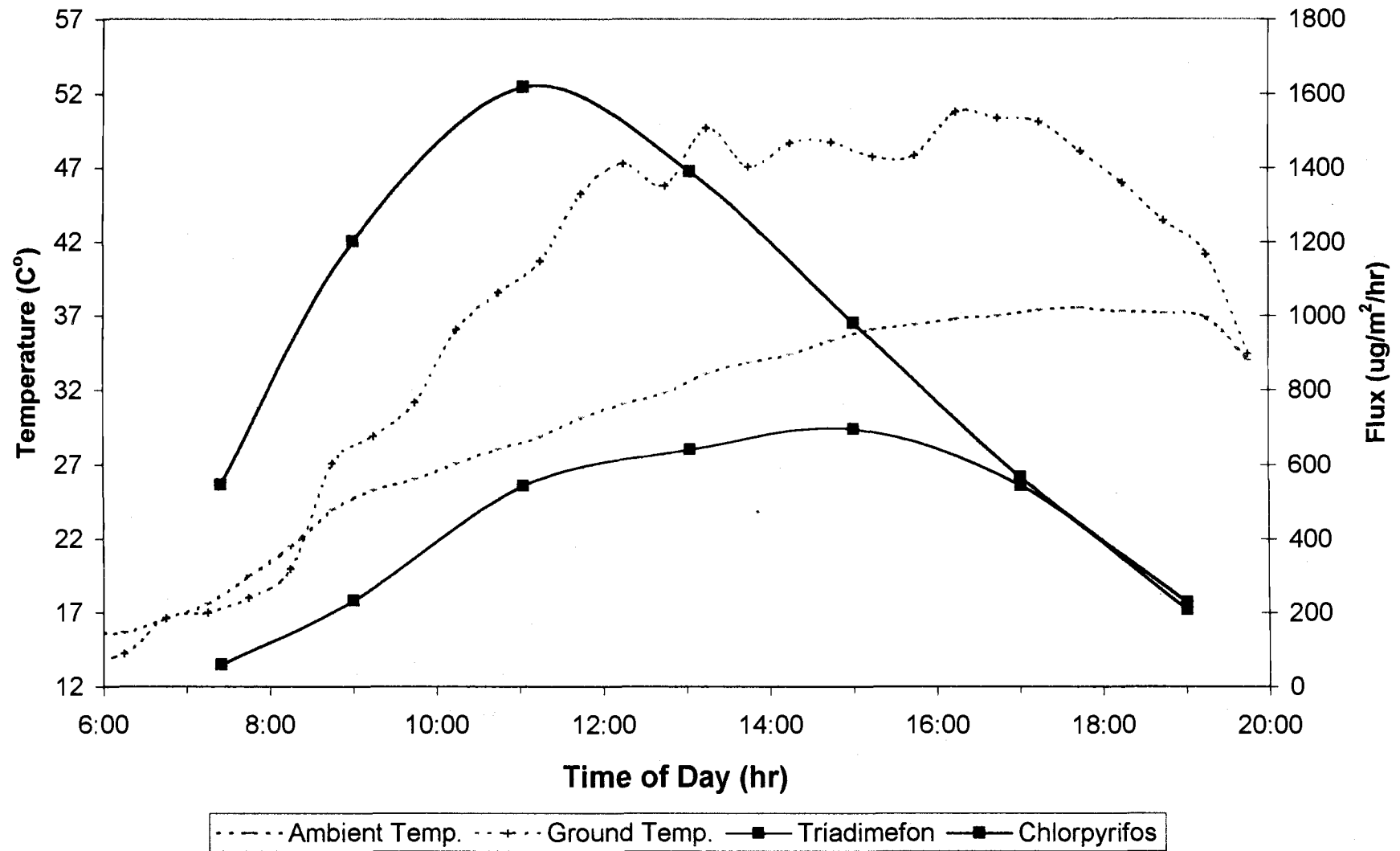
$C = C_0 \cdot \exp(-kT(\text{days}))$

Solar Radiation and Temperature Day 0, App.1 '95 July 17, Julian 198



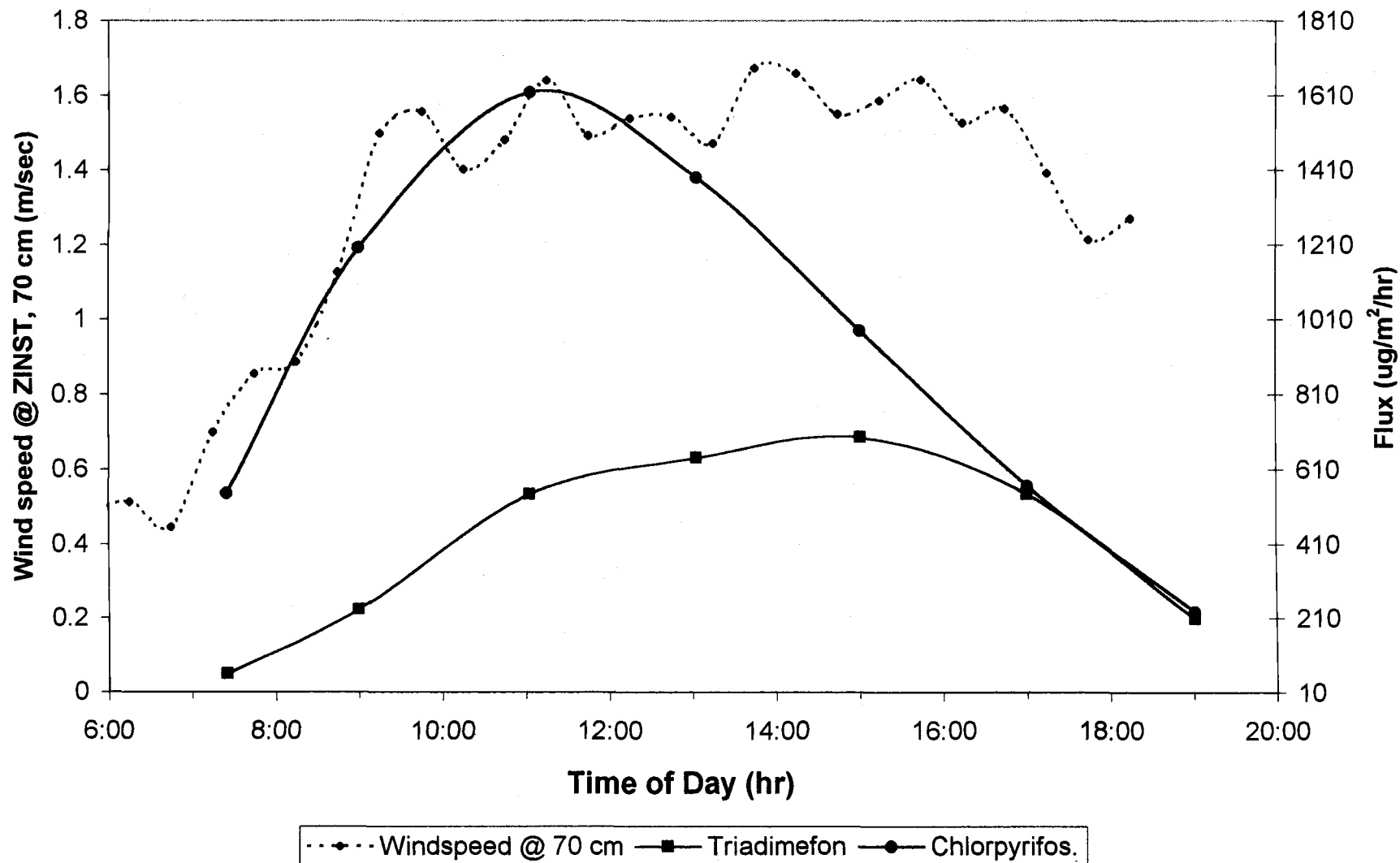
—•— Solar Radiation ···· Surface Temp. - - - Ambient Temp.

Flux and Temperature (C°)
Day 0, App.1 '95 July 17, Julian 198

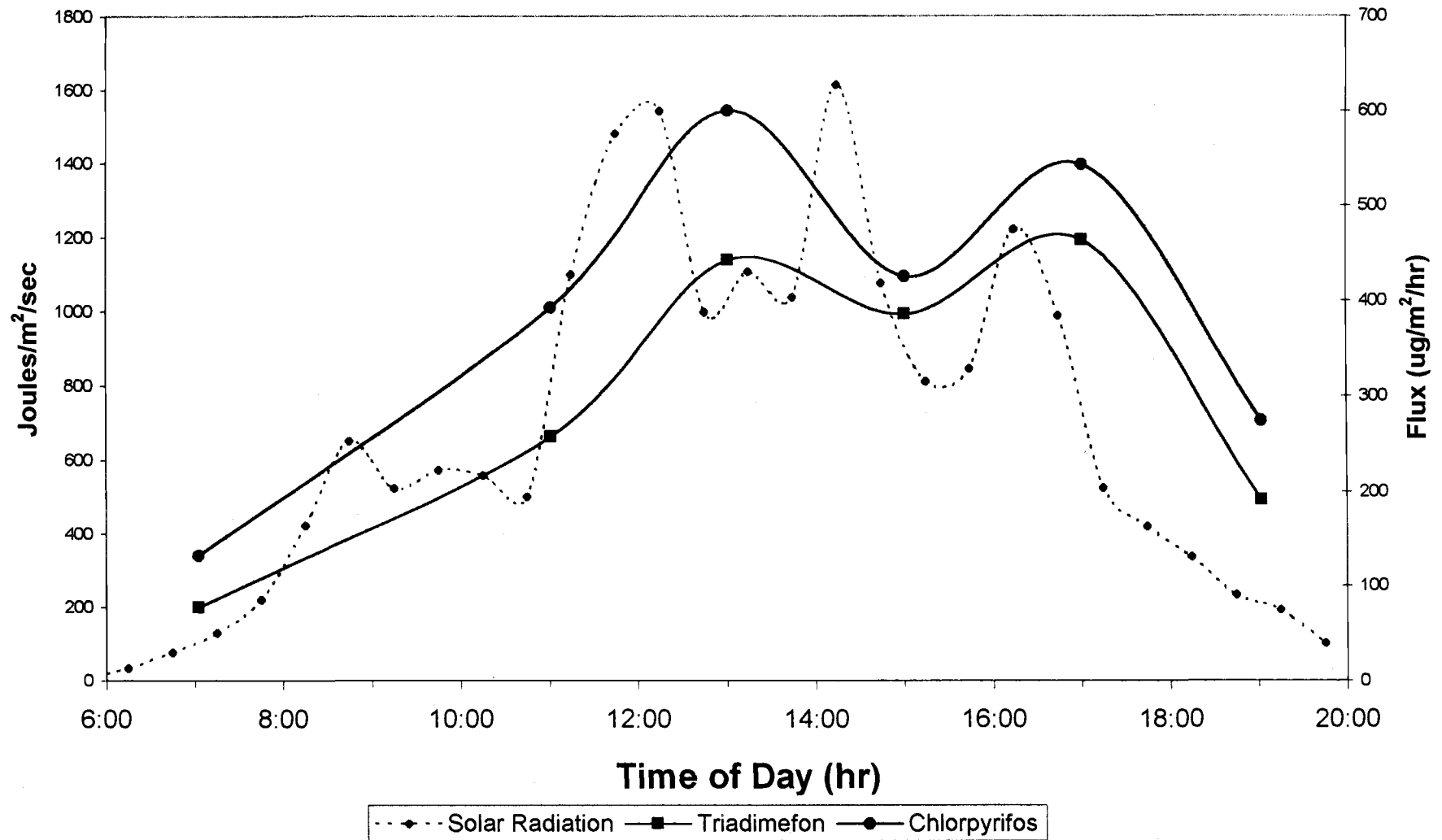


Windspeed and Flux

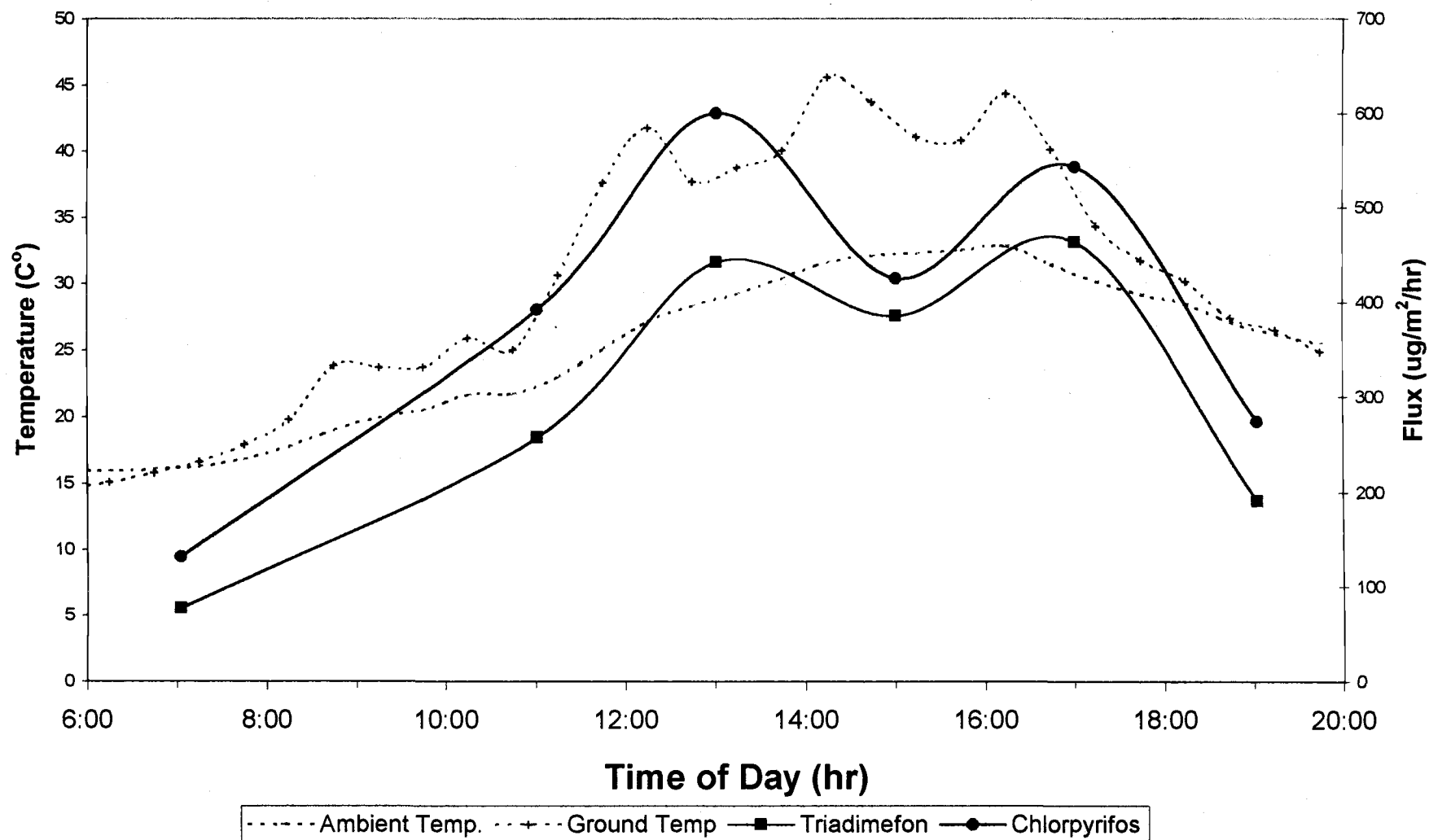
Day 0, App.1 '95 July 17, Julian 198



Solar Radiation vs. Flux
Day 1, App.1 '95, July 18, Julian 199

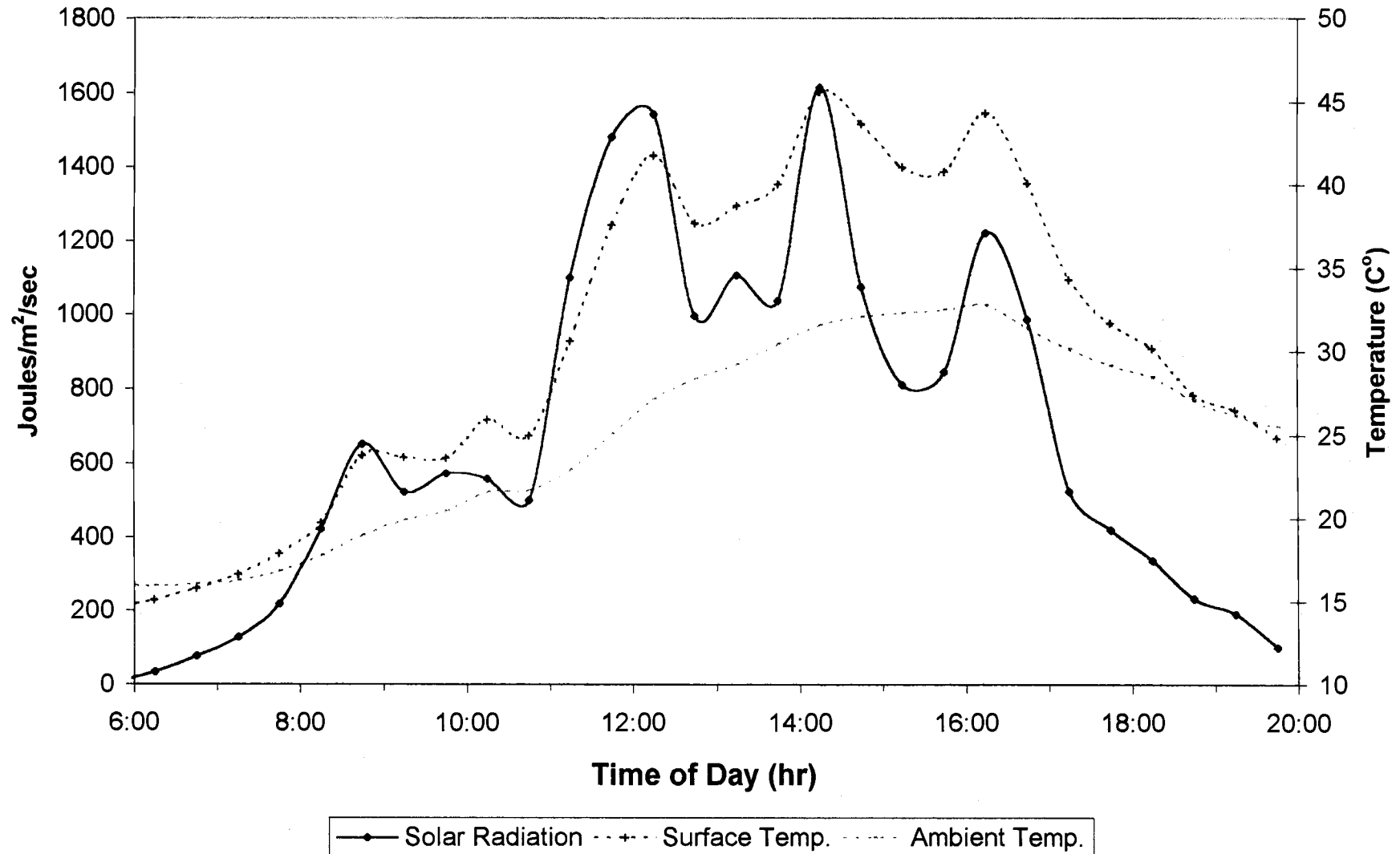


Flux and Temperature (C°)
Day 1, App.1 '95, July 18, Julian 199

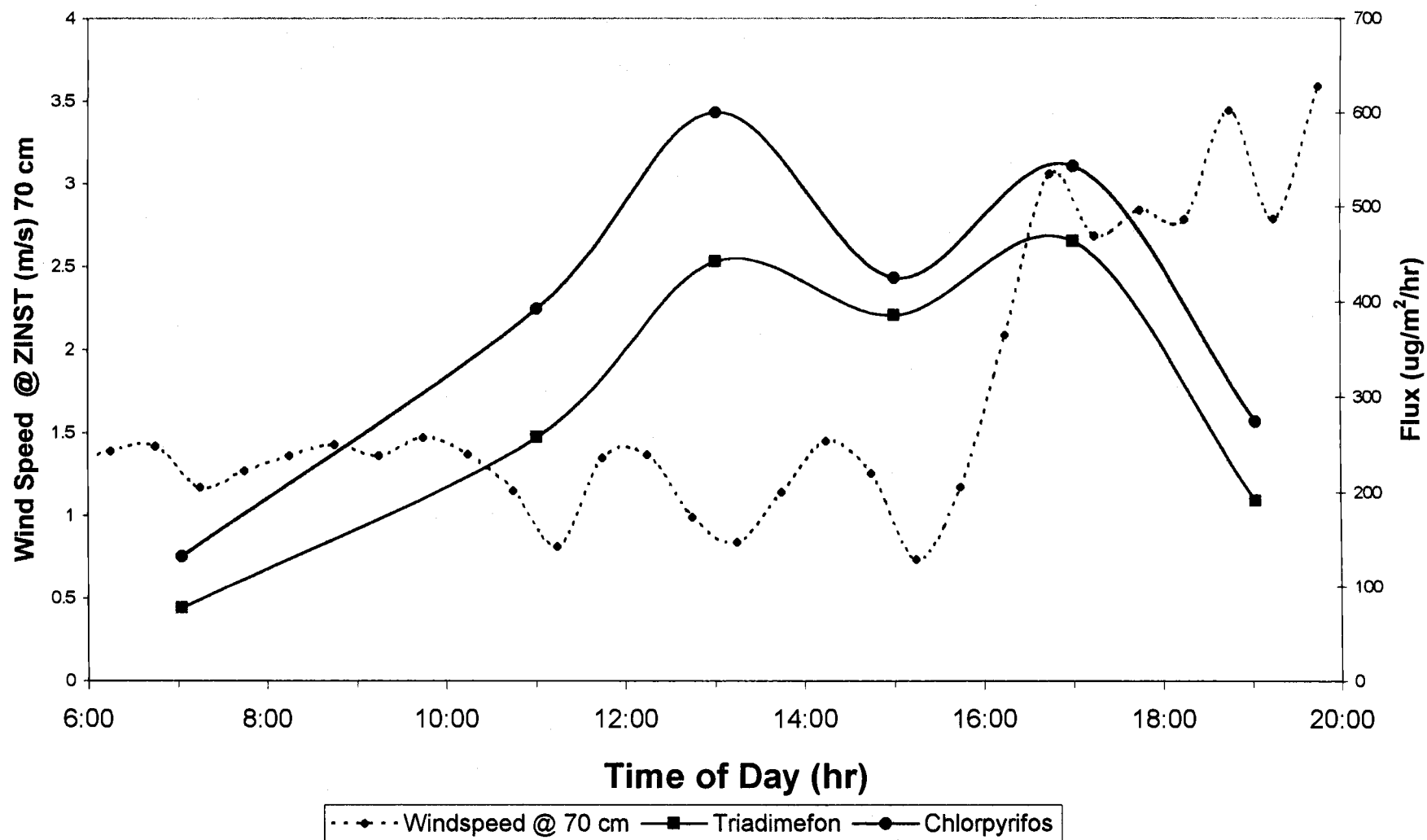


Solar Radiation and Temperature

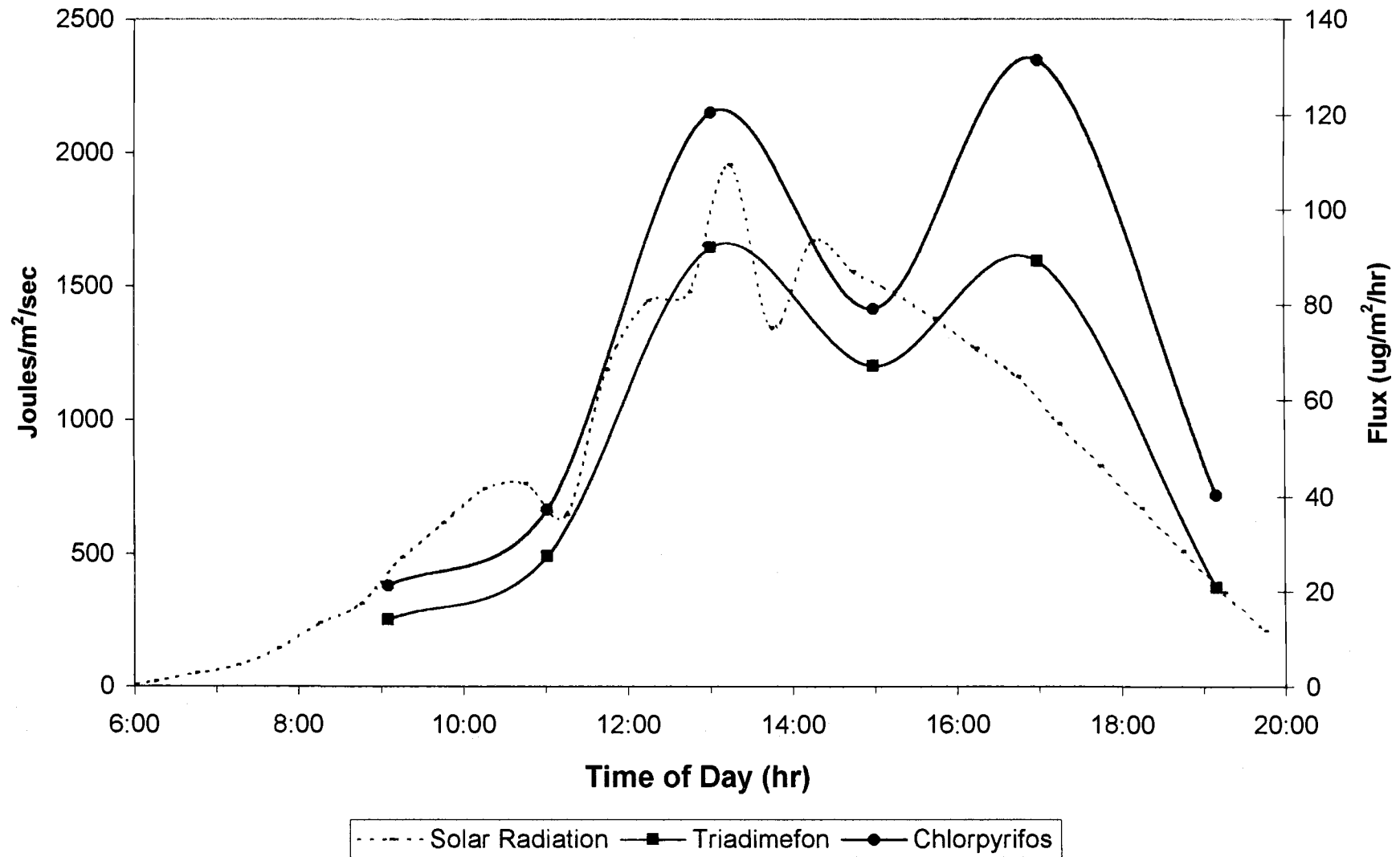
Day 1, App.1 '95 July 18, Julian 199



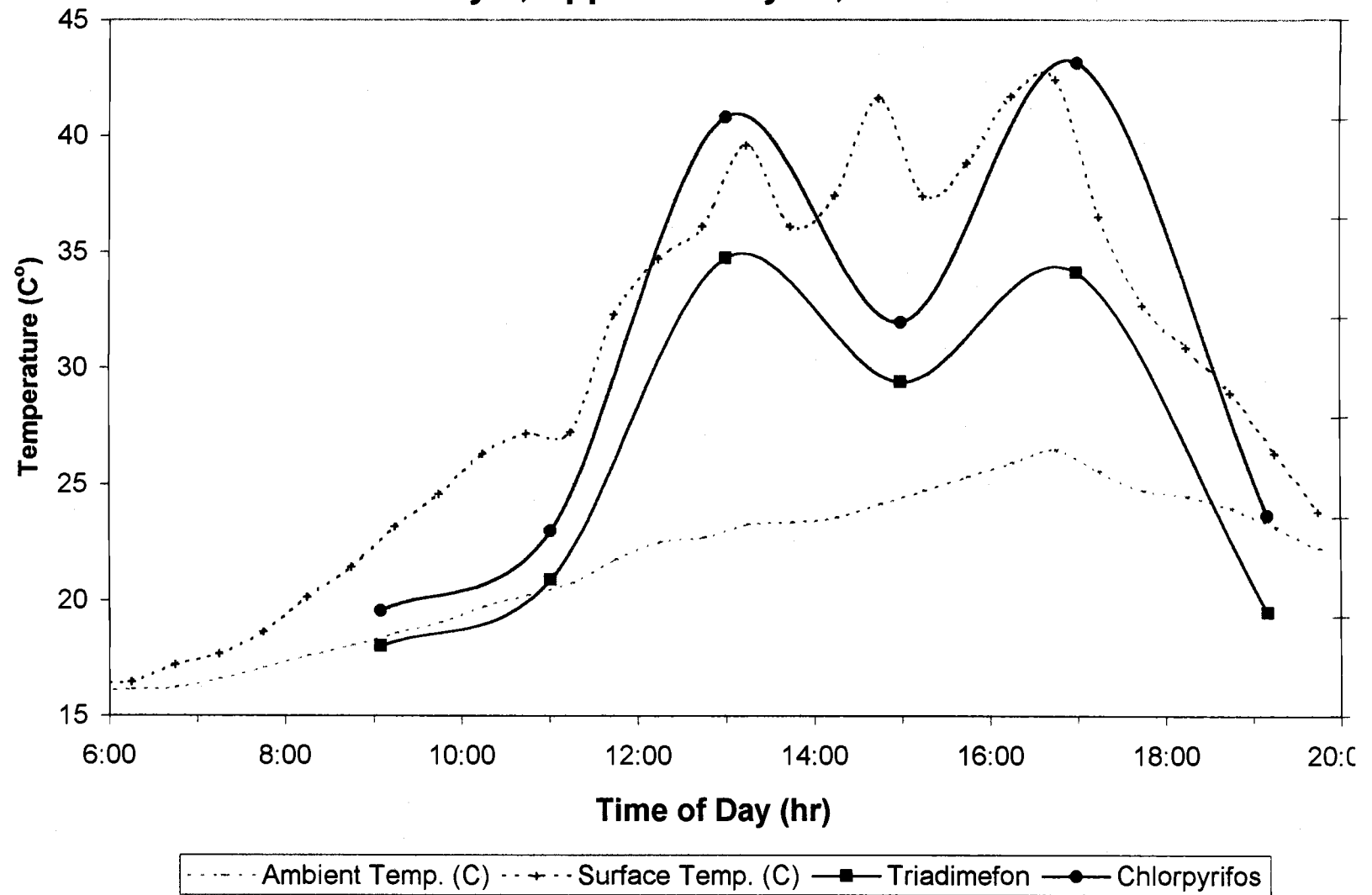
**Windspeed @ Height ZINST (70 cm) and Flux
Day 1, App.1 '95, July 18, Julian 199**



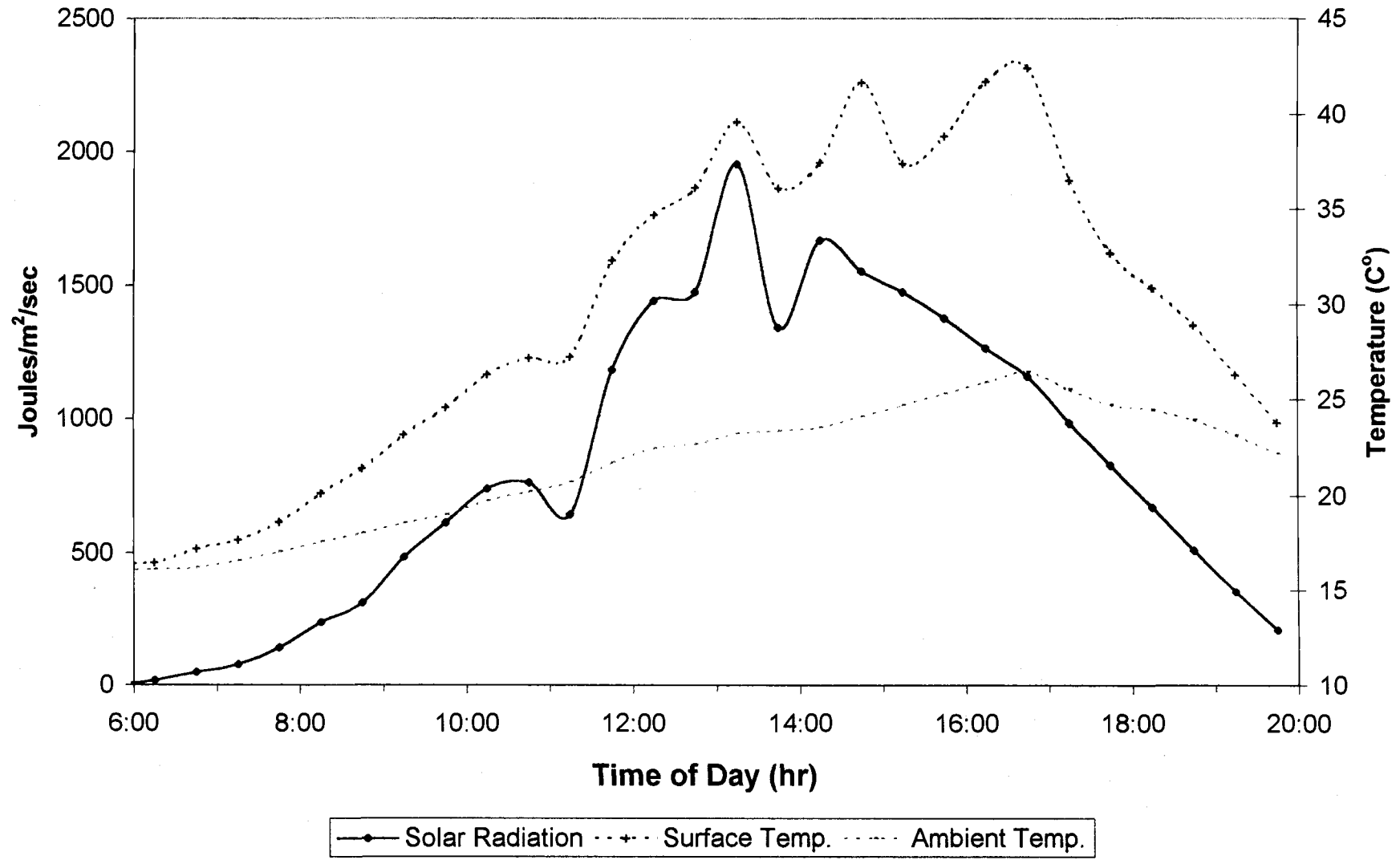
Solar Radiation and Flux
Day 7, App.1 '95 July 24, Julian 205



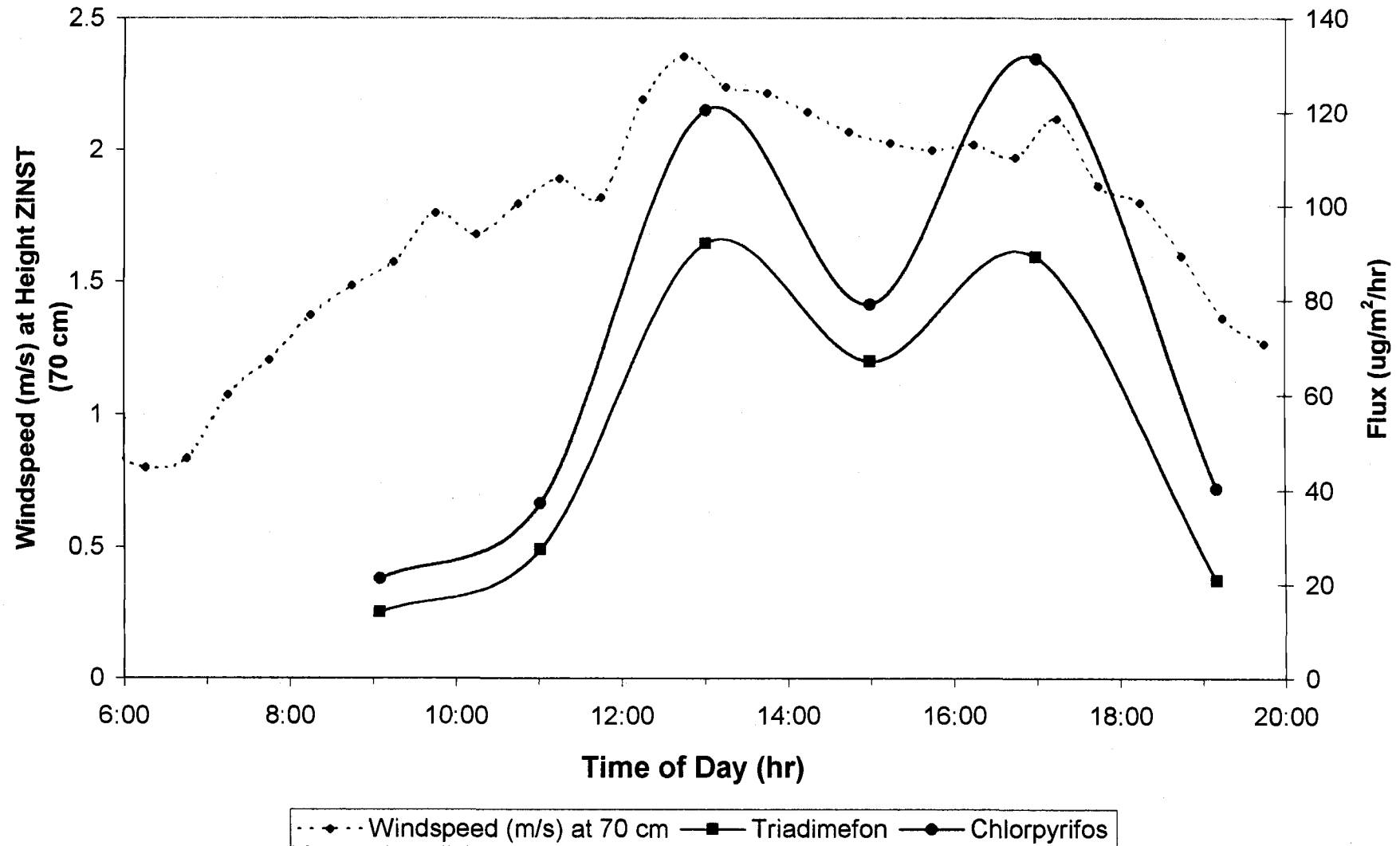
Flux and Temperature (C°)
Day 7, App.1 '95 July 24, Julian 205



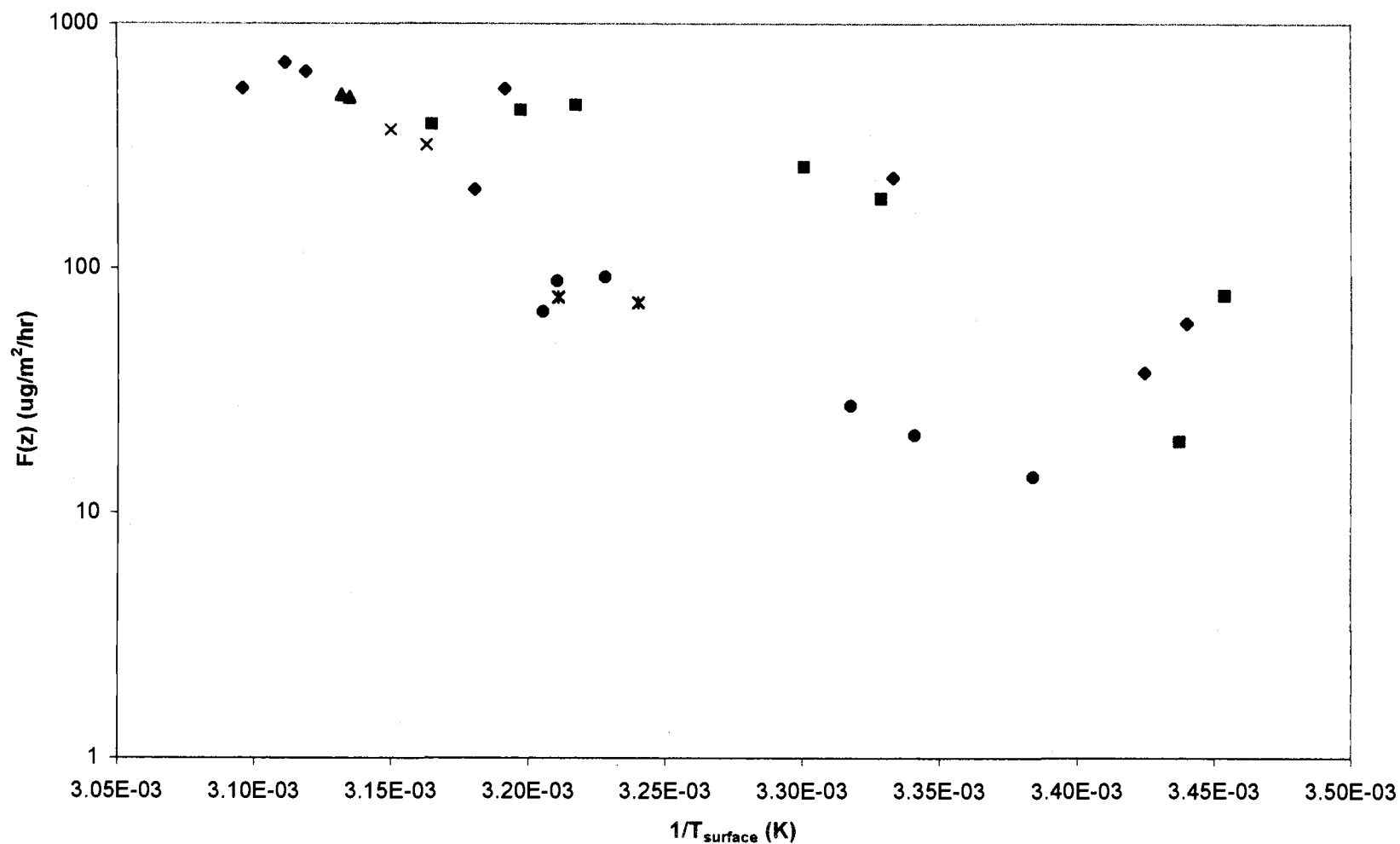
Solar Radiation and Temperature Day 7, App.1 '95 July 24, Julian 205



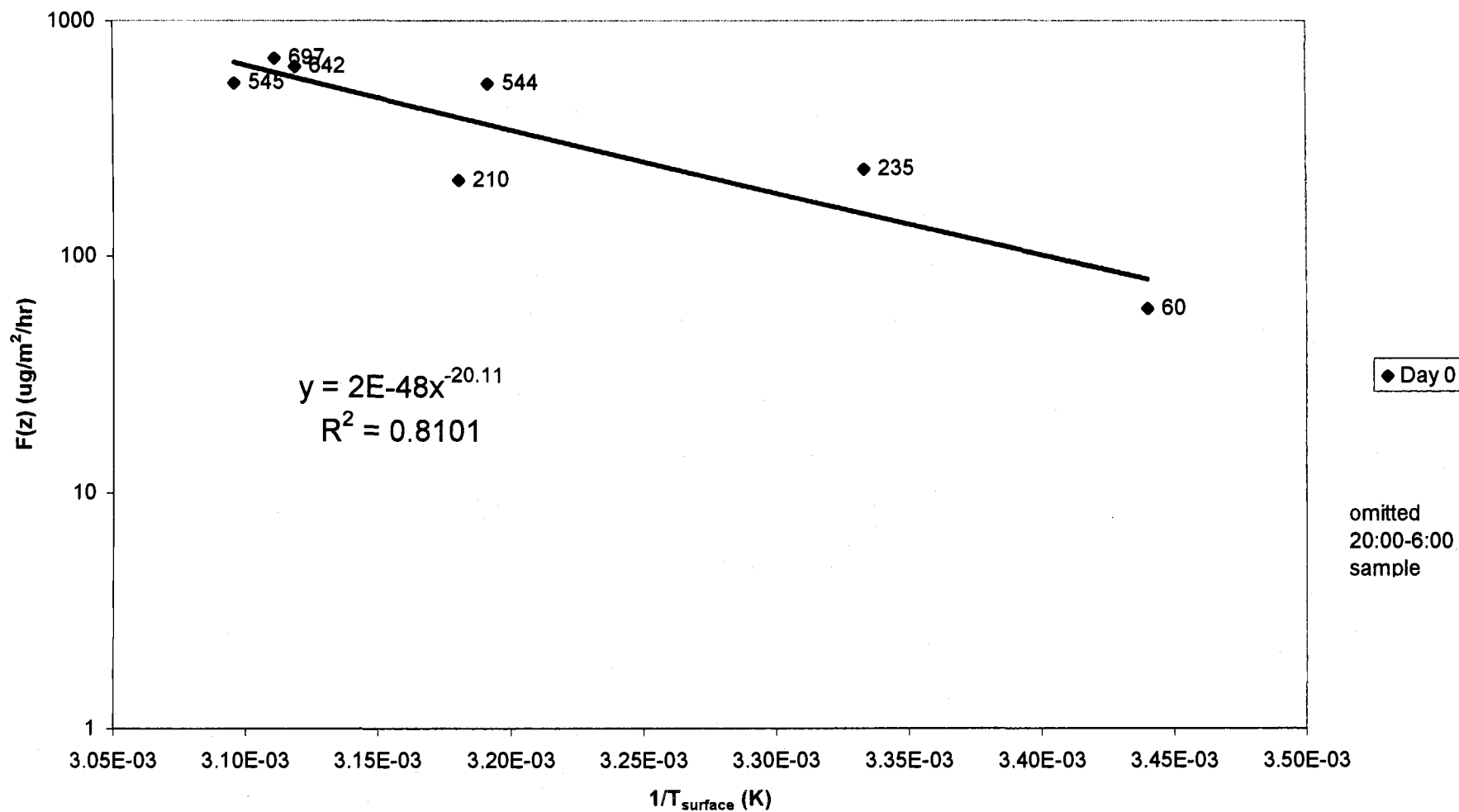
Windspeed and Flux
Day 7, App.1 '95 July 24, Julian 205



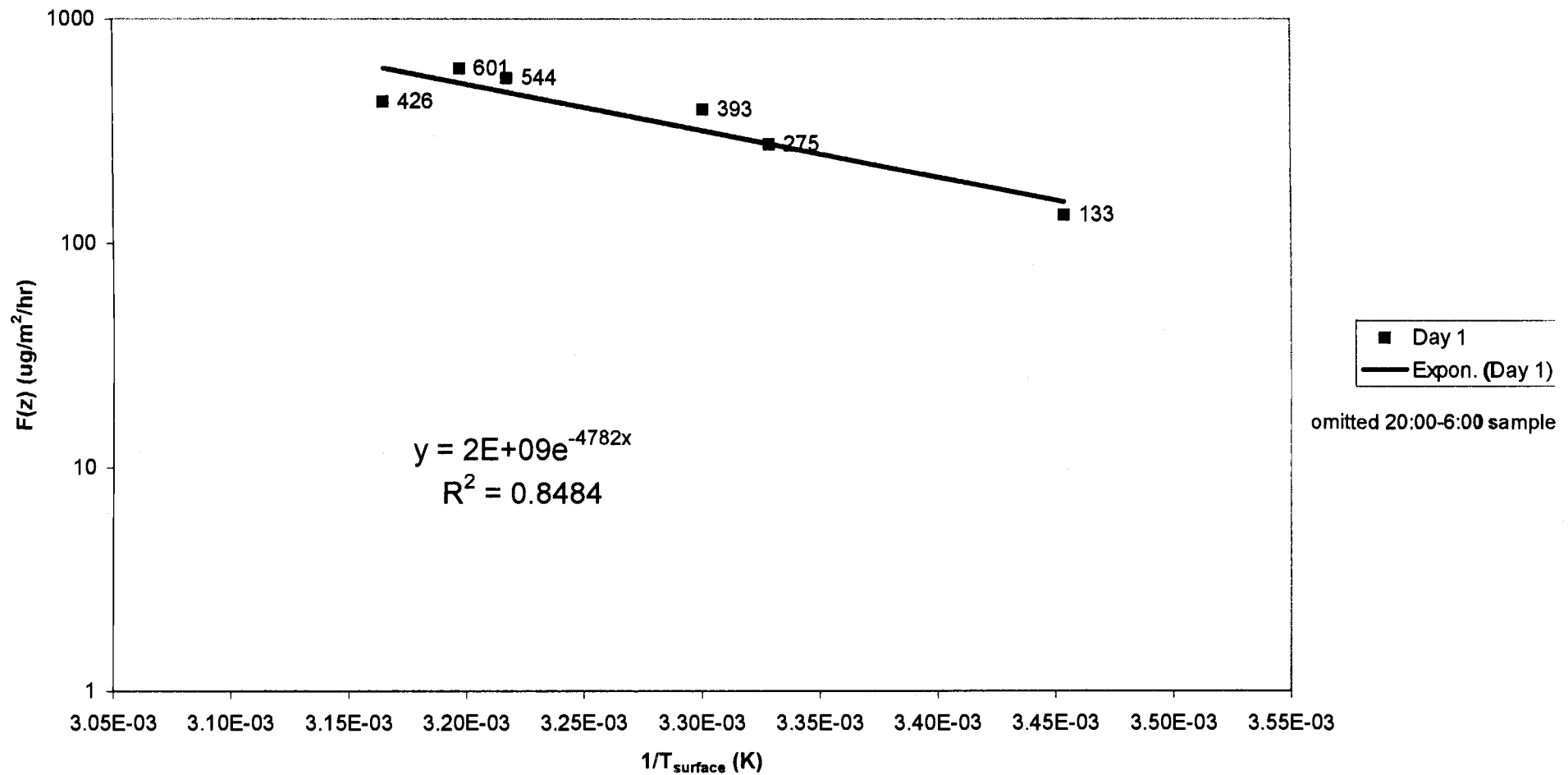
Triadimefon: Flux ($\mu\text{g}/\text{m}^2/\text{hr}$) vs. $1/T_{\text{surface}}$ (K)
Day 0-7, App.1 '95 July 17-24, Julian 198-205



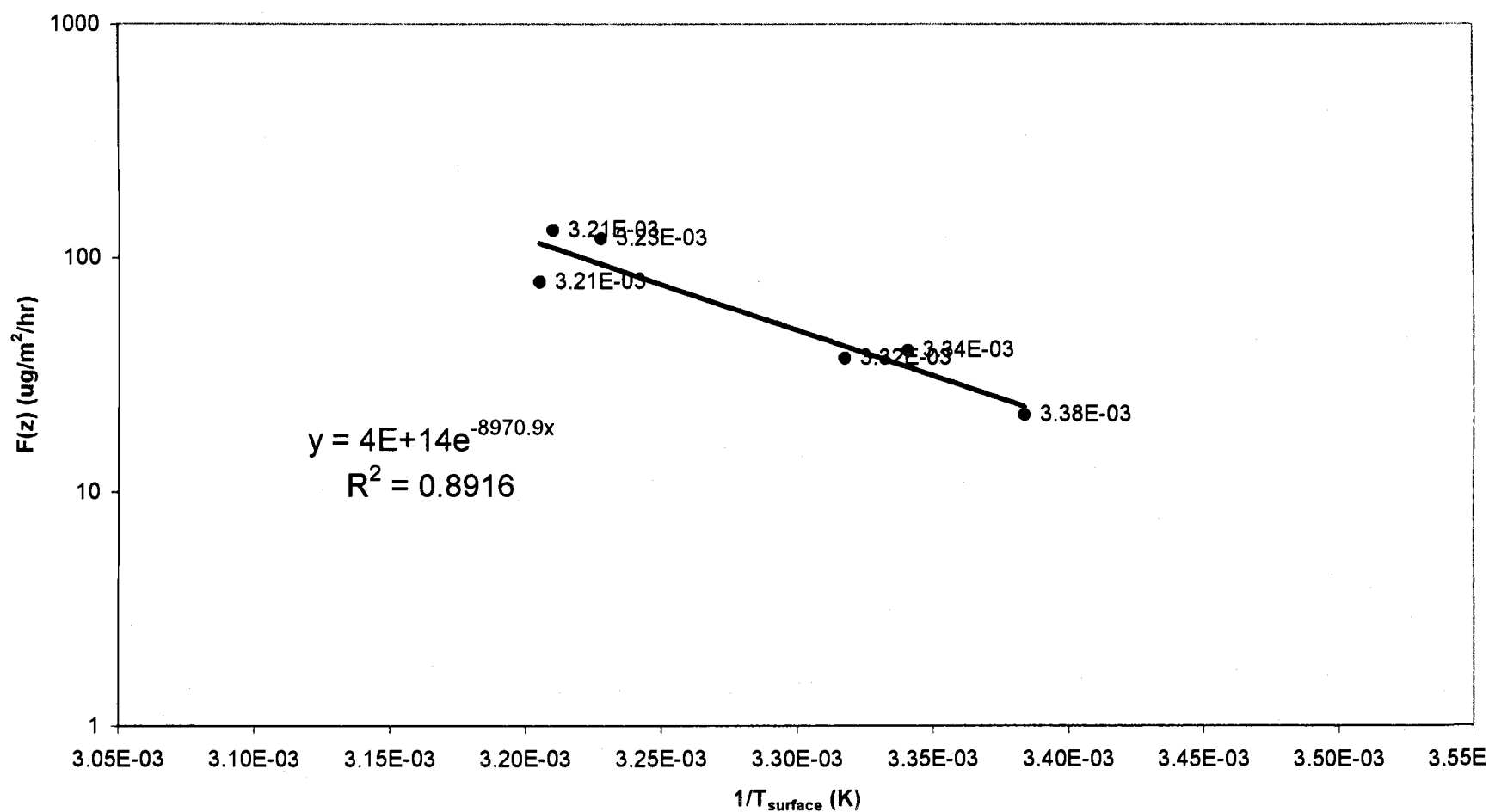
Triadimefon: Flux ($\mu\text{g}/\text{m}^2/\text{hr}$) vs. $1/T_{\text{surface}}$ (K)
Day 0, App.1 '95 July 17, Julian 198



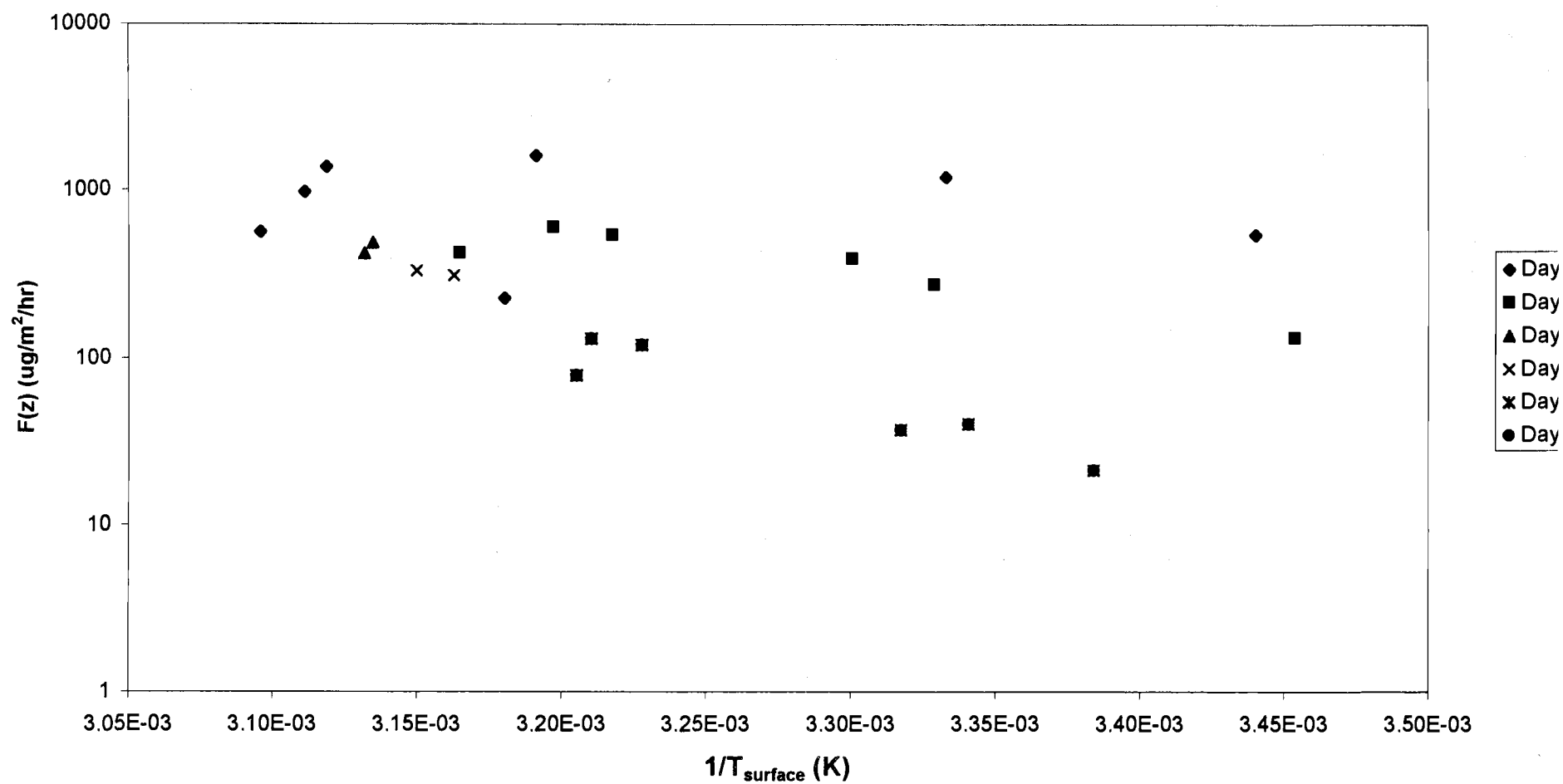
Triadimefon: Flux ($\mu\text{g}/\text{m}^2/\text{hr}$) vs. $1/T_{\text{surface}}$ (K)
Day 1, App.1 '95 July 18, Julian 199



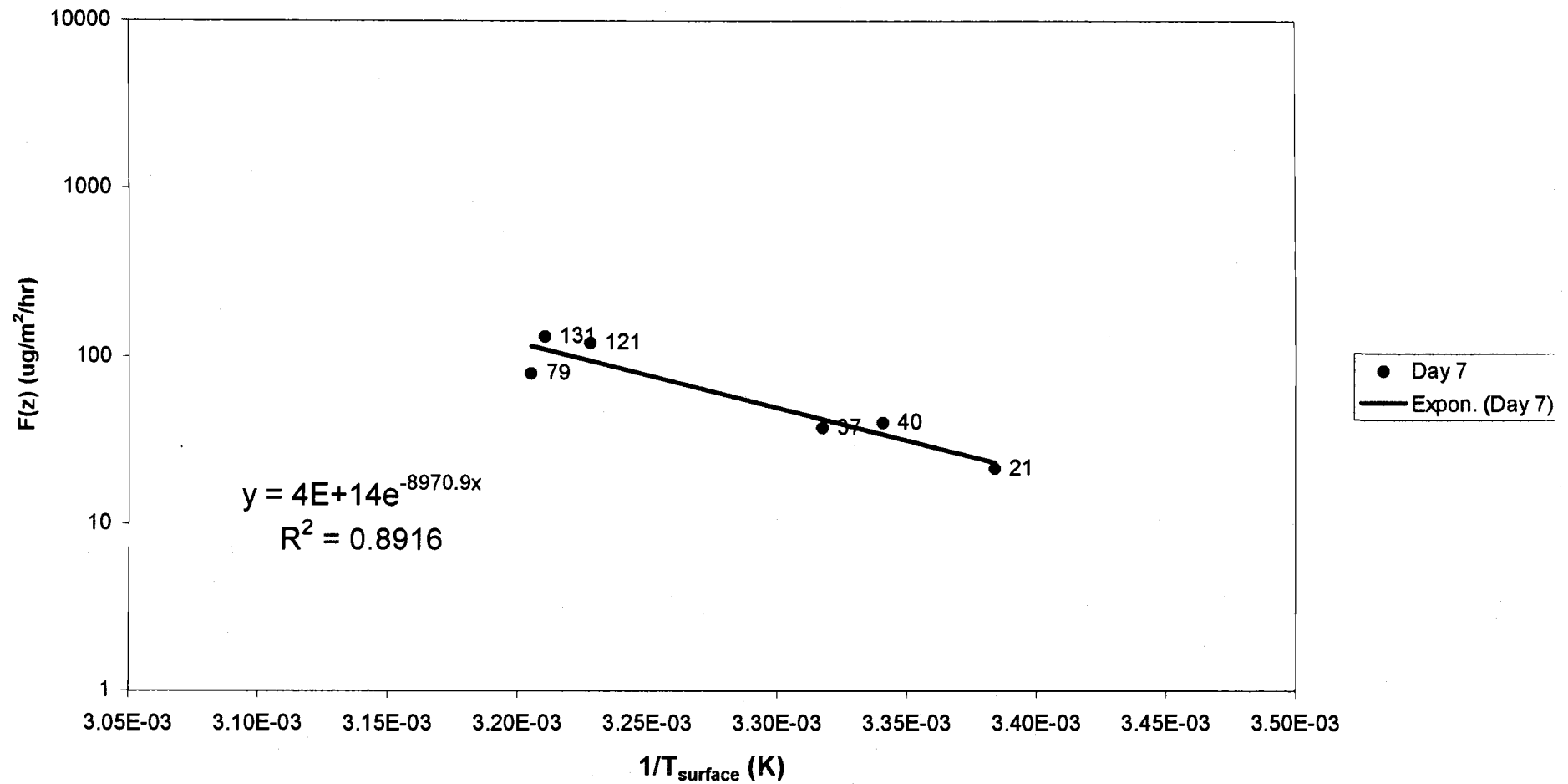
Triadimefon: Flux ($\mu\text{g}/\text{m}^2/\text{hr}$) vs. $1/T_{\text{surface}}$ (K)
 Day 7, App.1 '95 July 24, Julian 205



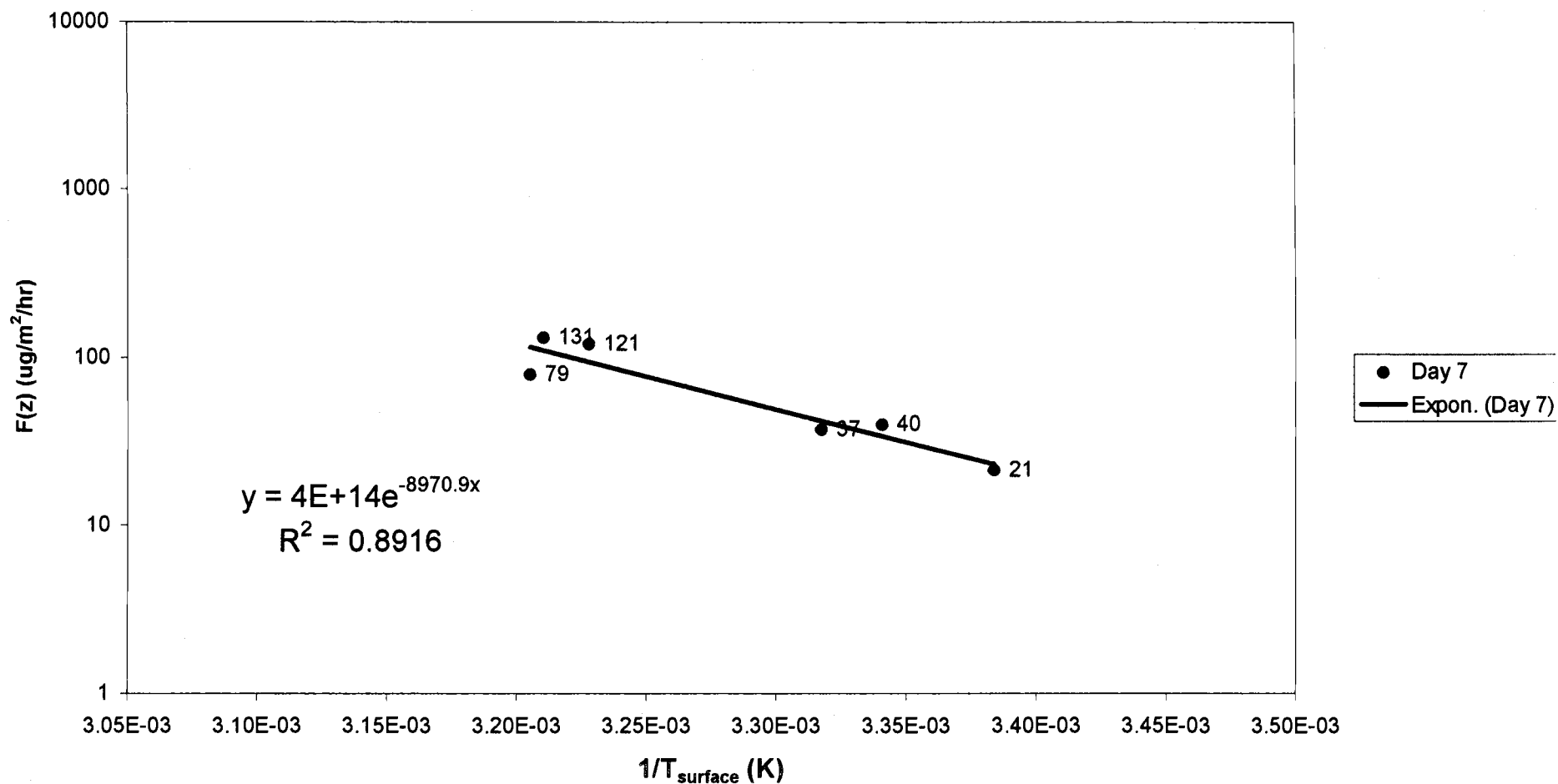
Chlorpyrifos: Flux ($\mu\text{g}/\text{m}^2/\text{hr}$) vs. $1/T_{\text{surface}}$ (K)
 Day 0-7, App.1 '95 July 17-24, Julian 198-205



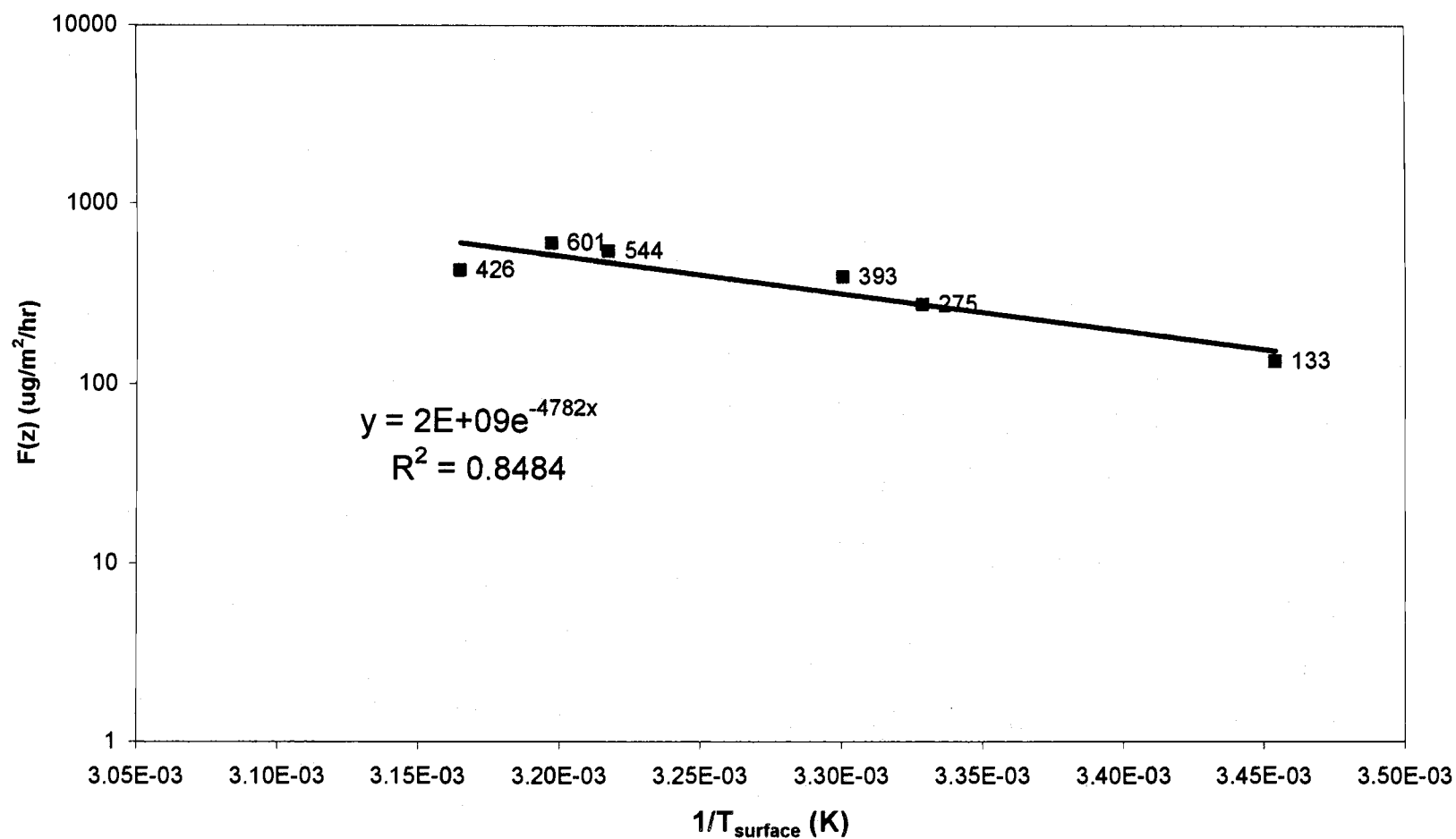
Chlorpyrifos: Flux ($\mu\text{g}/\text{m}^2/\text{hr}$) vs. $1/T_{\text{surface}}$ (K)
 Day 7, App.1 '95 July 24, Julian 205



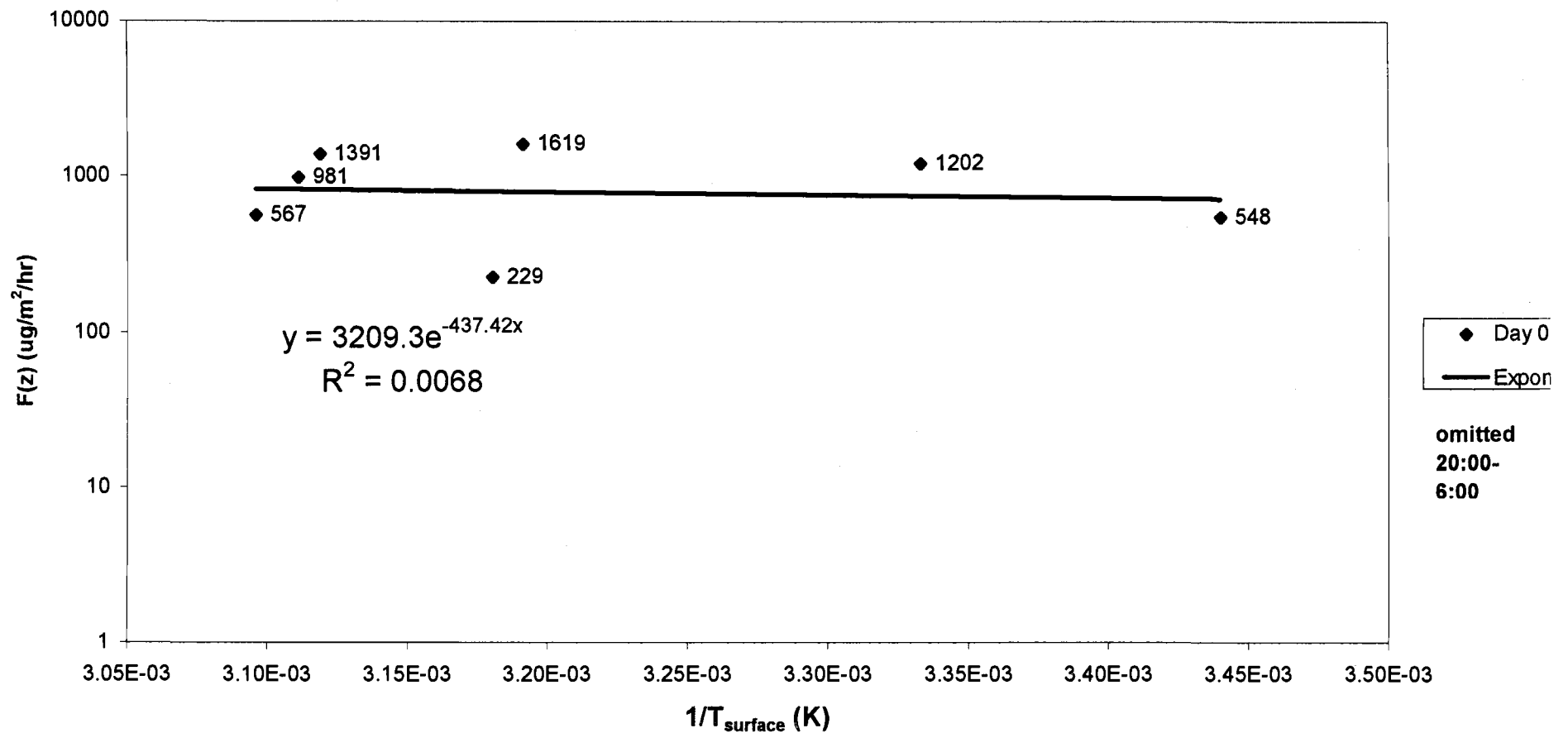
Chlorpyrifos: Flux ($\mu\text{g}/\text{m}^2/\text{hr}$) vs. $1/T_{\text{surface}}$ (K)
 Day 7, App.1 '95 July 24, Julian 205



Chlorpyrifos: Flux ($\mu\text{g}/\text{m}^2/\text{hr}$) vs. $1/T_{\text{surface}}$ (K)
Day 1, App.1 '95 July 18, Julian 199



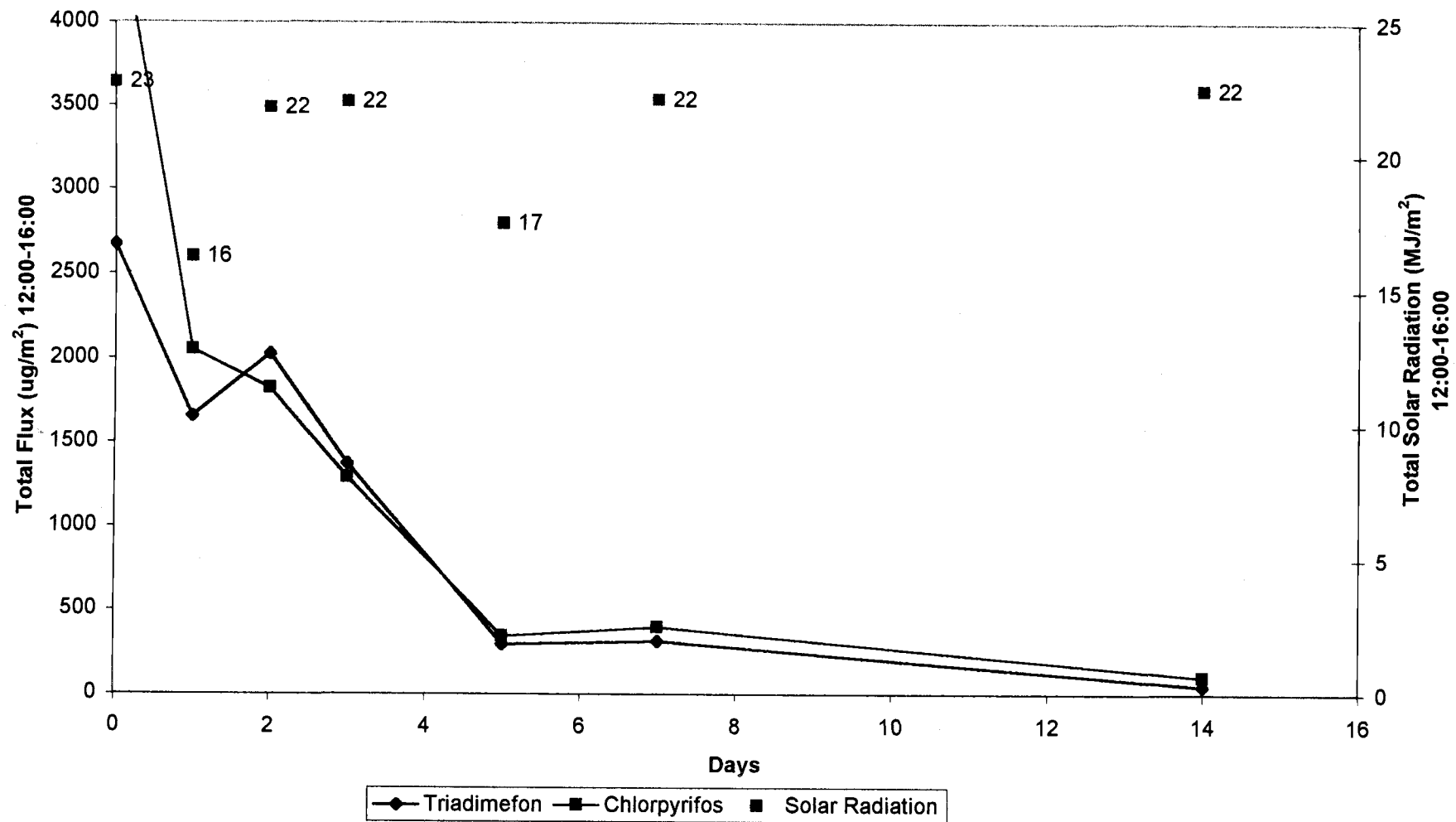
Chlorpyrifos: Flux ($\mu\text{g}/\text{m}^2/\text{hr}$) vs. $1/T_{\text{surface}}$ (K)
Day 0, App.1 '95 July 17, Julian 198



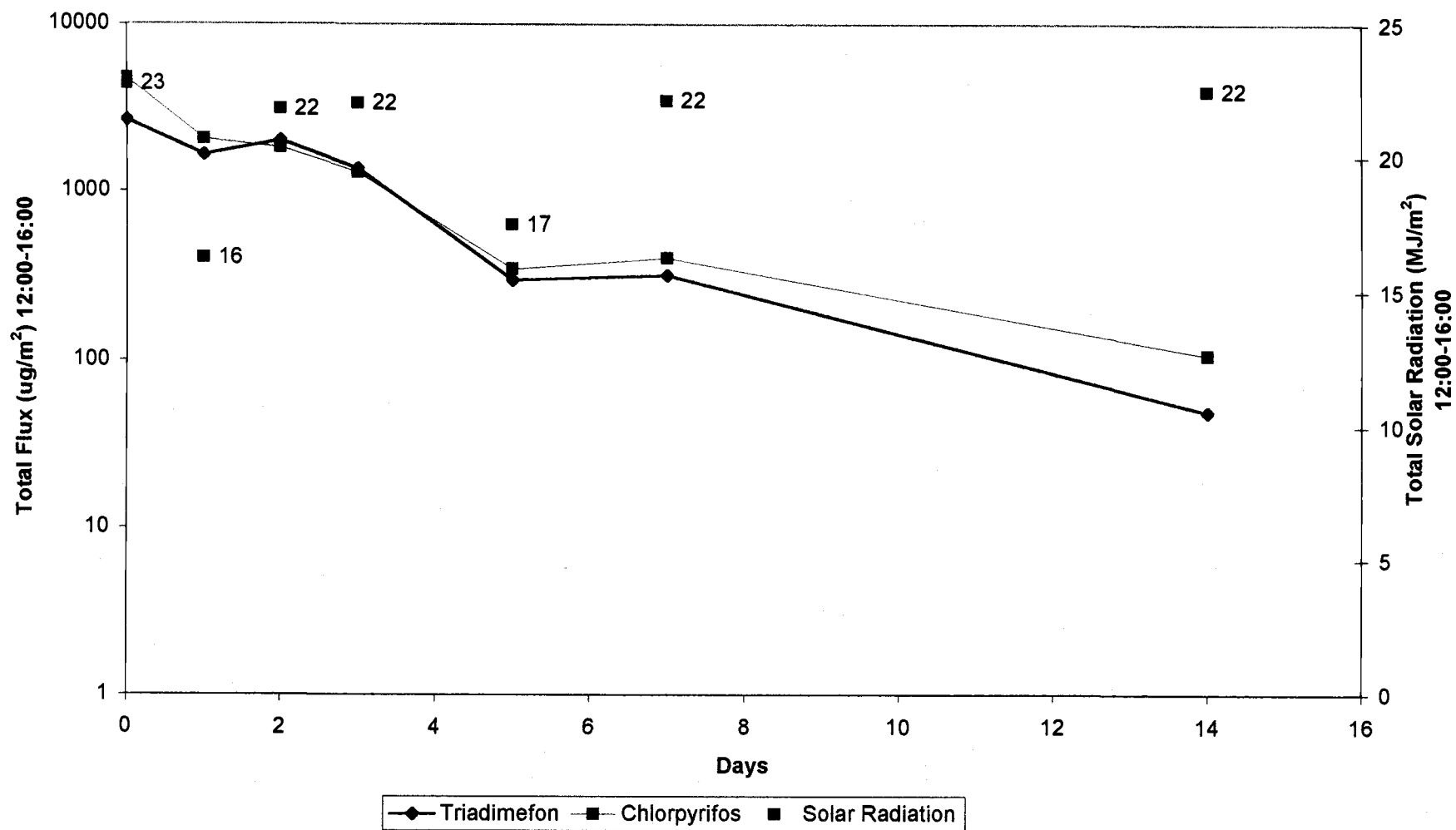
Peak Flux Values during 12:00-16:00 on Days 0,1,2,3,5,7,14,22
Application 1, 1995

Day	Total Flux (ug/m ²) 12:00-16:00		Total Solar Radiation 12:00-16:00 (MJ/m ²)	Flux/Solar Radiation (ug/MJ)	
	Triadimefon	Chlorpyrifos		Triadimefon	Chlorpyrifos
0	2677	4744	23	118	209
1	1657	2053	16	102	126
2	2030	1822	22	93	84
3	1375	1293	22	62	59
5	299	346	17	17	20
7	319	400	22	14	18
14	49	107	22	2	5
22	#VALUE!	#VALUE!	21	#VALUE!	

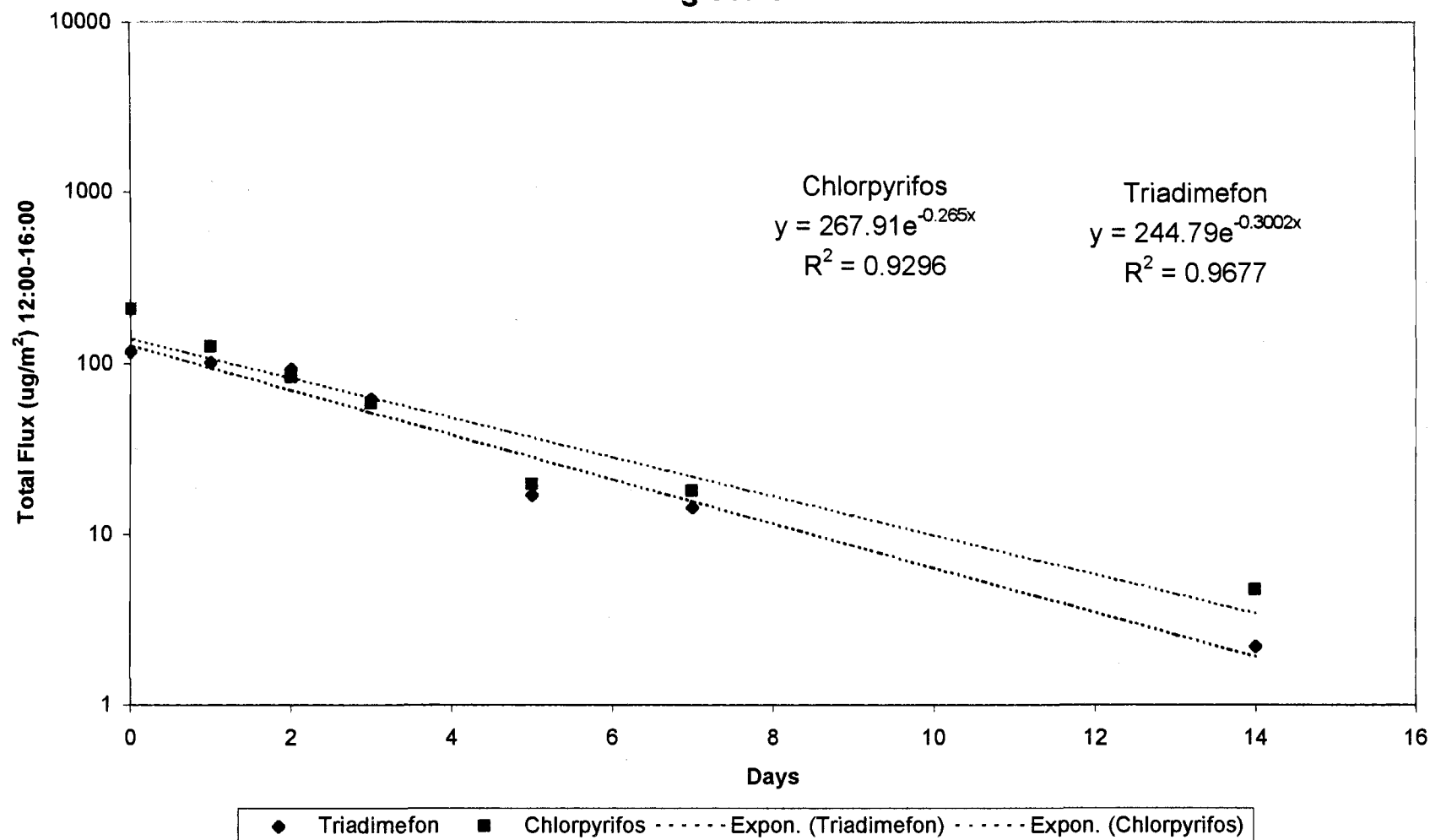
**Peak Flux ($\mu\text{g}/\text{m}^2$) during 12:00-16:00
following Application 1, July 17th 1995**



**Peak Flux ($\mu\text{g}/\text{m}^2$) during 12:00-16:00
following Application 1, July 17th 1995
log scale**



Peak Solar Radiation normalized Flux (Flux/S.R.)
12:00-16:00
on Days following Application 1, July 17th 1995
log scale



Appendix 5: Application 1, 1996

Source File: app196summarya

T1.App.1,96
Ch,96,1,0,SR.FI
Ch,96,1,0,T.F
Ch,96,1,0,SR.T
Ch,96,1,0,WS.FI
Ch,96,1,1,SR.FI
Ch,96,1,1,T.FI
Ch,96,1,1,SR.T
Ch,96,1,1,WS.FI
Ch,96,1,2,SR.FI
Ch,96,1,2,T.FI
Ch,96,1,2,SR.T
Ch,96,1,2,WS.FI
Ch,96,1,7,SR.FI
Ch,95,1,7,T.FI
Ch,96,1,7,SR.T
Ch,96,1,7,WS.FI

Source File: fluxratio3.xls

CCTr96,1,0.7
CCTr,96,1,0
CCTr,96,1,1
CCTr,96,1,2
CCTr,96,1,7
CCCI,96,1,0.7
CCCI,96,1,0
CCCI,96,1,1
CCCI,96,1,2
CCCI,96,1,7
CCEt.96,1,0.7
CCEt.96,1,0
CCEt.96,1,1
CCEt.96,1,2
CCEt.96,1,7

Source File: app196summarya

Solar Rad
Temp
Wind
Precip
Pk Flux Noon
Ch,PkFxNoon
CH,logPkFxNoon

Application 1, 1996 Airborne Residue

Application 1, 1996

											Wind Speed, (m/s) at (41 cm, 70 cm, 140 cm, 280 cm)			
	Air Sampling		Intermed.	Flux (ug/m ² /hr)			Surface	Ambient	1/T(K)	Solar Rad.	41	70	140	280
	Start	End		Time	Triadimefon	Chlorpyrifos	Ethofumesate	Temp. (C)	Temp. (C)	Surface	J/m ² sec			
Day 0 (June 12th)														
Julian 164	6:41	7:59	7:20		9	166	41	12.62	12.36	3.50E-03	382	0.68	0.78	0.83
	8:00	10:01	9:00		77	1046	284	22.22	15.40	3.39E-03	941	1.34	1.46	1.63
	10:01	12:00	11:00		242	2496	768	30.15	17.89	3.30E-03	1457	1.62	1.71	1.96
	12:00	14:00	13:00		450	1738	949	36.14	20.82	3.23E-03	1683	1.64	1.73	1.97
	14:01	16:06	15:03		405	1092	898	37.91	23.33	3.21E-03	1490	1.49	1.56	1.80
	16:07	17:56	17:01		341	944	851	32.33	23.82	3.27E-03	1083	2.81	3.07	3.58
	17:58	20:00	18:59		95	284	248	23.61	21.23	3.37E-03	469	3.05	3.36	3.90
	20:00	6:00	13:00		11	69	31	11.44	11.50	3.51E-03	7	1.29	1.43	1.65
Est.Total (6:00-20:00)					3238	15532	8079							
Day 1 (June 13th)	6:01	8:02	7:01		7	148	64	12.82	9.94	3.50E-03	247	0.73	0.78	0.84
Julian 165	8:03	10:00	9:01		83	325	203	23.34	14.74	3.37E-03	892	1.01	1.08	1.18
	10:02	12:00	11:01		172	598	414	32.19	17.06	3.27E-03	1235	1.27	1.36	1.50
	12:02	14:00	13:01		178	508	409	33.94	19.16	3.26E-03	1140	1.48	1.65	1.81
	14:01	16:00	15:00		198	436	374	35.87	21.17	3.24E-03	1231	1.29	1.40	1.54
	16:01	18:00	17:00		179	377	333	29.39	21.63	3.31E-03	797	1.83	2.03	2.30
	18:01	20:01	19:01		110	210	157	22.00	19.35	3.39E-03	474	3.31	3.63	4.28
	20:03	6:00	13:01		9	23	16	10.45	10.24	3.53E-03	8	1.01	1.13	1.29
Est.Total (6:00-20:00)					1636	4785	3596							
Day 2 (June 14th)	6:00	8:00	7:00		22	47	26	10.03	9.01	3.53E-03	312	0.80	0.92	0.98
Julian 166	8:06	10:01	9:03		47	152	138	18.06	12.47	3.43E-03	949	1.57	1.67	1.88
	10:03	12:00	11:01		123	308	308	25.70	15.63	3.35E-03	1463	1.68	1.78	2.01
	12:01	14:00	13:00		200	362	422	31.86	18.72	3.28E-03	1684	1.74	1.85	2.06
	14:01	16:01	15:01		220	335	418	32.32	21.11	3.27E-03	1562	1.72	1.85	2.09
	16:02	18:00	17:01		106	159	257	27.76	22.88	3.32E-03	1098	1.63	1.79	1.99
	18:01	20:00	19:00		49	57	128	21.32	22.62	3.40E-03	475	1.52	1.66	1.88
	20:01	6:00	13:00		6	11	12	10.68	11.05	3.52E-03	8	0.79	0.89	1.00
					1534	2840	3392							
Day 3 (June 15th)	12:05	14:05	13:05		258	320	371	34.70	19.80	3.25E-03	1666	1.34	1.52	1.68
Julian 167														
Day 6 (June 18th)	12:02	14:00	13:01		126	215	176	32.25	16.67	3.27E-03	1745	1.32	1.50	1.60
Julian 170														

Application 1, 1996 Airborne Residue

	Air Sampling		Intermed.	Flux (ug/m ² /hr)			Surface	Ambient	1/T(K)	Solar Rad.	WS 1 (cm/s)	WS 2 (cm/s)	WS 3 (cm/s)	WS 4 (cm/s)
	Start	End	Time	Triadlme fon	Chlorpyrifos	Ethofumesate	Temp. (C)	Temp. (C)	Surface	J/m ² sec	0.41 m	0.70 m	1.40 m	2.8 m
Day 7 (June 19th)														
Julian 171	6:01	8:00	7:00	3	9	9	9.91	11.24	3.53E-03	321	1.12	1.15	1.40	1.47
	8:01	10:00	9:00	62	107	99	17.72	13.85	3.44E-03	967	1.70	1.72	2.01	2.15
	10:00	12:01	11:00	40	69	60	26.45	17.15	3.34E-03	1439	1.79	1.84	2.13	2.27
	12:04	14:00	13:02	76	101	111	31.30	20.67	3.28E-03	1732	1.77	1.94	2.18	2.32
	14:01	16:00	15:00	113	108	155	30.14	23.53	3.30E-03	1561	1.82	1.99	2.23	2.37
	16:01	18:00	17:00	79	70	68	28.92	25.25	3.31E-03	1136	1.70	1.88	2.09	2.21
	18:00	20:00	19:00	13	12	21	23.71	25.28	3.37E-03	517	1.34	1.49	1.62	1.63
Est.Total (6:00-20:00)				745	929	1005								
Day 14 (June 26th)	6:00	8:00	7:00	#VALUE!	3	#VALUE!	11.68	11.56	3.51E-03	278	0.62	0.67	0.73	0.69
Julian 178	8:01	10:00	9:00	13	30	28	21.61	16.48	3.39E-03	892	0.86	0.95	0.99	0.85
	10:00	12:00	11:00	12	36	23	35.41	19.30	3.24E-03	1380	1.28	1.38	1.53	1.54
	12:00	14:00	13:00	28	79	49	42.28	22.29	3.17E-03	1611	1.26	1.40	1.53	1.57
	14:01	16:00	15:00	8	19	12	39.79	24.02	3.20E-03	1442	1.36	1.56	1.67	1.73
	16:00	18:00	17:00	#VALUE!	24	#VALUE!	31.38	24.41	3.28E-03	1151	3.45	3.84	4.44	4.97
	18:00	20:00	19:00	#VALUE!	#VALUE!	17	25.62	21.68	3.35E-03	549	3.55	3.93	4.55	5.13
Est.Total (6:00-20:00)				#VALUE!	2242	#VALUE!								
Day 21 (July 3rd)	6:00	8:00	7:00	6	12	10	15.42	14.15	3.47E-03	248	1.10	1.27	1.42	0.73
Julian 185	8:01	10:00	9:00	39	31	30	23.92	18.49	3.37E-03	806	1.03	1.17	1.23	1.21
	10:00	12:00	11:00	10	23	18	29.89	21.34	3.30E-03	1212	1.49	1.68	1.83	1.90
	12:00	14:01	13:00	16	39	27	30.77	23.49	3.29E-03	1145	2.24	2.55	2.85	3.14
	14:01	15:59	15:00	#VALUE!	37	28	31.32	22.82	3.28E-03	1344	3.02	3.34	3.87	4.26
	16:00	18:00	17:00	#VALUE!	18	#VALUE!	25.80	22.00	3.35E-03	463	2.45	2.73	3.17	3.48
	18:01	20:00	19:00	#VALUE!	#VALUE!	#VALUE!	20.29	19.69	3.41E-03	121	2.46	2.77	3.22	3.50
Est.Total (6:00-20:00)				#VALUE!	4805	#VALUE!								

Solar Radiation		Day 0	Day 1	Day 2	Day 3	Day 6	Day 7	Day 14	Day 21
Julian Date, 1996		0	1	2	3	6	7	14	21
Time	Time(hr)	164	165	166	167	170	171	178	185
600	5:45	20.28	18.51	20.37	12.44	6.733	14.46	18.83	12.87
630	6:15	75.7	103.2	78.1	84.1	17.12	66.55	69.86	38.33
700	6:45	219.4	202.5	228.7	247	73.9	235.9	209.7	102.7
730	7:15	390.8	190.1	393.3	353.4	130.1	411.1	335.2	375.8
800	7:45	536.2	491.2	548.5	542.3	273.6	569.3	495.3	475.3
830	8:15	706	608.6	710	710	494.9	731	601.5	398.1
900	8:45	868	834	878	865	806	892	827	824
930	9:15	1022	909	1032	1015	1033	1056	985	970
1000	9:45	1167	1215	1174	1155	1230	1190	1154	1031
1030	10:15	1303	1425	1307	1284	480.1	1330	1334	870
1100	10:45	1418	1387	1425	1403	273.7	1422	1401	1161
1130	11:15	1512	628.1	1523	1500	955	1397	1453	1558
1200	11:45	1595	1501	1598	1579	1616	1605	1330	1258
1230	12:15	1649	1433	1653	1635	1727	1691	1521	1558
1300	12:45	1689	1130	1688	1666	1705	1725	1611	1474
1330	13:15	1709	790	1700	1683	1785	1730	1664	910
1400	13:45	1685	1205	1693	1678	1763	1780	1647	638.9
1430	14:15	1655	1506	1663	1552	1270	1544	1674	1332
1500	14:45	1537	1090	1616	1327	1657	1670	1492	1410
1530	15:15	1506	818	1537	1556	1343	1568	1445	1416
1600	15:45	1262	1511	1432	1041	1083	1463	1155	1218
1630	16:15	1301	828	1311	1280	890	1342	1410	773
1700	16:45	1158	695	1176	1210	1012	1214	1203	405.1
1730	17:15	1013	695.3	1030	1021	1076	1069	1063	345.2
1800	17:45	860	968	875	886	906	917	926	329.7
1830	18:15	701	709	713	718	747	757	776	211.1
1900	18:45	544.9	543.2	552.1	529.4	577.5	593.3	624.9	172.6
1930	19:15	390	392.6	390.2	422.3	422.2	434.2	481	72.8
2000	19:45	240.8	250.9	245.4	200.3	276.6	283.7	312.6	27.41
MJ/m ²		25781.25	52250220				53952300	51455340	37510578
Time (hr) 8:00-20:00		8:00-20:00					8:00-20:00	8:00-20:00	8:00-20:00

Temperature C°--Surface and Ambient

Julian Date, 1996		164				165				166				167			
Time	Time(hr)	Ambient	Ground1	Ground2	Groundavg	Ambient	Ground1	Ground2	Groundavg	Ambient	Ground1	Ground2	Groundavg	Ambient	Ground1	Ground2	Groundavg
600	6:00	7.55	8.07	6.962	7.516	7.81	9.26	8.17	8.715	7.03	7.99	6.795	7.3925	6.762	7.4	7.07	7.235
630	6:30	7.78	8.85	7.71	8.28	8.09	9.99	9.32	9.655	7.23	8.41	7.23	7.82	7.04	7.96	7.7	7.83
700	7:00	10.17	10.15	9.66	9.905	9.69	12.2	12.21	12.205	8.5	9.22	8.73	8.975	9.01	9.57	9.95	9.76
730	7:30	13.07	11.57	11.49	11.53	10.34	13.08	13.02	13.05	9.63	9.71	10	9.855	10.3	10.7	11.15	10.925
800	8:00	13.85	16.34	16.51	16.425	11.62	16.11	16.6	16.355	10.67	13.22	13.72	13.47	12.56	15.55	15.93	15.74
830	8:30	14.41	19.62	18.78	19.2	13.41	19.09	19	19.045	11.41	15.61	15.11	15.36	13.78	19.3	19.49	19.395
900	9:00	15.3	22.92	20.59	21.755	14.65	22.92	21.95	22.435	12.17	18.04	16.74	17.39	15.13	22.44	20.56	21.5
930	9:30	15.7	24.32	21.58	22.95	15.16	25.39	23.32	24.355	12.88	19.63	17.92	18.775	15.49	24.86	22.39	23.625
1000	10:00	16.19	26.68	23.26	24.97	15.74	28.77	26.24	27.505	13.42	21.7	19.76	20.73	15.73	26.1	23.96	25.03
1030	10:30	16.92	27.9	26.12	27.01	16.52	32.66	32.06	32.36	14.41	23.47	22.73	23.1	15.97	27.43	26.9	27.165
1100	11:00	17.51	30.26	28.39	29.325	17.26	33.72	35.43	34.575	15.27	25.42	25.38	25.4	16.88	29.51	29.92	29.715
1130	11:30	18.28	32.31	30.69	31.5	16.72	26.53	27.71	27.12	15.97	25.87	26.57	26.22	17.64	30.51	32.1	31.305
1200	12:00	18.84	33.32	32.18	32.75	17.75	33.85	35.59	34.72	16.85	27.51	28.68	28.095	18.43	32.03	33.49	32.76
1230	12:30	19.62	34.05	33.99	34.02	18.43	36.08	38.31	37.195	17.7	30.63	30.84	30.735	18.91	32.53	34.52	33.525
1300	13:00	20.42	35.32	35.93	35.625	19.21	33.33	35.84	34.585	18.47	31.75	32	31.875	19.49	33.37	35.5	34.435
1330	13:30	21.35	36.48	38.14	37.31	19.32	29.27	31.69	30.48	19.09	31.5	32.22	31.86	20.2	34.53	36.02	35.275
1400	14:00	21.9	35.61	39.63	37.62	19.69	32.49	34.53	33.51	19.6	32.85	33.05	32.95	20.59	34.74	36.42	35.58
1430	14:30	22.73	36.37	41.49	38.93	20.57	36.22	39.47	37.845	20.06	31.48	32.71	32.095	21.25	35.22	36.61	35.915
1500	15:00	23.14	35.1	41.05	38.075	21	32.6	37.92	35.26	20.98	32.93	33.1	33.015	21.49	33.69	35.22	34.455
1530	15:30	23.56	35.34	41.64	38.49	20.96	30.17	33.87	32.02	21.36	31.92	31.82	31.87	21.94	36.1	36.15	36.125
1600	16:00	23.89	33.52	38.8	36.16	22.13	36.23	40.46	38.345	22.04	32.83	31.76	32.295	22.57	34.24	33.92	34.08
1630	16:30	24.28	33.48	32.75	33.115	21.71	29.82	30.8	30.31	22.36	31.69	26.64	29.165	22.71	34.3	30.88	32.59
1700	17:00	24.53	33.87	33.67	33.77	22.19	30.11	30.81	30.46	22.88	30.29	27.54	28.915	22.42	31.89	30.67	31.28
1730	17:30	23.47	31.97	32.67	32.32	21.39	27.41	28.23	27.82	23.2	28.38	27.21	27.795	22.31	28.92	29.51	29.215
1800	18:00	23	29.98	30.27	30.125	21.24	27.62	30.28	28.95	23.08	25.65	24.7	25.175	21.76	25.58	27.07	26.325
1830	18:30	22.2	27.61	27.09	27.35	20.81	25.71	26.68	26.195	23.12	23.63	22.98	23.305	20.67	22.29	23.96	23.125
1900	19:00	21.7	25.61	23.82	24.715	19.8	23.11	22.57	22.84	23.1	22.31	21.56	21.935	19.65	20.66	21.01	20.835
1930	19:30	20.94	23.11	21.43	22.27	18.71	21.05	20.01	20.53	23.07	21.55	20.51	21.03	19.03	19.77	19.62	19.695
2000	20:00	20.07	20.62	19.59	20.105	18.08	18.54	18.34	18.44	21.2	19.16	18.89	19.025	18.22	17.83	17.98	17.905

Temperature C°--Surface and Ambient

Julian Date, 1996	170				171				178				185			
Time(hr)	Ambient	Ground1	Ground2	Groundavg	Ambient	Ground1	Ground2	Groundavg	Ambient	Ground1	Ground2	Groundavg	Ambient	Ground1	Ground2	Groundavg
6:00	7.59	9.47	9.32	9.395	9.95	7.17	8.21	7.69	8.75	8.72	9.78	9.25	13.33	13.95	14.07	14.01
6:30	7.87	9.81	9.69	9.75	10.08	7.32	8.37	7.845	9.13	9.24	10.12	9.68	13.28	13.82	13.87	13.845
7:00	8.17	10.14	10.05	10.095	11.08	7.85	8.94	8.395	10.91	10.6	10.86	10.73	13.43	14.03	14.09	14.06
7:30	8.7	11.13	11.13	11.13	11.56	8.85	9.66	9.255	12.64	11.71	11.72	11.715	14.42	15.71	15.17	15.44
8:00	9.29	12.46	12.69	12.575	12.25	15.07	13.25	14.16	13.56	14.99	14.16	14.575	15.48	18.68	17.95	18.315
8:30	10.17	14.61	14.96	14.785	12.69	16.73	14.18	15.455	14.47	16.97	16.74	16.855	16.4	19.58	19.02	19.3
9:00	11.96	18.95	18.89	18.92	13.27	18.55	15.2	16.875	15.89	19.9	20.1	20	18.67	23.86	22.7	23.28
9:30	13.22	22.33	21.23	21.78	14.51	20.97	16.91	18.94	17.07	23.09	22.85	22.97	19.2	26.39	25.18	25.785
10:00	14.28	25.4	23.82	24.61	14.92	21.5	17.71	19.605	18.48	27.39	25.85	26.62	19.69	27.67	26.94	27.305
10:30	13.94	20.27	20.31	20.29	15.89	23.96	21.68	22.82	18.75	32.67	32.74	32.705	20.23	27.75	27.05	27.4
11:00	11.74	15.81	15.73	15.77	16.8	26.94	27.91	27.425	18.79	33.78	34.75	34.265	20.62	28.71	28.13	28.42
11:30	12.52	20.01	20.06	20.035	17.49	26.45	28.12	27.285	19.58	37.03	37.75	37.39	21.97	32.54	32.07	32.305
12:00	14.56	27.72	28.51	28.115	18.4	25.97	30.53	28.25	20.07	36.81	37.74	37.275	22.55	31.68	31.19	31.435
12:30	15.88	30.34	31.15	30.745	19.34	27.8	33.03	30.415	21.18	39.94	40.69	40.315	23.63	35.17	34.67	34.92
13:00	16.7	31.83	32.33	32.08	20.3	28.03	33.63	30.83	22.11	40.57	42.26	41.415	23.98	32.89	32.55	32.72
13:30	16.8	32.72	32.98	32.85	20.96	28.4	33.9	31.15	22.65	42.39	44.31	43.35	24.37	30.47	30.68	30.575
14:00	17.31	33.12	33.55	33.335	22.08	30.47	35.17	32.82	23.23	43.05	45.03	44.04	21.96	24.94	24.79	24.865
14:30	17.5	25.99	25.37	25.68	22.52	30.54	30.46	30.5	24.02	44.1	45.43	44.765	21.78	28.67	28.45	28.56
15:00	18.09	25.72	24.34	25.03	23.23	31.94	29.24	30.59	24.45	44.05	44.82	44.435	22.91	32.83	32.4	32.615
15:30	18.3	24.66	23.18	23.92	23.9	31.63	27.91	29.77	23.69	36.66	36.69	36.675	23.18	32	32.21	32.105
16:00	18.42	22.03	21.22	21.625	24.48	31.27	28.15	29.71	23.9	33.38	33.22	33.3	23.4	31.72	32.26	31.99
16:30	18.06	21.73	19.07	20.4	24.8	31.02	28.81	29.915	25.22	33.05	33.65	33.35	23.16	29.36	30.06	29.71
17:00	18.63	22.69	20.67	21.68	25.3	30.56	28.66	29.61	24.78	31.31	31.69	31.5	22.26	24.98	25.67	25.325
17:30	19.04	23.45	23.05	23.25	25.41	28.68	29.72	29.2	24.19	30.55	30.9	30.725	21.69	24.01	24.68	24.345
18:00	19.31	22.18	22.41	22.295	25.5	26.11	27.78	26.945	23.45	29.82	30.03	29.925	20.89	23.57	24.07	23.82
18:30	19.32	20.27	21.52	20.895	25.55	25.41	25.68	25.545	22.89	28.44	28.67	28.555	20.58	21.78	22.26	22.02
19:00	19.37	22.51	20.03	21.27	25.46	24.87	23.86	24.365	22.09	26.54	26.9	26.72	20.12	20.41	20.93	20.67
19:30	18.83	20.49	19.22	19.855	25.17	23.88	22.54	23.21	21.49	24.76	25.27	25.015	19.38	19.26	19.67	19.465
20:00	18.57	18.89	17.92	18.405	24.94	22.89	20.54	21.715	20.23	21.84	22.51	22.175	18.68	18.82	19.15	18.985

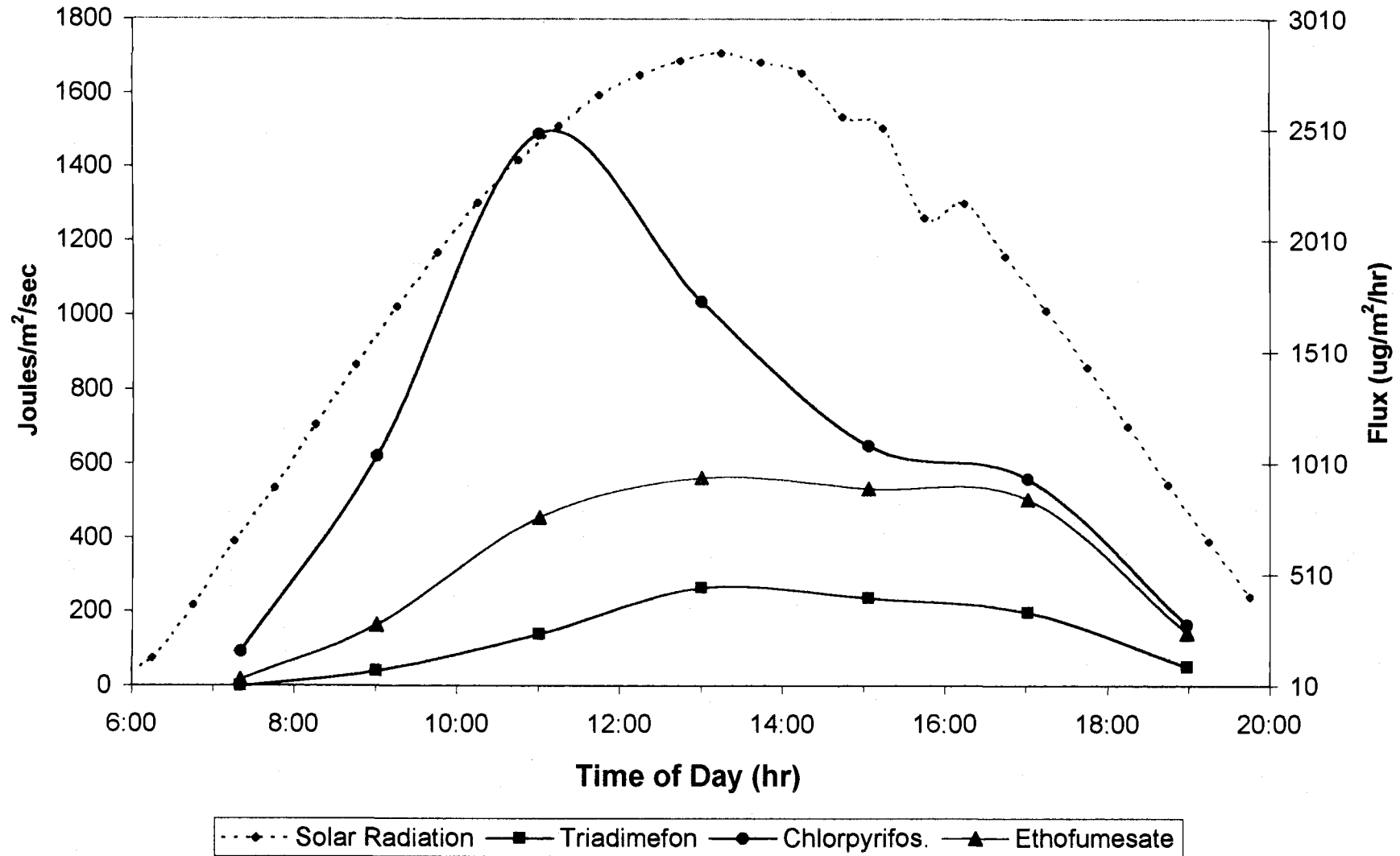
Wind Speed Profile June 12th, 1996 Application 1, Day 0, Julian Date 164

Time	Height (cm) log Ht-->	41	70	140	280	u* (m/s) Value	u* (m/s) Std. Err	Zo (m) Value	Zo (m) Std. Err	L (m) Value	L (m) Std. Err	R squared
600	6:00	0.447	0.495	0.507	0.447	0.06	0.01	0.013	-0.0050	-5.80	-0.71	1.00
630	6:30	0.458	0.498	0.495	0.447	0.04	0.01	0.003	-0.0048	-5.43	-1.78	0.98
700	7:00	0.473	0.548	0.518	0.453	0.06	0.03	0.011	-0.0285	-5.22	-3.82	0.91
730	7:30	0.617	0.691	0.773	0.547	0.16	0.04	0.063	-0.0449	-5.47	-1.79	0.98
800	8:00	0.944	1.087	1.187	1.049	0.18	0.01	0.039	-0.0054	-6.67	-0.41	1.00
830	8:30	1.211	1.418	1.514	1.552	0.16	0.04	0.017	-0.0188	-9.90	-5.07	0.99
900	9:00	1.097	1.247	1.355	1.323	0.15	0.01	0.019	-0.0032	-8.37	-0.60	1.00
930	9:30	1.568	1.606	1.859	1.896	0.11	0.09	0.002	-0.0088	-17.67	-43.46	0.96
1000	10:00	1.5	1.582	1.795	1.836	0.13	0.06	0.003	-0.0084	-14.40	-16.48	0.98
1030	10:30	1.72	1.744	2.063	2.119	0.13	0.12	0.002	-0.0112	-23.63	-93.58	0.95
1100	11:00	1.585	1.675	1.91	1.978	0.13	0.06	0.003	-0.0082	-17.38	-23.66	0.99
1130	11:30	1.483	1.631	1.825	1.902	0.15	0.02	0.007	-0.0040	-14.26	-4.11	1.00
1200	12:00	1.687	1.773	2.031	2.125	0.13	0.07	0.002	-0.0070	-23.69	-49.58	0.99
1230	12:30	1.572	1.661	1.887	1.981	0.12	0.05	0.002	-0.0054	-24.32	-44.00	0.99
1300	13:00	1.696	1.789	2.021	2.104	0.13	0.05	0.002	-0.0051	-19.97	-29.41	0.99
1330	13:30	1.645	1.753	1.988	2.016	0.16	0.06	0.006	-0.0107	-12.32	-10.22	0.99
1400	14:00	1.639	1.7	1.998	2.055	0.14	0.10	0.004	-0.0154	-18.15	-40.38	0.97
1430	14:30	1.436	1.527	1.711	1.743	0.12	0.04	0.004	-0.0067	-12.90	-10.07	0.99
1500	15:00	1.615	1.644	1.957	1.989	0.13	0.12	0.003	-0.0176	-17.32	-47.60	0.95
1530	15:30	1.478	1.57	1.787	1.84	0.13	0.05	0.004	-0.0091	-15.14	-16.31	0.99
1600	16:00	1.448	1.516	1.739	1.741	0.13	0.07	0.005	-0.0142	-11.76	-13.63	0.97
1630	16:30	1.547	1.581	1.852	1.886	0.12	0.10	0.002	-0.0122	-17.43	-44.75	0.95
1700	17:00	2.577	2.821	3.287	3.625	0.24	0.06	0.005	-0.0074	-120.57	-643.21	1.00
1730	17:30	3.655	4.065	4.766	5.352	0.36	0.07	0.007	-0.0066	670.77	14005.50	1.00
1800	18:00	3.446	3.793	4.426	4.976	0.30	0.07	0.004	-0.0053	68.89	175.62	1.00
1830	18:30	3.67	4.054	4.724	5.313	0.33	0.06	0.005	-0.0050	85.34	234.18	1.00
1900	19:00	3.006	3.33	3.877	4.358	0.27	0.05	0.005	-0.0048	121.68	426.48	1.00
1930	19:30	2.976	3.265	3.784	4.262	0.24	0.05	0.003	-0.0037	42.29	61.41	1.00
2000	20:00	2.548	2.787	3.214	3.653	0.18	0.03	0.002	-0.0020	20.86	13.82	1.00

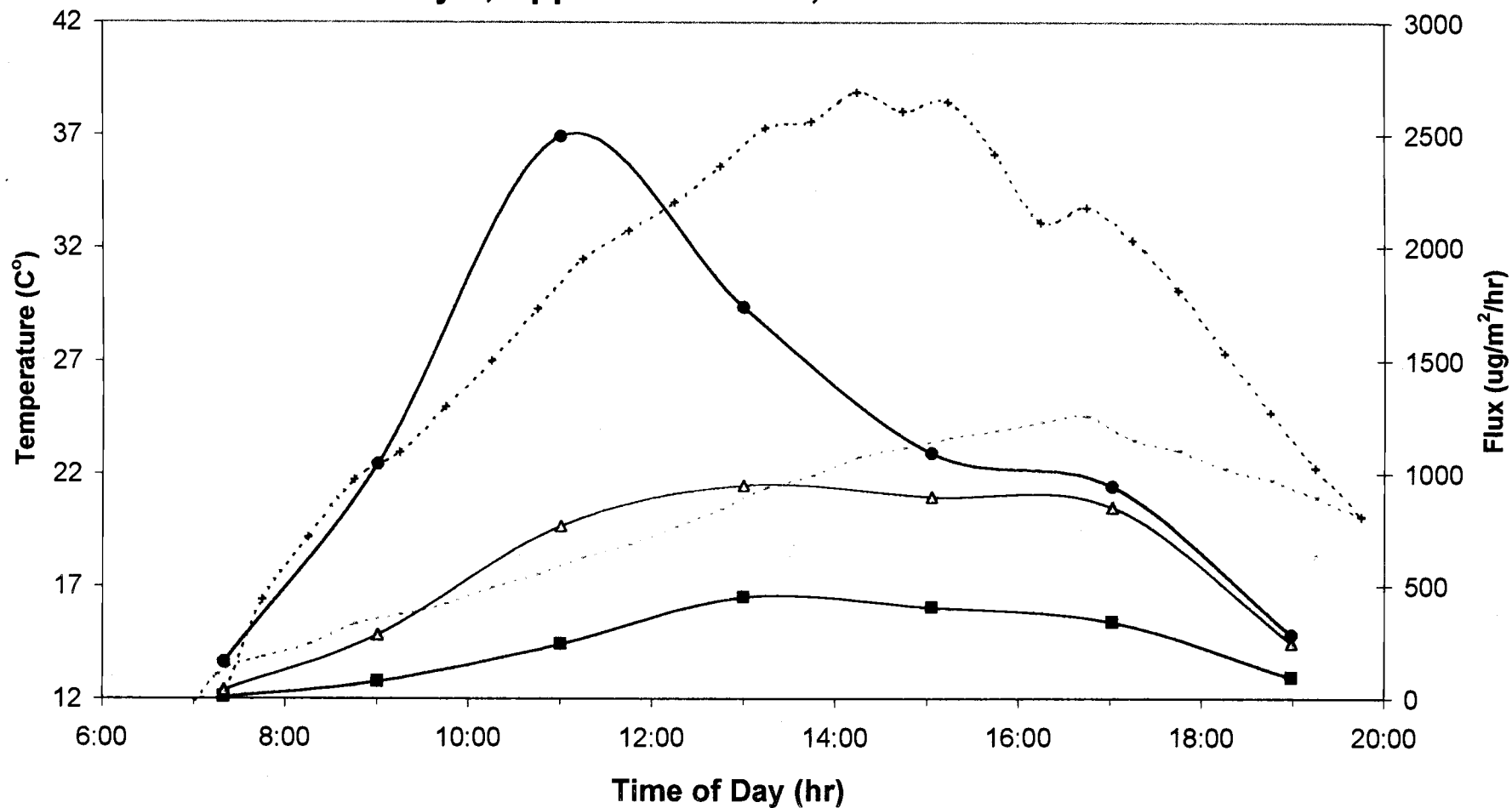
Wind Speed Profile June 13th, 1996 Application 1, Day 1, Julian Date 165

Height (cm)	41	70	140	280	u* (m/s)	u* (m/s)	Zo (m)	Zo (m)	L (m)	L (m)	R squared
Time (hrs)	-0.89	-0.36	0.34	1.03	Value	Std. Err	Value	Std. Err	Value	Std. Err	
6:00	0.447	0.613	0.599	0.517	0.13	0.059	0.074	-0.0920	-6	4.0	0.91
6:30	0.75	0.747	0.909	0.817	0.09	0.085	0.015	-0.0580	-8	11.0	0.81
7:00	0.515	0.556	0.557	0.529	0.04	0.012	0.001	-0.0024	-6	2.7	0.96
7:30	0.62	0.675	0.701	0.611	0.08	0.003	0.012	-0.0018	-6	0.3	1.00
8:00	1.022	1.138	1.182	1.173	0.10	0.02	0.005	-0.0066	-8.33	3.55	0.98
8:30	0.795	0.886	0.874	0.725	0.11	0.02	0.014	-0.0113	-5.06	1.24	0.99
9:00	0.933	1.02	1.137	1.13	0.28	0.03	0.062	-0.0229	-4.32	0.66	1.00
9:30	1.028	1.095	1.201	1.182	0.26	0.03	0.048	-0.0177	-4.23	0.60	1.00
10:00	1.268	1.304	1.499	1.542	0.27	0.01	0.042	-0.0029	-5.31	0.15	1.00
10:30	1.265	1.344	1.485	1.491	0.11	0.03	0.003	-0.0052	-10.92	6.38	0.99
11:00	1.214	1.28	1.405	1.456	0.08	0.02	0.001	-0.0015	-18.34	16.87	0.99
11:30	1.272	1.408	1.542	1.605	0.12	0.00	0.006	-0.0007	-13.32	0.73	1.00
12:00	1.329	1.41	1.583	1.609	0.11	0.04	0.004	-0.0073	-12.73	10.58	0.99
12:30	1.529	1.683	1.841	1.941	0.13	0.00	0.004	-0.0007	-16.51	1.60	1.00
13:00	1.222	1.384	1.483	1.481	0.15	0.02	0.012	-0.0071	-9.02	2.10	1.00
13:30	1.457	1.609	1.771	1.835	0.14	0.00	0.006	-0.0007	-12.88	0.66	1.00
14:00	1.719	1.941	2.156	2.261	0.20	0.01	0.011	-0.0017	-13.44	1.08	1.00
14:30	1.409	1.552	1.675	1.755	0.12	0.01	0.003	-0.0019	-14.72	4.20	1.00
15:00	1.408	1.443	1.652	1.731	0.08	0.07	0.000	-0.0027	-65.28	590.72	0.97
15:30	1.118	1.202	1.338	1.359	0.10	0.02	0.005	-0.0060	-11.84	6.07	0.99
16:00	1.243	1.408	1.514	1.555	0.14	0.02	0.009	-0.0074	-10.69	3.66	1.00
16:30	1.182	1.337	1.456	1.47	0.15	0.01	0.013	-0.0040	-9.80	1.27	1.00
17:00	0.977	1.081	1.127	1.145	0.08	0.02	0.003	-0.0045	-9.79	5.19	0.99
17:30	1.94	2.182	2.495	2.708	0.21	0.01	0.010	-0.0031	-23.40	5.99	1.00
18:00	3.236	3.533	4.118	4.586	0.27	0.08	0.004	-0.0060	117.89	641.41	1.00
18:30	3.226	3.524	4.169	4.73	0.27	0.09	0.004	-0.0070	29.21	48.19	1.00
19:00	3.677	4.037	4.765	5.388	0.32	0.09	0.005	-0.0072	43.32	90.95	1.00
19:30	3.427	3.754	4.447	5.032	0.30	0.10	0.005	-0.0080	38.99	81.90	1.00
20:00	2.929	3.207	3.723	4.195	0.23	0.05	0.003	-0.0039	38.06	55.21	1.00

Solar Radiation and Flux **Day 0, App.1 '96 June 12, Julian 164**

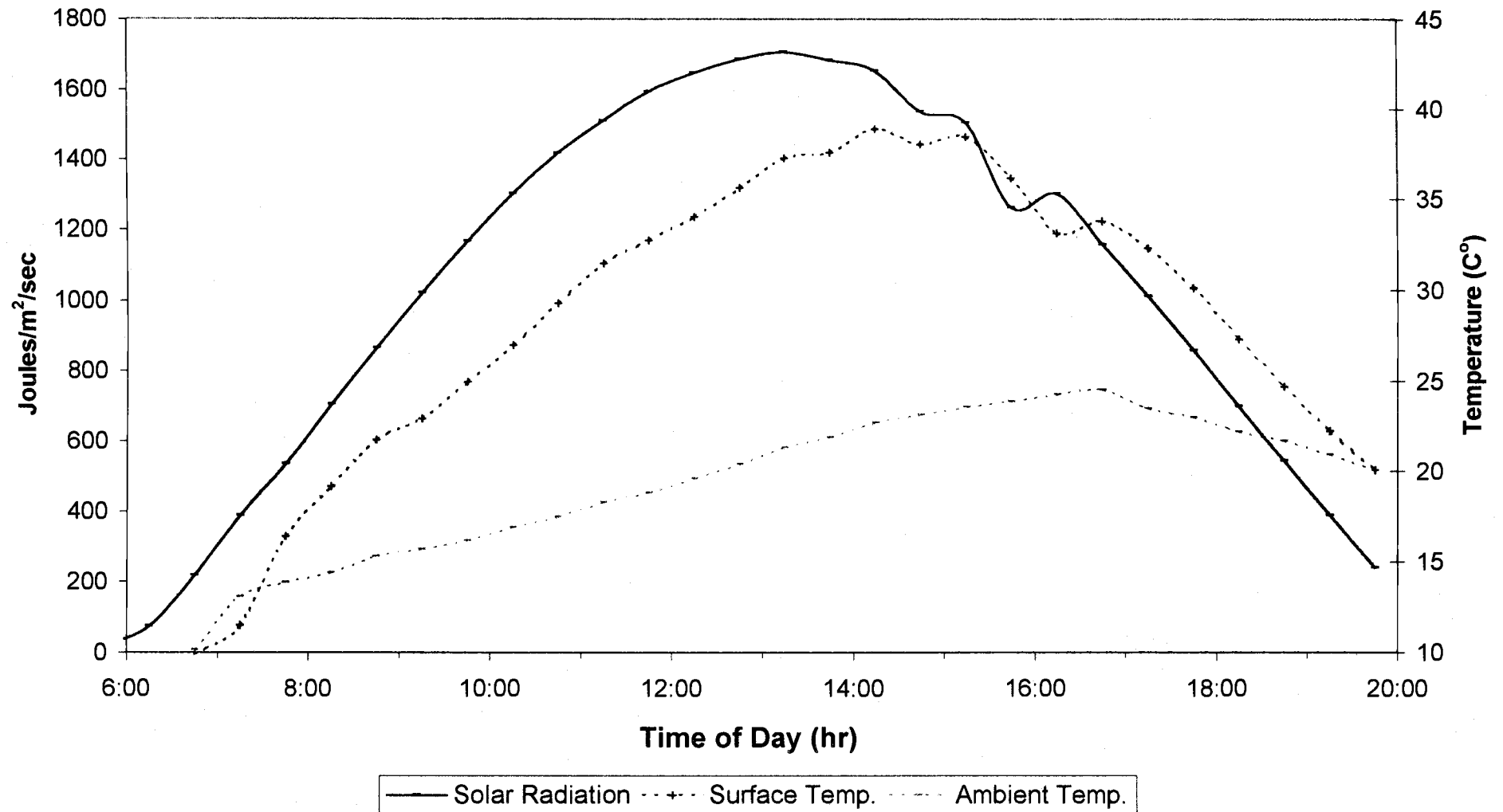


Flux and Temperature (C°) Day 0, App.1 '96 June 12, Julian 164

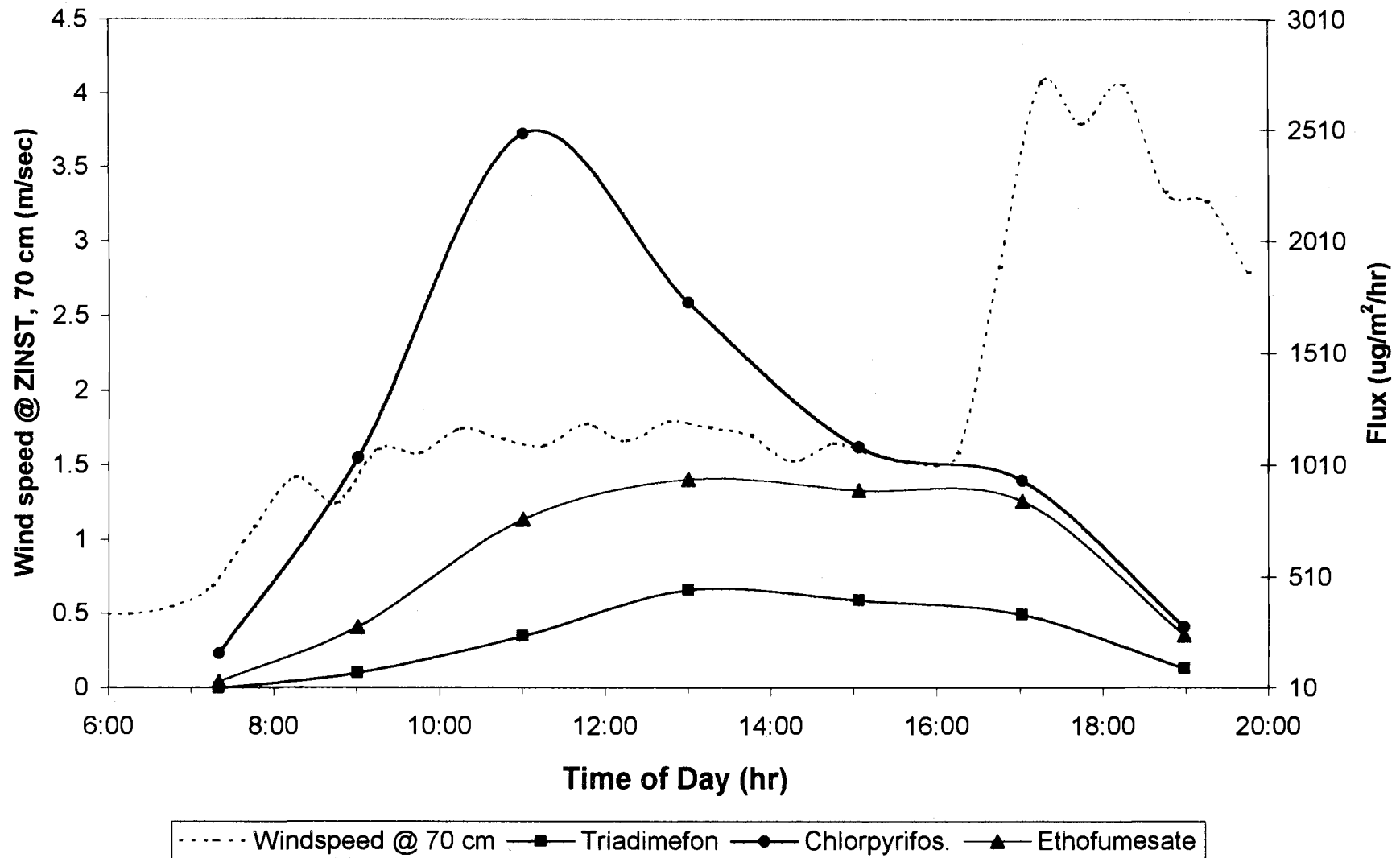


..... Ambient Temp.+.... Ground Temp. —■— Triadimefon —●— Chlorpyrifos —△— Ethofumesate

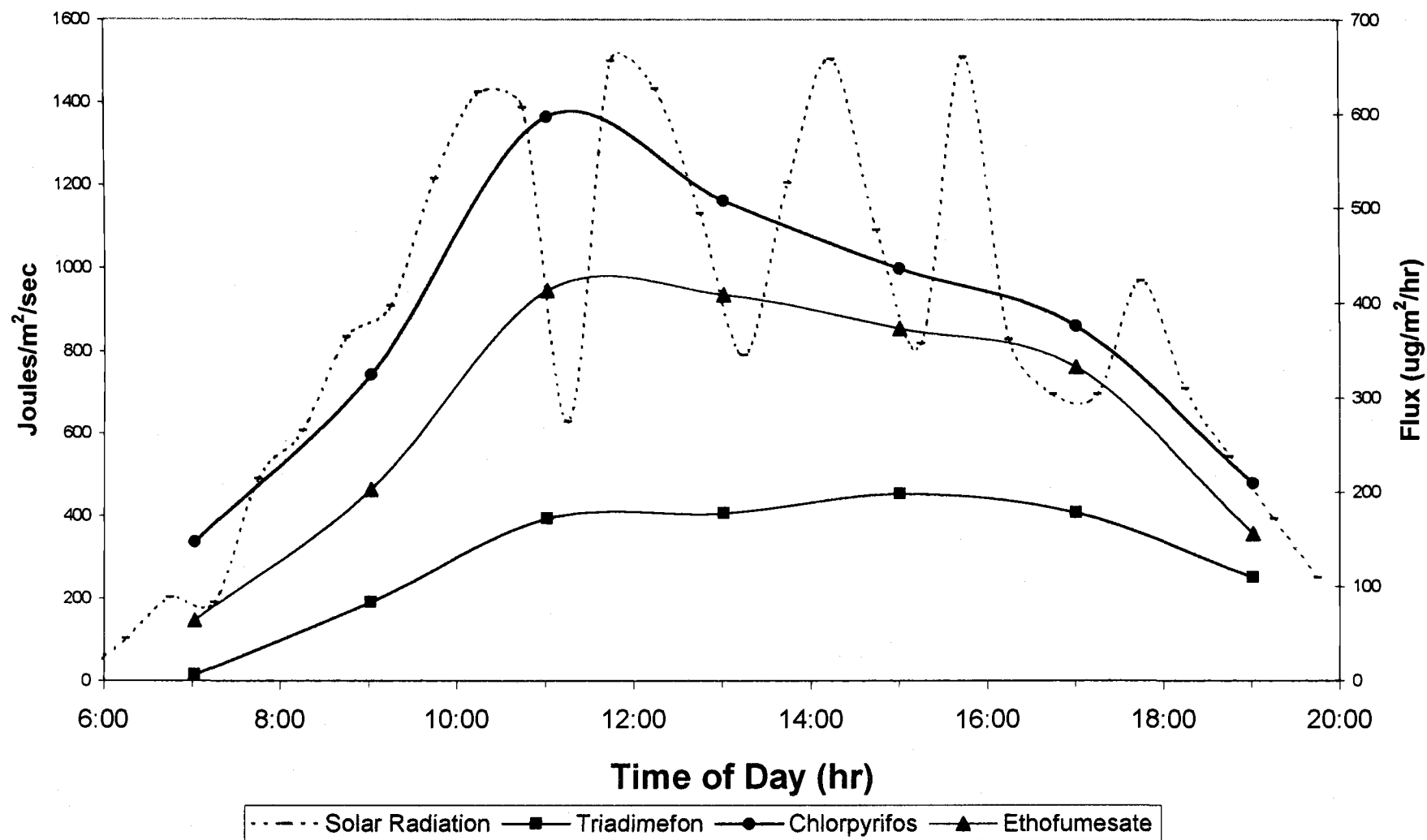
Solar Radiation and Temperature
Day 0, App.1 '96 June 12, Julian 164



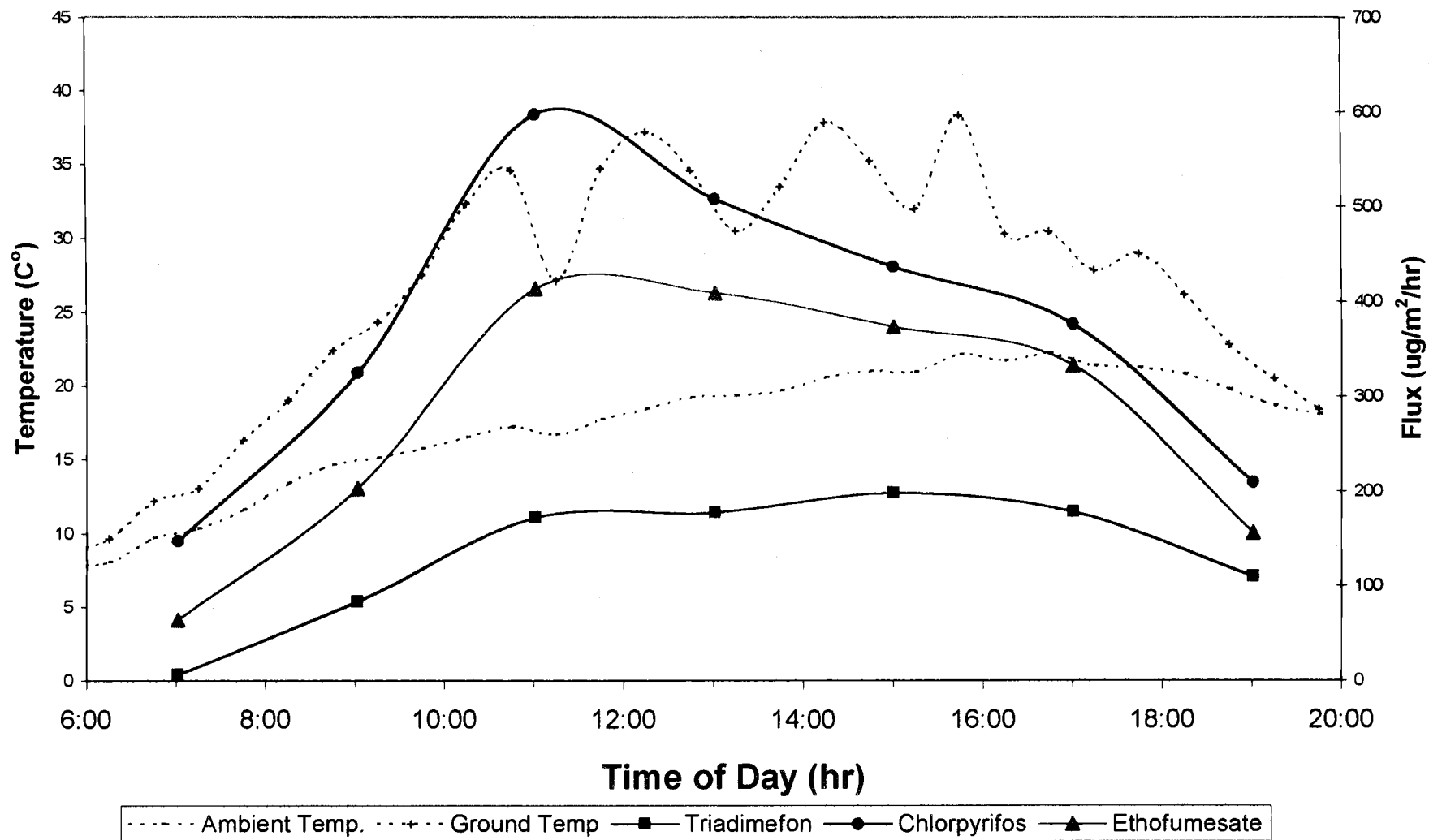
Windspeed and Flux **Day 0, App.1 '96 June 12, Julian 164**



Solar Radiation vs. Flux
Day 1, App.1 '96 June 13, Julian 165

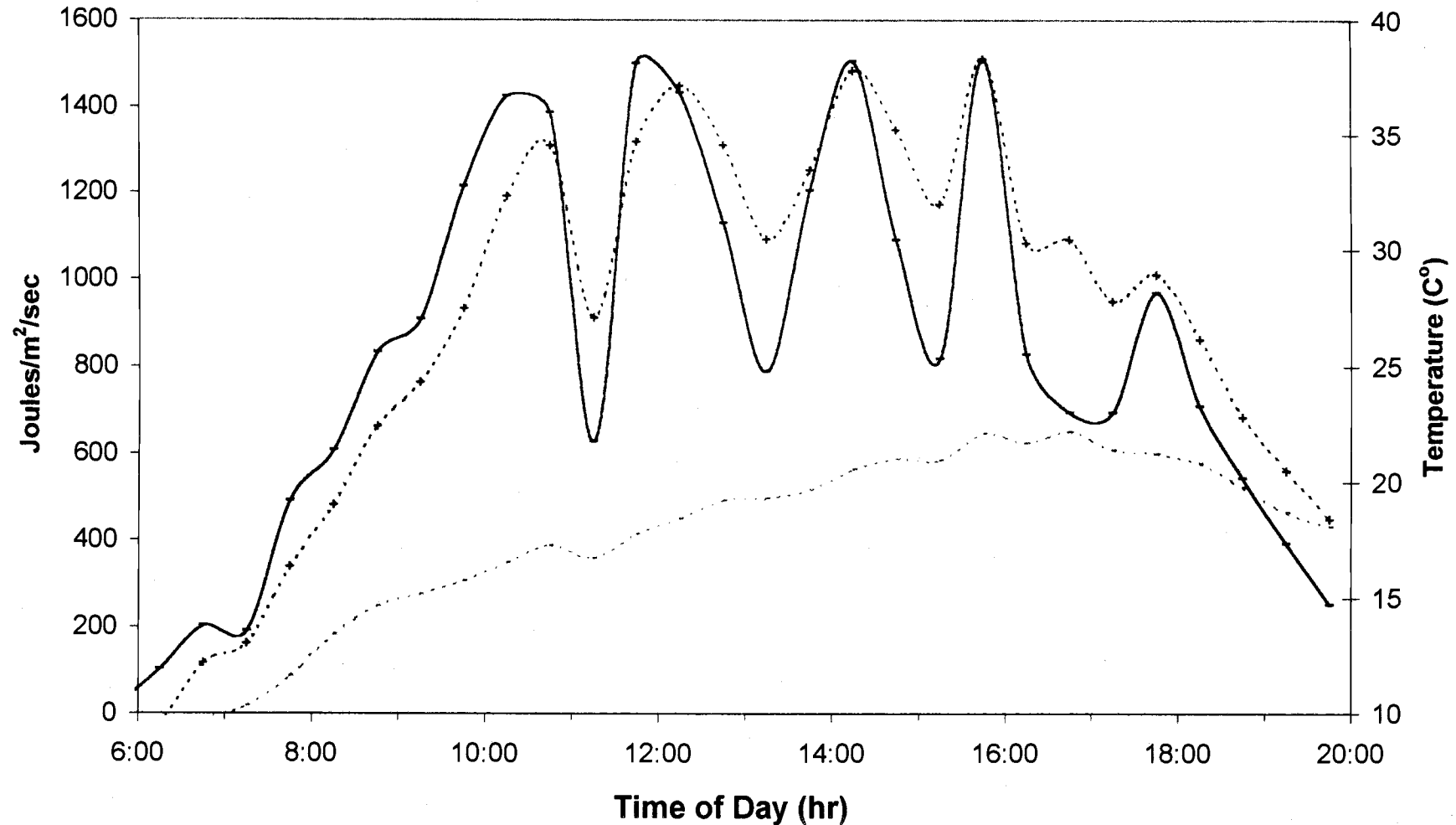


Flux and Temperature (C°) **Day 1, App.1 '96 June 13, Julian 165**



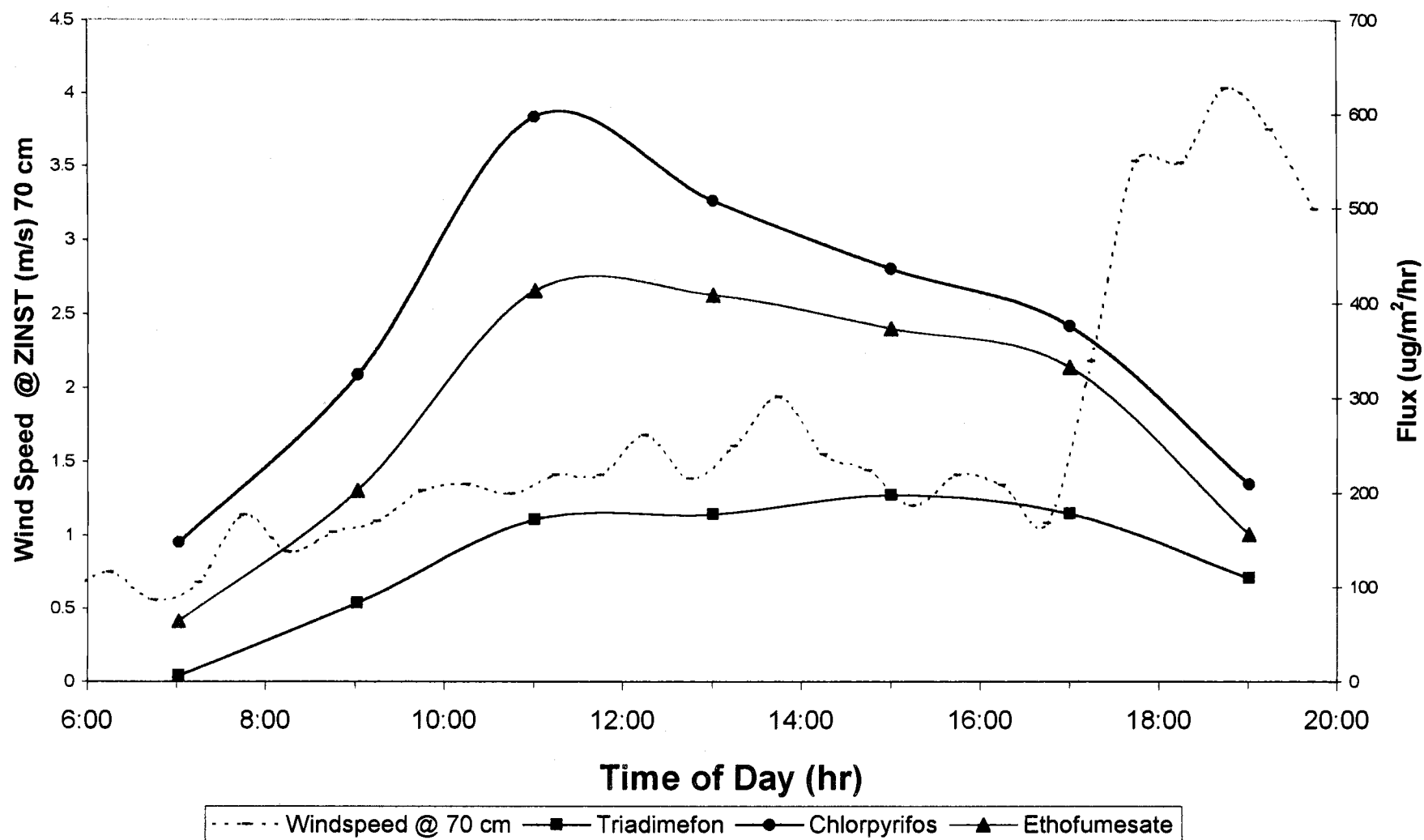
Solar Radiation and Temperature

Day 1, App.1 '96 June 13, Julian 165

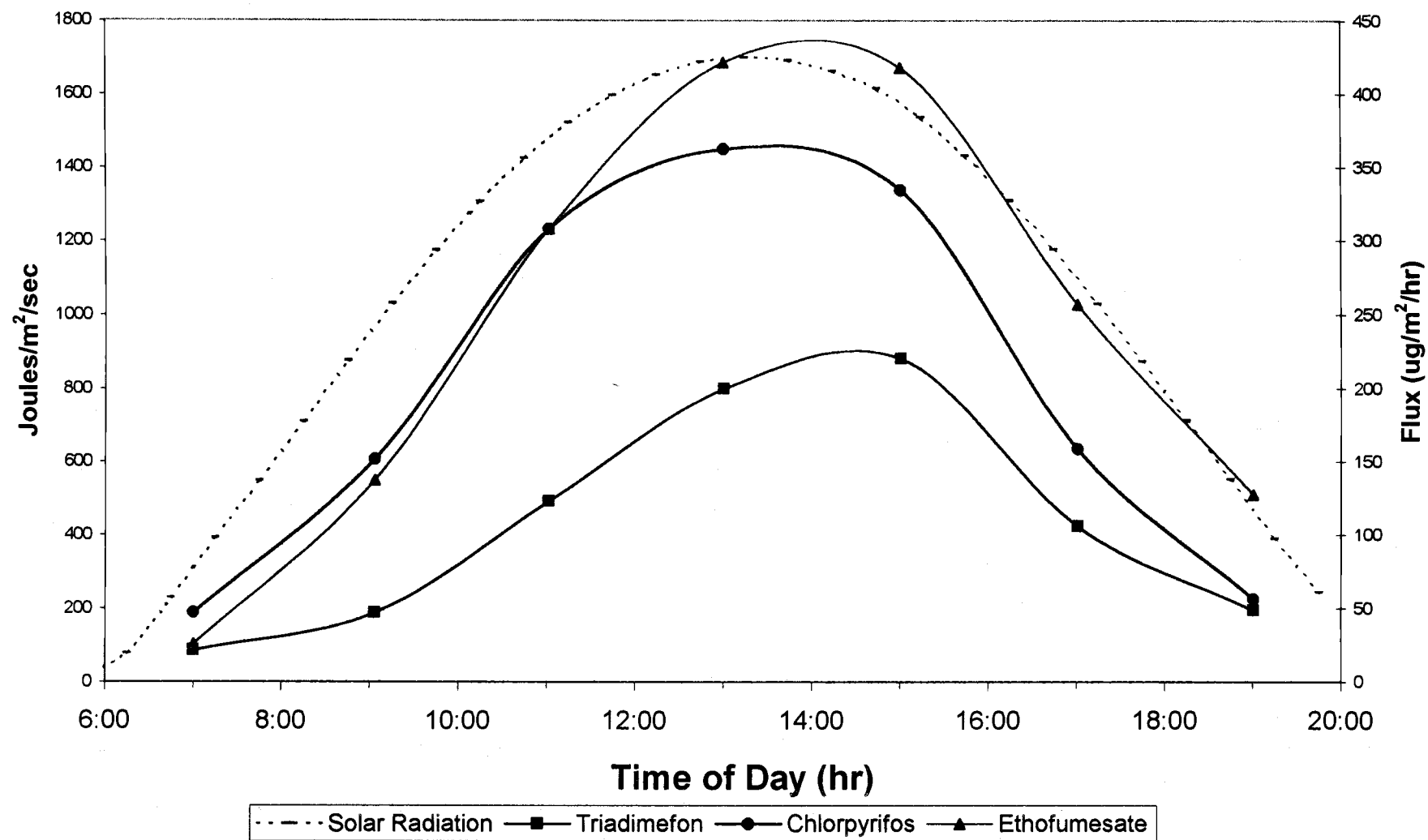


— Solar Radiation ···+··· Surface Temp. ····· Ambient Temp.

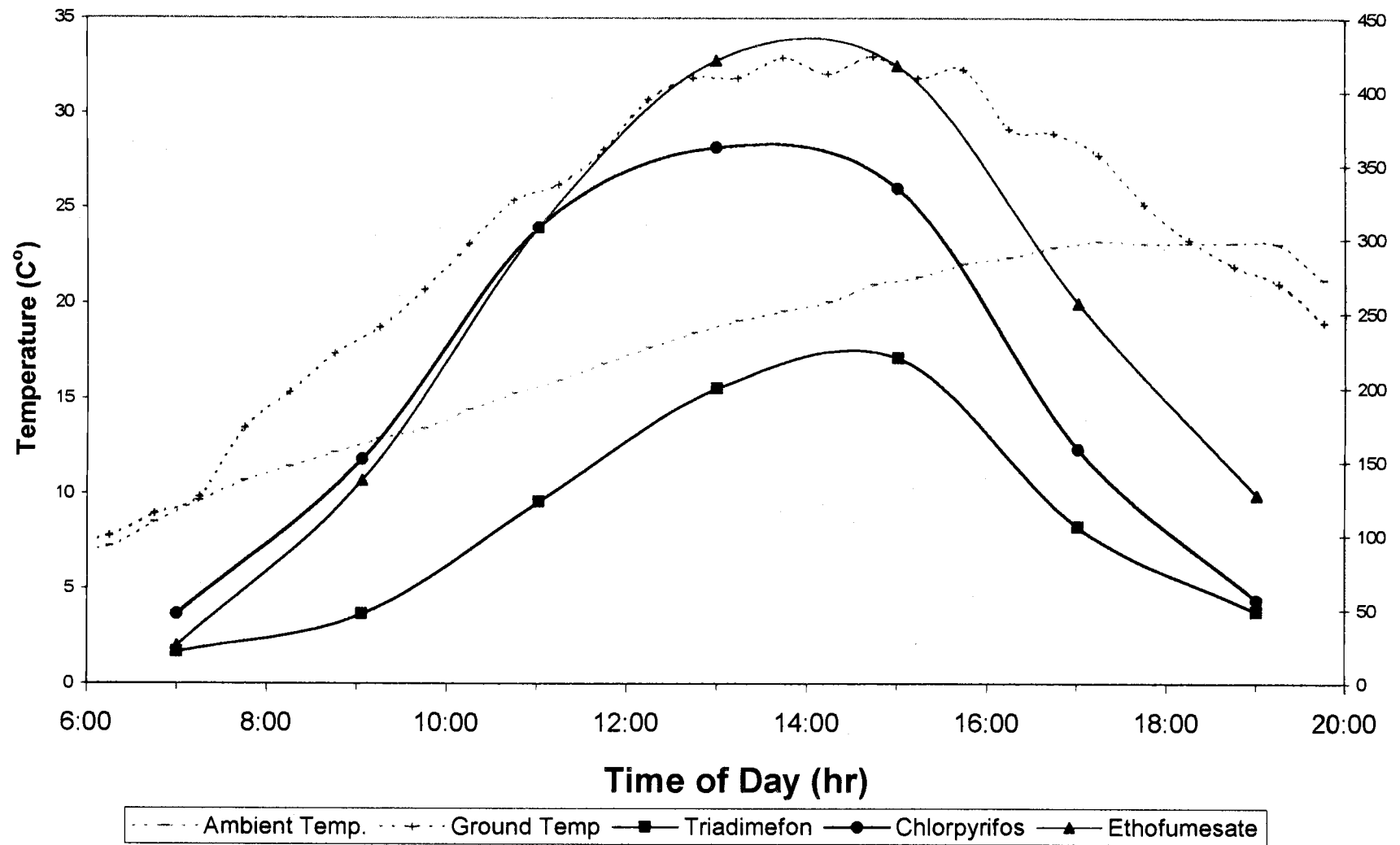
**Windspeed @ Height ZINST (70 cm) and Flux
Day 1, App.1 '96 June 13, Julian 165**



Solar Radiation vs. Flux
Day 2, App.1 '96 June 14, Julian 166

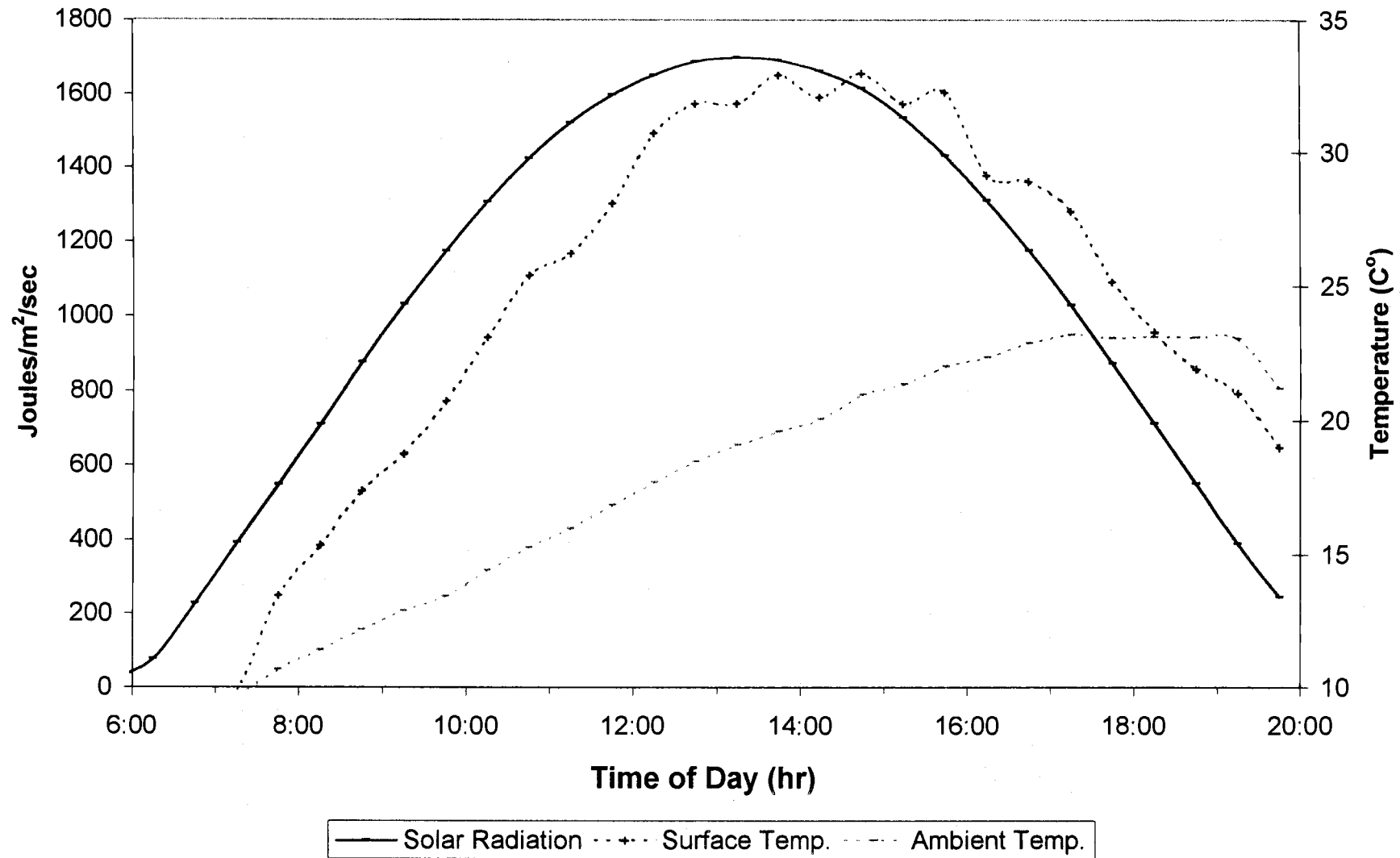


Flux and Temperature (C°)
Day 2, App.1 '96 June 14, Julian 166

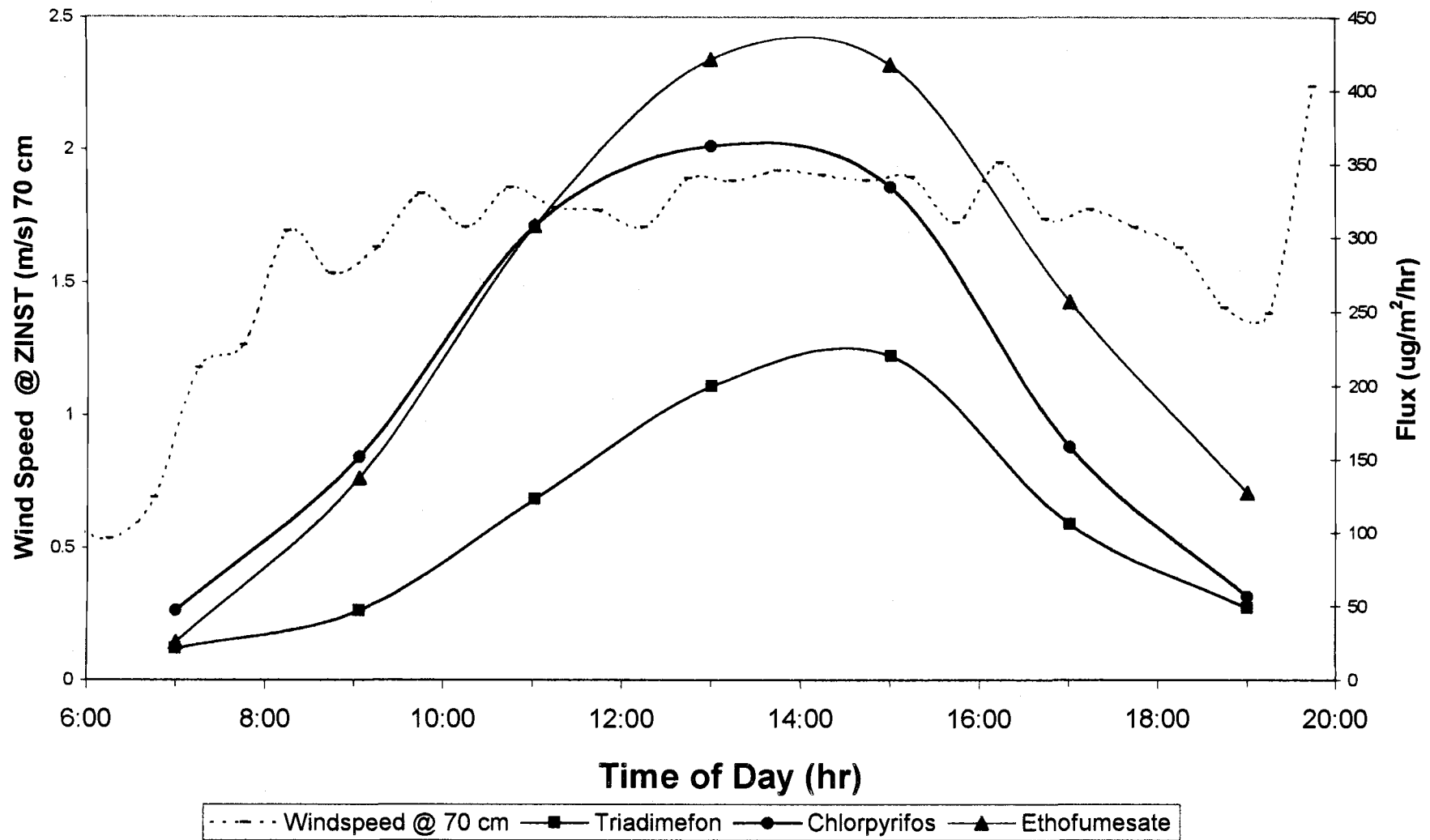


Solar Radiation and Temperature

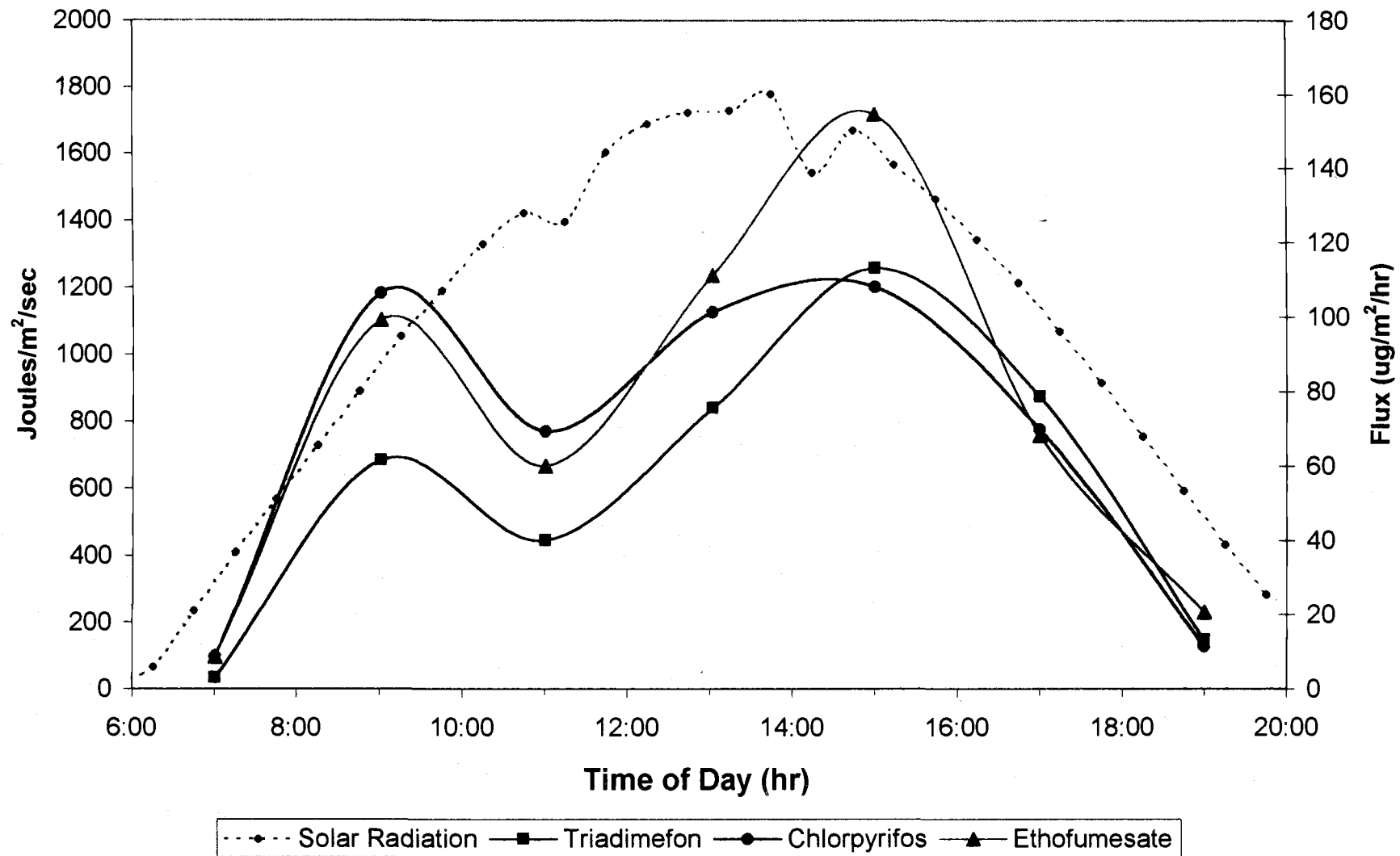
Day 2, App.1 '96 June 14, Julian 166



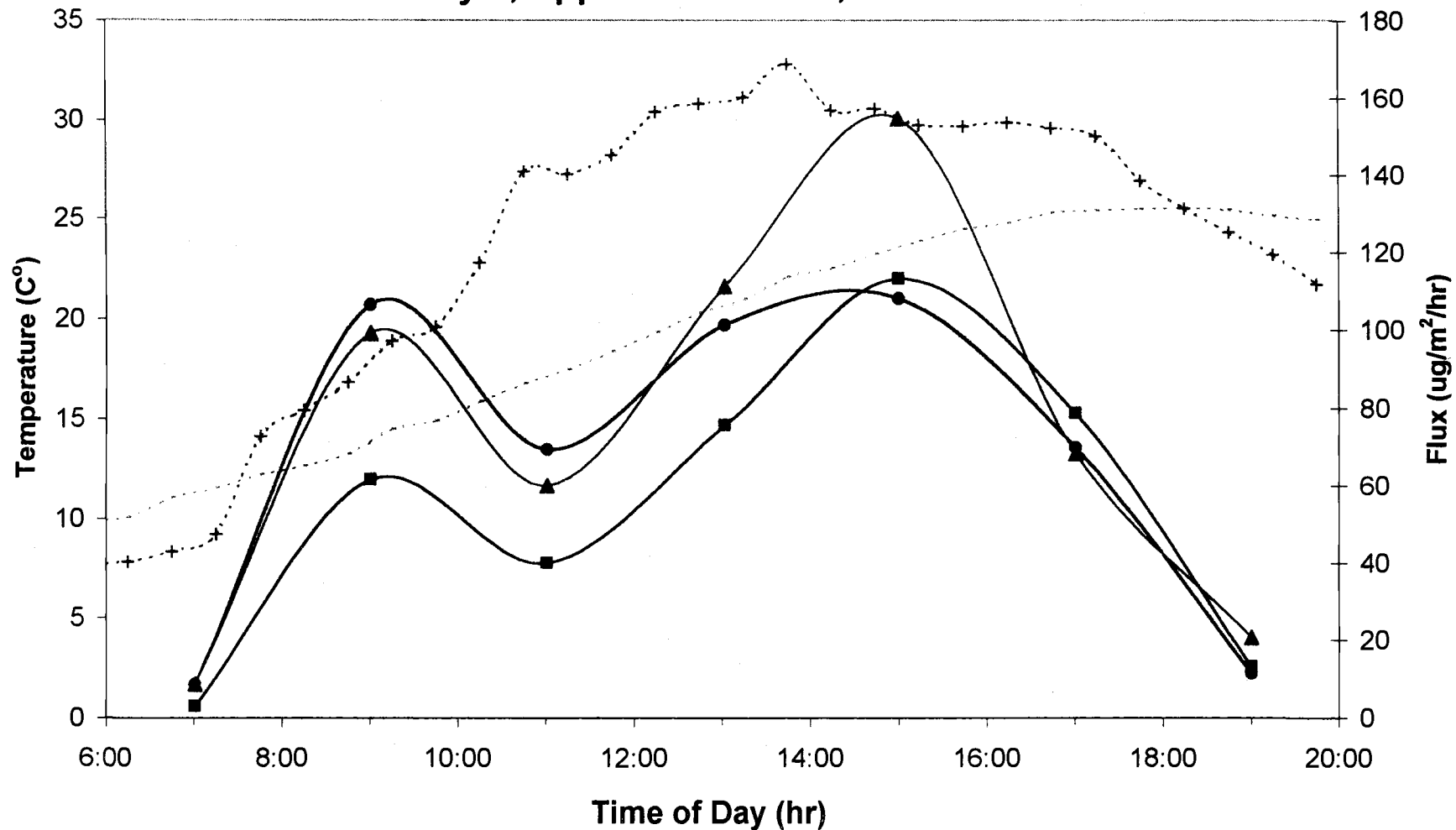
Windspeed @ Height ZINST (70 cm) and Flux
Day 1, App.1 '96 June 13, Julian 165



Solar Radiation and Flux
Day 7, App.1 '96 June 19, Julian 171



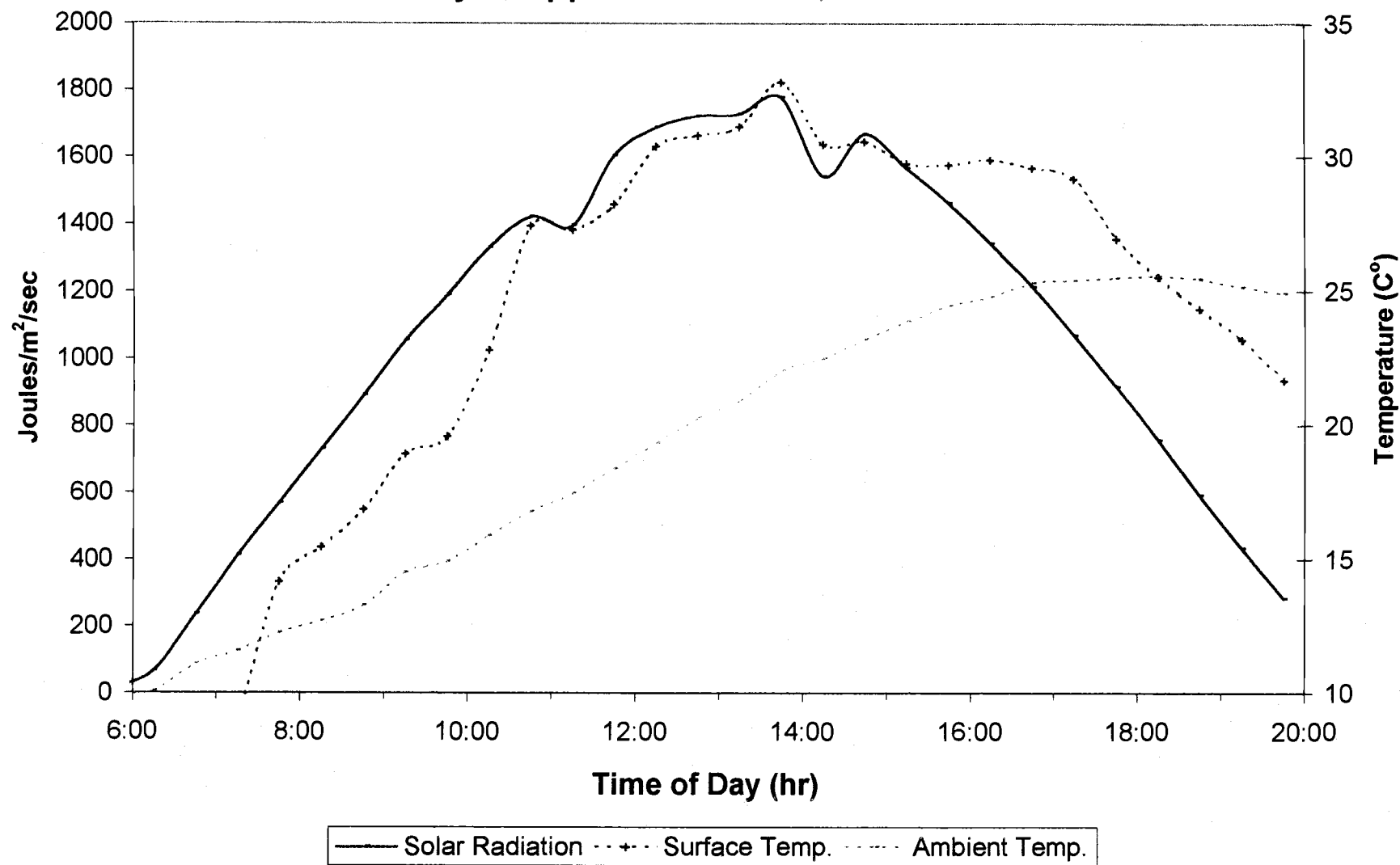
Flux and Temperature (C°) Day 7, App.1 '96 June 19, Julian 171



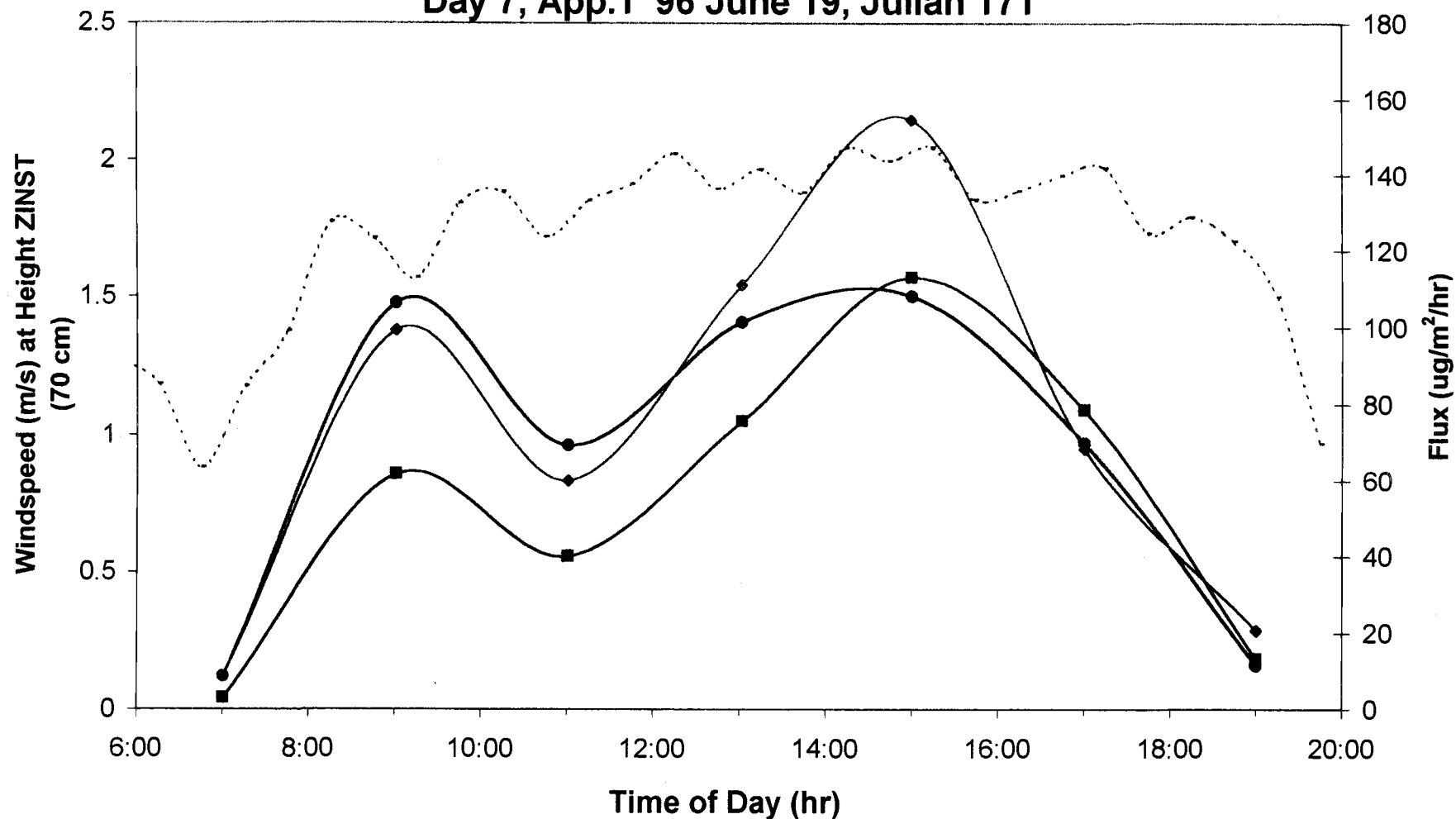
--- Ambient Temp. (C) .. + .. Surface Temp. (C) —■— Triadimefon —●— Chlorpyrifos —▲— Ethofumesate

Solar Radiation and Temperature

Day 7, App.1 '96 June 19, Julian 171

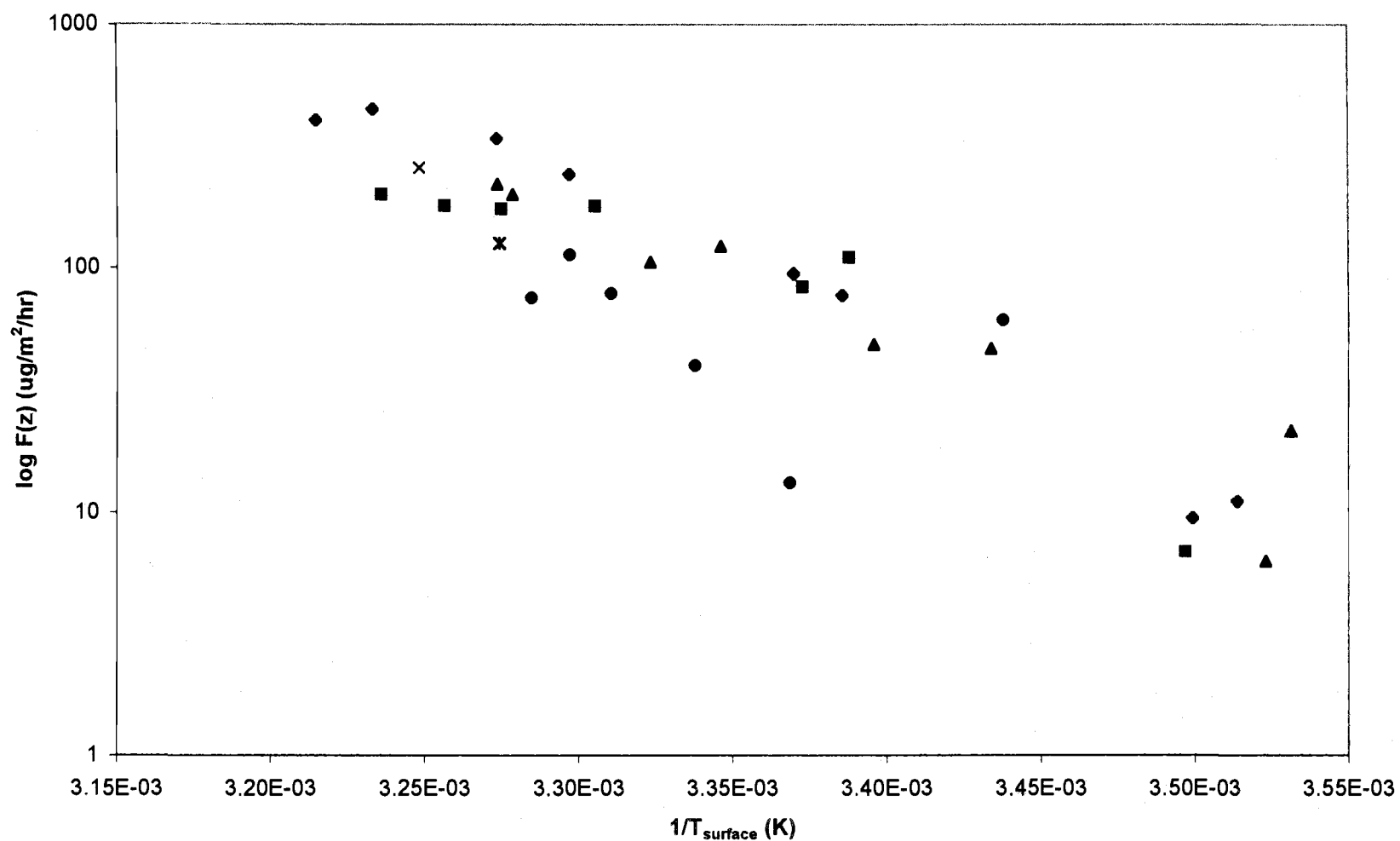


Windspeed and Flux **Day 7, App.1 '96 June 19, Julian 171**

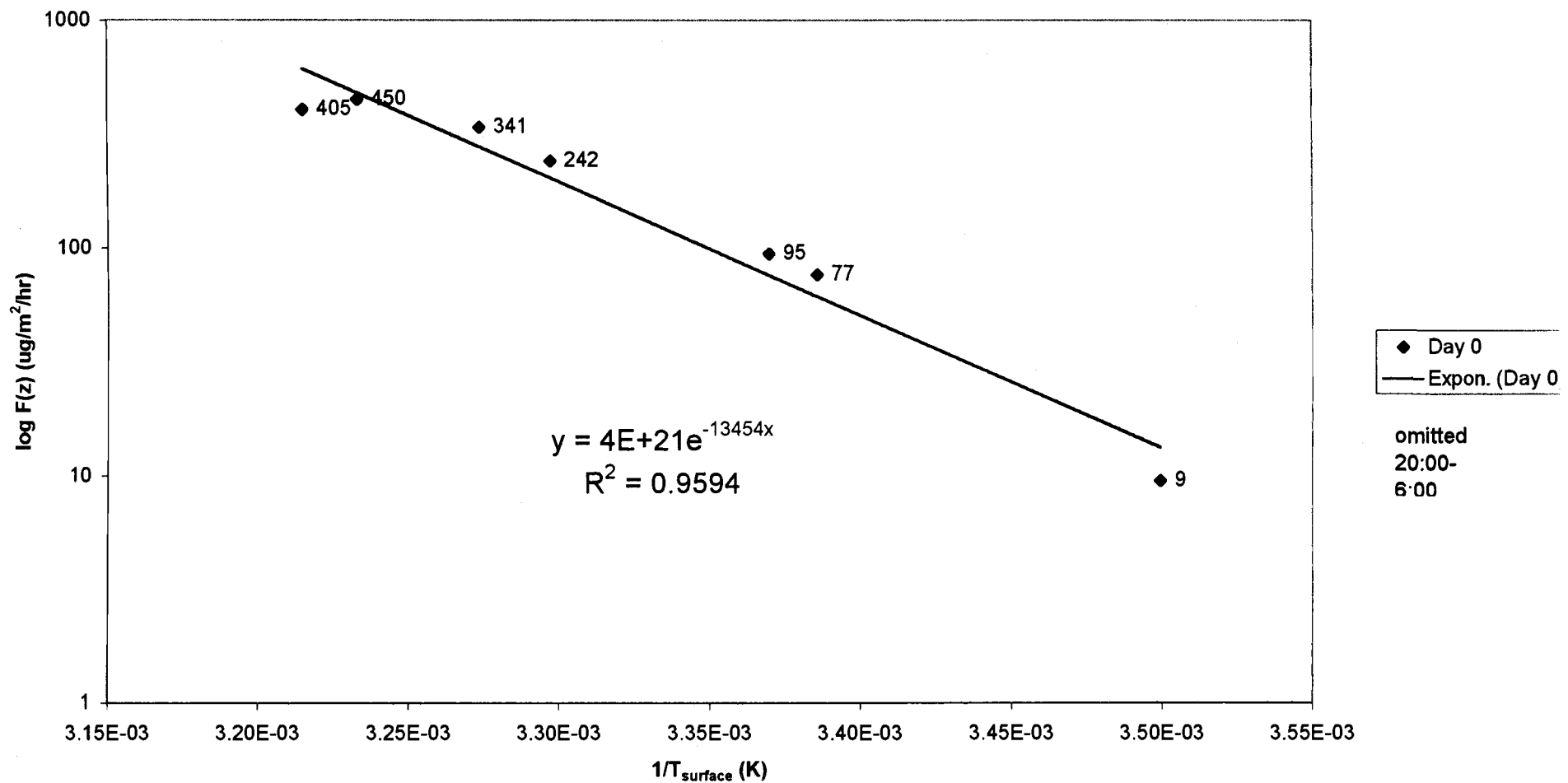


..... Windspeed (m/s) at 70 cm —■— Triadimefon —●— Chlorpyrifos —◆— Ethofumesate

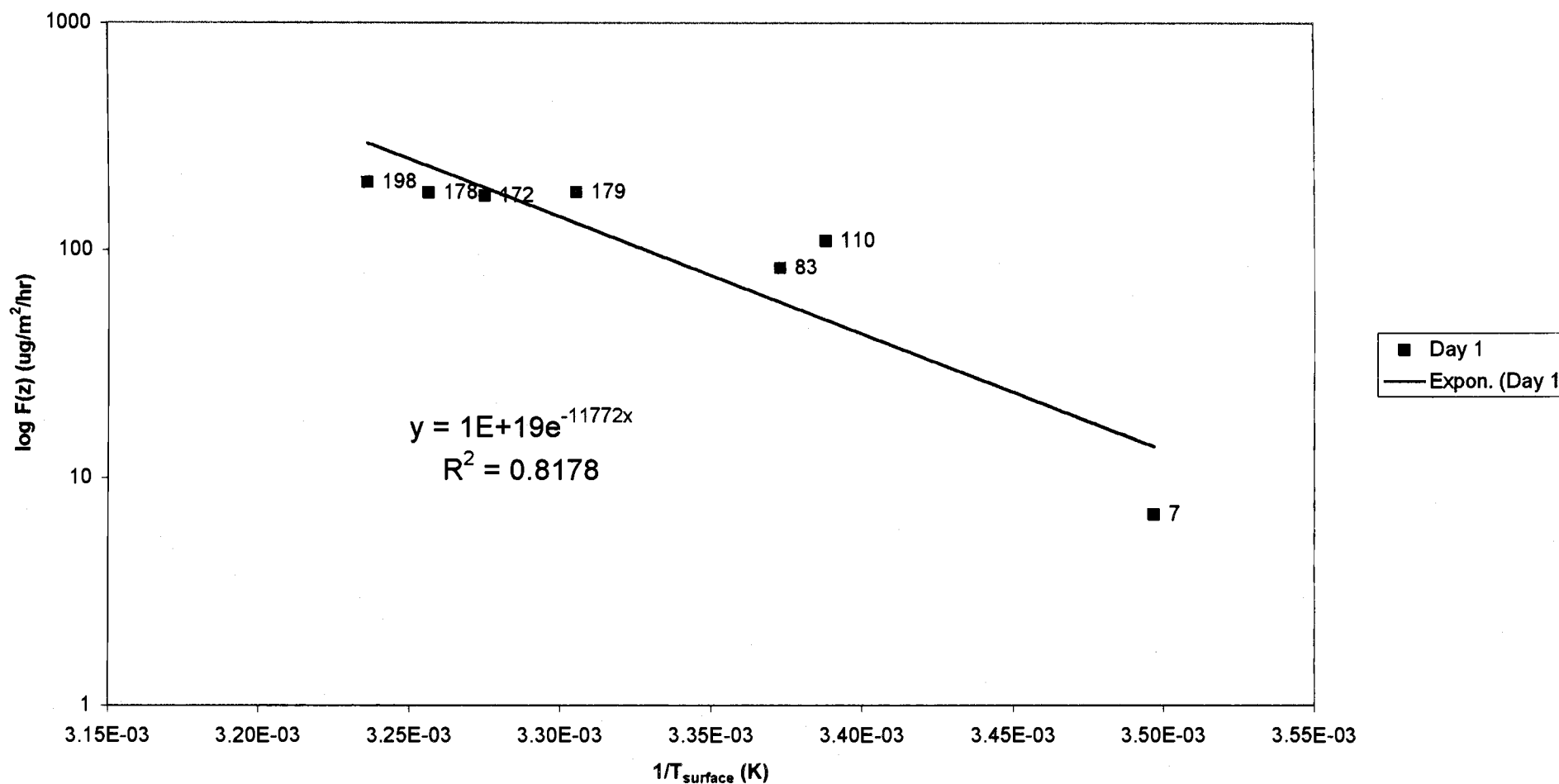
Triadimefon: Flux ($\mu\text{g}/\text{m}^2/\text{hr}$) vs. $1/T_{\text{surface}}$ (K)
Day 0-7, App.1 '96 June 12-19, Julian 164-171



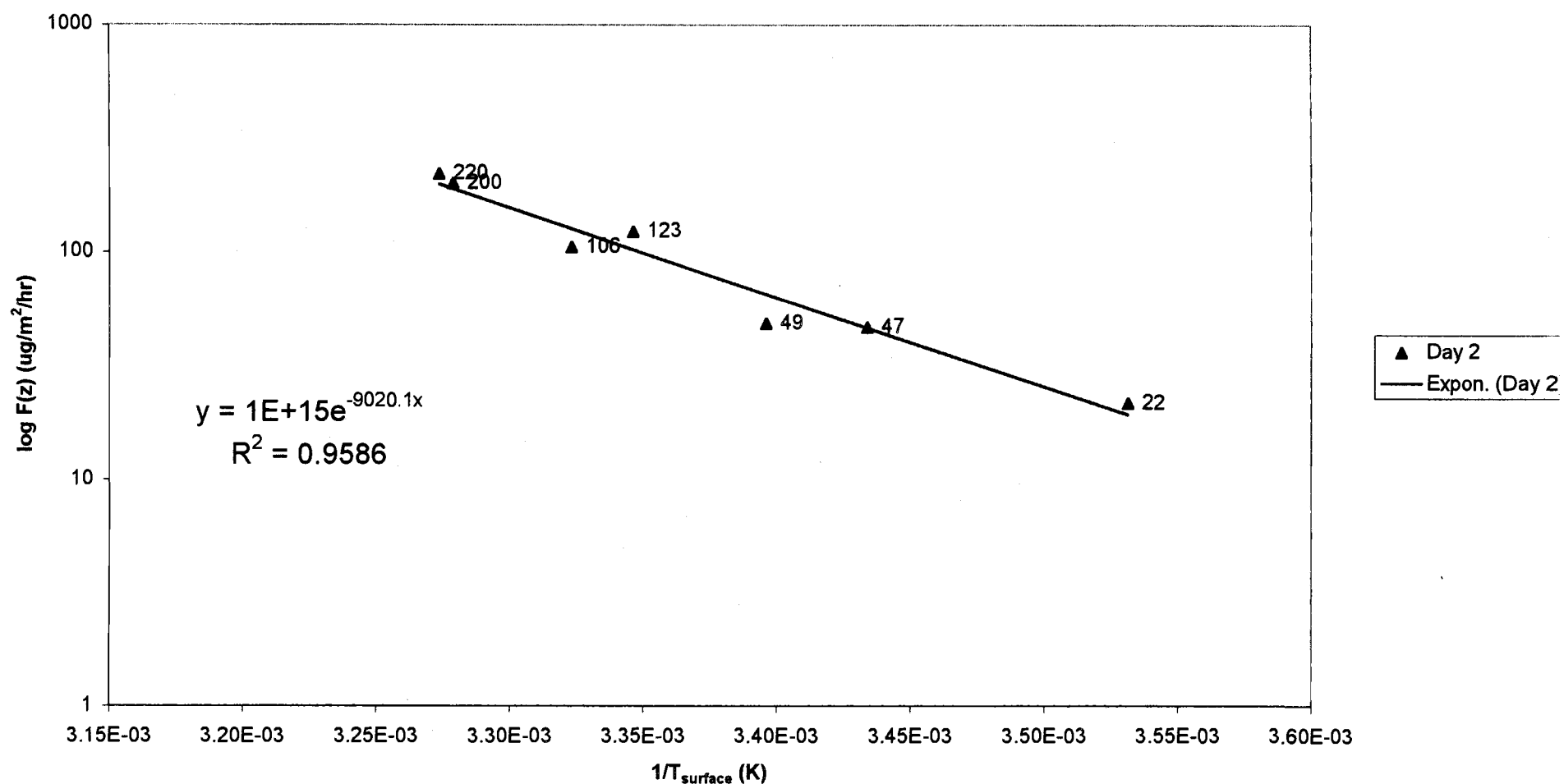
Triadimefon: Flux ($\mu\text{g}/\text{m}^2/\text{hr}$) vs. $1/T_{\text{surface}}$ (K)
 Day 0, App.1 '96 June 12, Julian 164



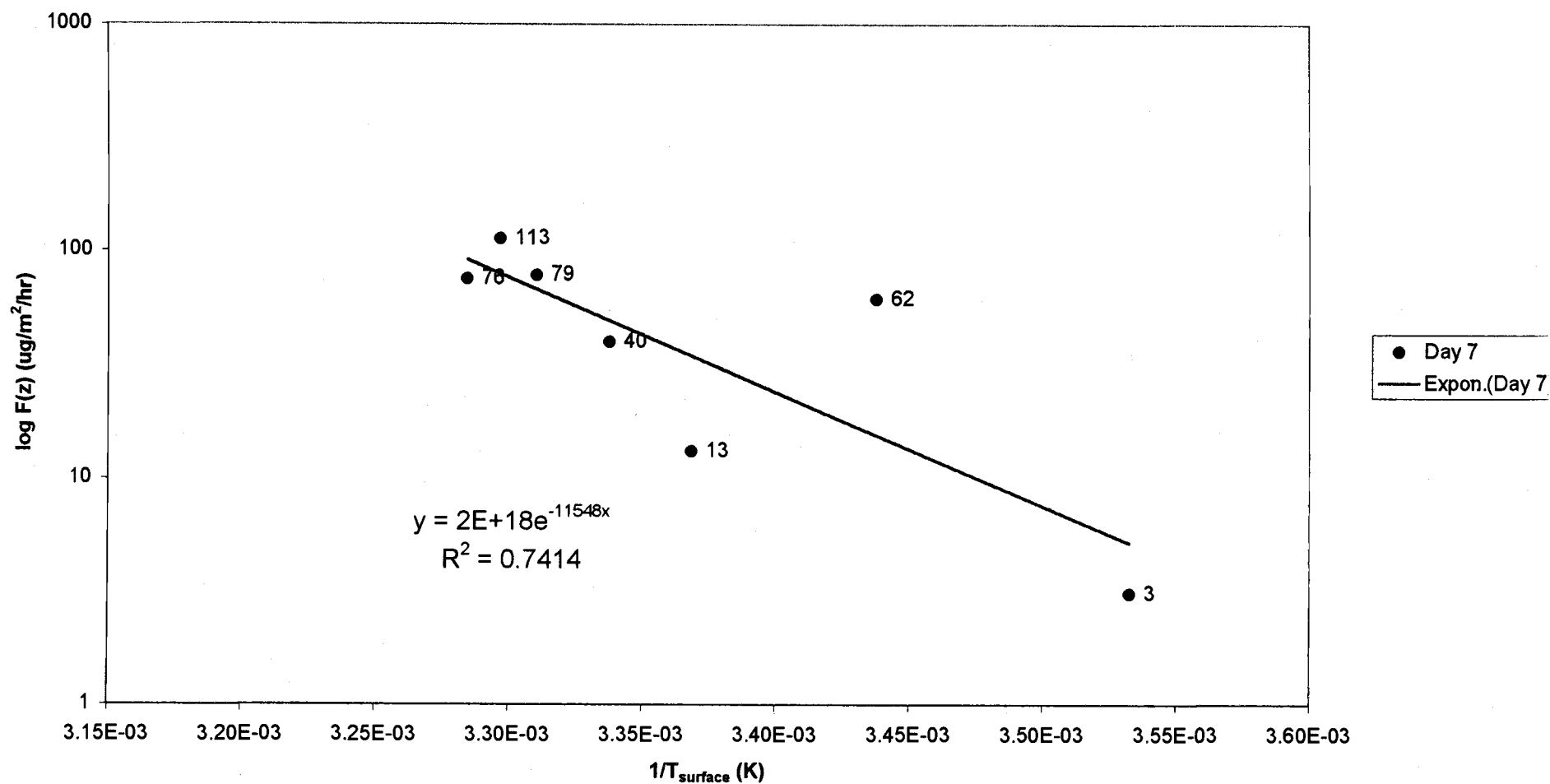
Triadimefon: Flux ($\mu\text{g}/\text{m}^2/\text{hr}$) vs. $1/T_{\text{surface}}$ (K)
Day 1, App.1 '96 June 13, Julian 165



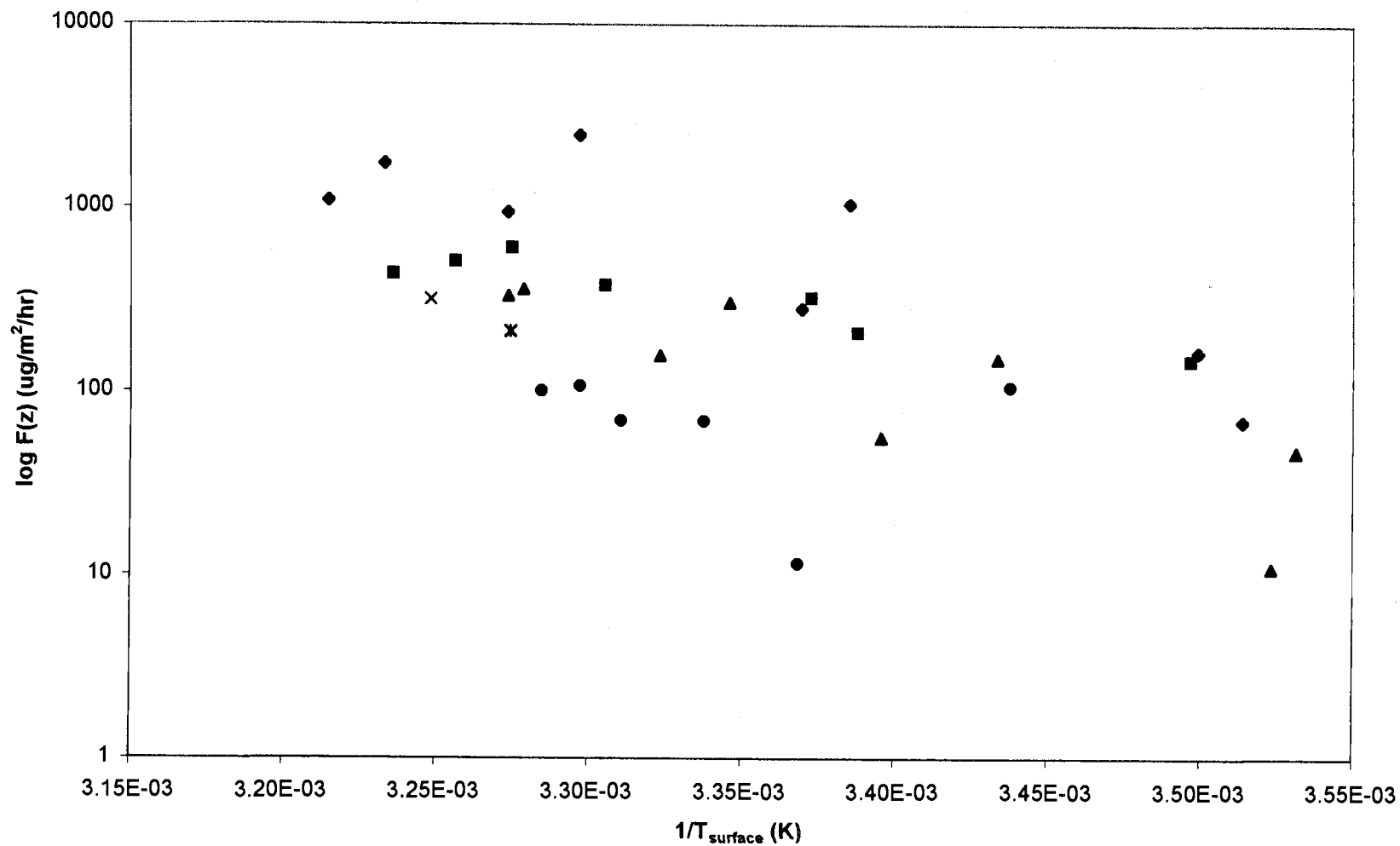
Triadimefon: Flux ($\mu\text{g}/\text{m}^2/\text{hr}$) vs. $1/T_{\text{surface}}$ (K)
 Day 2, App.1 '96 June 14, Julian 166



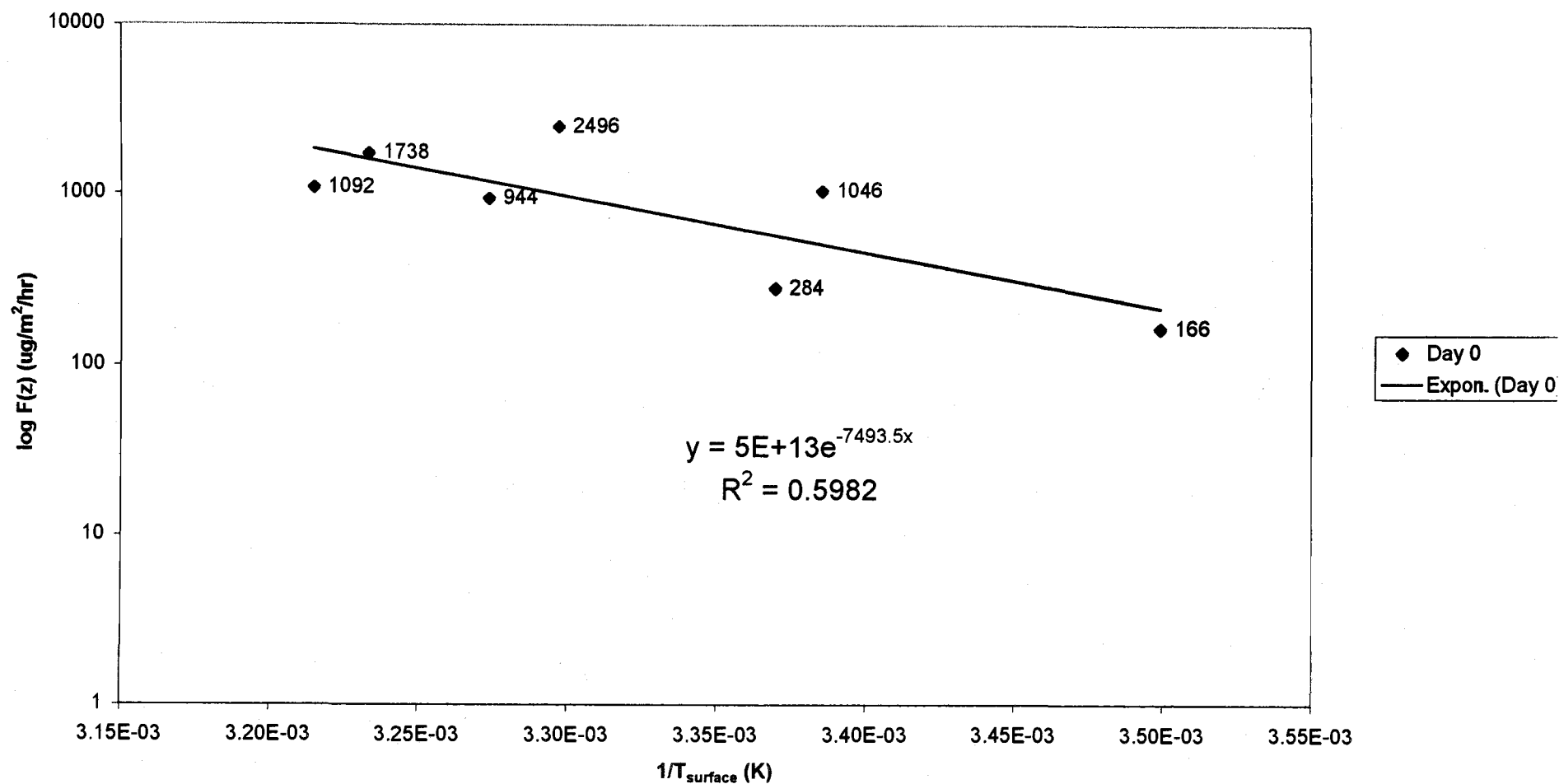
Triadimefon: Flux ($\mu\text{g}/\text{m}^2/\text{hr}$) vs. $1/T_{\text{surface}}$ (K)
Day 7, App.1 '96 June 19, Julian 171



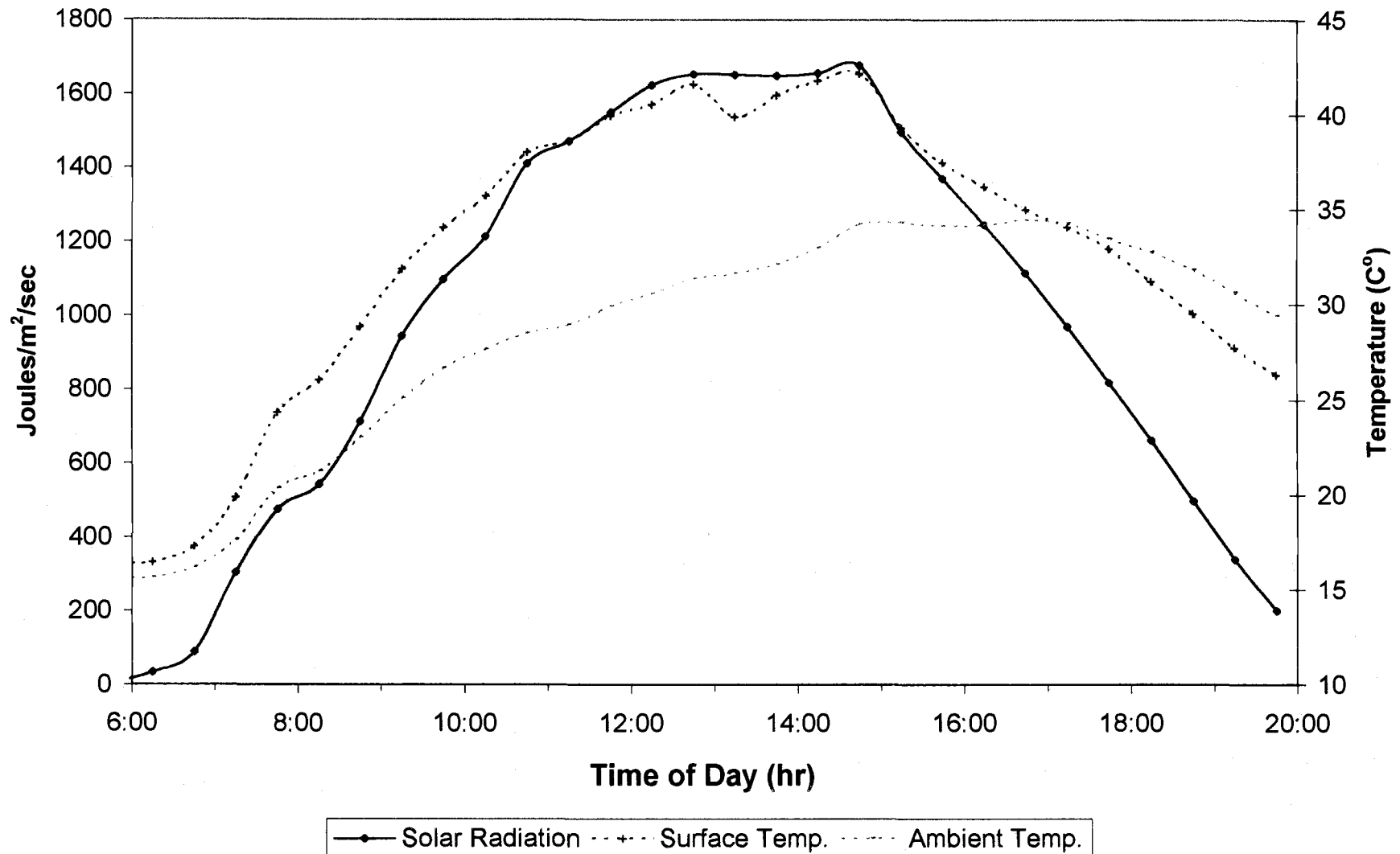
Chlorpyrifos: Flux ($\mu\text{g}/\text{m}^2/\text{hr}$) vs. $1/T_{\text{surface}}$ (K)
Day 0-7, App.1 '96 June 12-19, Julian 164-171



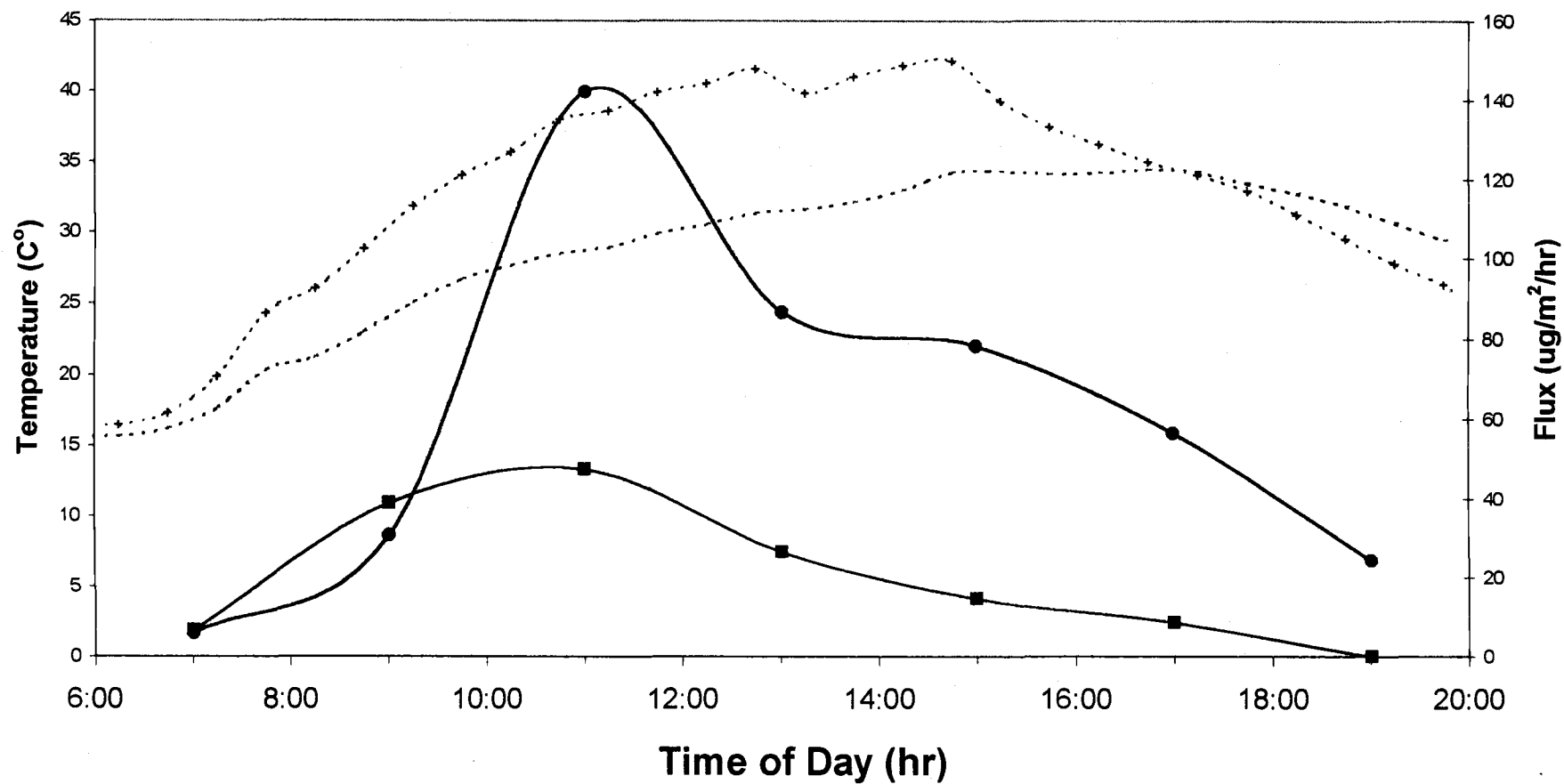
Chlorpyrifos: Flux ($\mu\text{g}/\text{m}^2/\text{hr}$) vs. $1/T_{\text{surface}}$ (K)
Day 0, App.1 '96 June 12, Julian 164



Solar Radiation and Temperature **Day 1, App.2 '96 July 24, Julian 206**

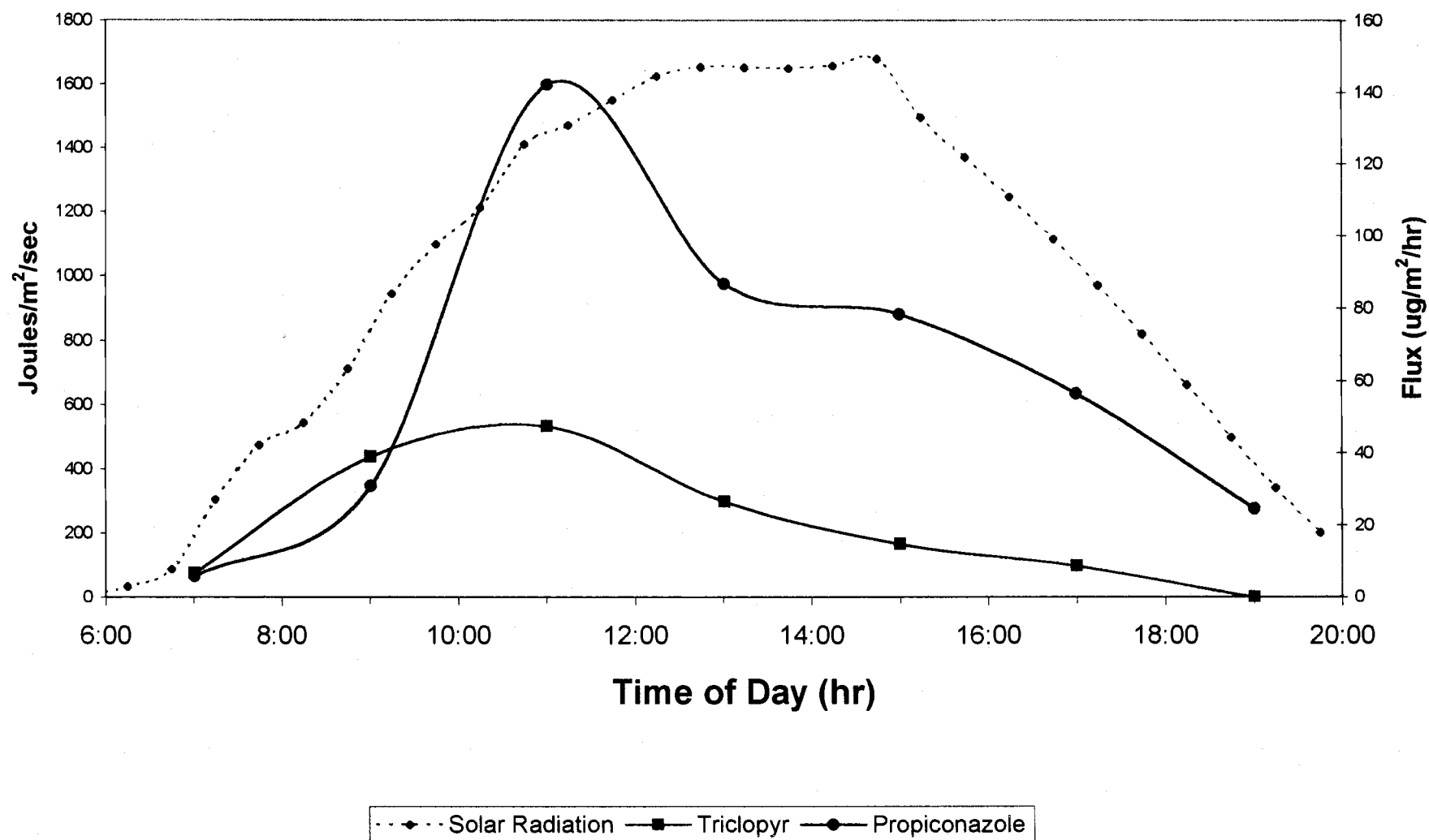


Flux and Temperature (C°)
Day 1, App.2 '96 July 24, Julian 206

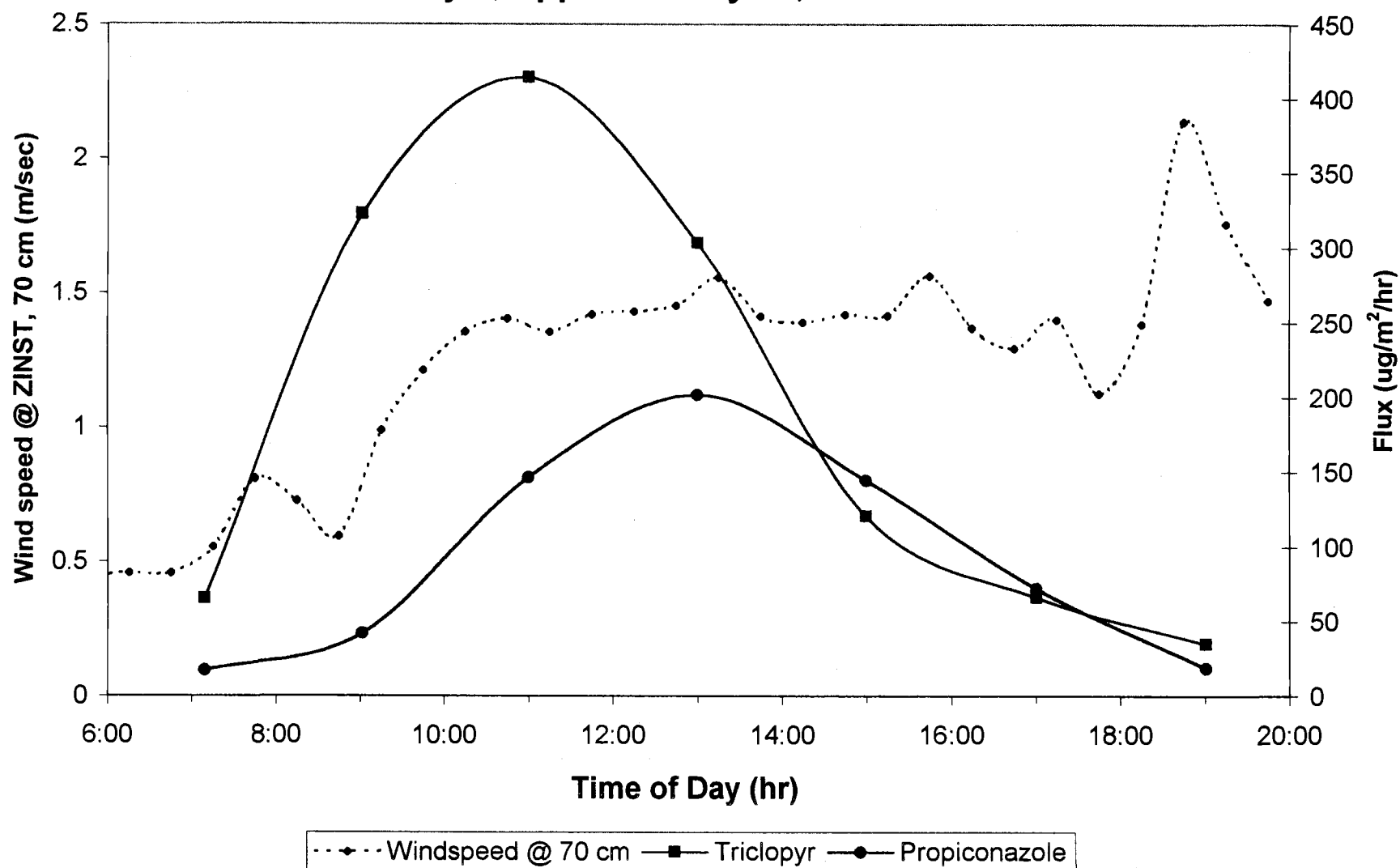


----- Ambient Temp. - - + - - Ground Temp -■- Triclopyr -●- Propiconazole

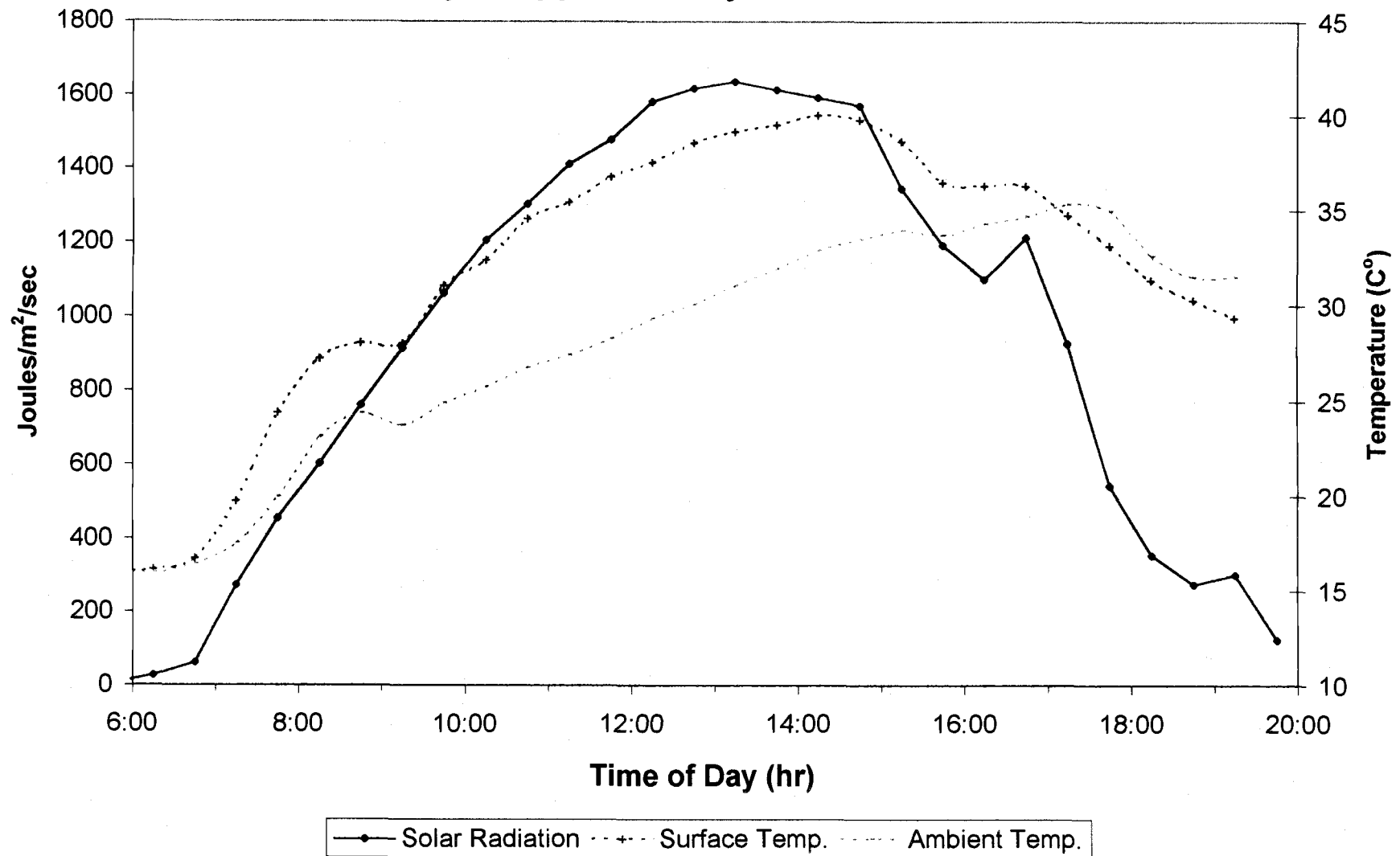
Solar Radiation vs. Flux
Day 1, App.2 '96 July 24, Julian 206



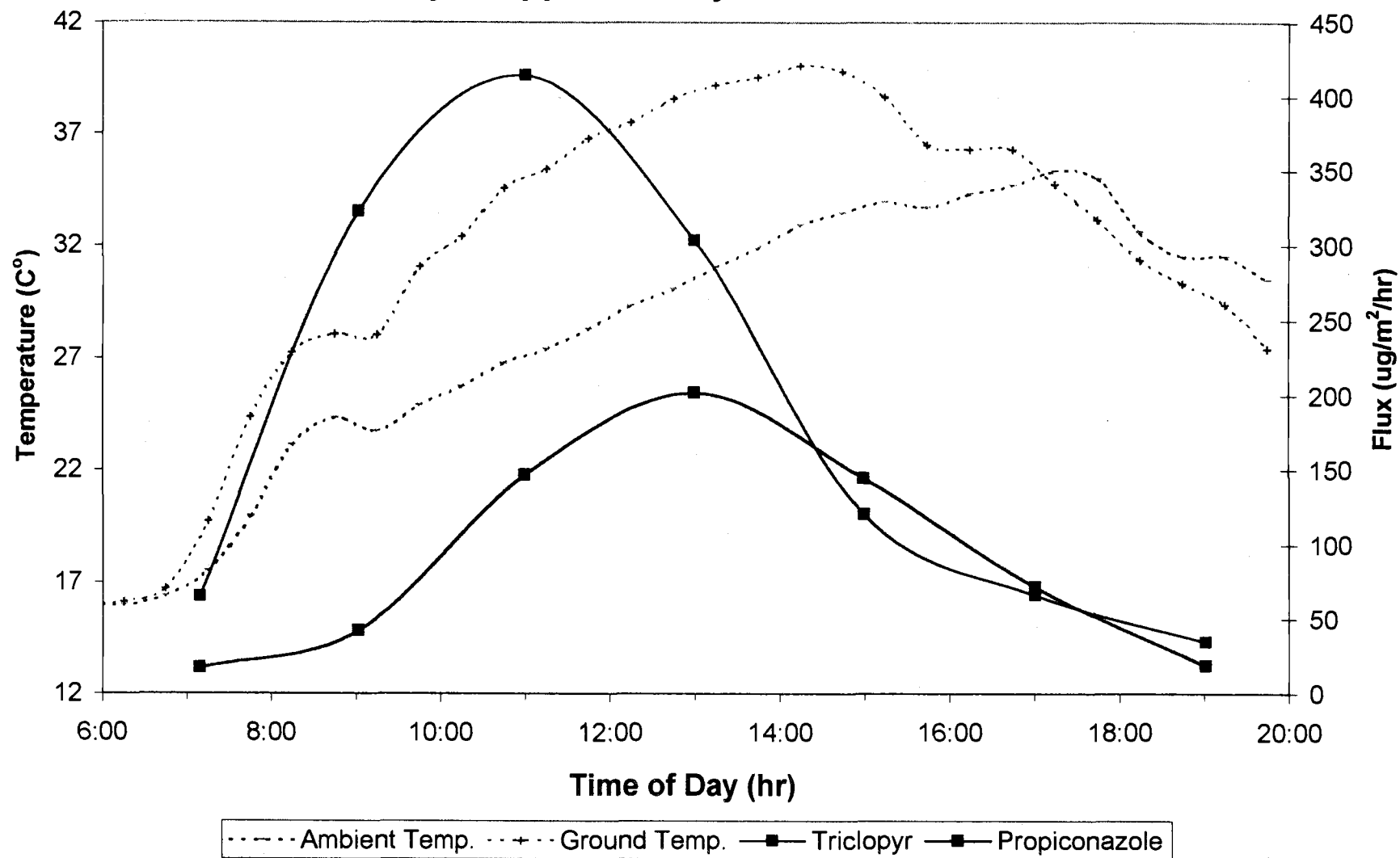
Windspeed and Flux **Day 0, App.2 '96 July 23, Julian 205**



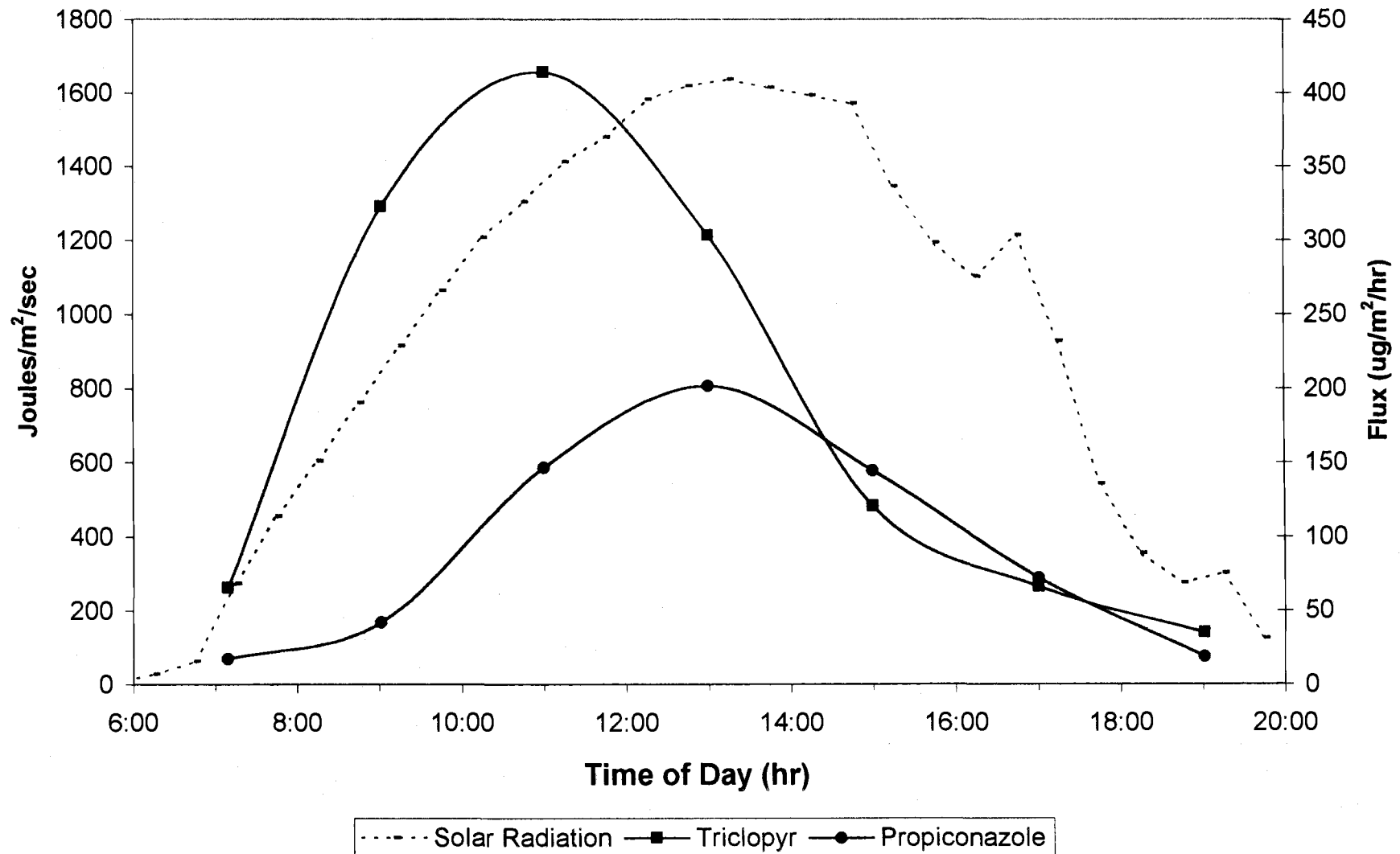
Solar Radiation and Temperature Day 0, App.2 '96 July 23, Julian 205



Flux and Temperature (C°) Day 0, App.2 '96 July 23, Julian 205



Solar Radiation and Flux **Day 0, App.2 '96 July 23, Julian 205**



Peak Flux Values during 12:00-14:00 on Days 0,1,2,3,5,7,13,21

Application 2, 1996

Day	Total Flux (ug/m ²) 12:00-14:00		Total Solar Radiation (MJ/m ²)	Flux/Solar Radiation (ug/MJ)	
	Triclopyr	Propiconazole		Triclopyr	Propiconazole
0	606	404	12	52	35
1	53	173	12	4	15
2	9	118	12	1	10
3	#VALUE!	86	11	#VALUE!	7
5	#VALUE!	17	6	#VALUE!	3
7	#VALUE!	59	11	#VALUE!	5
13	#VALUE!	#VALUE!	10	#VALUE!	#VALUE!
21	#VALUE!	#VALUE!	#VALUE!	#VALUE!	#VALUE!

Precipitation Record: Application 2 1996

July 23-Aug 13, 1996

(Corvallis/Hyslop readings listed on website: <ftp://chaos.ats.orst.edu/pub/oregon/dly/prec1862.1f>)

Experiment Date	Calendar Date	Julian Date	Precipitation (hundredths of inches)	Precipitation (mm)
0	7/23/96	205		
1	7/24/96	206		
2	7/25/96	207		
3	7/26/96	208		
4	7/27/96	209		
5	7/28/96	210		
6	7/29/96	211		
7	7/30/96	212		
8	7/31/96	213		
9	8/1/96	214		
10	8/2/96	215	14	3.6
11	8/3/96	216	T	
12	8/4/96	217		
13	8/5/96	218		
14	8/6/96	219		
15	8/7/96	220		
16	8/8/96	221		
17	8/9/96	222		
18	8/10/96	223		
19	8/11/96	224		
20	8/12/96	225		
21	8/13/96	226		
22	8/14/96	227		

T-trace

Wind speed Profile July 24th, 1996 Application 2, Day 1, Julian Date 206

Height (cm)	41	70	140	280	u* (m/s)	u* (m/s)	Zo (m)	Zo (m)	L (m)	L (m)	
Time (hrs)	-0.89	-0.36	0.34	1.03	Value	Std. Err	Value	Std. Err	Value	Std. Err	R ²
6:00	0.463	0.512	0.555	0.455	0.083849	0.01	0.033	-0.0192	-6	-1.32	0.99
6:30	0.496	0.514	0.55	0.49	0.046833	0.02	0.004	-0.0090	-6	-3.00	0.94
7:00	0.478	0.531	0.513	0.471	0.042263	0.02	0.003	-0.0092	-5	-3.87	0.91
7:30	0.481	0.49	0.517	0.493	0.025006	0.01	0.000	-0.0006	-7	-4.80	0.92
8:00	0.505	0.568	0.549	0.485	0.055977	0.02	0.007	-0.0156	-5	-2.97	0.94
8:30	0.51	0.607	0.533	0.469	0.056445	0.06	0.006	-0.0354	-5	-6.40	0.83
9:00	0.664	0.79	0.698	0.589	0.083756	0.07	0.010	-0.0419	-5	-5.13	0.88
9:30	0.638	0.705	0.605	0.535	0.028045	0.06	0.000	-0.0004	-3	-7.10	0.89
10:00	0.834	0.94	0.894	0.815	0.078801	0.05	0.004	-0.0137	-5	-4.47	0.88
10:30	0.756	0.85	0.83	0.855	0.046009	0.05	0.000	-0.0034	-9	-17.11	0.83
11:00	0.974	1.138	1.154	1.178	0.107426	0.06	0.008	-0.0223	-9	-8.87	0.94
11:30	1.123	1.249	1.303	1.316	0.10118	0.03	0.004	-0.0057	-9	-4.58	0.99
12:00	1.062	1.174	1.219	1.245	0.08383	0.03	0.002	-0.0042	-10	-6.49	0.98
12:30	1.151	1.269	1.343	1.284	0.128339	0.01	0.009	-0.0017	-7	-0.47	1.00
13:00	1.119	1.196	1.257	1.18	0.101928	0.01	0.004	-0.0016	-7	-0.74	1.00
13:30	1.285	1.284	1.428	1.396	0.068197	0.07	0.000	-0.0018	-10	-20.23	0.88
14:00	1.365	1.406	1.602	1.642	0.092664	0.06	0.001	-0.0053	-19	-42.25	0.97
14:30	1.06	1.163	1.199	1.157	0.097284	0.02	0.004	-0.0042	-7	-2.13	0.99
15:00	1.243	1.34	1.435	1.404	0.113327	0.01	0.004	-0.0017	-8	-1.05	1.00
15:30	1.45	1.558	1.675	1.733	0.099316	0.00	0.001	-0.0001	-14	-0.49	1.00
16:00	1.335	1.296	1.53	1.546	0.062882	0.12	0.000	-0.0017	-44	-608.31	0.88
16:30	1.276	1.309	1.505	1.515	0.097518	0.07	0.002	-0.0096	-14	-25.58	0.95
17:00	1.137	1.162	1.347	1.32	0.100316	0.07	0.004	-0.0169	-11	-16.09	0.93
17:30	1.929	2.149	2.469	2.701	0.196583	0.02	0.008	-0.0044	-34	-22.55	1.00
18:00	2.256	2.485	2.895	3.185	0.21915	0.05	0.007	-0.0078	-61	-142.68	1.00
18:30	2.482	2.756	3.207	3.567	0.241861	0.04	0.007	-0.0059	-117	-386.21	1.00
19:00	2.44	2.732	3.217	3.553	0.275676	0.05	0.012	-0.0101	-41	-54.48	1.00
19:30	2.331	2.586	3.043	3.432	0.221798	0.05	0.006	-0.0070	110	427.97	1.00
20:00	2.054	2.27	2.638	3.012	0.165085	0.03	0.003	-0.0028	26	18.21	1.00

Wind speed Profile July 23rd, 1996 Application 2, Day 0, Julian Date 205

	Height (cm)	41	70	140	280	u* (m/s)	u* (m/s)	Zo (m)	Zo (m)	L (m)	L (m)	
Time	log Ht-->	-0.89	-0.36	0.34	1.03	Value	Std. Err	Value	Std. Err	Value	Std. Err	R ²
600	6:00	0.447	0.447	0.447	0.447	-4.1E-16	0.00	#NUM!	#NUM!	-6	-8.18	1.00
630	6:30	0.447	0.46	0.447	0.447	0.003413	0.01	0.000	0.0000	-5	-17.79	0.48
700	7:00	0.447	0.46	0.447	0.447	0.003413	0.01	0.000	0.0000	-5	-17.79	0.48
730	7:30	0.458	0.557	0.465	0.458	0.031188	0.08	0.001	-0.0104	-5	-15.06	0.52
800	8:00	0.58	0.811	0.76	0.678	0.160977	0.10	0.066	-0.1192	-6	-5.66	0.85
830	8:30	0.553	0.729	0.621	0.47	0.124828	0.09	0.042	-0.1065	-5	-4.70	0.89
900	9:00	0.486	0.598	0.461	0.447	0.024086	0.10	0.000	-0.0018	-3	-16.33	0.62
930	9:30	0.85	0.991	0.913	0.829	0.090895	0.08	0.006	-0.0265	-5	-5.81	0.83
1000	10:00	1.105	1.214	1.251	1.303	0.069791	0.03	0.001	-0.0021	-13	-14.53	0.98
1030	10:30	1.313	1.358	1.48	1.488	0.076373	0.03	0.000	-0.0014	-12	-12.52	0.98
1100	11:00	1.366	1.407	1.521	1.538	0.067435	0.03	0.000	-0.0005	-14	-16.08	0.98
1130	11:30	1.255	1.357	1.436	1.407	0.10953	0.00	0.003	-0.0002	-8	-0.12	1.00
1200	12:00	1.443	1.421	1.642	1.679	0.061833	0.10	0.000	-0.0007	-106	-3010.05	0.92
1230	12:30	1.318	1.433	1.529	1.549	0.108405	0.01	0.003	-0.0008	-10	-1.02	1.00
1300	13:00	1.41	1.454	1.618	1.683	0.073289	0.05	0.000	-0.0010	-35	-129.53	0.98
1330	13:30	1.42	1.557	1.687	1.695	0.14081	0.00	0.006	-0.0006	-10	-0.36	1.00
1400	14:00	1.403	1.413	1.607	1.645	0.07191	0.08	0.000	-0.0016	-29	-150.32	0.95
1430	14:30	1.344	1.392	1.595	1.623	0.104212	0.07	0.002	-0.0089	-15	-26.44	0.97
1500	15:00	1.463	1.421	1.734	1.763	0.088299	0.15	0.001	-0.0081	-43	-524.28	0.90
1530	15:30	1.468	1.417	1.711	1.706	0.086191	0.15	0.001	-0.0068	-22	-145.38	0.86
1600	16:00	1.488	1.564	1.729	1.715	0.121784	0.04	0.003	-0.0059	-10	-7.26	0.98
1630	16:30	1.431	1.371	1.622	1.583	0.074415	0.14	0.000	-0.0033	-15	-70.74	0.79
1700	17:00	1.324	1.295	1.553	1.475	0.111092	0.13	0.003	-0.0235	-10	-22.25	0.81
1730	17:30	1.503	1.402	1.693	1.619	0.075121	0.18	0.000	-0.0033	-13	-69.77	0.68
1800	18:00	1.126	1.126	1.257	1.186	0.076856	0.07	0.001	-0.0062	-8	-10.99	0.82
1830	18:30	1.265	1.384	1.542	1.604	0.121793	0.01	0.006	-0.0036	-14	-4.36	1.00
1900	19:00	1.947	2.139	2.461	2.688	0.180455	0.03	0.005	-0.0056	-46	-69.00	1.00
1930	19:30	1.619	1.758	2.04	2.241	0.137897	0.04	0.004	-0.0066	-178	-1592.18	1.00
2000	20:00	1.328	1.471	1.708	1.772	0.168907	0.04	0.016	-0.0157	-14	-7.81	0.99

Ground Temperature C°

Julian Date,	218	218	218	218	226	226	226	226
Time(hr)	Ambient	Ground1	Ground2	Groundavg	Ambient	Ground1	Ground2	Groundavg
6:00	13.81	12.76	13.63	0.153	12.75	13.44	12.86	13.15
6:30	12.94	9.84	12.34	11.09	12.66	13.34	12.8	13.07
7:00	12.75	12.65	13.62	13.135	12.75	13.52	13.07	13.295
7:30	13.73	14.18	13.93	14.055	13.63	14.25	14.11	14.18
8:00	14.62	15.79	14.57	15.18	15.36	16.2	17.65	16.925
8:30	14.96	17.76	16.19	16.975	16.8	18.93	23.32	21.125
9:00	15.54	20.49	17.94	19.215	18.62	21.52	25.53	23.525
9:30	16.49	24.79	20.83	22.81	21.72	24.35	28.2	26.275
10:00	16.99	23.31	20.36	21.835	23.25	26.4	29.3	27.85
10:30	16.92	20.66	19.11	19.885	23.86	28.06	30.12	29.09
11:00	17.61	22.48	21.18	21.83	24.72	30.47	31.79	31.13
11:30	17.9	22.12	21.06	21.59	25.74	33.88	34.59	34.235
12:00	17.56	22.48	21.1	21.79	26.94	36.53	36.71	36.62
12:30	17.29	22.21	20.61	21.41	27.91	39	38.22	38.61
13:00	18.39	26.54	23.58	25.06	28.37	39.11	38.7	38.905
13:30	19.53	30.97	25.54	28.255	29.05	35.31	40.19	37.75
14:00	20.62	32.85	26.7	29.775	30.07	35.43	38.55	36.99
14:30	20.08	24.65	21.93	23.29	30.59	35.48	38.74	37.11
15:00	19.74	24.85	22.17	23.51	31.77	40.06	42.44	41.25
15:30	20.93	28.63	27.25	27.94	32.56	32.08	31.09	31.585
16:00	20.49	24.7	25.65	25.175	32.88	34.87	34.17	34.52
16:30	20.89	28.74	28.92	28.83	33.68	36.63	36.27	36.45
17:00	21.75	32.26	30.73	31.495	32.96	34.77	33.54	34.155
17:30	22.21	31.45	32.23	31.84	31.38	32.21	31.34	31.775
18:00	22.44	26.24	27.71	26.975	30.59	29.97	31.73	30.85
18:30	21.68	21.61	21.55	21.58	29.9	29.38	30.34	29.86
19:00	21.32	19.78	19.67	19.725	28.68	27.32	28.41	27.865
19:30	20.1	16.15	16.29	16.22	27.24	25.51	26.11	25.81
20:00	19.17	14.74	14.82	14.78	26.01	23.45	23.48	23.465

Ground Temperature C°

Julian Date,	208	208	208	208	210	210	210	210	212	212	212	212
Time(hr)	Ambient	Ground1	Ground2	Groundavg	Ambient	Ground1	Ground2	Groundavg	Ambient	Ground1	Ground2	Groundavg
6:00	14.33	16.01	16.13	16.07	15.26	16.56	16.47	16.515	16.25	14.76	15.35	15.055
6:30	14.27	16.11	16.17	16.14	14.93	16.6	16.64	16.62	15.95	14.84	15.4	15.12
7:00	14.73	16.78	16.74	16.76	15.16	17.3	17.45	17.375	15.87	15.49	15.76	15.625
7:30	15.73	18.79	18.48	18.635	15.72	18.48	18.25	18.365	17.07	18.9	17.97	18.435
8:00	17.66	22.73	22.1	22.415	16.53	19.46	19.13	19.295	18.69	21.83	21.17	21.5
8:30	19.44	24.82	24.48	24.65	17.23	20.14	19.82	19.98	19.08	23.21	23.12	23.165
9:00	20.82	27.23	26.94	27.085	17.75	20.56	20.5	20.53	19.26	24.42	24.8	24.61
9:30	22.12	30.76	29.94	30.35	18.06	21.05	20.39	20.72	19.89	25.76	25.49	25.625
10:00	23.27	32.88	32.15	32.515	18.15	21.09	20.56	20.825	20.8	27.71	26.71	27.21
10:30	24.67	34.73	34.22	34.475	18.17	20.69	20.22	20.455	21.3	28.06	26.45	27.255
11:00	25.7	37.01	36.28	36.645	18.2	20.01	20.12	20.065	22.25	29.47	27.39	28.43
11:30	27.21	38.49	38.25	38.37	18.35	20.54	20.26	20.4	23.03	29.74	30.27	30.005
12:00	28.25	39.42	39.47	39.445	18.36	21.22	20.93	21.075	23.6	31.22	33.41	32.315
12:30	29.14	40.06	40.65	40.355	19.04	22.18	22.1	22.14	24.57	32.79	35.85	34.32
13:00	30.24	40.48	41.48	40.98	20.13	24.52	25.31	24.915	25.06	32.84	35.66	34.25
13:30	31.13	40.4	41.97	41.185	21.8	29.34	30.06	29.7	25.75	32.95	35.78	34.365
14:00	32.38	42.12	42.76	42.44	22.79	30.27	30.64	30.455	26.8	33.59	36.47	35.03
14:30	32.86	42.61	42.28	42.445	24.9	34.7	35	34.85	27.38	33.57	36.63	35.1
15:00	33.66	41.02	41.12	41.07	25.48	34.25	34.06	34.155	27.76	33.17	35.42	34.295
15:30	34.14	40.45	38.75	39.6	25.97	33.28	33.2	33.24	28.09	32.33	33.24	32.785
16:00	34.47	38.58	37.17	37.875	26.83	32.31	32.3	32.305	28.33	31.45	33.47	32.46
16:30	34.59	37.72	36.32	37.02	27.14	30.41	30.8	30.605	28.72	30.24	32.32	31.28
17:00	34.04	34.75	34.97	34.86	27.47	29.66	30.35	30.005	28.75	28.17	30.11	29.14
17:30	33.42	32.37	33.84	33.105	27.77	28.14	29.29	28.715	29.14	26.99	29.25	28.12
18:00	32.76	30.66	32.82	31.74	27.06	26.39	27.53	26.96	28.34	26.86	28.75	27.805
18:30	32.05	29.58	30.98	30.28	26.31	25.25	26.13	25.69	26.8	26.2	27.29	26.745
19:00	31.2	28.3	28.91	28.605	26.04	24.71	25.41	25.06	25.8	24.79	25.4	25.095
19:30	30.3	27.08	27.11	27.095	25.34	23.88	24.5	24.19	24.68	23.58	23.78	23.68
20:00	29.24	25.69	25.59	25.64	24.79	23.15	23.67	23.41	23.55	22.3	22.41	22.355

Ground Temperature C°

Julian Date, 1996	205	205	205	205	206	206	206	206	207	207	207	207	
Time	Time(hr)	Ambient	Ground1	Ground2	Groundavg	Ambient	Ground1	Ground2	Groundavg	Ambient	Ground1	Ground2	Groundavg
600	6:00	16.03	15.81	16.13	15.97	15.61	16.37	16.38	16.375	14.02	15.14	15.23	15.185
630	6:30	15.96	16	16.27	16.135	15.65	16.43	16.5	16.465	13.96	15.23	15.13	15.18
700	7:00	16.4	16.72	16.76	16.74	16.2	17.35	17.26	17.305	14.43	15.82	15.57	15.695
730	7:30	17.53	20.06	19.44	19.75	17.63	20.21	19.58	19.895	15.74	18.58	17.68	18.13
800	8:00	19.97	25.27	23.55	24.41	20.37	24.93	23.79	24.36	17.61	22.58	21.54	22.06
830	8:30	23.15	28.27	26.27	27.27	21.26	26.71	25.43	26.07	18.59	25.32	24.37	24.845
900	9:00	24.36	28.85	27.33	28.09	23.04	29.6	28.12	28.86	20.53	28.77	27.43	28.1
930	9:30	23.74	28.58	27.52	28.05	25.11	32.71	31.04	31.875	22.47	31.39	30.01	30.7
1000	10:00	24.91	31.41	30.72	31.065	26.7	34.6	33.51	34.055	24.02	33.39	32.26	32.825
1030	10:30	25.75	32.66	32.14	32.4	27.68	36.15	35.31	35.73	25.4	35.14	34.17	34.655
1100	11:00	26.79	34.93	34.2	34.565	28.52	38.61	37.47	38.04	26.39	36.26	35.71	35.985
1130	11:30	27.42	35.5	35.38	35.44	28.94	38.98	38.32	38.65	27.15	35.53	35.76	35.645
1200	12:00	28.3	36.76	36.82	36.79	29.93	40.02	39.93	39.975	27.54	34.79	35.93	35.36
1230	12:30	29.34	37.14	37.96	37.55	30.57	40.5	40.63	40.565	28.69	36.76	37.97	37.365
1300	13:00	30.07	38.13	39.03	38.58	31.37	41.15	42.1	41.625	29.69	38	39.3	38.65
1330	13:30	31.04	38.32	40.04	39.18	31.64	38.83	40.99	39.91	30.71	38.89	40.01	39.45
1400	14:00	31.91	38.58	40.48	39.53	32.13	40.14	42	41.07	31.12	37.15	39.29	38.22
1430	14:30	32.92	38.99	41.14	40.065	33	41.22	42.45	41.835	32.13	38.65	39.94	39.295
1500	15:00	33.46	38.98	40.65	39.815	34.25	42.14	42.24	42.19	32.93	38.15	38.59	38.37
1530	15:30	33.94	38.61	38.76	38.685	34.31	39.73	38.93	39.33	33.42	37.34	36.59	36.965
1600	16:00	33.71	36.78	36.24	36.51	34.14	38.14	36.86	37.5	33.67	35.98	34.98	35.48
1630	16:30	34.31	37.04	35.59	36.315	34.2	36.84	35.63	36.235	33.51	33.84	34.05	33.945
1700	17:00	34.68	37.29	35.34	36.315	34.43	35.53	34.5	35.015	33.86	32.03	32.72	32.375
1730	17:30	35.33	34.87	34.63	34.75	34.29	33.78	34.38	34.08	34.01	30.36	31.84	31.1
1800	18:00	34.99	32.74	33.56	33.15	33.49	32.07	33.81	32.94	33.97	29.51	31.94	30.725
1830	18:30	32.63	31.11	31.6	31.355	32.77	30.55	31.93	31.24	34.18	28.79	30.88	29.835
1900	19:00	31.5	30.16	30.46	30.31	31.86	29.2	29.88	29.54	34.73	28.51	29.34	28.925
1930	19:30	31.5	29.37	29.43	29.4	30.65	27.65	27.88	27.765	33.76	27.87	27.85	27.86
2000	20:00	30.46	27.4	27.46	27.43	29.45	26.35	26.36	26.355	30.33	26.2	26.08	26.14

Solar Radiation		Day 0	Day 1	Day 2	Day 3	Day 5	Day 7	Day 13	Day 21
Julian Date, 1996		0	1	2	3	5	7	13	21
Time	Time(hr)	205	206	207	208	210	212	218	226
600	5:45	5.185	4.535	4.302	3.62	1.718	1.779	1.078	0.153
630	6:15	28.59	34.66	24.59	25.92	28.96	18.46	14.28	5.156
700	6:45	62.23	89.2	57.11	71.9	89.6	64.77	56.75	39.93
730	7:15	273.2	304.8	269	246.3	164.1	256.7	175.4	93.9
800	7:45	454.6	475.9	449.3	409.8	184.3	398.7	378.1	342.6
830	8:15	604.6	544.5	608.7	562.2	237.8	559.2	506.8	474.5
900	8:45	763	713	778	731	273	717	747	640.6
930	9:15	916	945	935	885	234.9	879	981	798
1000	9:45	1064	1098	1081	1033	195	1027	768	947
1030	10:15	1207	1214	1223	1171	129.6	1153	656.5	1101
1100	10:45	1304	1412	1348	1289	139.6	1284	1000	1282
1130	11:15	1413	1472	1450	1395	122.9	1392	937	1492
1200	11:45	1480	1552	1526	1486	190.3	1476	1064	1551
1230	12:15	1583	1626	1588	1550	362.2	1536	860	1566
1300	12:45	1620	1655	1624	1598	775	1570	1425	1505
1330	13:15	1638	1653	1644	1617	1138	1588	1674	1485
1400	13:45	1616	1650	1636	1611	1006	1591	1624	1405
1430	14:15	1595	1658	1608	1578	1577	1562	449.7	1405
1500	14:45	1573	1679	1555	1528	1249	1509	658.5	1444
1530	15:15	1346	1497	1477	1444	1077	1430	786	1358
1600	15:45	1192	1371	1381	1341	1016	1335	464.6	1260
1630	16:15	1100	1246	1265	1223	656.7	1219	949	1138
1700	16:45	1213	1114	1140	1102	815	1090	1239	1006
1730	17:15	929	971	995	961	800	951	1038	861
1800	17:45	543.9	820	836	806	324	796	903	706
1830	18:15	355	663.1	673.3	654.1	291.2	638.2	531.6	549.1
1900	18:45	274.8	498.8	506.7	497.1	248	475	396.8	393.6
1930	19:15	301.8	341.3	346	343.8	147.3	322.1	103.1	252.1
2000	19:45	124.7	201.4	202.2	200.1	86	183.8	69.01	108.5
MJ/m ²		25781.25	47180520				48027600	36377478	45127800
Time (hr) 8:00-20:00		8:00-20:00					8:00-20:00	8:00-20:00	8:00-20:00

Application 2, 1996 Airborne Residue

	Air Sampling Period		Intermed.	Flux (ug/m ² /hr)		Surface Temp. (C)	Ambient Temp. (C)	1/T(K) Surface	Solar Rad. J/m ² sec	WS 1 (m/s) 0.41 m	WS 2 (m/s) 0.70 m	WS 3 (m/s) 1.40 m	WS 4 (m/s) 2.8 m
	Start	End		Triclopyr	Propiconazole								
Day 7 (July 30th)	6:00	8:00	7:00	#VALUE!	#VALUE!	17.67	16.90	3.44E-03	185	0.65	0.47	0.73	0.71
Julian 212	8:01	10:00	9:00	#VALUE!	4	25.15	19.76	3.35E-03	796	1.42	0.67	1.71	1.79
	10:01	12:00	11:00	#VALUE!	19	29.50	22.55	3.30E-03	1326	1.72	1.65	2.07	2.18
	12:01	14:02	13:01	#VALUE!	30	34.49	25.55	3.25E-03	1571	1.67	1.67	1.98	2.07
	14:03	16:00	15:01	#VALUE!	20	33.66	27.89	3.26E-03	1459	1.60	1.67	1.92	1.97
	16:01	18:00	17:00	#VALUE!	23	29.09	28.74	3.31E-03	1014	1.61	1.75	2.01	2.11
	18:01	20:00	19:00	#VALUE!	#VALUE!	24.47	25.21	3.36E-03	405	2.44	2.77	3.30	3.75
Est.Total (6:00-20:00)													
Day 13 (August 5th)	6:00	8:00	7:00	#VALUE!	2	13.37	13.51	3.49E-03	156	144.53	44.70	198.88	216.93
Julian 218	8:00	10:00	9:00	#VALUE!	#VALUE!	20.21	16.00	3.41E-03	751	219.73	209.15	292.75	324.03
	10:01	12:00	11:00	#VALUE!	22	21.27	17.50	3.40E-03	914	235.23	264.35	308.70	342.50
	12:01	14:00	13:00	#VALUE!	#VALUE!	26.13	18.96	3.34E-03	1396	190.23	215.25	245.68	264.93
	14:01	16:00	15:00	#VALUE!	#VALUE!	24.98	20.31	3.35E-03	590	125.90	143.50	162.18	166.63
	16:00	18:00	17:00	#VALUE!	#VALUE!	29.79	21.82	3.30E-03	1032	150.30	173.65	194.93	203.10
	18:01	20:24	19:12	#VALUE!	#VALUE!	18.08	20.57	3.43E-03	275	139.13	161.35	185.03	196.58
Est.Total (6:00-20:00)													
Day 21 (August 13th)	6:00	8:45	7:22	#VALUE!	#VALUE!	14.37	13.60	3.48E-03	120	47.15	47.80	50.73	45.90
Julian 226	8:00	10:00	9:00	#VALUE!	#VALUE!	24.69	20.10	3.36E-03	715	82.83	56.85	99.48	89.58
	10:01	12:01	11:01	#VALUE!	#VALUE!	32.77	25.32	3.27E-03	1357	122.48	128.70	147.30	144.23
	12:10	14:00	13:05	#VALUE!	#VALUE!	38.06	28.85	3.21E-03	1490	109.98	122.63	129.80	125.28
	14:01	16:02	15:01	#VALUE!	#VALUE!	36.12	31.95	3.23E-03	1367	78.90	99.58	102.03	90.30
	16:02	18:01	17:01	#VALUE!	#VALUE!	33.31	32.15	3.26E-03	928	216.48	247.20	287.00	311.90
Est.Total (6:00-20:00)													

Application 2, 1996 Airborne Residue

All diffusion coefficients adjusted for temperature using $[T(K)/T(25^{\circ}C)]^{1.75}$

Application 2, 1996

										WS 1 (m/s)	WS 2 (m/s)	WS 3 (m/s)	WS 4 (m/s)
										0.41 m	0.70 m	1.40 m	2.8 m
										41	70	140	280
Air Sampling Period		Intermed.	Flux (ug/m ² /hr)		Surface	Ambient	1/T(K)	Solar Rad.					
Day 0 (July 23rd)	Start	End	Time	Triclopyr	Propiconazole	Temp. (C)	Temp. (C)	Surface	J/m ² sec				
Julian 205	6:15	8:03	7:09	66	17	19.26	17.47	3.42E-03	205	0.51	0.64	0.57	0.51
	8:03	10:00	9:01	323	42	28.62	24.04	3.31E-03	837	0.94	1.04	1.03	1.02
	10:00	12:00	11:00	414	147	34.80	27.07	3.25E-03	1351	1.35	1.40	1.53	1.54
	12:00	14:00	13:00	303	202	38.71	30.59	3.21E-03	1614	1.39	1.45	1.63	1.66
	14:00	16:00	15:00	121	145	38.77	33.51	3.21E-03	1427	1.46	1.44	1.70	1.69
	16:01	18:00	17:00	66	72	35.13	34.83	3.24E-03	946	1.30	1.30	1.51	1.47
	18:01	20:01	19:01	35	19	29.62	31.52	3.30E-03	264	1.59	1.75	2.03	2.19
	20:04	6:00	13:02	3	1	19.74	20.62	3.41E-03	3	0.64	0.70	0.76	0.73
Est.Total (6:00-20:00)				2656	1290								
Day 1 (July 24th)	6:01	8:00	7:00	7	6	19.51	17.46	3.42E-03	226	0.49	0.53	0.53	0.48
Julian 206	8:01	10:00	9:00	39	31	30.22	24.03	3.30E-03	825	0.66	0.76	0.68	0.60
	10:01	12:00	11:00	47	142	38.10	28.77	3.21E-03	1413	0.98	1.10	1.13	1.15
	12:02	14:00	13:01	26	87	40.79	31.43	3.19E-03	1646	1.23	1.29	1.41	1.38
	14:00	16:00	15:00	15	78	40.21	33.93	3.19E-03	1551	1.27	1.34	1.46	1.46
	16:00	18:00	17:00	9	56	34.57	34.10	3.25E-03	1038	1.65	1.78	2.05	2.18
	18:01	20:00	19:00	#VALUE!	24	28.73	31.18	3.31E-03	426	2.33	2.59	3.03	3.39
	20:00	6:00	13:00	0	1	18.67	18.91	3.43E-03	4	0.62	0.68	0.75	0.72
Est.Total (6:00-20:00)				286	801								
Day 2 (July 25th)	6:01	8:00	7:00	#VALUE!	3	17.77	15.44	3.44E-03	200	0.51	0.57	0.65	0.55
Julian 207	8:12	10:00	9:06	6	18	29.12	21.40	3.31E-03	851	0.79	0.87	0.90	0.79
	10:01	12:00	11:00	5	41	35.41	26.62	3.24E-03	1387	1.16	1.13	0.97	1.32
	12:00	13:55	12:57	4	59	38.42	30.05	3.21E-03	1623	1.51	1.27	0.81	1.86
	13:55	16:00	14:57	4	75	37.53	33.04	3.22E-03	1505	1.45	1.50	1.71	1.76
	16:01	18:00	17:00	#VALUE!	33	32.04	33.84	3.28E-03	1059	1.55	1.55	1.84	1.85
	18:01	20:00	19:00	#VALUE!	20	28.19	33.25	3.32E-03	432	1.28	1.42	1.65	1.75
	20:01	6:00	13:00	0	#VALUE!	19.02	19.19	3.42E-03	4	0.72	0.86	0.96	0.97
Day 3 (July 26th)	12:00	14:00	13:00	#VALUE!	43	41.24	30.72	3.18E-03	1594	1.01	1.16	1.21	1.14
Julian 208													
Day 5 (July 28th)	12:00	14:00	13:00	#VALUE!	8	26.80	20.94	3.33E-03	820	0.93	0.97	1.15	1.15
Julian 210													

Appendix 6: Application 2, 1996

Source File: app296summary

T1.App.2,96
Ch,96,2,0,SR.FI
Ch,96,2,0,T.F
Ch,96,2,0,SR.T
Ch,96,2,0,WS.FI
Ch,96,2,1,SR.FI
Ch,96,2,1,T.FI
Ch,96,2,1,SR.T
Ch,96,2,1,WS.FI
Ch,96,2,2,SR.FI
Ch,96,2,2,T.FI
Ch,96,2,2,SR.T
Ch,96,2,2,WS.FI
Ch,96,2,7,SR.FI
Ch,96,2,7,T.FI
Ch,96,2,7,SR.T
Ch,95,2,7,WS.FI

Source File: fluxratio3.xls

CCTrpyr,96,2,0.7
CCTrpyr,96,2,0
CCTrpyr,96,2,1
CCTrpyr,96,2,2
CCPr,96,2,0.7
CCPr,96,2,0
CCPr,96,2,1
CCPr,96,2,2
CCPr,96,2,7

Source File: app296summary

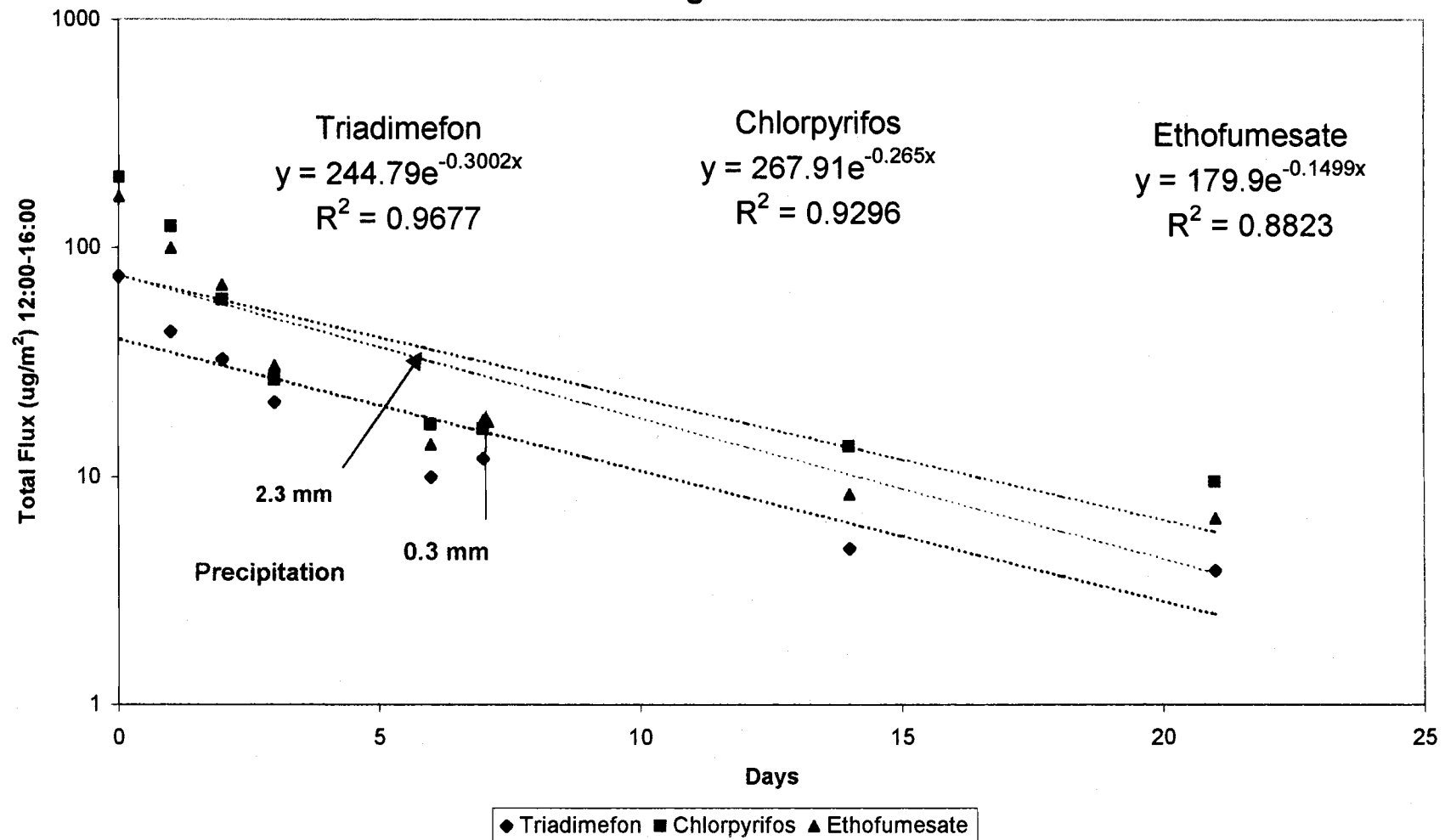
Solar Rad
Temp
Wind
Precip
Pk Flux Noon
Ch,PkFxNoon
Ch,logPkFxNoon

Peak Solar Radiation normalized Flux (Flux/S.R.)

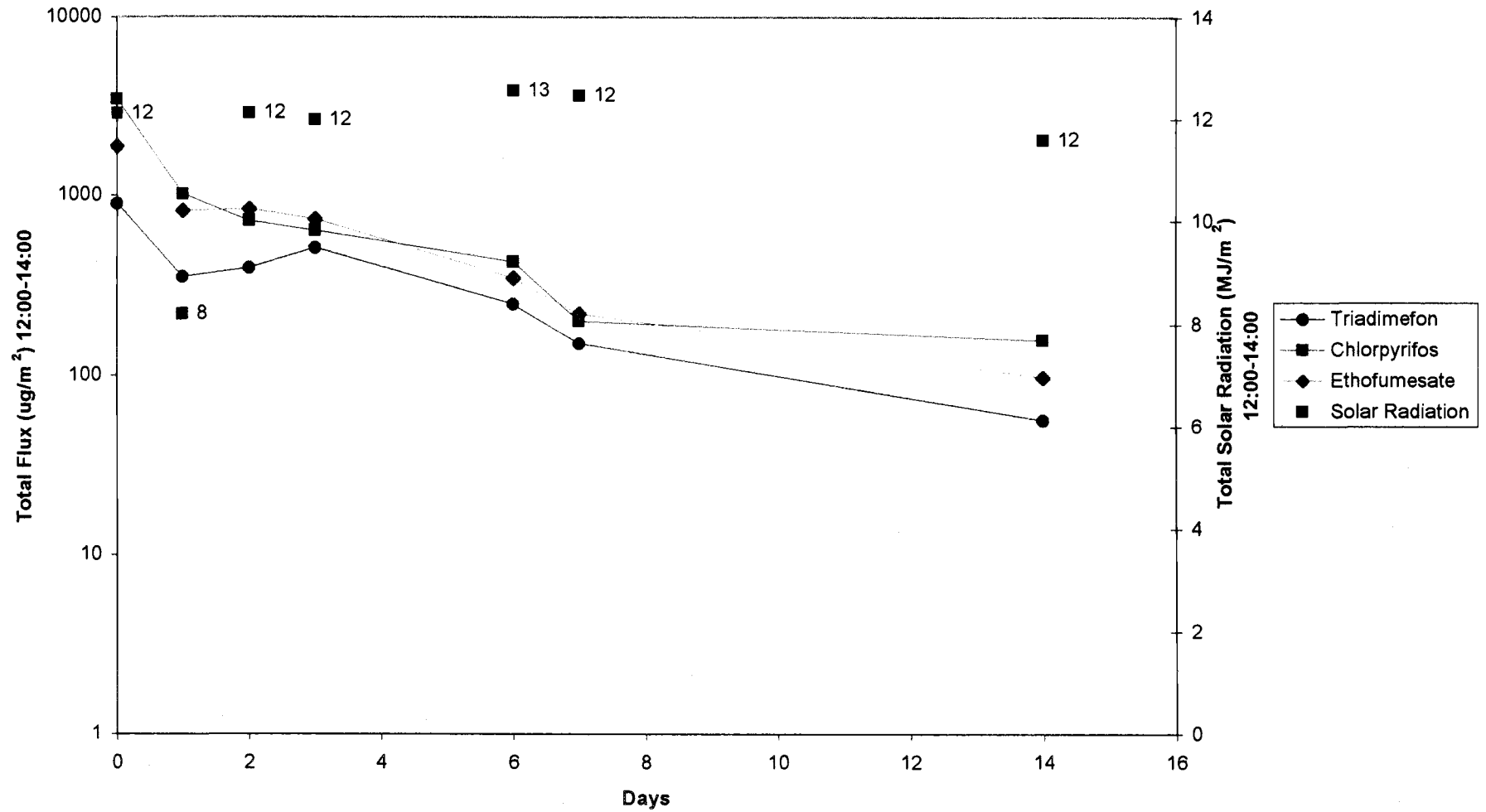
12:00-14:00

following Application 1, June 12th 1996

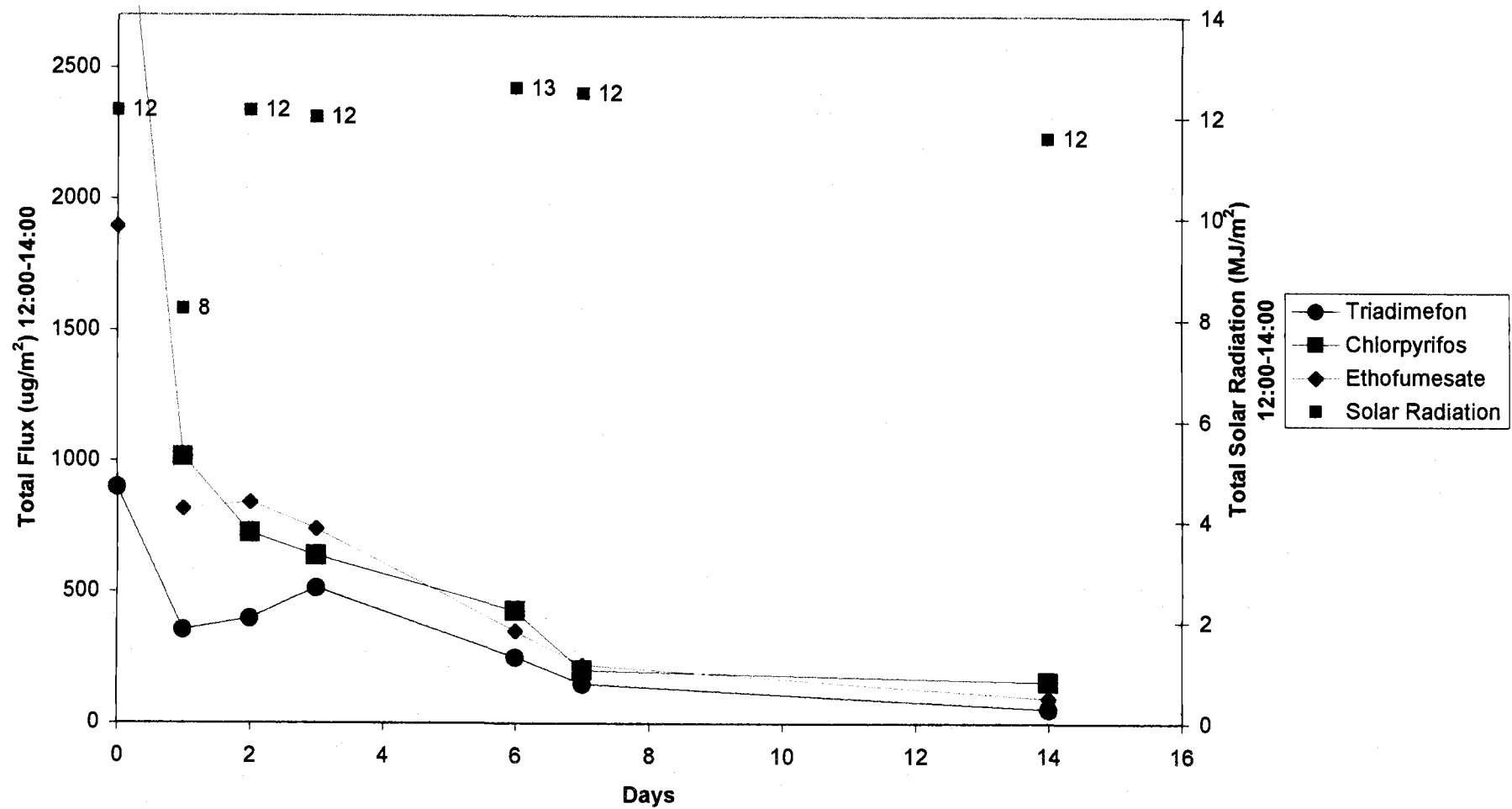
log scale



Peak Flux ($\mu\text{g}/\text{m}^2$) during 12:00-14:00
following Application 1, June 12th 1996
log scale



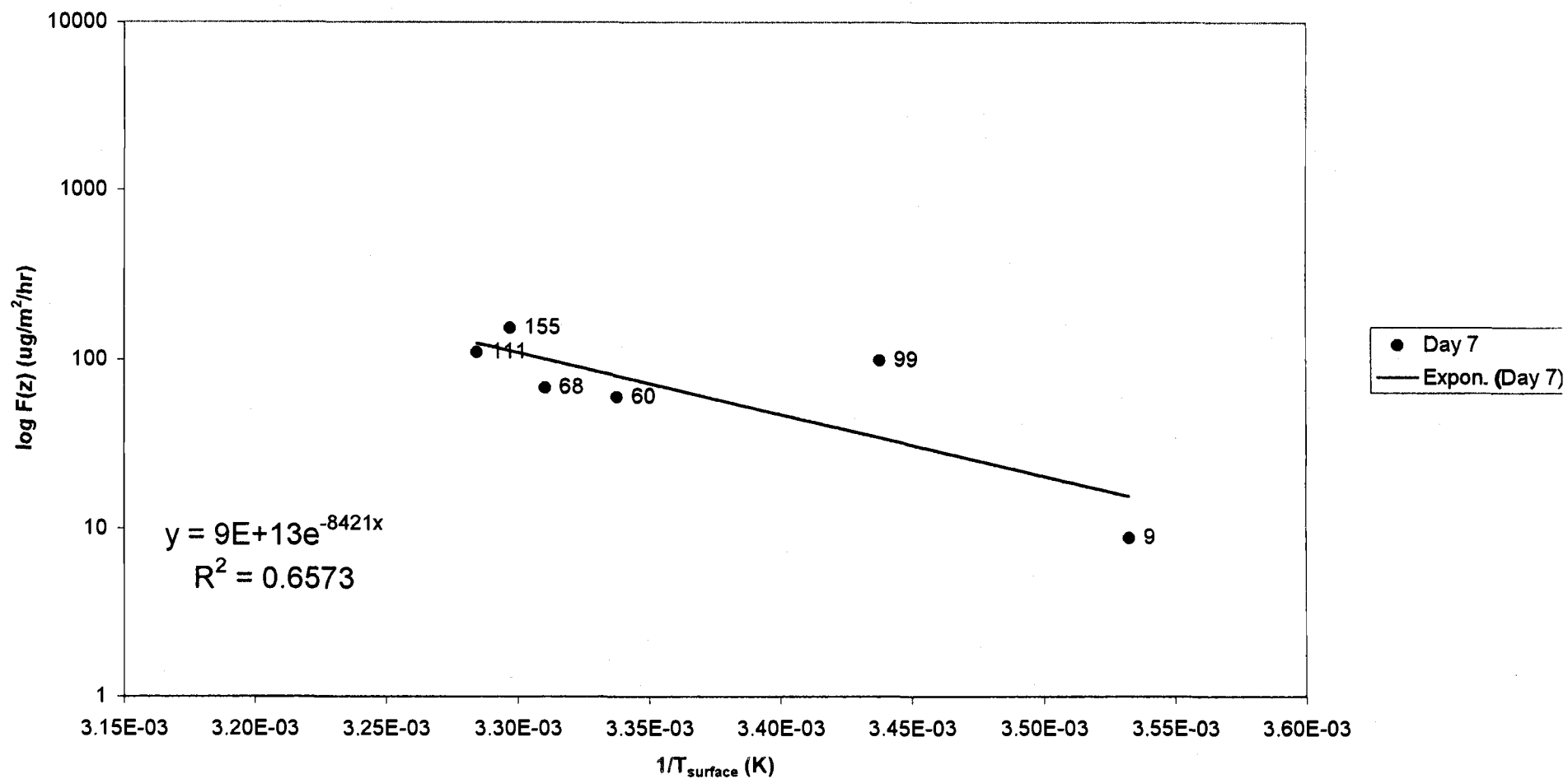
**Peak Flux ($\mu\text{g}/\text{m}^2$) during 12:00-14:00
following Application 1, June 12th 1996**



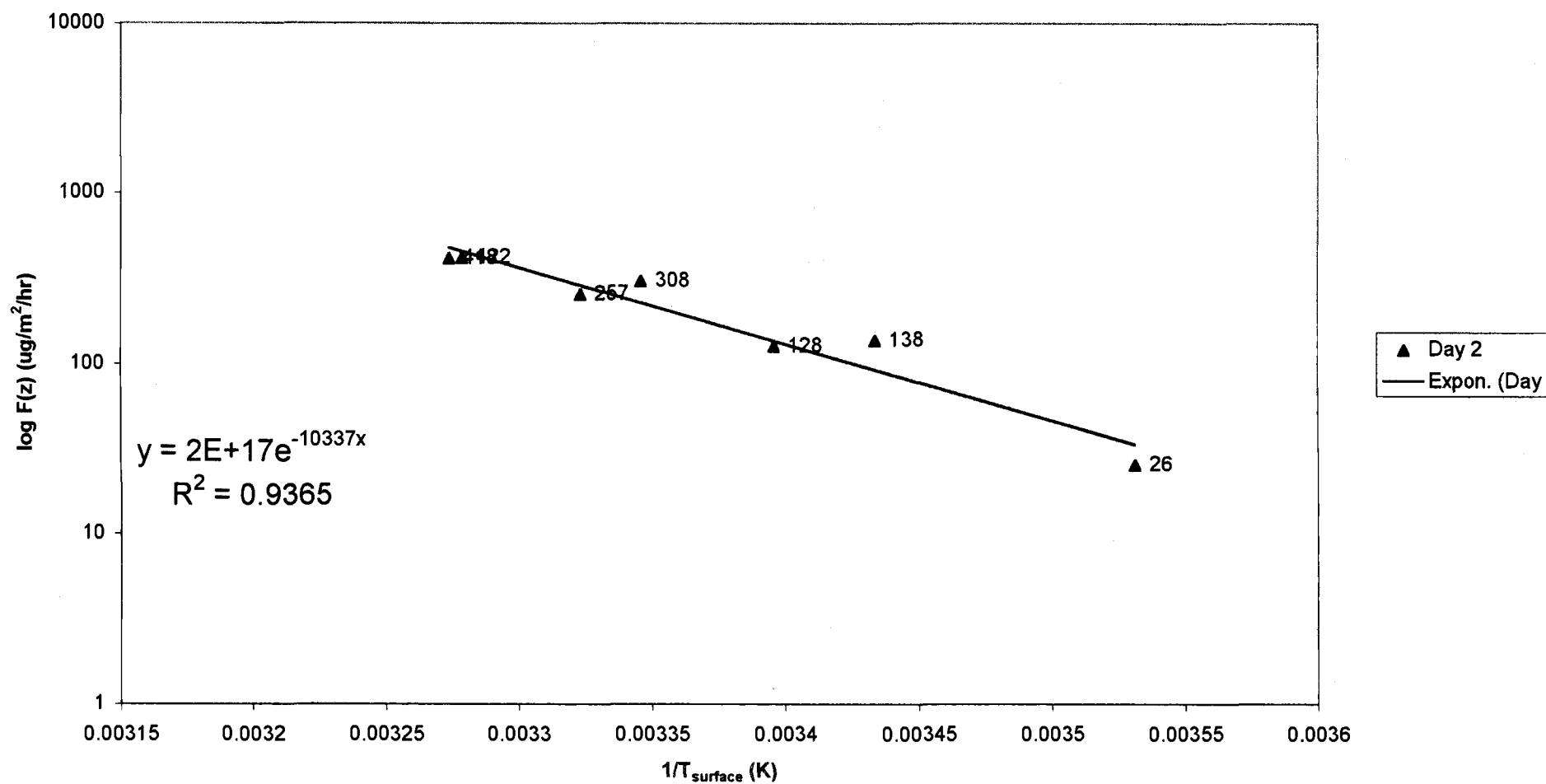
Peak Flux Values during 12:00-16:00 on Days 0,1,2,3,6,7,14,21
Application 1, 1996

Day	Total Flux (ug/m ²) 12:00-14:00			Total Solar Radiation 12:00-14:00 (MJ/m ²)		Flux/Solar Radiation (ug/MJ)		
	Triadimefon	Chlorpyrifos	Ethofumesate			Triadimefon	Chlorpyrifos	Ethofumesate
0	811	2183	1797	11		76	204	167
1	356	1016	818	8		43	124	100
2	399	725	843	12		33	60	70
3	258	320	371	12		21	27	31
6	126	215	176	13		10	17	14
7	151	203	222	12		12	16	18
14	57	159	98	12		5	14	8
21	32	78	54	8		4	9	7

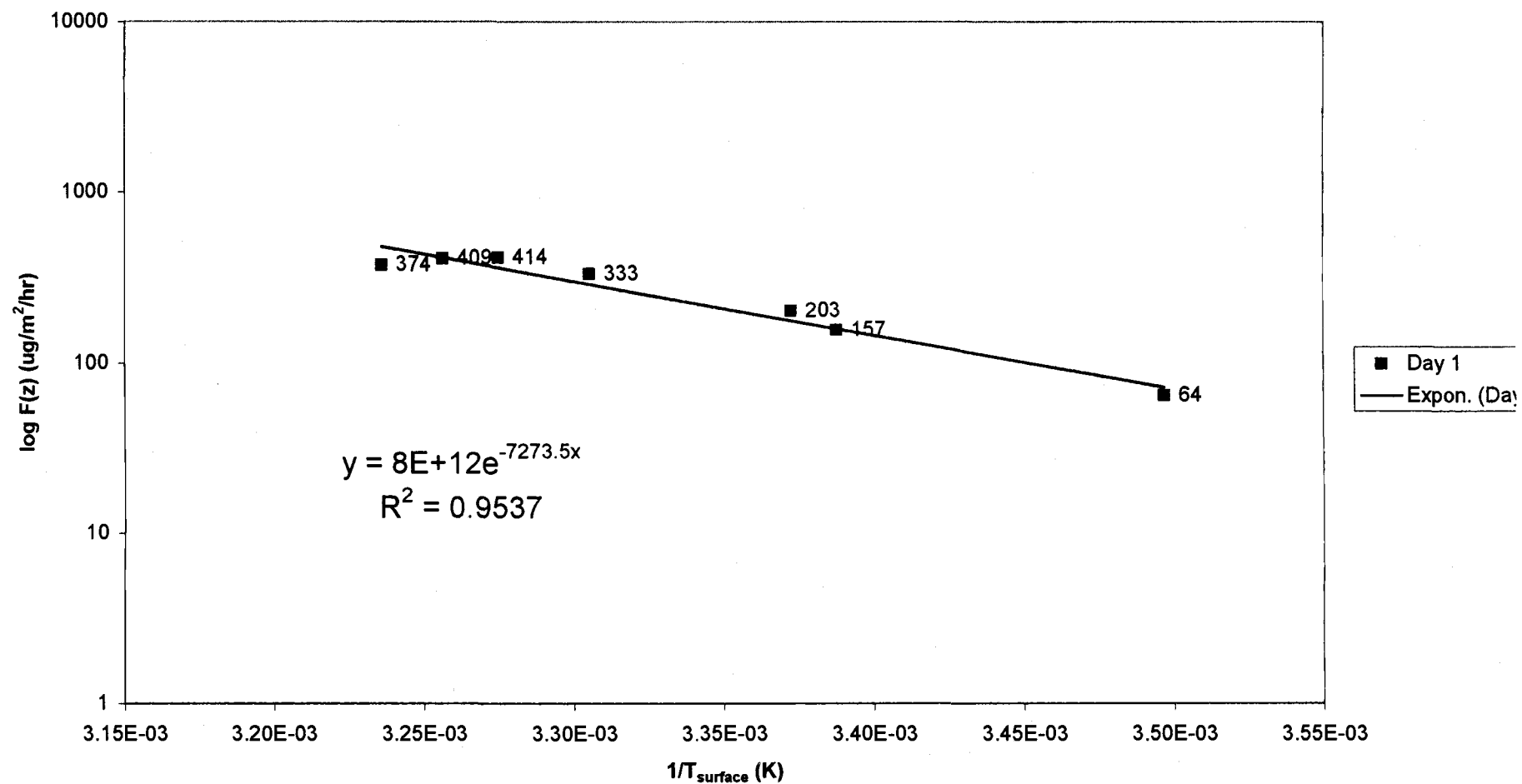
Ethofumesate: Flux ($\mu\text{g}/\text{m}^2/\text{hr}$) vs. $1/T_{\text{surface}}$ (K)
Day 7, App.1 '96 June 19, Julian 171



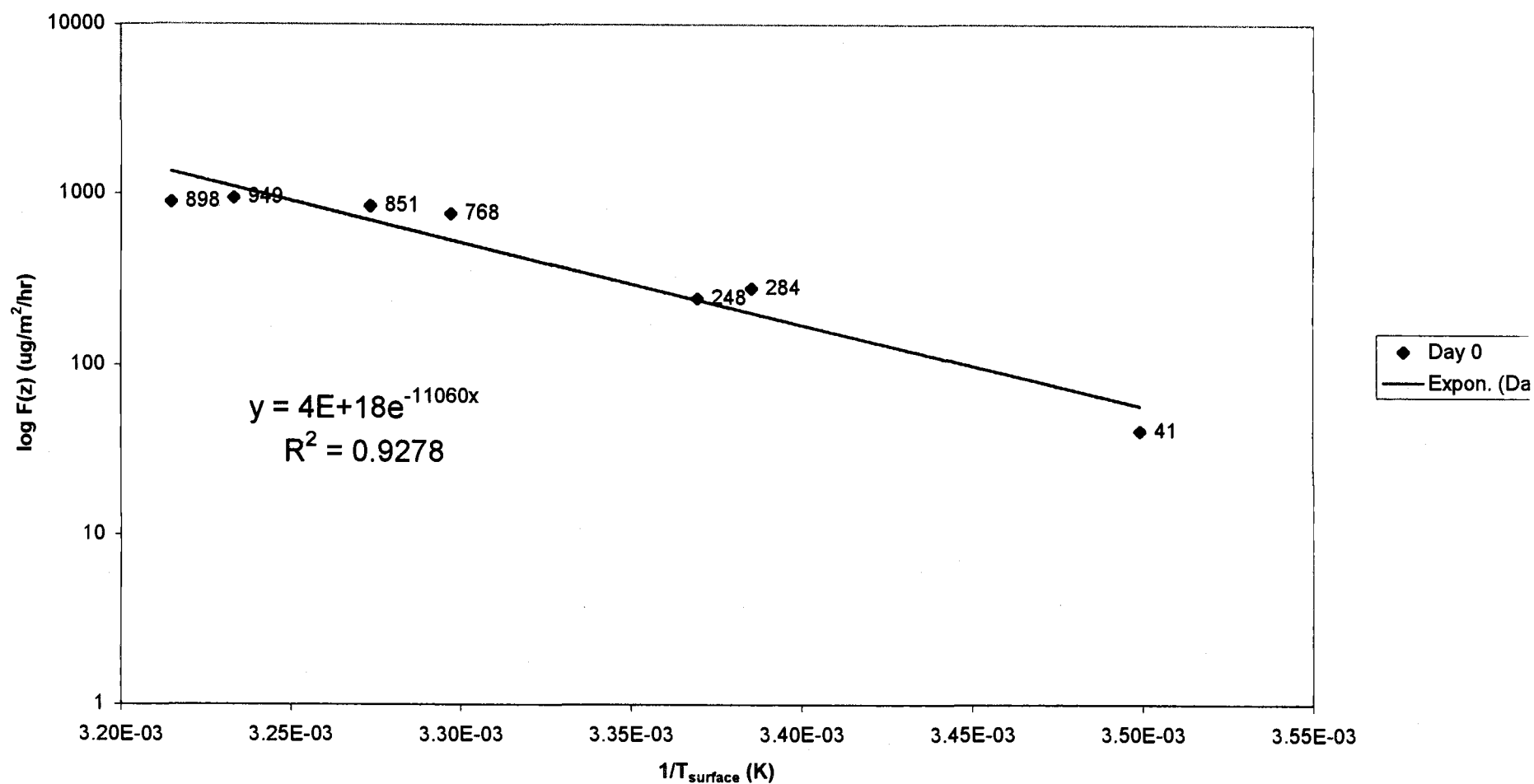
Ethofumesate: Flux (ug/m²/hr) vs. 1/T_{surface} (K)
Day 2, App.1 '96 June 14, Julian 171



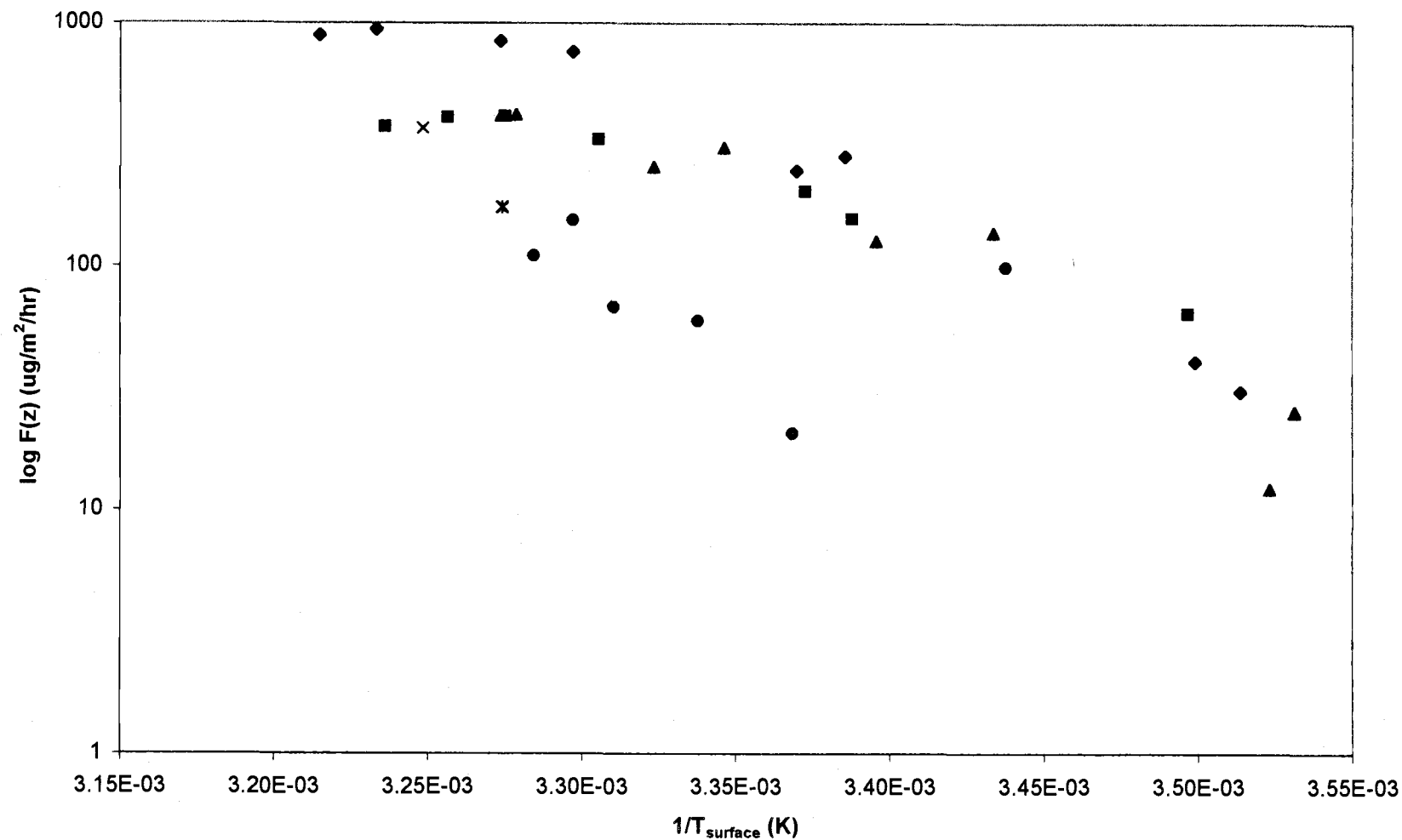
Ethofumesate: Flux (ug/m²/hr) vs. 1/T_{surface} (K)
Day 1, App.1 '96 June 13, Julian 165



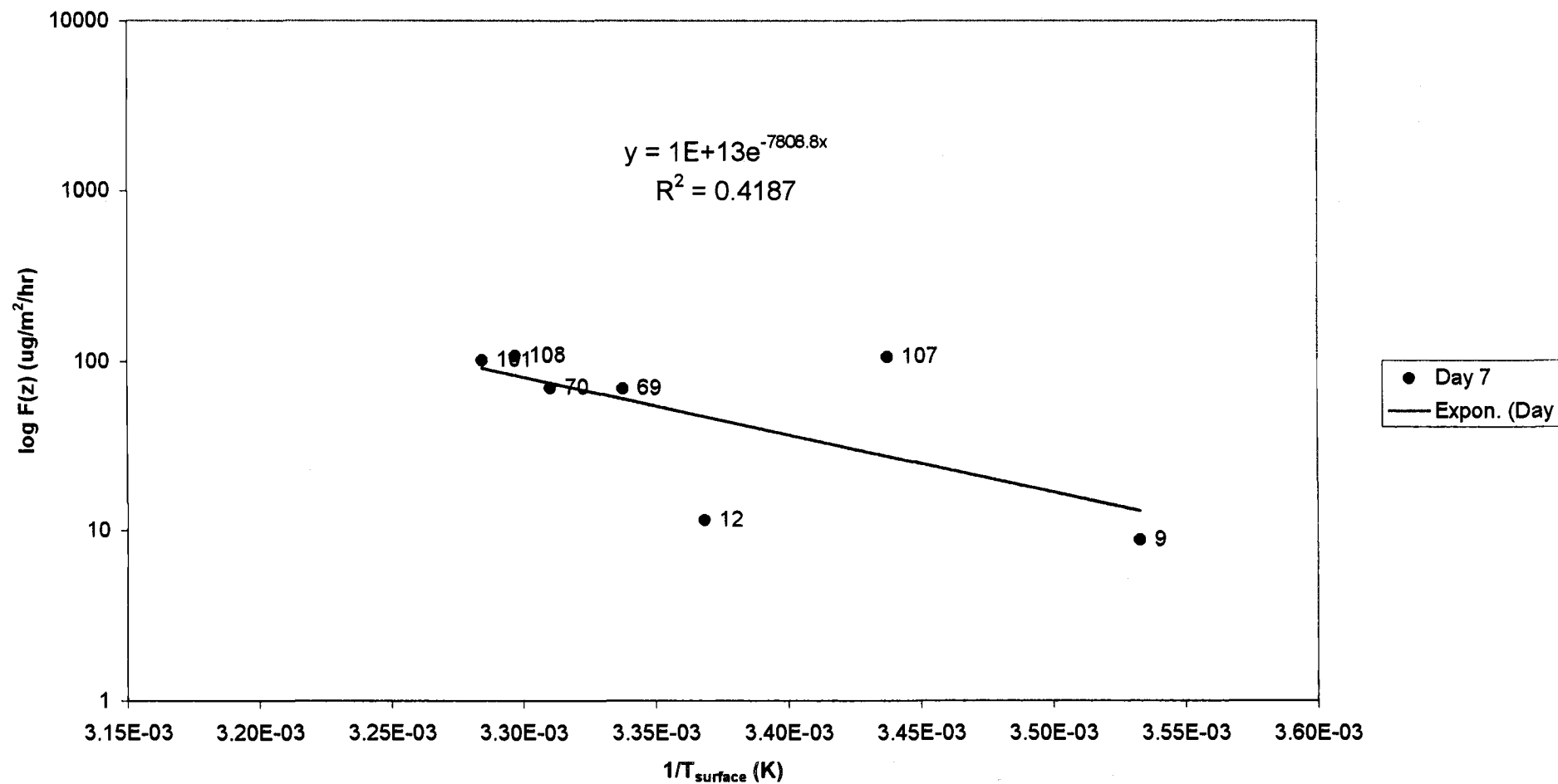
Ethofumesate: Flux ($\mu\text{g}/\text{m}^2/\text{hr}$) vs. $1/T_{\text{surface}}$ (K)
Day 0, App.1 '96 June 12, Julian 164



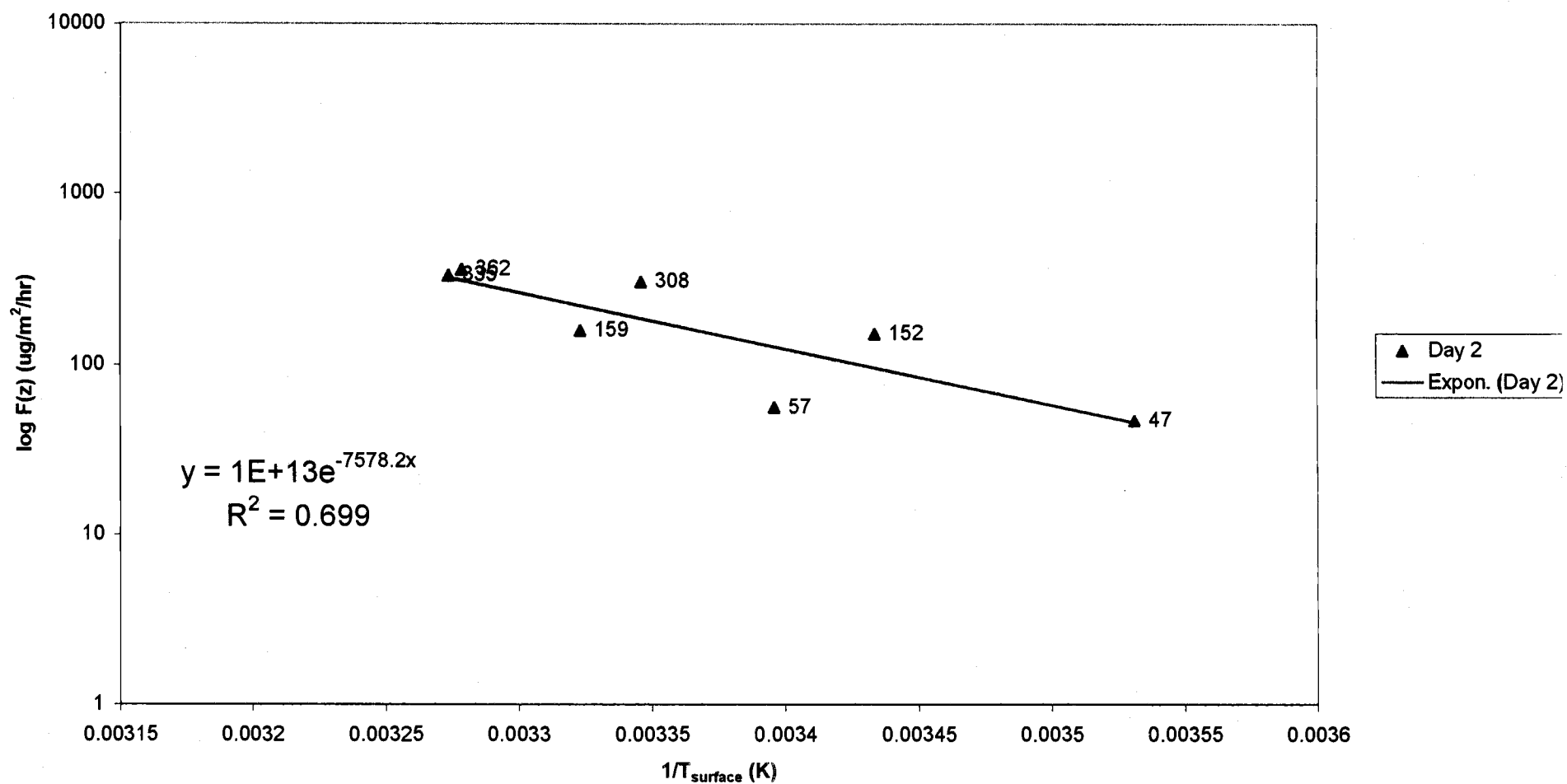
Ethofumesate: Flux ($\mu\text{g}/\text{m}^2/\text{hr}$) vs. $1/T_{\text{surface}}$ (K)
Day 0-7, App.1 '96 June 12-19, Julian 164-171



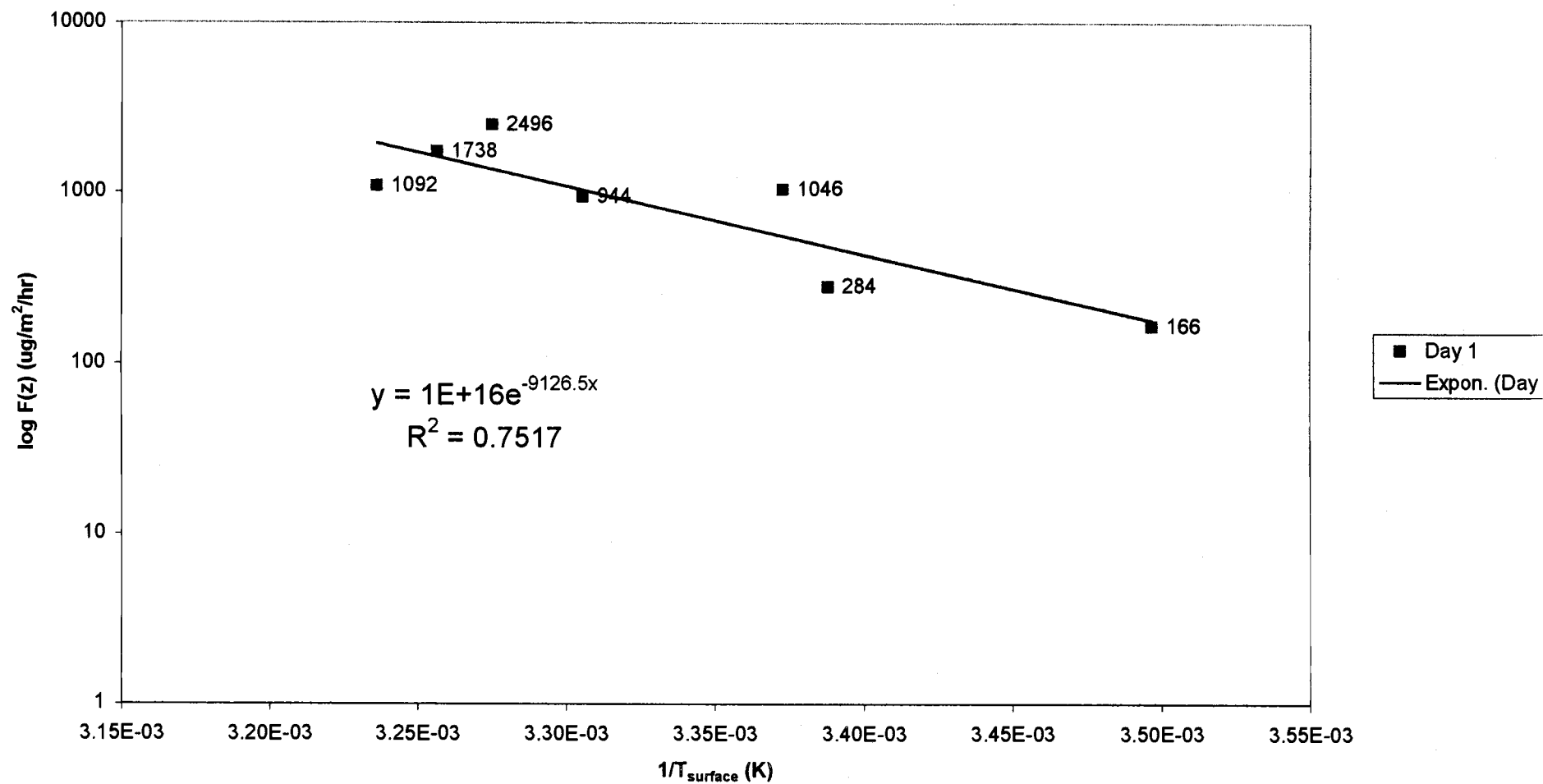
Chlorpyrifos: Flux ($\mu\text{g}/\text{m}^2/\text{hr}$) vs. $1/T_{\text{surface}}$ (K)
 Day 7, App.1 '96 June 19, Julian 171



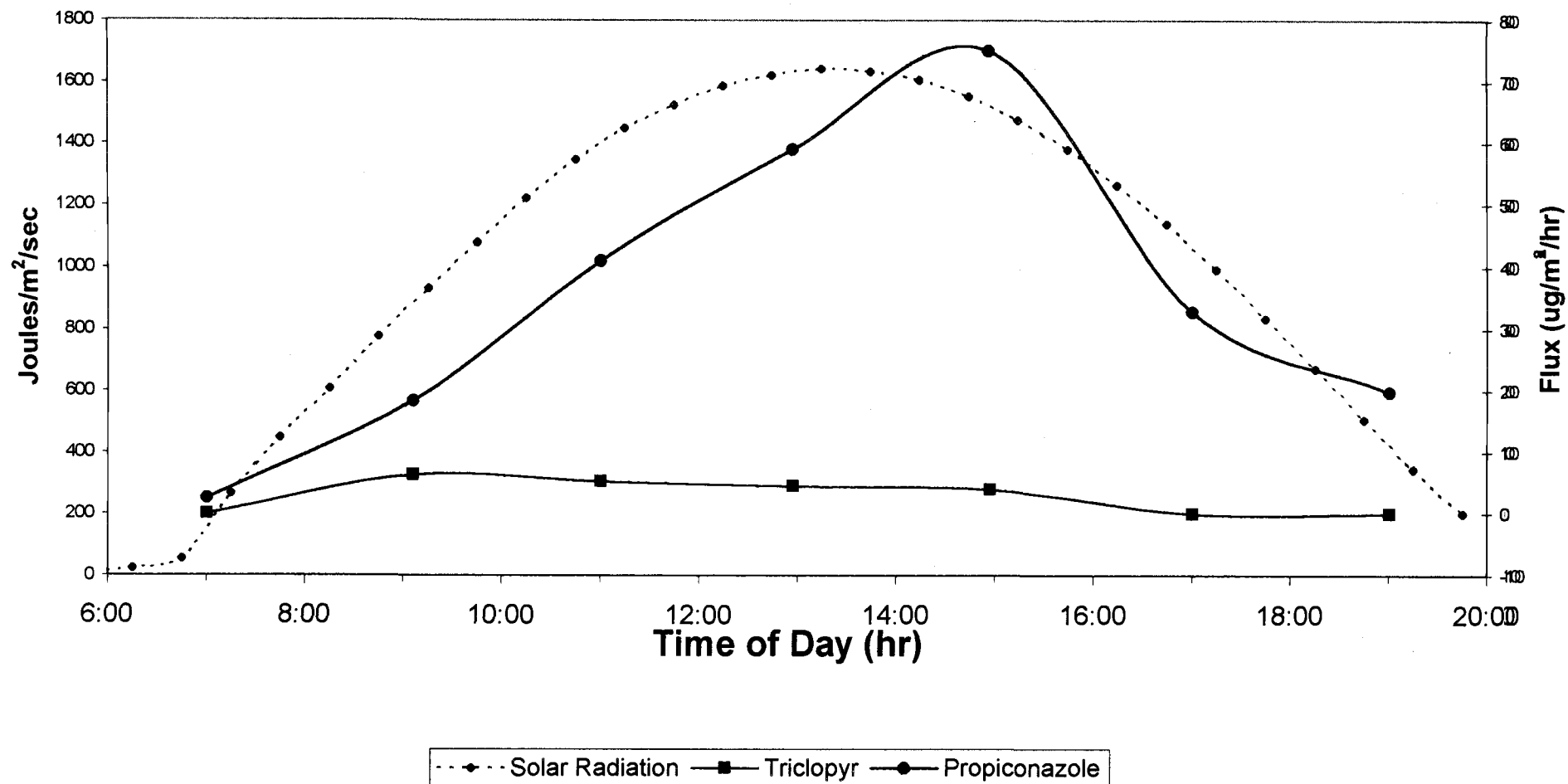
Chlorpyrifos: Flux ($\mu\text{g}/\text{m}^2/\text{hr}$) vs. $1/T_{\text{surface}}$ (K)
Day 2, App.1 '96 June 14, Julian 166



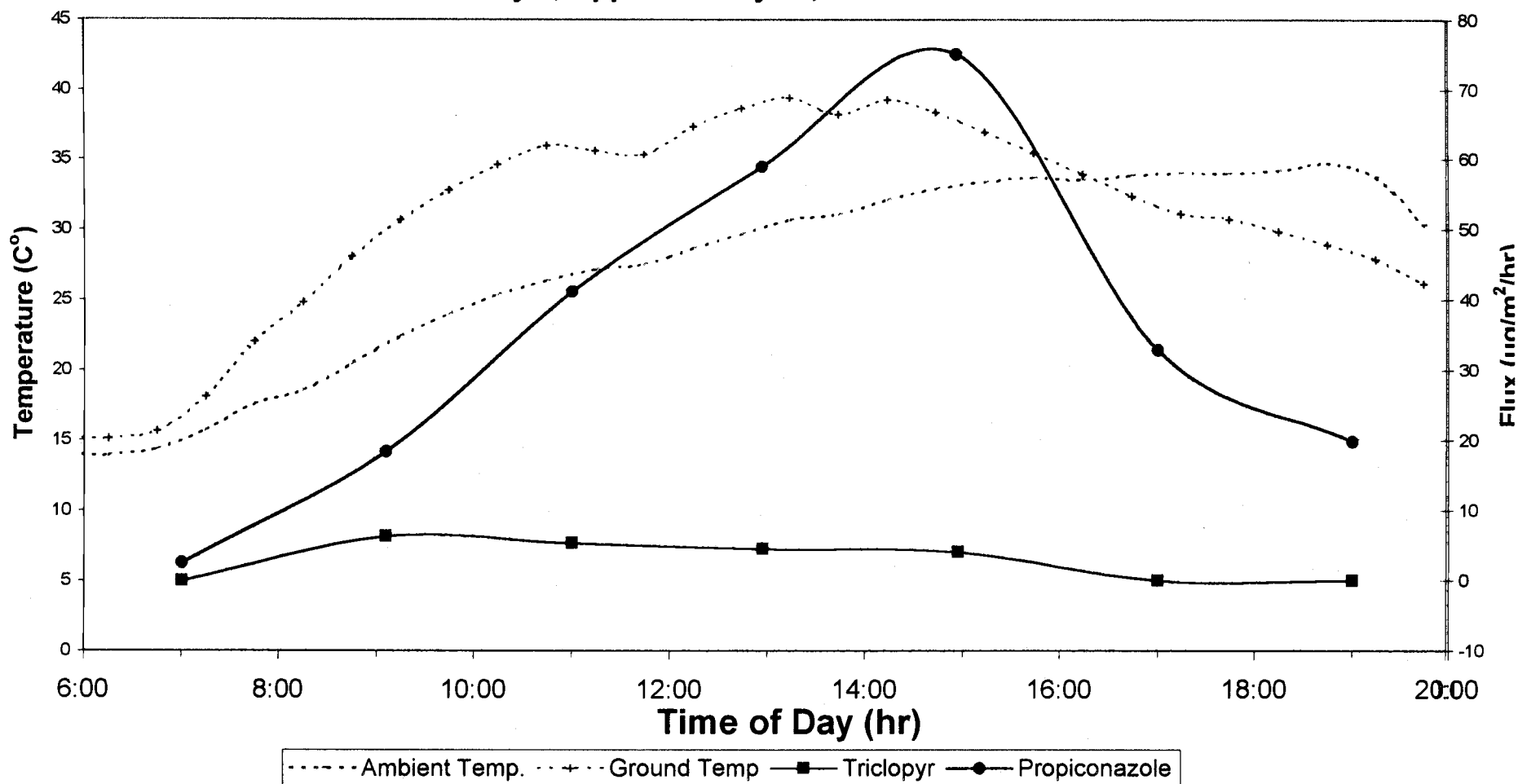
Chlorpyrifos: Flux ($\mu\text{g}/\text{m}^2/\text{hr}$) vs. $1/T_{\text{surface}}$ (K)
Day 1, App.1 '96 June 13, Julian 165



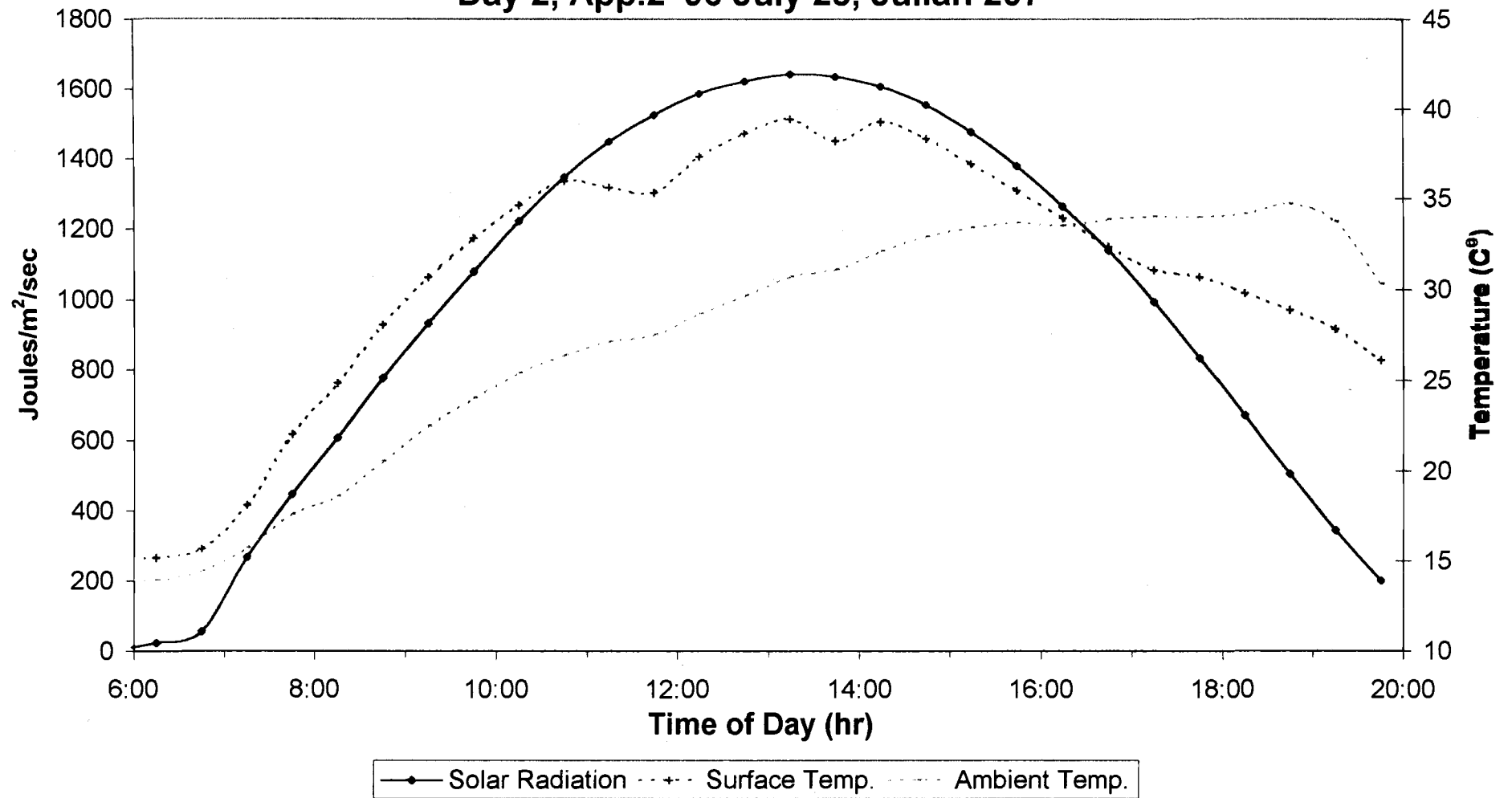
Solar Radiation vs. Flux **Day 2, App.2 '96 July 25, Julian 207**



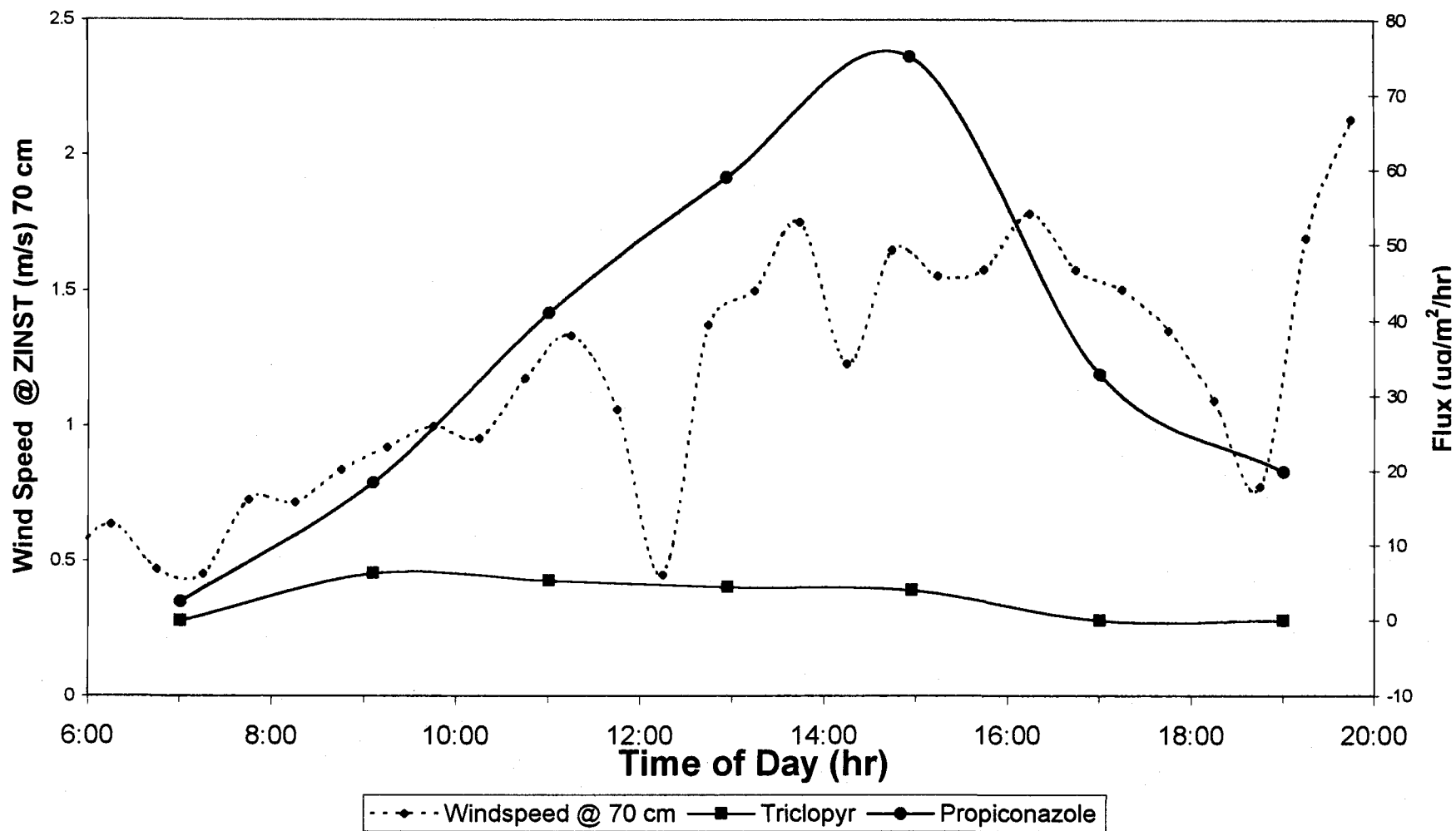
Flux and Temperature (C°)
Day 2, App.2 '96 July 25, Julian 207



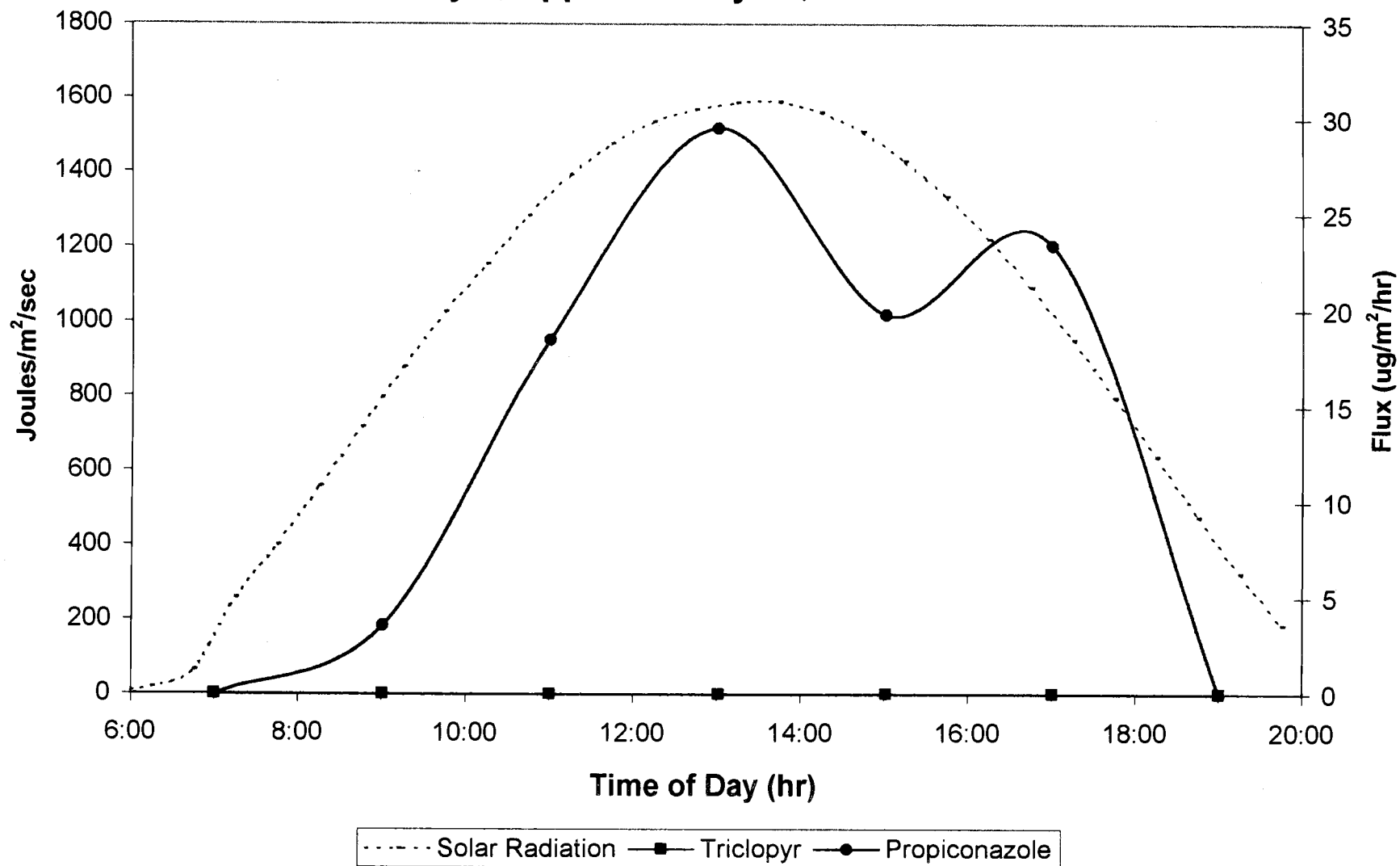
Solar Radiation and Temperature Day 2, App.2 '96 July 25, Julian 207



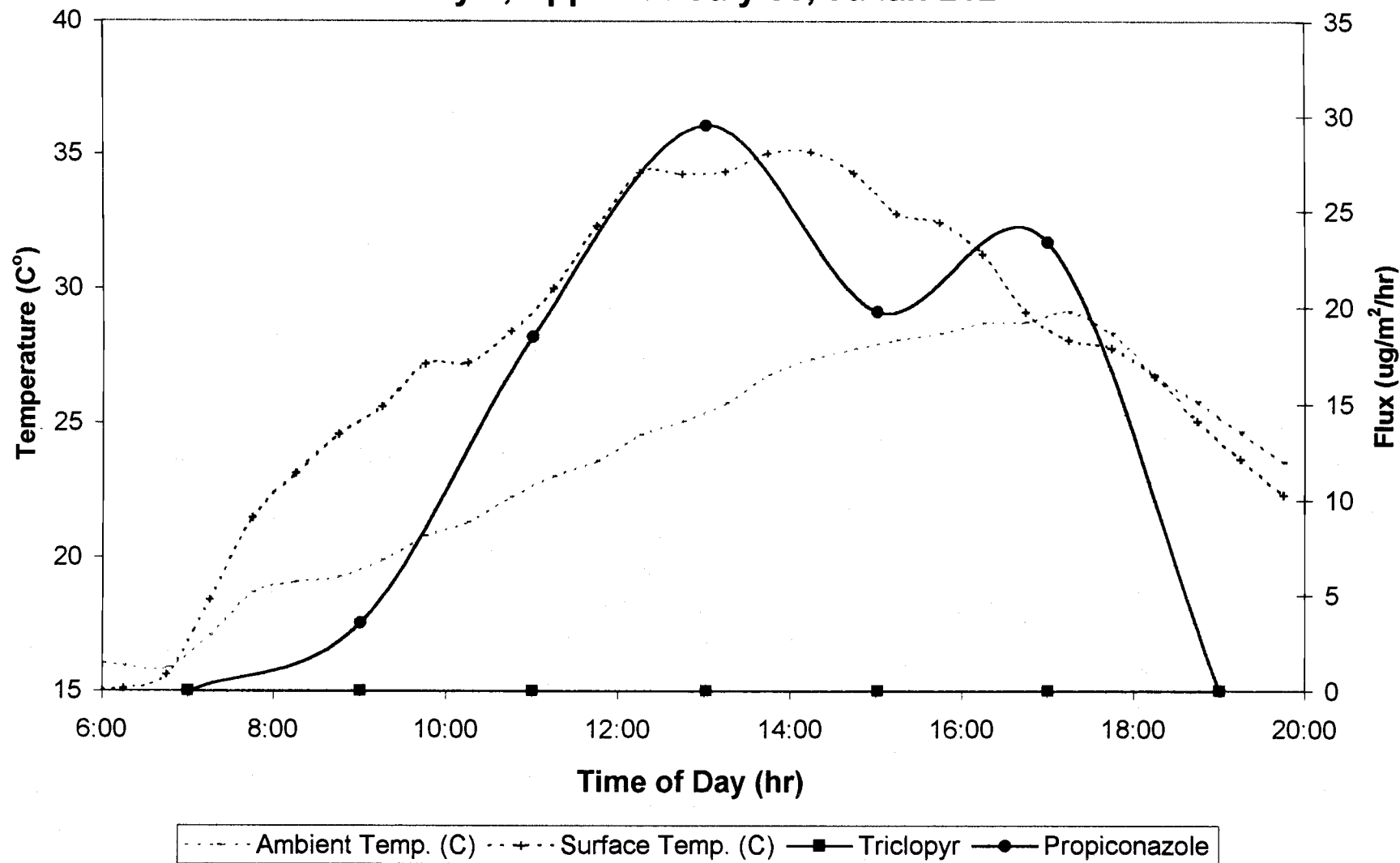
Windspeed @ Height ZINST (70 cm) and Flux
Day 2, App.2 '96 July 25, Julian 207



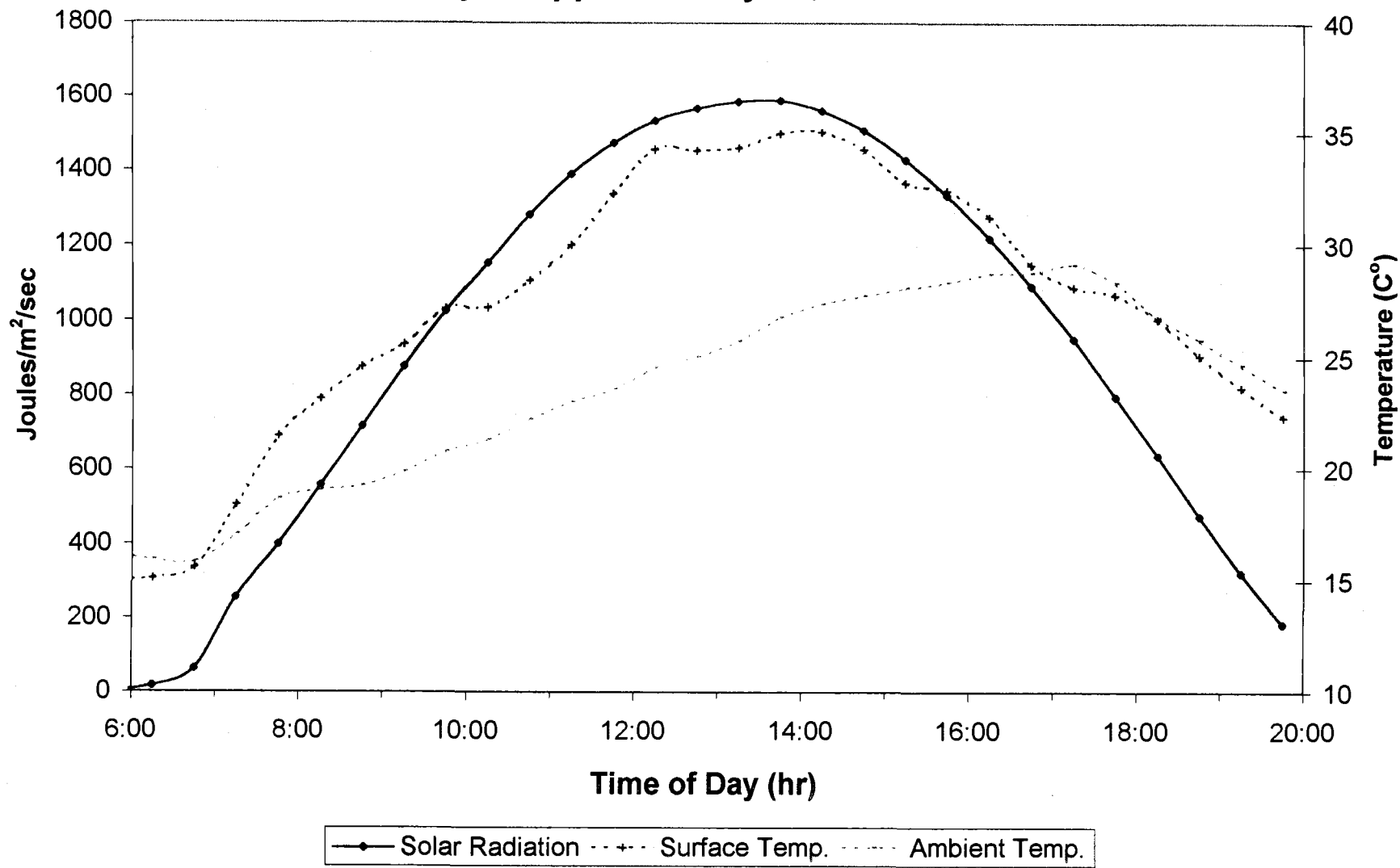
Solar Radiation and Flux
Day 7, App.2 '96 July 30, Julian 212



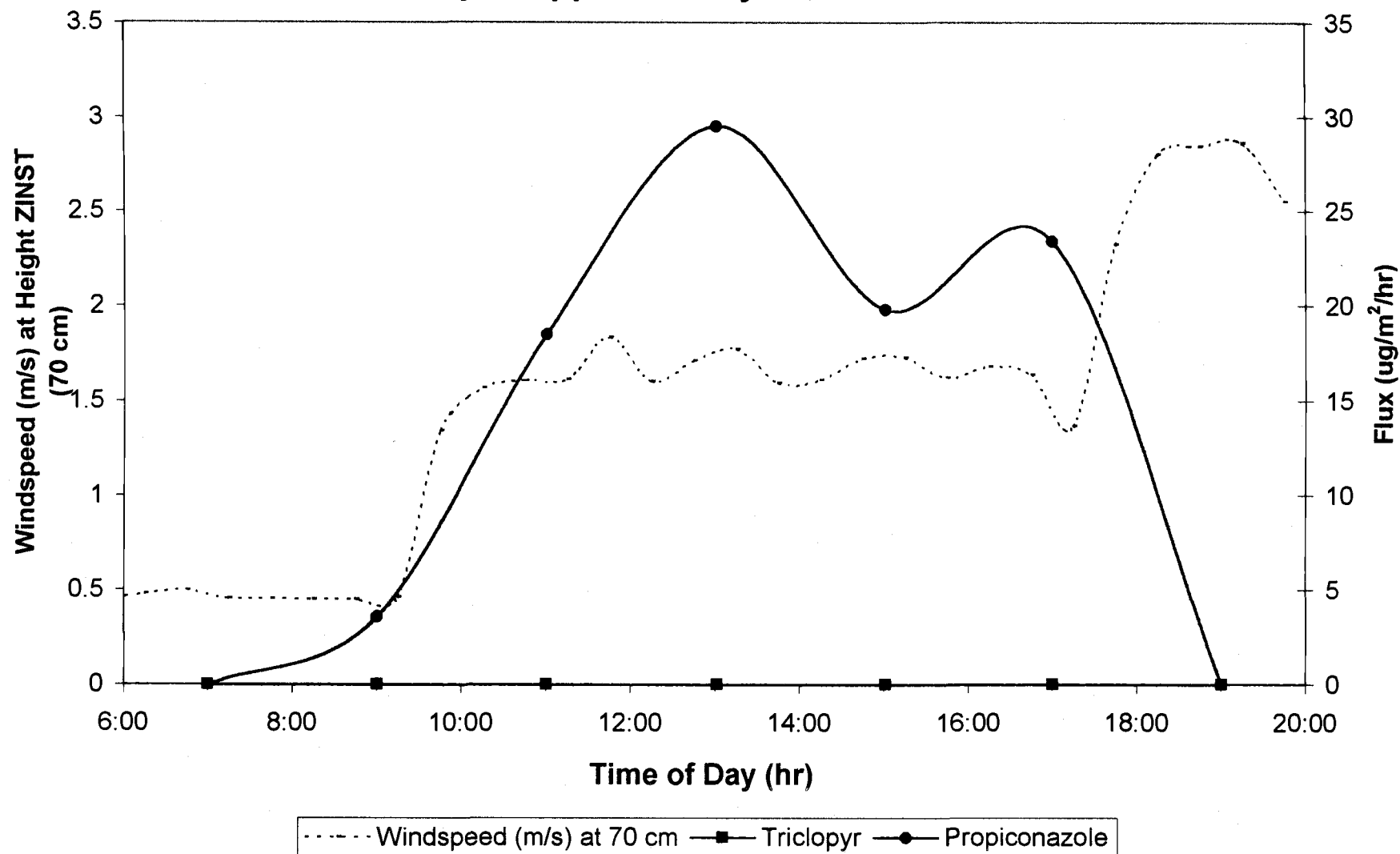
Flux and Temperature (C°) Day 7, App.2 '96 July 30, Julian 212



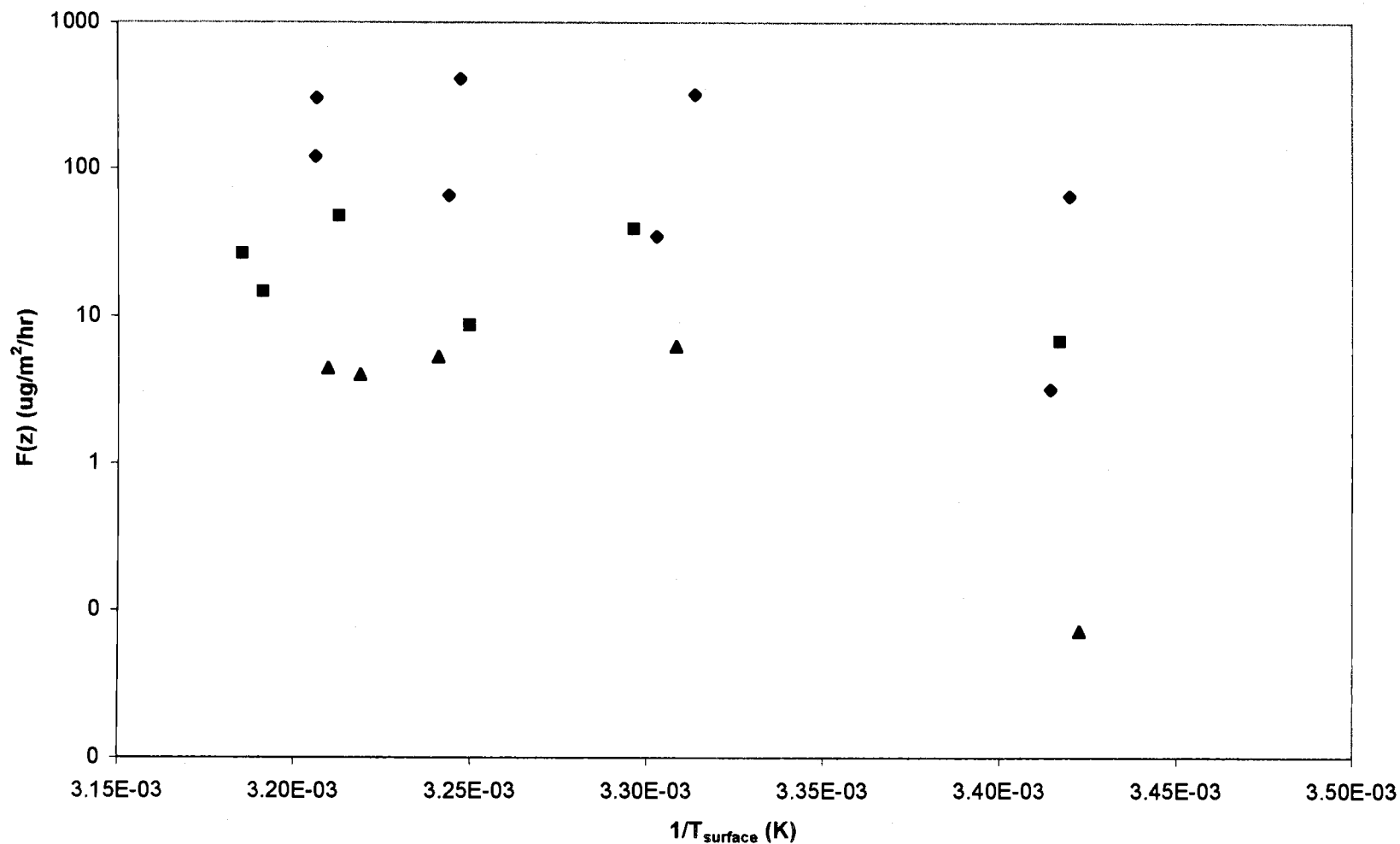
Solar Radiation and Temperature **Day 7, App.2 '96 July 30, Julian 212**



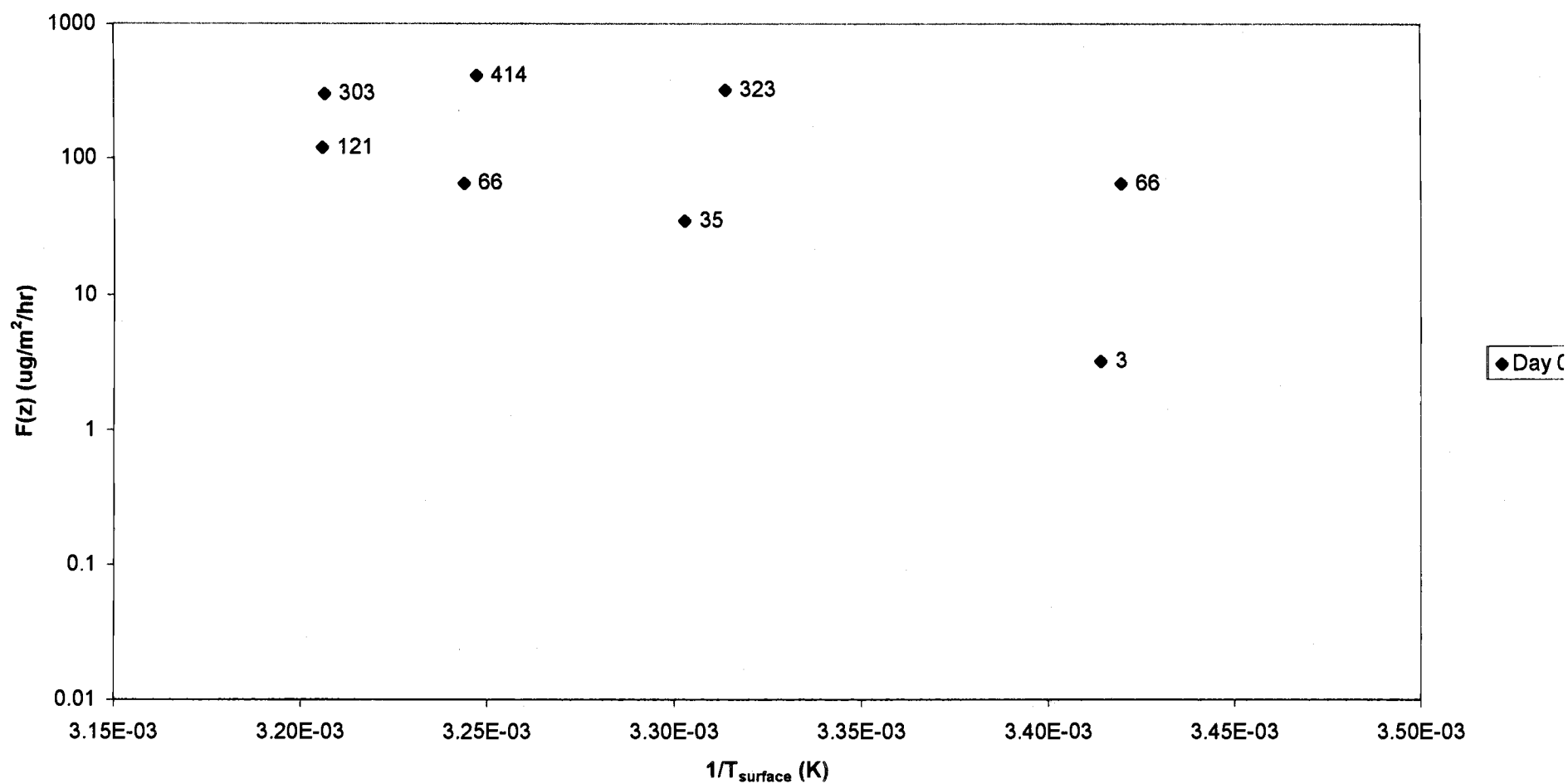
Windspeed and Flux Day 7, App.2 '96 July 30, Julian 212



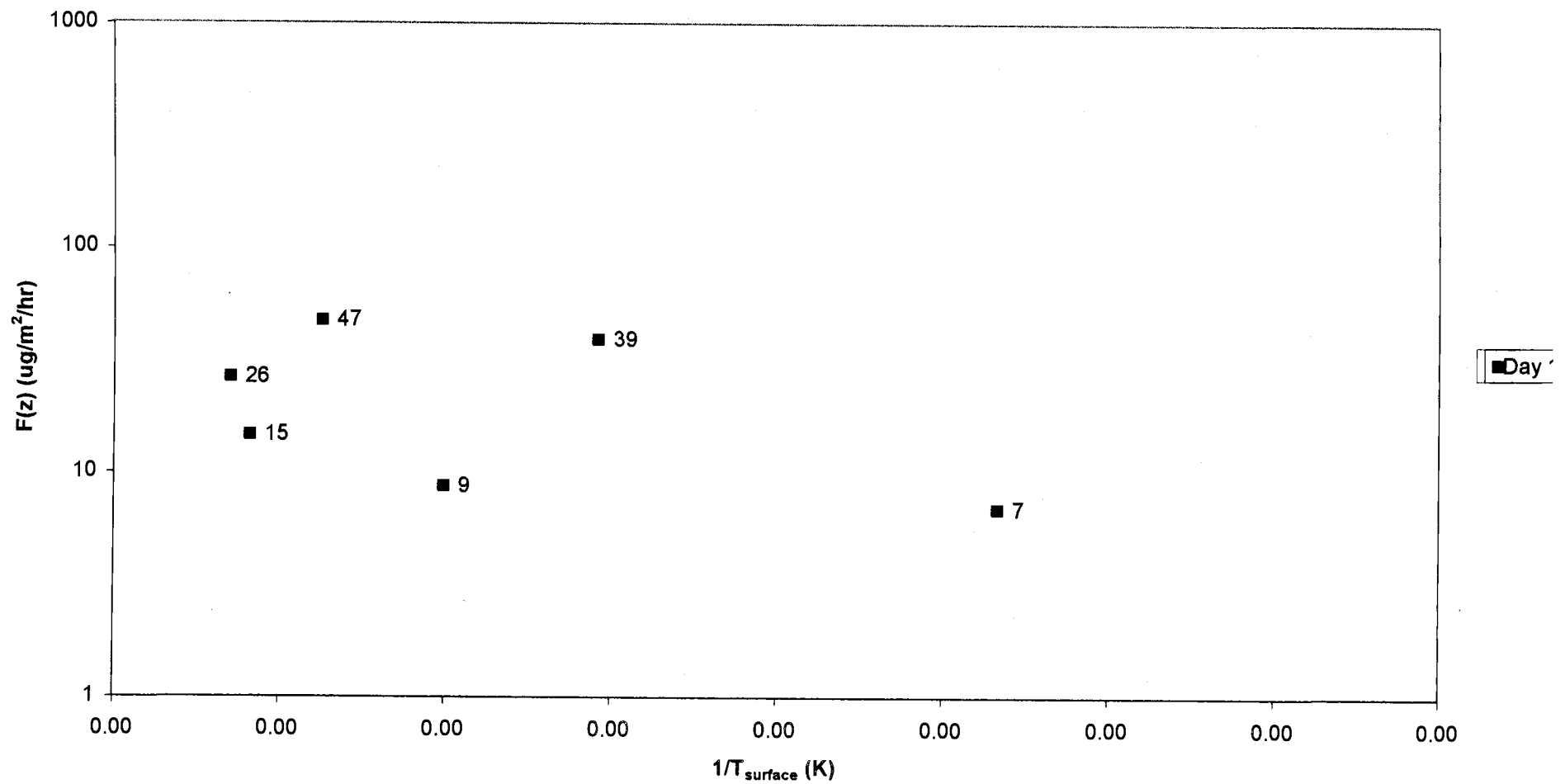
Triclopyr: Flux ($\mu\text{g}/\text{m}^2/\text{hr}$) vs. $1/T_{\text{surface}}$ (K)
 Day 0-7, App.2 '96 July 23-30, Julian 205-212



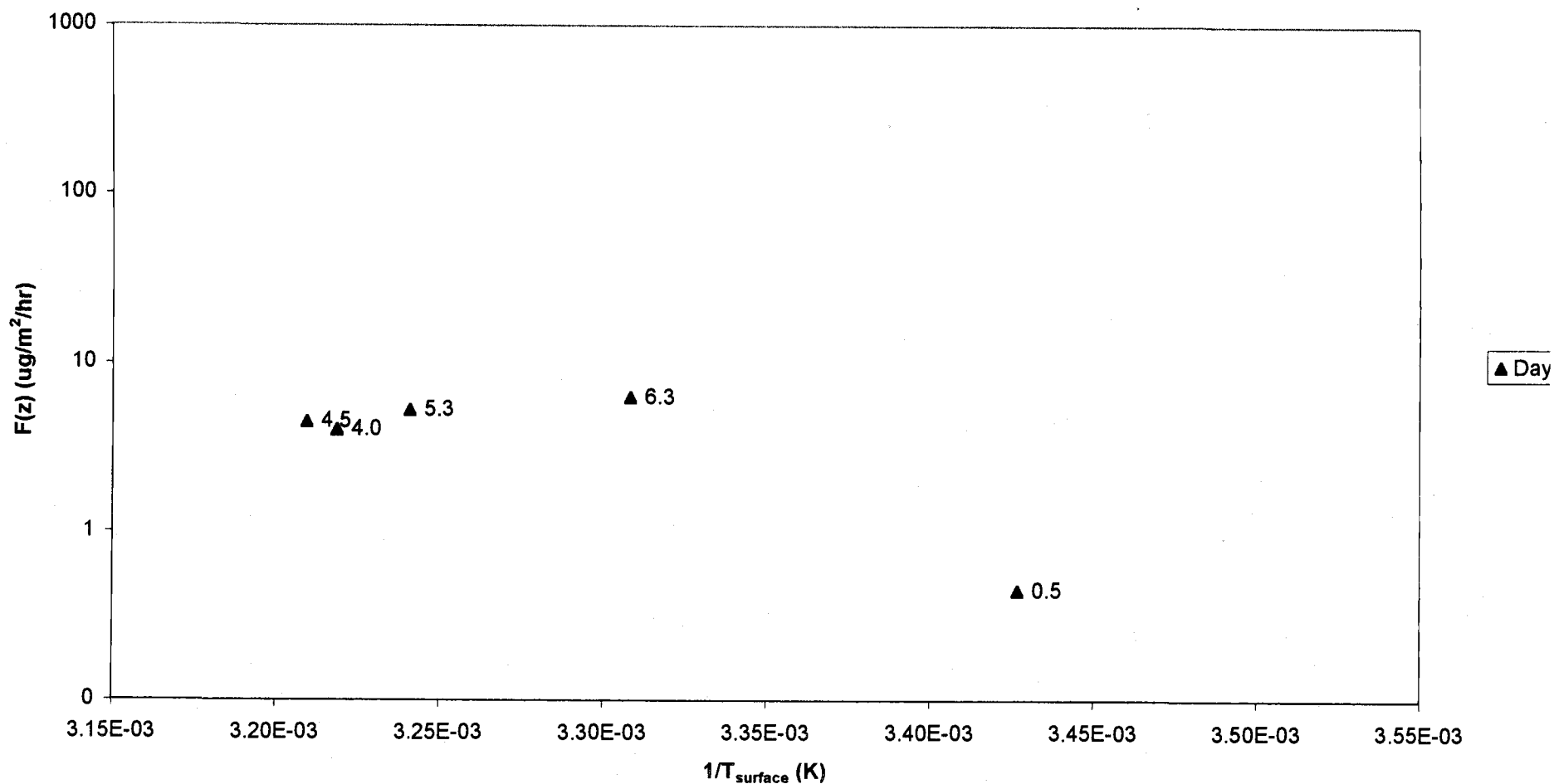
Triclopyr: Flux ($\mu\text{g}/\text{m}^2/\text{hr}$) vs. $1/T_{\text{surface}}$ (K)
Day 0, App.2 '96 July 23, Julian 205



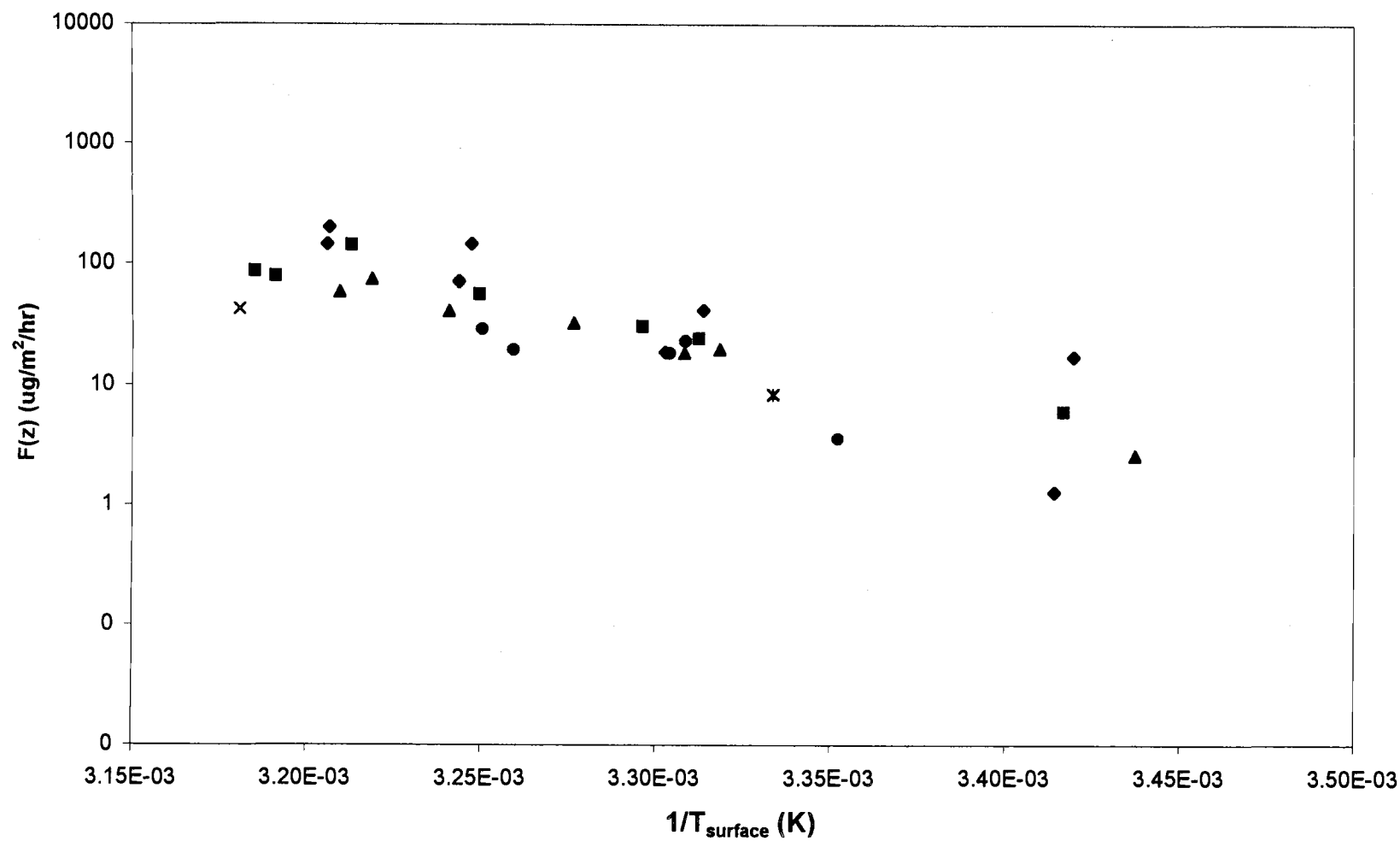
Triclopyr: Flux ($\mu\text{g}/\text{m}^2/\text{hr}$) vs. $1/T_{\text{surface}}$ (K)
Day 1, App.2 '96 July 24, Julian 206



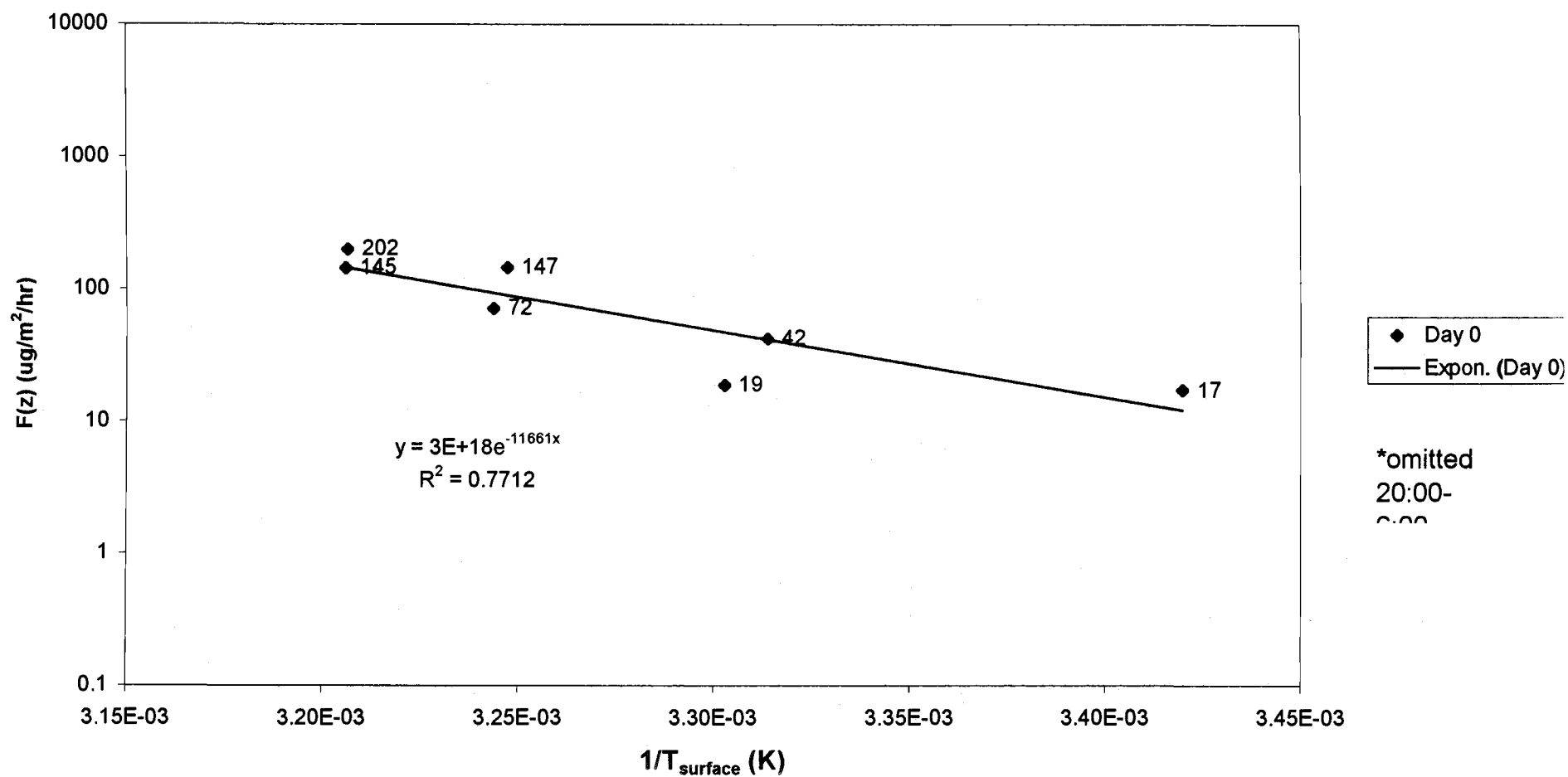
Triclopyr: Flux ($\mu\text{g}/\text{m}^2/\text{hr}$) vs. $1/T_{\text{surface}}$ (K)
Day 2, App.2 '96 July 25, Julian 207



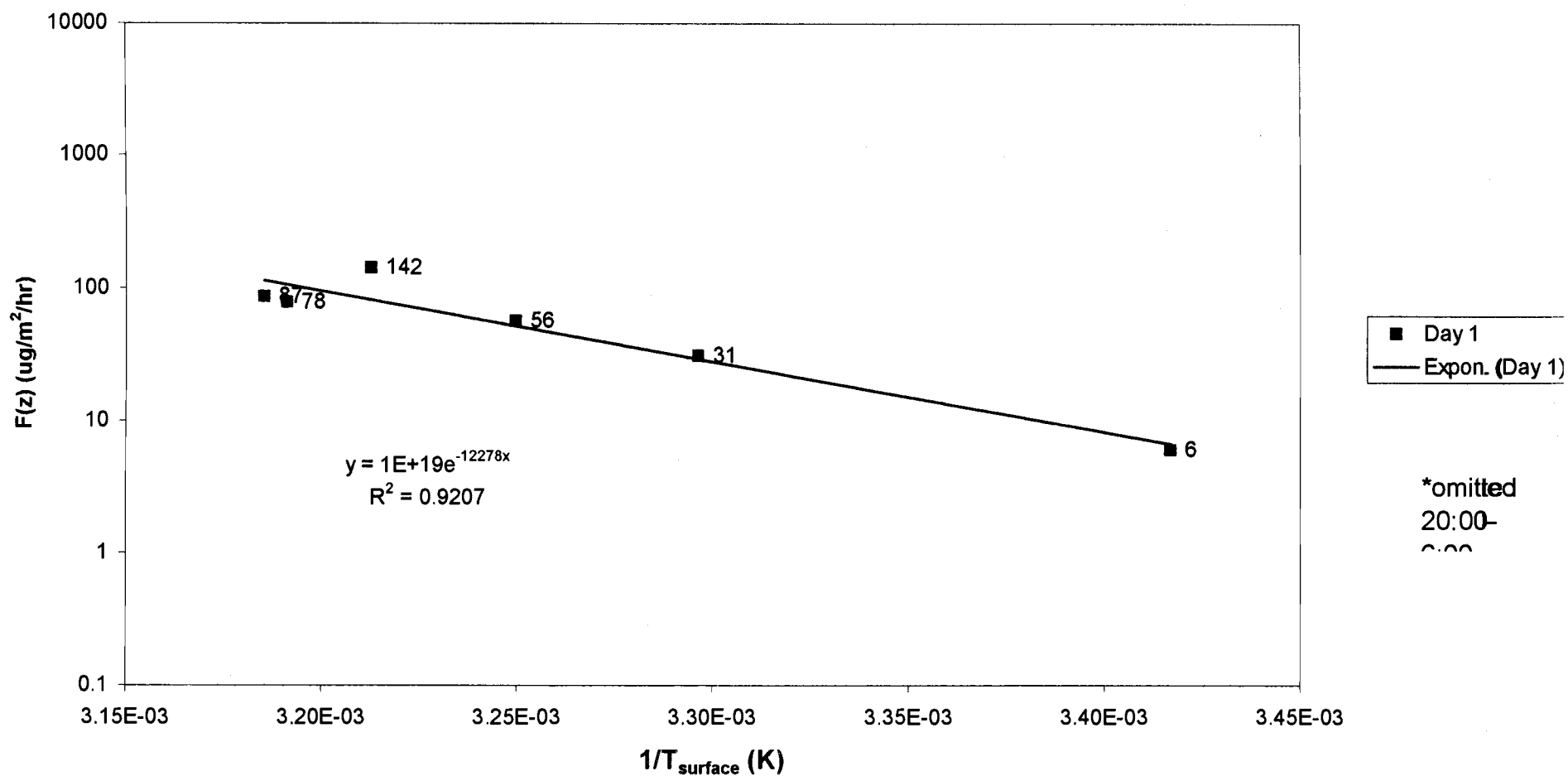
Propiconazole: Flux ($\mu\text{g}/\text{m}^2/\text{hr}$) vs. $1/T_{\text{surface}}$ (K)
Day 0-7, App.2 '96 July 23-30, Julian 205-212



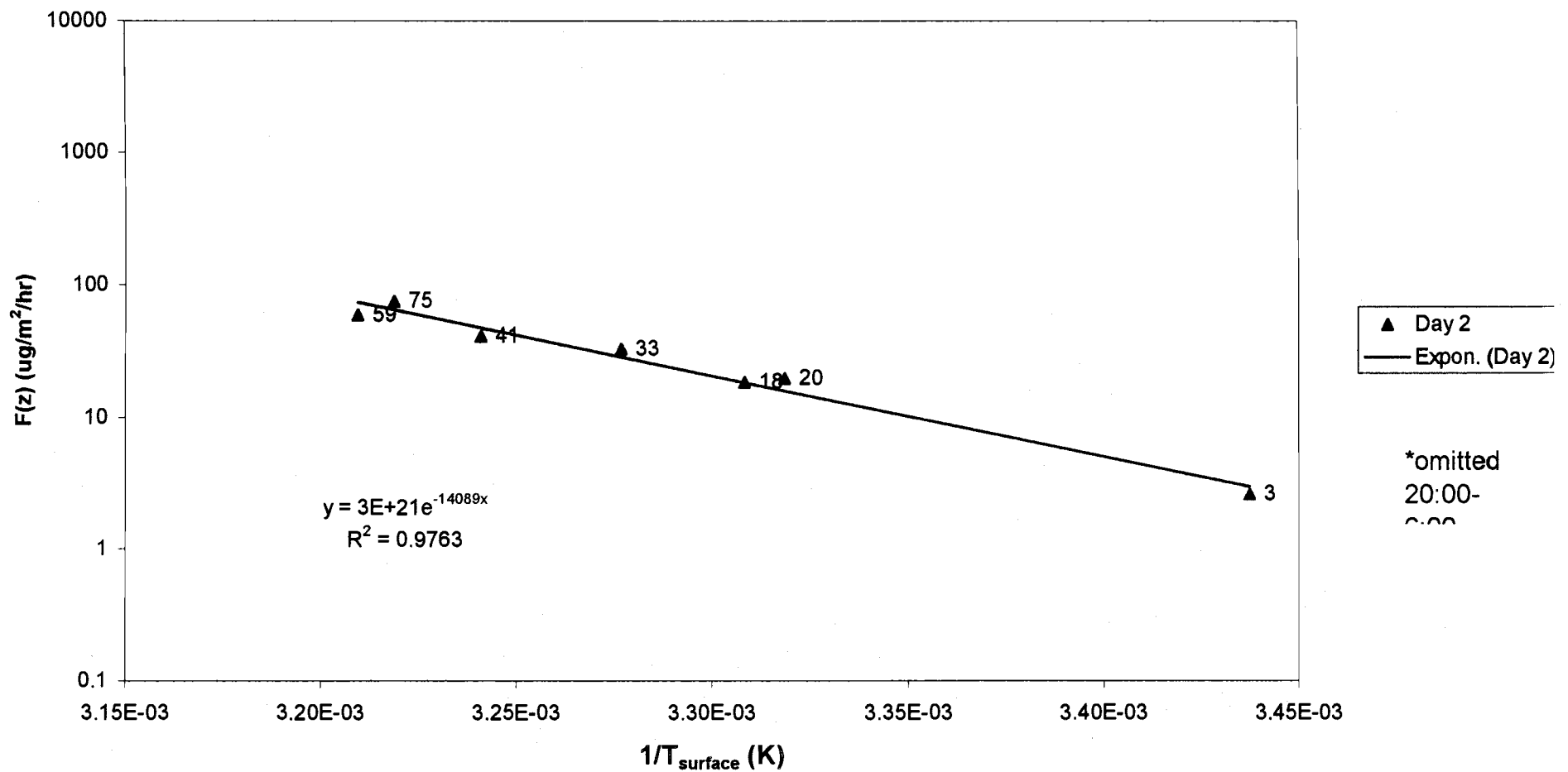
Propiconazole: Flux ($\mu\text{g}/\text{m}^2/\text{hr}$) vs. $1/T_{\text{surface}}$ (K)
Day 0, App.2 '96 July 23, Julian 205



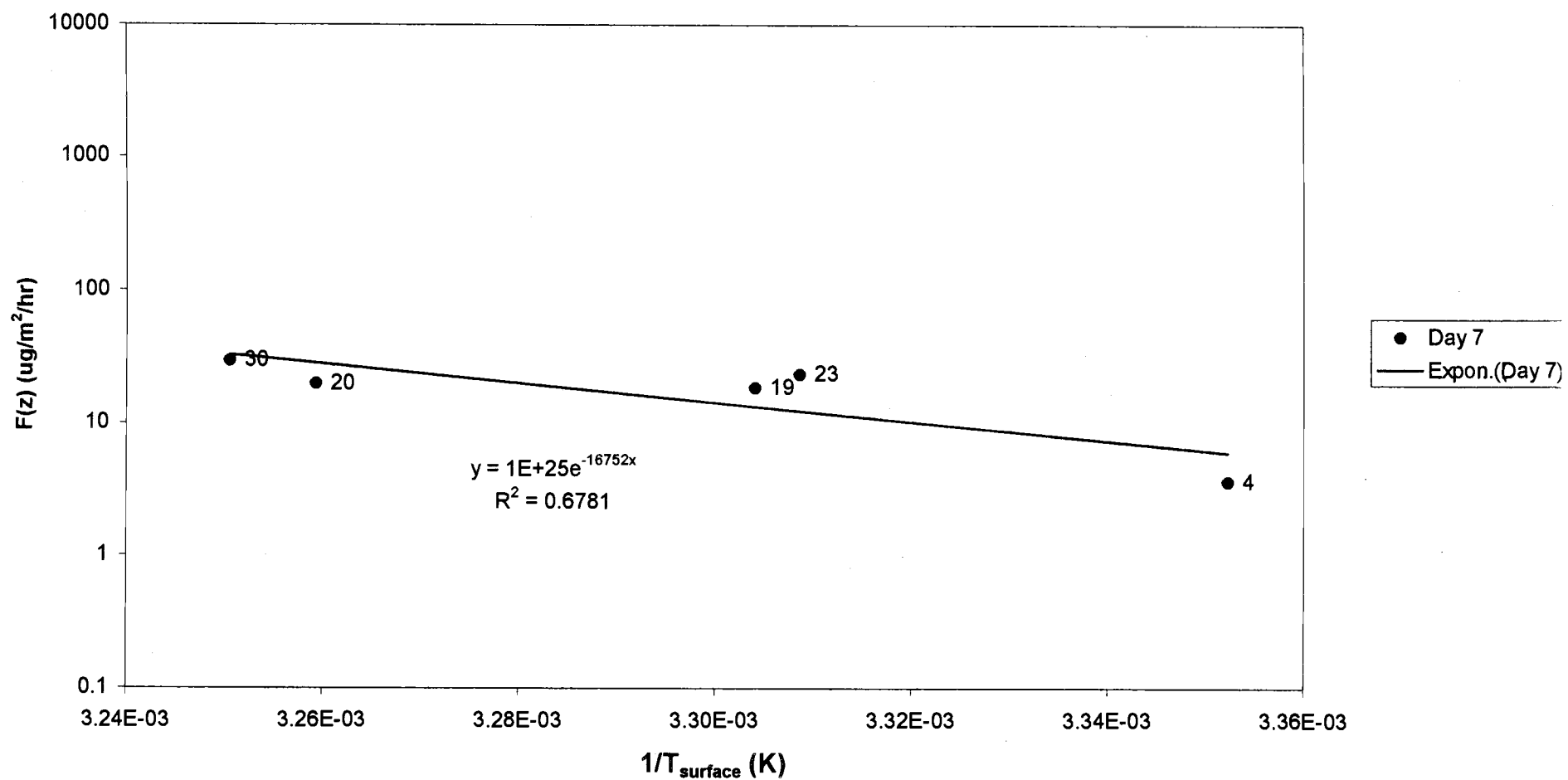
Propiconazole: Flux (ug/m²/hr) vs. 1/T_{surface} (K)
Day 1, App.2 '96 July 24, Julian 206



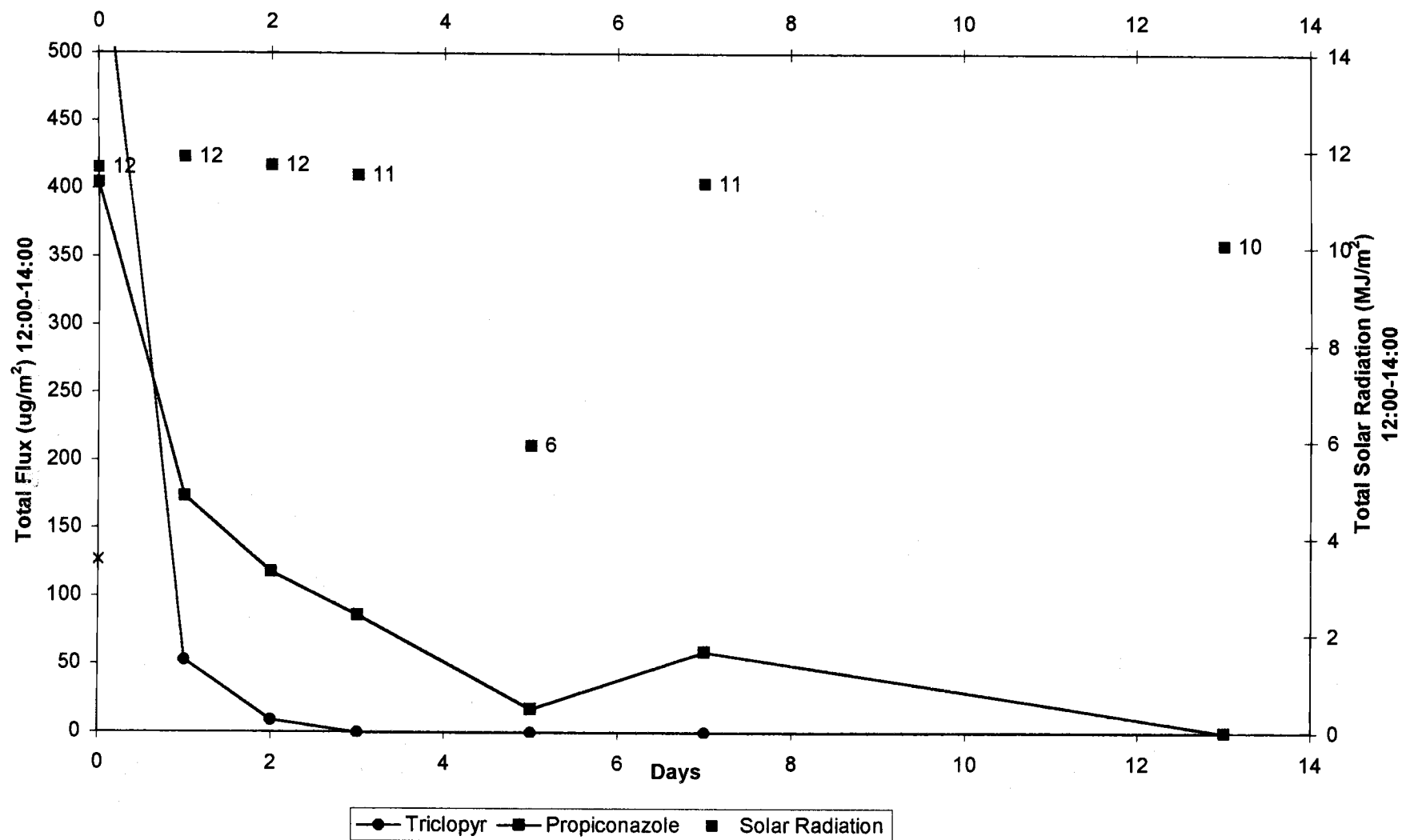
Propiconazole: Flux (ug/m²/hr) vs. 1/T_{surface} (K)
Day 2, App.2 '96 July 25, Julian 207



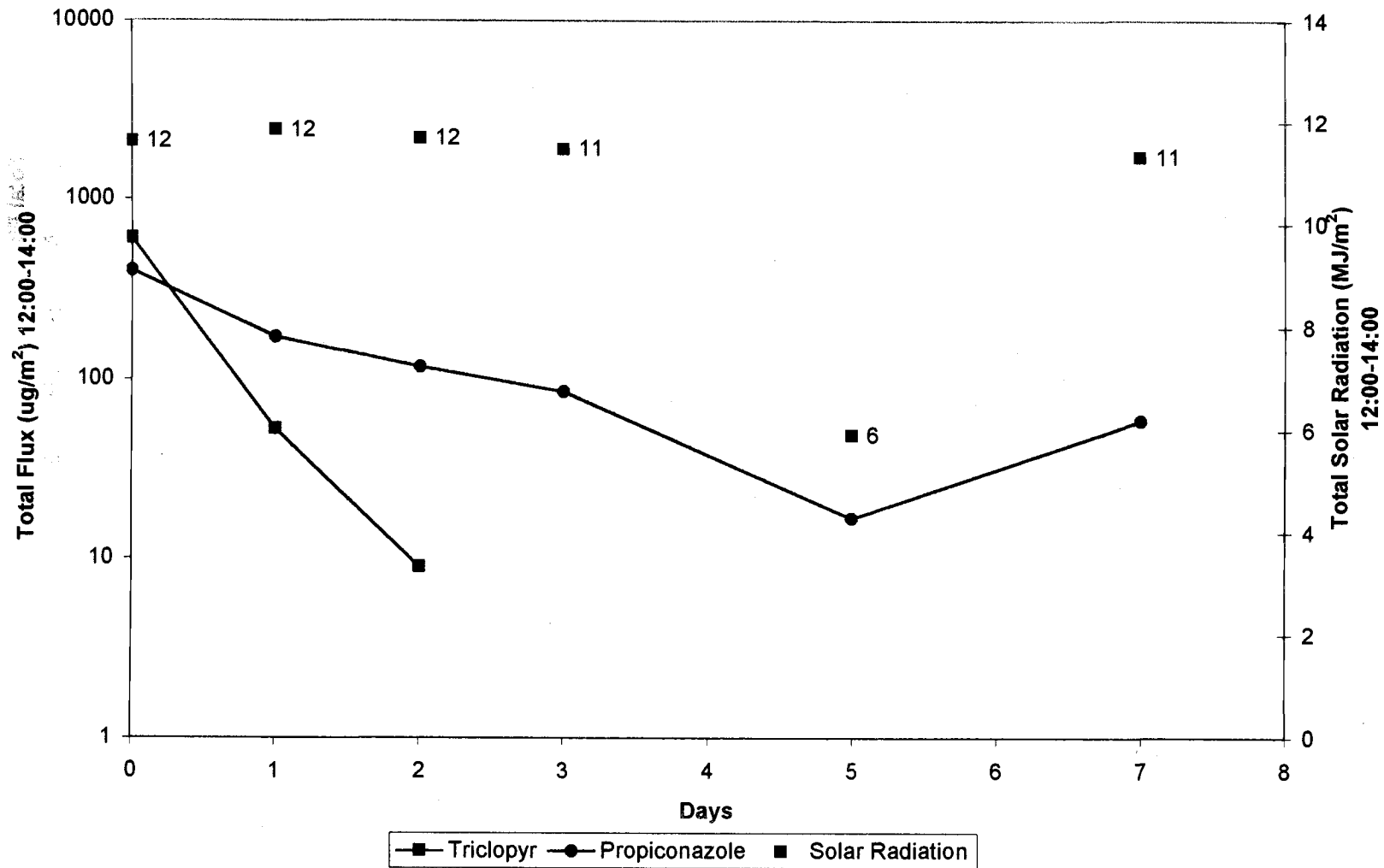
Propiconazole: Flux ($\mu\text{g}/\text{m}^2/\text{hr}$) vs. $1/T_{\text{surface}}$ (K)
Day 7, App.2 '96 July 30, Julian 212



**Peak Flux ($\mu\text{g}/\text{m}^2$) during 12:00-14:00
following Application 2, July 23rd 1996**



Peak Flux ($\mu\text{g}/\text{m}^2$) during 12:00-14:00
following Application 2, July 23rd 1996
log scale

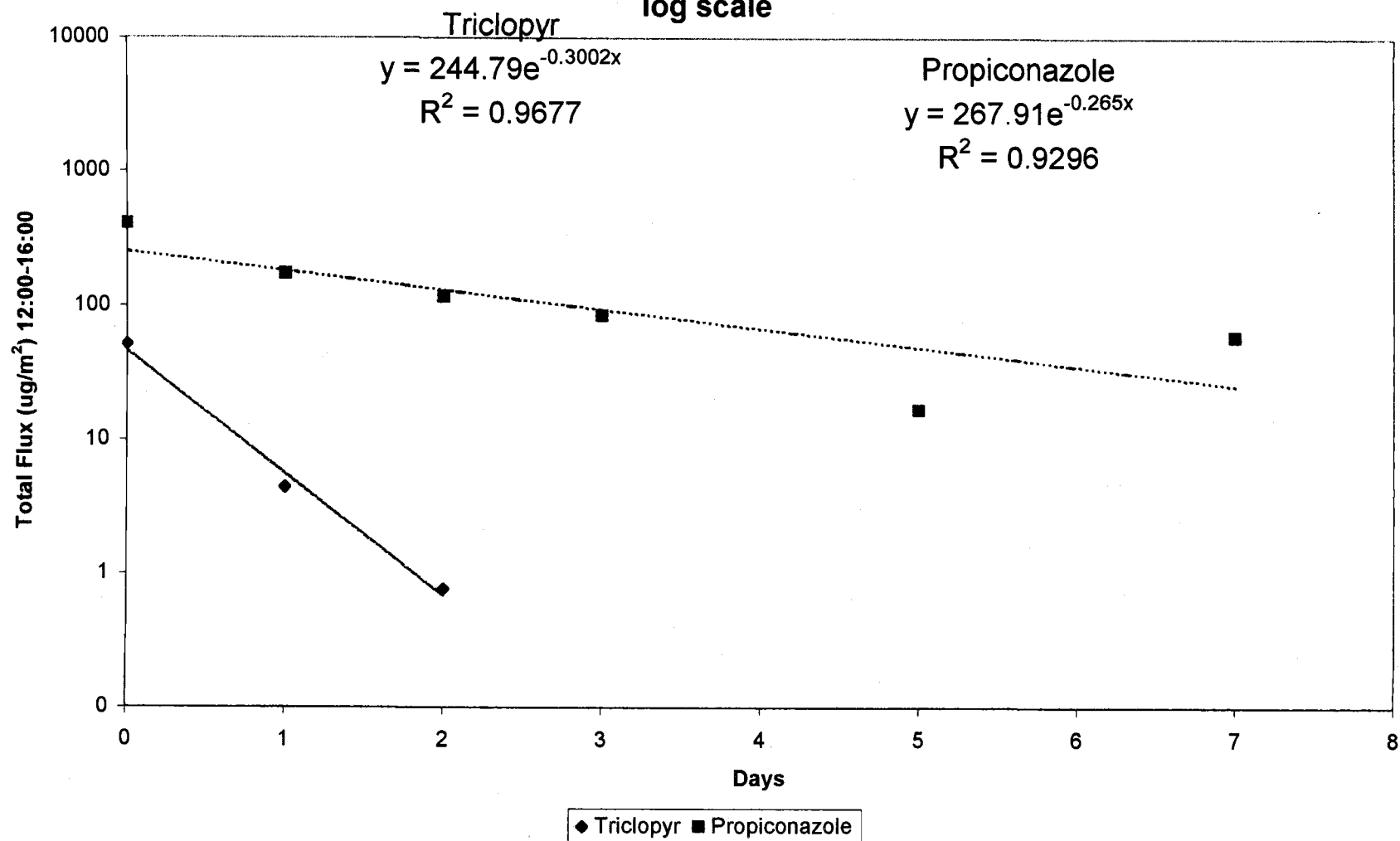


Peak Solar Radiation normalized Flux (Flux/S.R.)

12:00-14:00

following Application 2, July 23rd 1996

log scale



Appendix 7: Backward-Time Lagrangian-Stochastic Model

Source File: resistsummary5.xls

lagrange

Backward Lagrangian Stochastic Technique calculation of $Q/(u^*c)$
calculation $z_0=0.0045$ m, 22.8 m x 22.8 m, $z=0.73$ m courtesy of Thomas Flesch [46]

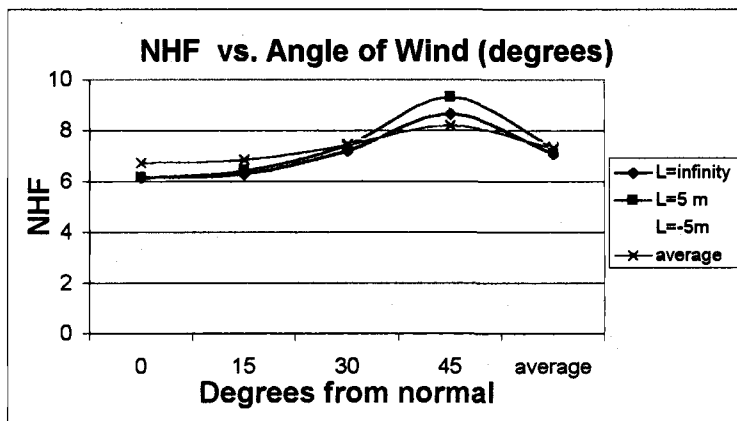
	Average	Deviation	%
Average for R=13.8 m, L= -5 m, L=infinity	6.7	0.5	+/- 9

Angle (0 degrees wind perpendicular to upwind face of square, 45 degrees wind diagonal across square)

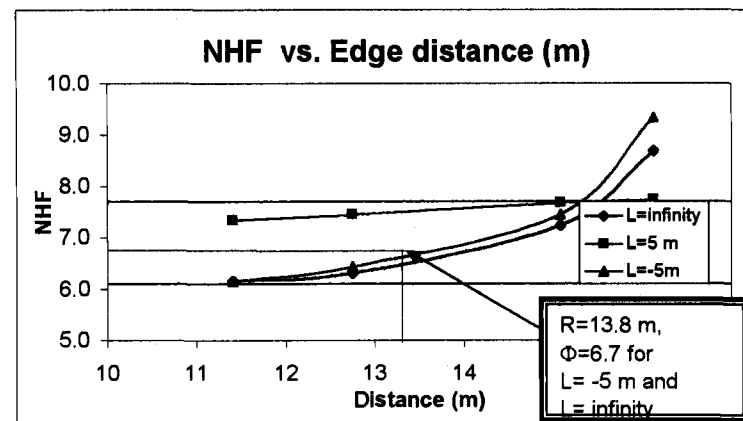
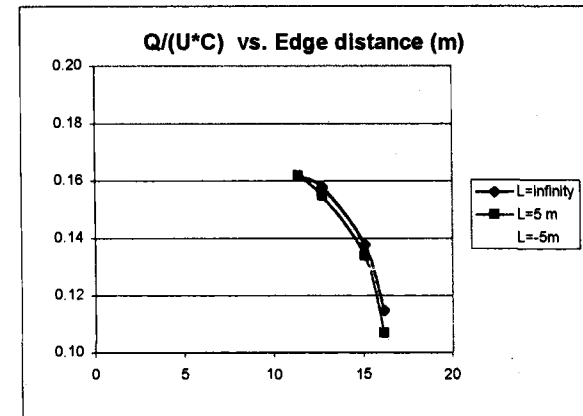
		0	15	30	45
Atmospheric	L=infinity	0.162	0.158	0.138	0.115
Stability	L=5 m	0.162	0.155	0.134	0.107
	L=-5m	0.136	0.134	0.13	0.129

NHF *Angle (0 degrees wind perpendicular to upwind face of square, 45 degrees wind diagonal across square)*

		0	15	30	45	average
Atmospheric Stability	L=infinity	6.17	6.33	7.25	8.70	7.11
	L=-5m	7.35	7.46	7.69	7.75	7.56
	L=5 m	6.17	6.45	7.46	9.35	7.36
	average	6.76	6.90	7.47	8.22	7.34



NHF	Upwind Distance to the edge of the treated plot				
L=infinity	11.4	12.75	15.08	16.12	average
L=5m	6.17	6.33	7.25	8.70	7.11
L=5m	7.35	7.46	7.69	7.75	7.56
L=5m	6.17	6.45	7.46	9.35	7.36
average	6.76	6.90	7.47	8.22	7.34



Appendix 8: Wind profiles and aerodynamic resistance

Source File: resistsummary6.xls

95,1,0,ht vs.WS

96,1,0,ht vs.WS

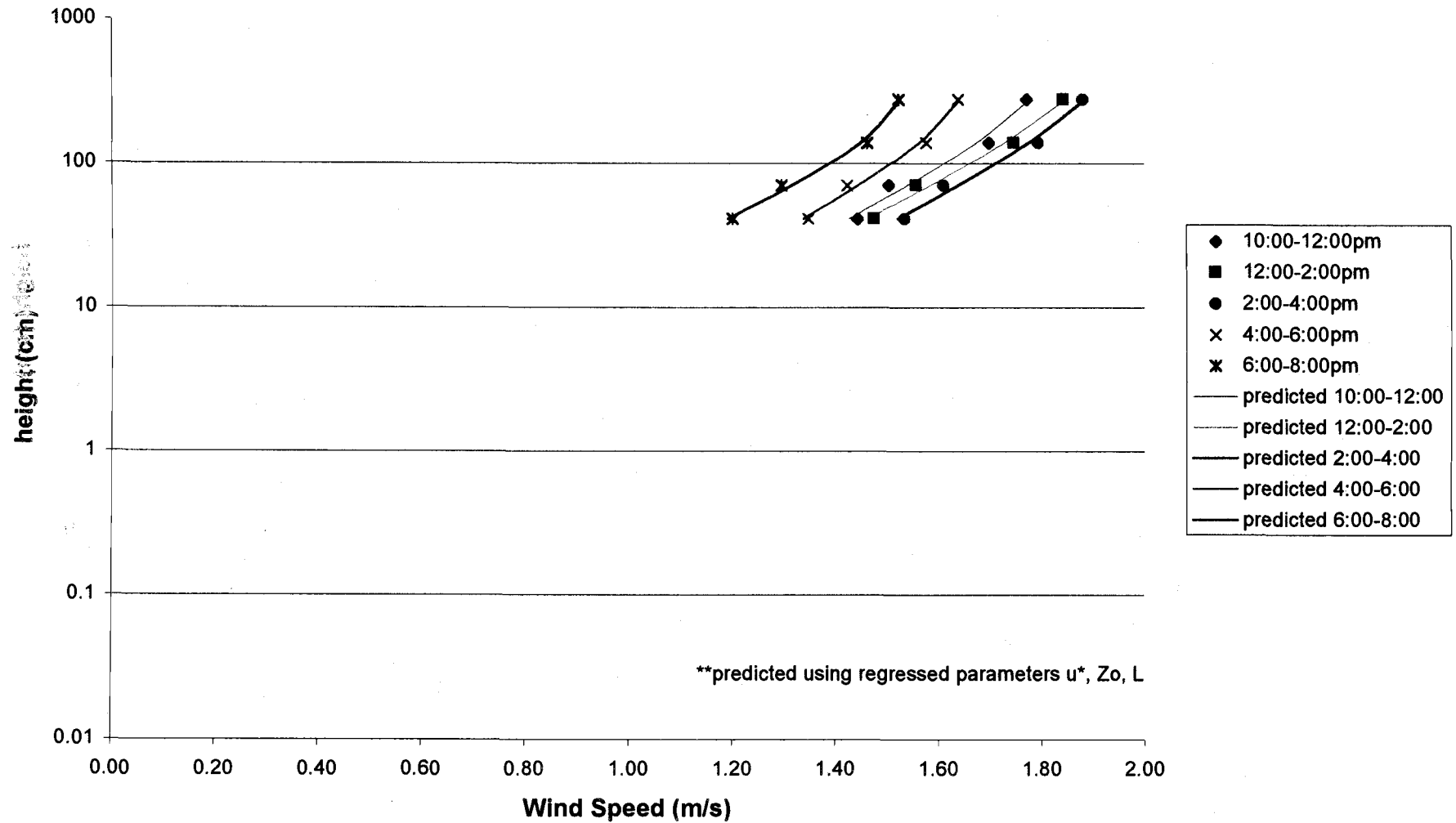
96,2,0,ht vs.WS

Source File: windsum.xls

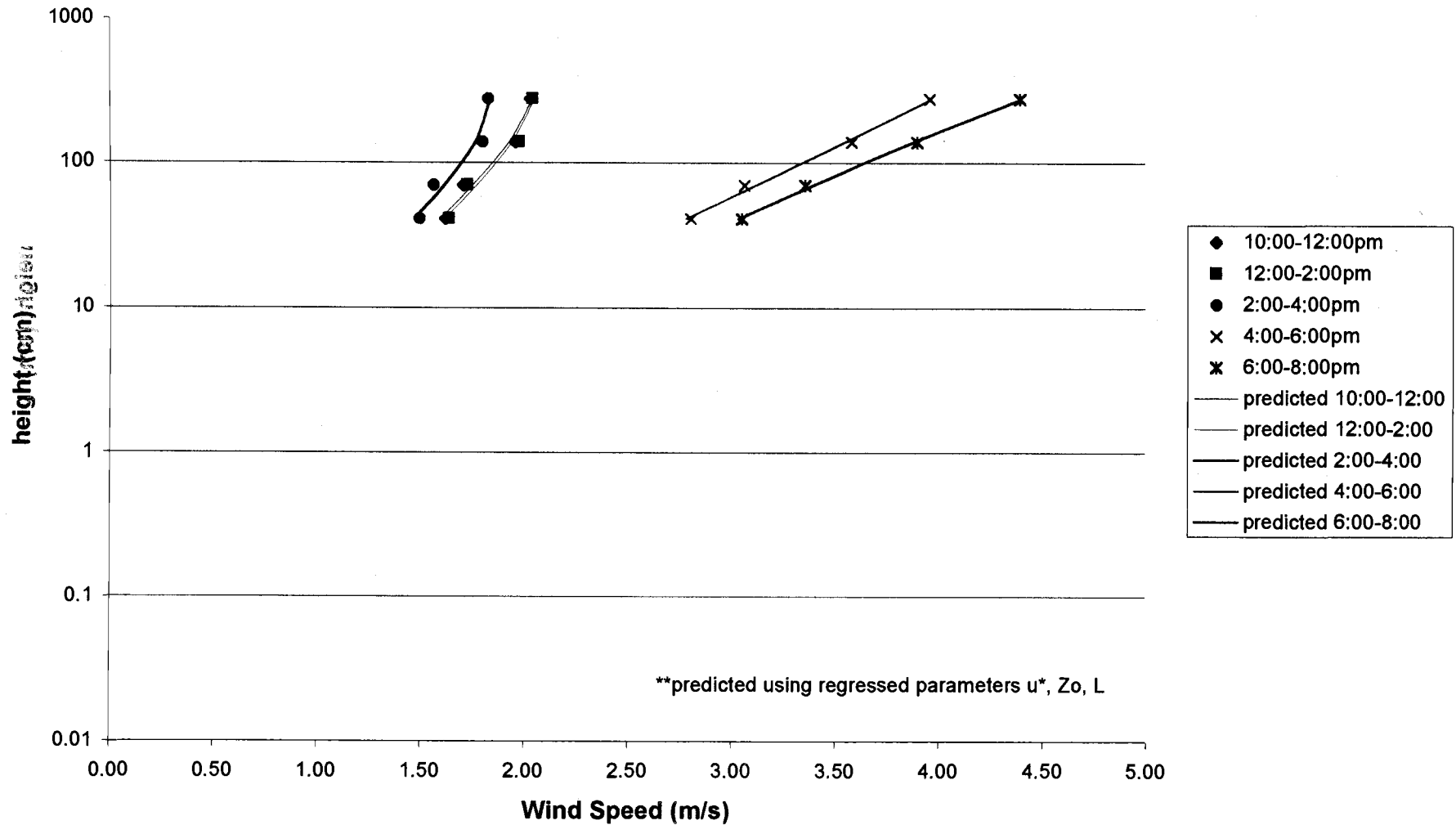
ZovsResumm

summary

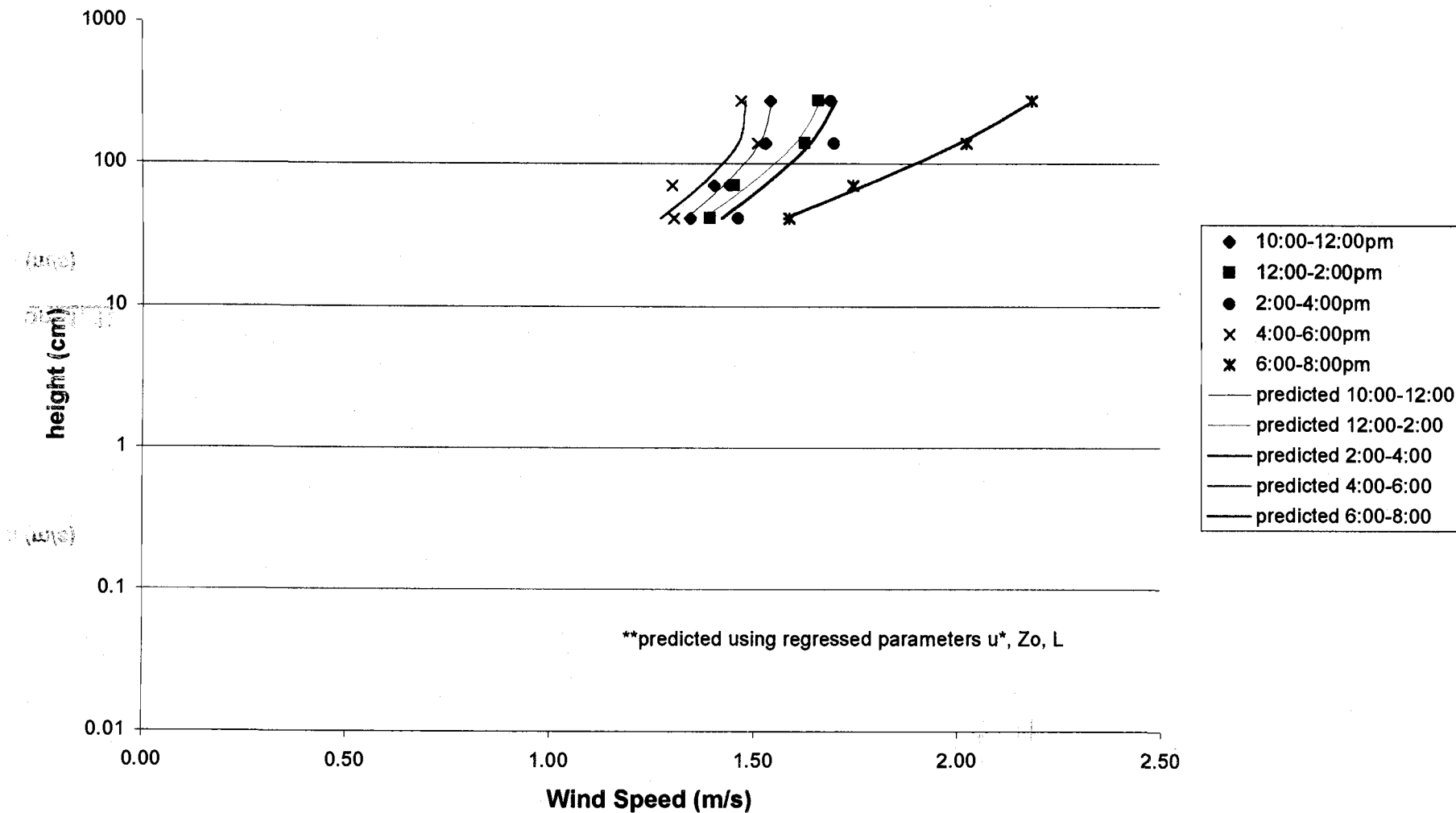
In ht (cm) vs W.S. (m/s) Day 0, App.1 '95 July 17, Julian 198



ln ht (cm) vs W.S. (m/s) **Day 0, App.1 '96 June 12, Julian 164**



In ht (cm) vs W.S. (m/s)
Day 0, App.2 '96 July 23, Julian 205



PARAMETERS DETERMINED FROM REGRESSION

$u(z) = u^*/k[\ln(z/z_0) + 4.7z/L]$ for $z=41, 70, 140, 280$ cm

*for half hour intervals between 9:00-20:00

Day 0, App. 1, 1995, 7:30-20:00

	average	min.	max.	stdev.
u@70cm (m/s)	1.42	0.713	1.872	0.28
u* (m/s)	0.10	0.05	0.21	0.03
Zo (m)	0.0025	4.53E-05	0.0150	0.0036
Re*	18.44	0.19	193.24	39.35
L (m)	-22.9	-9.0	39.7	31.7

Day 1, App. 1, 1995, 5:30-20:00

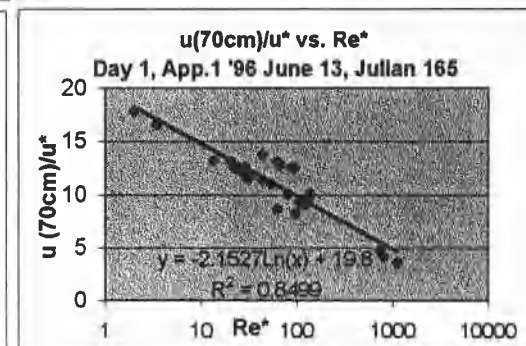
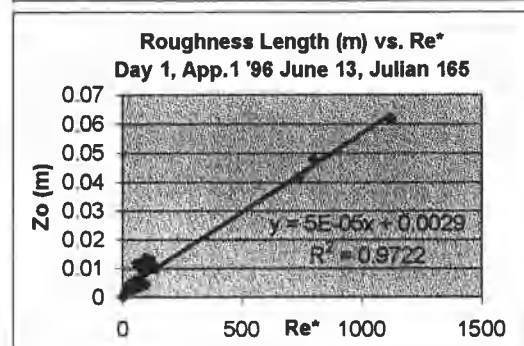
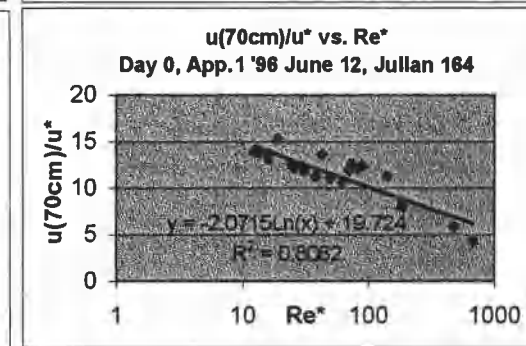
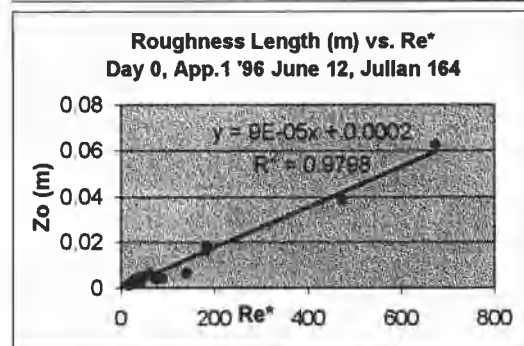
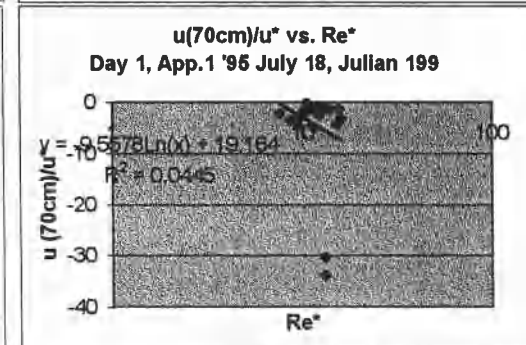
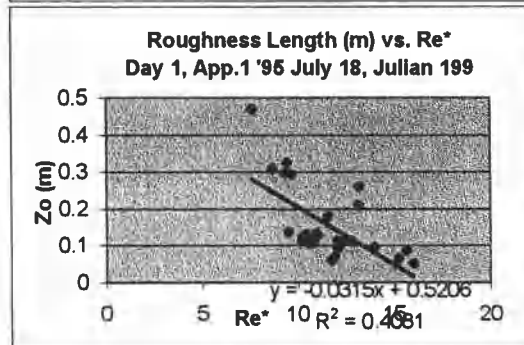
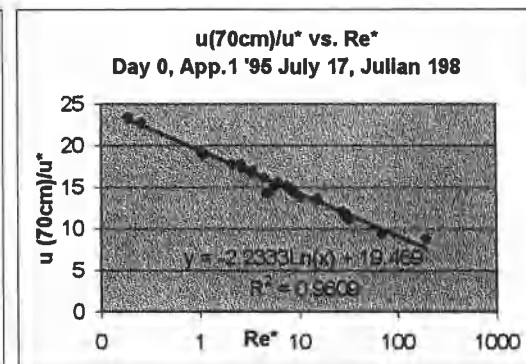
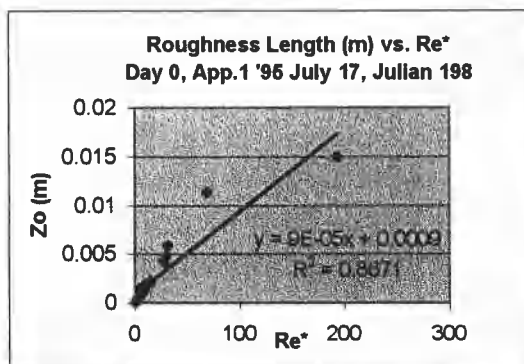
	average	min.	max.	stdev.
u@70cm (m/s)	1.70	0.74	3.59	0.82
u* (m/s)	0.16	0.05	0.47	0.10
Zo (m)	0.0064	0.0008	0.0218	0.0047
Re*	89.4	2.7	670.8	134.9
L (m)	-10.0	-7.7	-27.8	45.4

Day 0, App. 1, 1996, 7:30-20:00

	average	min.	max.	stdev.
u@70cm (m/s)	2.10	1.09	4.07	0.91
u* (m/s)	0.18	0.11	0.36	0.07
Zo (m)	0.0063	0.0017	0.0389	0.0080
Re*	70.1	12.3	474.0	97.6
L (m)	-21.2	-6.7	20.9	21.4

Day 1, App. 1, 1996, 7:00-20:00

	average	min.	max.	stdev.
u@70cm (m/s)	1.79	0.68	4.04	0.96
u* (m/s)	0.17	0.08	0.32	0.08
Zo (m)	0.0112	0.0004	0.0618	0.0152
Re*	154.3	2.0	1122.1	278.0
L (m)	-12.0	-4.2	29.2	13.1



*note: regressions only conducted when $u(41\text{cm}) > 0.6$ m/s

windsum.xls, 5/18/99

PARAMETERS DETERMINED FROM REGRESSION

$u(z)=u^*/k[\ln(z/z_0)+4.7z/L]$ for $z=41, 70, 140, 280$ cm

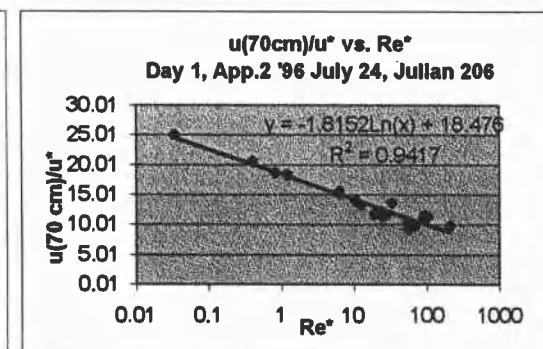
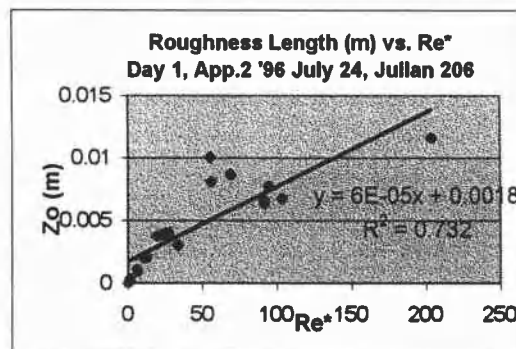
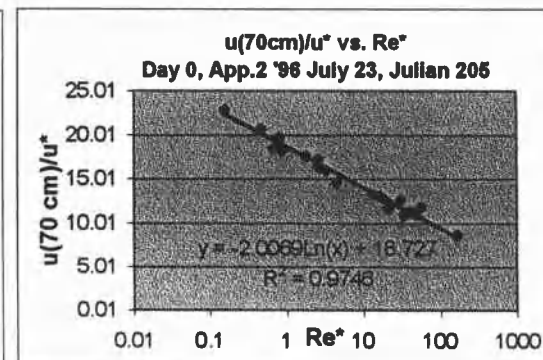
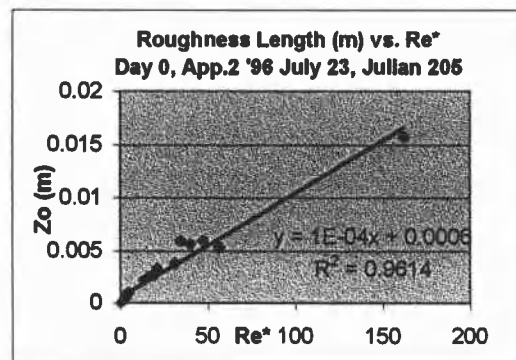
*for half hour intervals between 9:00-20:00

Day 0, App. 2, 1996, 9:00-20:00

	average	min.	max.	stdev.
$u@70\text{cm}$ (m/s)	1.42	0.99	2.14	0.22
u^* (m/s)	0.10	0.06	0.18	0.03
z_0 (m)	0.0028	4.40E-05	0.0158	0.0036
Re^*	21.8	0.2	162.3	35.7
L (m)	-13.7	-5.2	-177.9	22.7

Day 1, App. 2, 1996, 8:30-20:00

	average	min.	max.	stdev.
$u@70\text{cm}$ (m/s)	1.51	0.71	2.76	0.64
u^* (m/s)	0.12	0.03	0.28	0.07
z_0 (m)	0.0043	1.81E-05	0.0116	0.0034
Re^*	42.4	3.30E-02	203.5	48.6
L (m)	-10.7	-3.0	26.3	12.1



*note: regressions only conducted when $u(41\text{cm}) > 0.6$ m/s

Appendix 9: Flux normalization

Source File: fluxratio3.xls

boundary2

Application 1, 1995

Day 0 (July 17th)

Time	Flux (ug/m ² /hr)	
	Triadimefon	Chlorpyrifos
6:00-8:00	60	548
8:00-10:00	235	1202
10:00-12:00	544	1619
12:00-14:00	642	1391
14:00-16:00	697	981
16:00-18:00	545	567
18:00-20:00	210	229
20:00-6:00	38	61
Est.Average (6:00-6:00)	371	825
Est. Deviation (+/-)		

Normalized Flux Values

Flux/S.V.D(T)*. (m/hr)	
Triadimefon	Chlorpyrifos
6.85	2.73
6.56	2.01
2.35	0.63
1.07	0.26
1.05	0.17
0.67	0.08
0.78	0.08
3.50	0.26
2.85	0.78
2.56	1.02

Normalized Flux Values

Flux/S.D.*S.V.D(S.T.)*. (m ³ /hr/ug) 10 ⁻³	
Triadimefon	Chlorpyrifos
22.45	19.96
21.50	14.68
7.72	4.63
3.50	1.89
3.44	1.23
2.20	0.61
2.57	0.58
11.49	1.89
9.36	5.69
8.39	7.43

Surface Temp. (C)	Ambient Temp. (C)
17.55	18.58
26.85	24.23
40.19	28.59
47.49	32.46
48.28	35.55
49.86	37.18
41.28	36.35
18.86	22.02
36.29	29.37

Application 1, 1996

Day 0 (June 12th)

Time	Flux (ug/m ² /hr)		
	Triadimefon	Chlorpyrifos	Ethofumesate
6:00-8:00	9	166	41
8:00-10:00	77	1046	284
10:00-12:00	242	2496	768
12:00-14:00	450	1738	949
14:00-16:00	405	1092	898
16:00-18:00	341	944	851
18:00-20:00	95	284	248
20:00-6:00	11	69	31
Est.Average (6:00-6:00)	231	1109	577
Est. Deviation (+/-)			

Normalized Flux Values		
Flux/S.V.D(T)*. (m/hr)		
Triadimefon	Chlorpyrifos	Ethofumesate
2.35	1.52	
4.28	2.99	3.78
4.19	2.88	
3.37	1.04	
2.38	0.54	
4.33	0.86	
4.27	0.69	3.30
3.34	0.73	0.41
3.60	1.50	3.54
0.79	0.92	1.58

Normalized Flux Values		
Flux/S.D.*S.V.D(S.T.)*. (m ³ /hr/ug) 10 ⁻³		
Triadimefon	Chlorpyrifos	Ethofumesate
7.72	8.16	
14.04	16.07	15.11
13.73	15.49	
11.03	5.61	
7.81	2.92	
14.19	4.60	
14.01	3.71	13.21
10.95	3.94	1.65
11.79	8.08	14.16
2.58	4.97	6.30

Surface Temp. (C)	Ambient Temp. (C)
12.62	12.36
22.22	15.40
30.15	17.89
36.14	20.82
37.91	23.33
32.33	23.82
23.61	21.23
11.44	11.50
27.86	19.26

Application 2, 1996

Day 0 (July 23rd)

Time	Flux (ug/m ² /hr)	
	Triclopyr	Propiconazole
6:00-8:00	66	17
8:00-10:00	323	42
10:00-12:00	414	147
12:00-14:00	303	202
14:00-16:00	121	145
16:00-18:00	66	72
18:00-20:00	35	19
20:00-6:00	3	1
Est.Average (6:00-6:00)	190	92
Est. Deviation (+/-)		

Normalized Flux Values	
Flux/S.V.D(T)*. (m/hr)	
Triclopyr	Propiconazole
6.55	2.24
7.98	5.48
4.27	
1.83	
0.72	
0.65	
0.75	
0.30	0.17
2.88	2.63
3.01	2.68

Normalized Flux Values	
Flux/S.D.*S.V.D(S.T.)*. (m ³ /hr/ug) 10 ⁻³	
Triclopyr	Propiconazole
57.42	10.35
70.03	25.39
37.49	
16.06	
6.35	
5.73	
6.56	
2.63	0.77
25.28	12.17
26.39	12.41

Surface Temp. (C)	Ambient Temp. (C)
19.26	17.47
28.62	24.04
34.80	27.07
38.71	30.59
38.77	33.51
35.13	34.83
29.62	31.52
19.74	20.62
30.58	27.45

*S.D. (Spray Density ug/m²) *S.V.D(T) (Saturated Vapor Density at Surface Temp (K) ug/m³, *S.T. (Surface Temperature)

app10.wpd

Calculation Table for Backward-time Lagrangian Stochastic method flux (equations 66 and 67).

Application 1, 1995

Application 1, 1995			Adjusted	Total Residue Collected		Airborne Conc. @ 73 cm		BTLSD Flux				
Air Sampling Period			Flow Rate	Total Flow	Triadimefon	Chlorpyrifos	Triadimefon	Chlorpyrifos	u(70 cm)		Triadimefon	Chlorpyrifos
Day 0 (July 17th)	Start	End	(m ³ /min)	(m ³)	(ug)	(ug)	(ug/m ³)	(ug/m ³)	m/s	Φ [46]	(ug/m ³)	(ug/m ³)
Julian 198	6:50	8:00	0.99	69.40	10.00	91.00	0.14	1.31	0.78	6.7	60.23	548.14
	8:00	10:00	0.99	118.97	41.00	210.00	0.34	1.77	1.27	6.7	234.75	1202.37
	10:00	12:06	0.92	109.89	74.00	220.00	0.67	2.00	1.50	6.7	544.47	1618.68
	12:06	14:00	1.03	117.34	90.00	195.00	0.77	1.66	1.56	6.7	641.89	1390.77
	14:02	16:00	0.98	115.50	93.00	131.00	0.81	1.13	1.61	6.7	696.55	981.17
	16:02	18:00	0.92	108.06	77.00	80.00	0.71	0.74	1.42	6.7	545.42	566.67
	18:02	20:00	0.92	108.06	32.50	35.50	0.30	0.33	1.30	6.7	209.56	228.91
	20:00	6:03	0.97	582.62	33.50	54.00	0.06	0.09	1.22	6.7	37.77	60.89
Est.Total (6:00-20:00)												

Application 1, 1996

Application 1, 1996		Adjusted	Total Residue Collected			Airborne Conc. @ 73 cm			BTLS Flux						
Air Sampling Period		Flow Rate	Total Flow	Triadimefon	Chlorpyrifos	Ethofumesate	Triadimefon	Chlorpyrifos	Ethofumesate	u(70 cm)	Φ [46]	Triadimefon	Chlorpyrifos	Ethofumesate	
Start	End	(m³/min)	(m³)	(ug)	(ug)	(ug)	(ug/m³)	(ug/m³)	(ug/m³)	m/s		(ug/m²/hr)	(ug/m²/hr)	(ug/m²/hr)	
Day 0 (June 12th)															
Julian 16	7:41	7:59	1.12	131.70	3.00	52.40	13.00	0.02	0.40	0.10	0.78	6.7	9.49	165.75	41.12
	8:00	10:01	1.18	142.76	14.00	190.00	51.50	0.10	1.33	0.38	1.46	6.7	77.10	1046.40	283.63
	10:01	12:00	1.05	125.24	33.00	341.00	105.00	0.26	2.72	0.84	1.71	6.7	241.51	2495.58	768.43
	12:00	14:00	1.12	133.93	65.00	251.00	137.00	0.49	1.87	1.02	1.73	6.7	450.02	1737.77	948.50
	14:01	16:06	1.08	134.74	65.00	175.00	144.00	0.48	1.30	1.07	1.56	6.7	405.48	1091.67	898.29
	16:07	17:56	0.98	106.38	22.00	61.00	55.00	0.21	0.57	0.52	3.07	6.7	340.59	944.36	851.47
	17:58	20:00	1.01	123.73	6.50	19.50	17.00	0.05	0.16	0.14	3.36	6.7	94.82	284.45	247.98
	20:00	6:00	1.15	692.60	10.00	62.00	27.80	0.01	0.09	0.04	1.43	6.7	11.13	69.01	30.95
Est.Total (6:00-20:00)															

All diffusion coefficients adjusted for temperature using $[T(K)/T(25^{\circ}C)]^{1.75}$

Application 2, 1996

Application 2, 1-06			Adjusted	Total Residue Collected		Airborne Conc. @ 73 cm					BTLSD Flux	
Air Sampling Period			Flow Rate	Total Flow	Triclopyr	Propiconazole	Triclopyr	Propiconazole	u(70 cm)		Triclopyr	Propiconazole
Day 0 (July 23rd)	Start	End	(m³/min)	(m³)	(ug)	(ug)	(ug/m³)	(ug/m³)	m/s	Φ [46]	(ug/m²)	(ug/m²)
Julian 2	6:15	8:03	1.07	115.25	22.00	5.80	0.19	0.05	0.64	6.7	65.57	17.29
	8:03	10:00	0.99	116.00	67.00	8.80	0.58	0.08	1.04	6.7	322.84	42.40
	10:00	12:00	0.94	112.92	62.00	22.00	0.55	0.19	1.40	6.7	414.37	147.03
	12:00	14:00	0.97	115.94	45.00	30.00	0.39	0.26	1.45	6.7	303.22	202.15
	14:00	16:00	0.80	96.26	15.00	18.00	0.16	0.19	1.44	6.7	120.84	145.00
	16:01	18:00	0.81	96.96	9.20	10.00	0.09	0.10	1.30	6.7	66.36	72.14
	18:01	20:01	0.83	99.29	3.70	2.00	0.04	0.02	1.75	6.7	34.95	18.89
	20:04	6:00	0.84	500.67	4.30	1.70	0.01	0.00	0.70	6.7	3.23	1.28

Calculation Table for Fugacity Flux (equations 3, 4, 7, 63)

Assumed Constants $x=13.8$ m, $z_0=0.0045$ m

Application 1, 1995

Air Sampling Period				Surface	u^* (m/s)	Stability	S.V.D. (T) $\mu\text{g}/\text{m}^3$		Triadimefon	Chlorpyrifos	Predicted Fugacity Flux	
Start	End	Temp. (C)	Value	Value	Value	Value	Triadimefon	Chlorpyrifos	r_T for 35	r_T for 35	Triadimefon	Chlorpyrifos
									(s/m)	(s/m)	$\mu\text{g}/\text{m}^2/\text{hr}$	$\mu\text{g}/\text{m}^2/\text{hr}$
Day 0 (July 17th)												
Julian 198	6:50	8:00	17.55	0.10	-10	9	200	227	230	140	3141	
	8:00	10:00	26.85	0.09	-20	36	598	250	254	515	8487	
	10:00	12:06	40.19	0.09	-27	231	2553	236	239	3531	38454	
	12:06	14:00	47.49	0.10	-32	601	5367	225	228	9605	84611	
	14:02	16:00	48.28	0.09	-29	665	5802	231	234	10346	89122	
	16:02	18:00	49.86	0.09	-19	812	6780	236	240	12365	101854	
	18:02	20:00	41.28	0.11	-16	268	2859	201	204	4785	50455	
Est.Total (6:00-20:00)												

Application 2, 1996

Air Sampling				Surface	u^* (m/s)	Stability	S.V.D. (T) $\mu\text{g}/\text{m}^3$			Triadimefon	Chlorpyrifos	Ethofumesate	Predicted Fugacity Flux		
Start	End	Temp. (C)	Value	Value	Value	Value	Triadimefon	Chlorpyrifos	Ethofumesate	r_T for 35	r_T for 35	r_T for 35	Triadimefon	Chlorpyrifos	Ethofumesate
										(s/m)	(s/m)	(s/m)	$\mu\text{g}/\text{m}^2/\text{hr}$	$\mu\text{g}/\text{m}^2/\text{hr}$	$\mu\text{g}/\text{m}^2/\text{hr}$
Day 0 (June 1st)															
Julian 164	6:41	7:59	12.62	0.13	-6	4	109			164	166	164	89	2367	
	8:00	10:01	22.22	0.14	-11	18	350	75		162	164	162	400	7676	1670
	10:01	12:00	30.15	0.13	-19	58	866			170	172	170	1223	18134	
	12:00	14:00	36.14	0.14	-17	134	1666			167	169	167	2884	35492	
	14:01	16:06	37.91	0.13	-14	170	2011			172	174	171	3574	41676	
	16:07	17:56	32.33	0.25	-254	79	1103			98	99	98	2884	39969	
	17:58	20:00	23.61	0.25	50	22	412	75		99	100	99	808	14826	2737
	20:00	6:00	11.44												
Est.Total (6:00-20:00)															

All diffusion coefficients adjusted for temperature using $[T(K)/T(25^\circ\text{C})]^{1.75}$

Application 2, 1996

Air Sampling Period				Surface	u^* (m/s)	L (m)	S.V.D. (T) $\mu\text{g}/\text{m}^3$		Predicted Fugacity Flux			
Start	End	Temp. (C)	Value	Value	Value	Value	Triclopyr	Propiconazole	r_T for 35	r_T for 35	Triclopyr	Propiconazole
									(s/m)	(s/m)	$\mu\text{g}/\text{m}^2/\text{hr}$	$\mu\text{g}/\text{m}^2/\text{hr}$
Day 0 (July 23rd)												
Julian 205	6:15	8:03	19.26	0.08	-5	10	8		252	258	143	108
	8:03	10:00	28.62	0.07	-7	40	8		306	313	476	89
	10:00	12:00	34.80	0.09	-12	97			243	249	1435	
	12:00	14:00	38.71	0.10	-15	166			221	226	2701	
	14:00	16:00	38.77	0.09	-16	167			231	236	2598	
	16:01	18:00	35.13	0.10	-11	102			221	226	1653	
	18:01	20:01	29.62	0.16	-27	47	8		143	146	1176	191

Appendix 10: Sample Calculation of Time Lagrangian Stochastic Dispersion model (BTLS)

BTLS

$$\bar{c} \text{ (ug/m}^3\text{)} = \frac{\text{total collected residue @ 73 cm (ug)}}{\text{sampler flow rate (m}^3\text{/hr)} * \text{sampling interval (hr)}}$$

$$F_{Z=0} = \frac{u_{70\text{cm}} * c_{73\text{cm}}}{\Phi_{(z=73\text{cm}, R=10\text{m}, z_0=0.2\text{cm})}}$$

$F_{Z=0}$ - flux of pesticide vapor from the turf grass ($\text{ug} * \text{m}^{-2} * \text{hr}^{-1}$)

$c_{73\text{cm}}$ - airborne concentration pesticide vapor at the sampling height above the turf plot (ug/m^3).

$u_{70\text{cm}}$ - the average wind speed (m/s) near the sampling height during the air sampling interval.

Φ - ideal flux (unit-less) defined as a factor which relates the product of the wind speed u and concentration profiles c at the sampling height to the rate of loss from the surface F . This value is generated by the BTLS method as a function of plot radius R , roughness length z_0 , sampling height, and atmospheric stability L [45, 56].

Fugacity Model

$$\ln P = -\frac{\Delta H}{RT} + \frac{\Delta S}{R}$$

$$S.V.D. (\text{g/m}^3) = \text{mol.wt} * \frac{P}{R * T}$$

$$r_T = \frac{1}{ku_*} \left[\ln \left(\frac{ku_* z}{D_a} \right) + \frac{4.7 * z}{L} \right]$$

$$F_z = \frac{ku_* [S.V.D.(T)]}{r_T}$$

BTLS Sample Calculation: Application 1, 1996, Day 0, 8:00-10:01, Chlorpyrifos.

$\Phi=6.7$, total collected residue @73 cm=190.00 ug, sampler flow rate=1.18 m^3/min , sampling interval=121 minutes, $u(70\text{ cm})=0.78\text{ m/s}$.

$$\bar{c} = (\text{ug} / \text{m}^3) = \frac{190.00 \text{ ug}}{1.18 \text{ m}^3 / \text{min} * 121 \text{ min}} = 1.33 \frac{\text{ug}}{\text{m}^3}$$

$$F_{Z=0} = \frac{1.46 \text{ m} / \text{s} * 1.33 \text{ ug} / \text{m}^3}{6.7} * 3600 \text{ s} = 1043 \approx 1046 \frac{\text{ug}}{\text{m}^2 * \text{hr}}$$

Fugacity Sample Calculation: Appl. Environ. Biol. 1990
 $\Delta H = 88604 \text{ J/mol}$, $\Delta S = 246.6 \text{ J/K/mol}$, mol. wt. = 350.6 g/mol,
 m , $x = 13.8 \text{ m}$, $T = 22.22^\circ\text{C}$, $z_0 = 0.0045 \text{ m}$

J-10:01, Chlorpyrifos.
 1.75 , $u^* = 0.14 \text{ m/s}$, $L = -11$

$$\ln p = \frac{-87604.2 (\text{J/mol})}{8.3145 (\text{J/K/mol}) * (273.15 + 22.22) (\text{K})} + \frac{246.6 + (\text{J/K/mol})}{8.3145 (\text{J/K/mol})} = -6.013$$

$$S.V.D. = \frac{\exp^{-6.013} (\text{pa})}{8.3145 (\text{J/K/mol}) * (273.15 + 22.2) (\text{K})} * \frac{350.6 (\text{g})}{(\text{mol})} * 1 \times 10^6 \left(\frac{\text{ug}}{\text{g}} \right) = 349.5 \left(\frac{\text{ug}}{\text{m}^3} \right)$$

$$D_a = 3.44 \times 10^{-6} (\text{m}^2/\text{s}) * \left(\frac{273.15 + 22.22}{298.15} \right)^{1.75} = 3.38 \times 10^{-6} (\text{m}^2/\text{s})$$

$$r_T = \frac{1}{0.14 (\text{m/s}) * 0.4} \ln \left(\frac{0.14 (\text{m/s}) * 0.4 * 0.3 * 13.8 (\text{m})^{4/5} * 0.0045 (\text{m})^{1/5}}{3.38 \times 10^{-6} (\text{m}^2/\text{s})} \right) + 4.7 \left(\frac{0.3 * 13.8 (\text{m})^{4/5} * 0.0045^{1/5} (\text{m})}{-11 (\text{m})} \right) = 163.8 \left(\frac{\text{s}}{\text{m}} \right)$$

$$F_z = \frac{349.5 (\text{ug/m}^3)}{163.8 (\text{s/m})} * 3600 \left(\frac{\text{s}}{\text{hr}} \right) = 7681 \cong 7676 \left(\frac{\text{ug}}{\text{m}^3} \right)$$